PACIFIC EARTHQUAKE ENGINEERING RESEARCH CENTER

Experimental and Computational Evaluation of Reinforced Concrete Bridge Beam-Column Connections for Seismic Performance

Clay J. Naito

Jack P. Moehle

Khalid M. Mosalam

Department of Civil and Environmental Engineering
University of California, Berkeley

A report on research sponsored by
the California Department of Transportation under Contract No. 59 A 131

PEER 2001/08
NOV. 2001

Experimental and Computational Evaluation of Reinforced Concrete Bridge Beam-Column Connections for Seismic Performance

Clay J. Naito
Jack P. Moehle
Khalid M. Mosalam
Department of Civil and Environmental Engineering
University of California, Berkeley

A report on research sponsored by
the California Department of Transportation under Contract No. 59 A 131

PEER Report 2001/08
Pacific Earthquake Engineering Research Center
College of Engineering
University of California, Berkeley
November 2001

Technical Report Documentation Page

1. Report No. PEER 2001/08	2. Government Accession No.	3. Recipient's Catalog No.
4. Title and Subtitle Experimental and Computational Evaluation of Reinforced Concrete Bridge Beam-Column Connections for Seismic Performance		5. Report Date November 2001 6. Performing Organization Code UCB/ENG-9374
7. Authors Clay J. Naito, Jack P. Moehle, and Khalid M. Mosalam		8. Performing Organization Report No. UCB/PEER 2001/08
9. Performing Organization Name and Address Pacific Earthquake Engineering Research Center 1301 South 46th Street Richmond, CA 94804		10. Work Unit No. (TRAIS) 11. Contract or Grant No. Contract No. 59 A 131
12. Sponsoring Agency Name and Address California Department of Transportation Engineering Service Center 1801 30th Street MS#9 Sacramento, CA 95816		13. Type of Report and Period Covered Research Report July 1995–December 1998 14. Sponsoring Agency Code National Science Foundation

15. Supplementary Notes

16. Abstract

Proper design of reinforced concrete bridge beam-column connections is imperative for the behavior of the bridge structure. While in the past this area was overlooked, resulting in bridge structure damage and in some cases collapse, current methods have overcompensated for these shortcomings. The presented research shows that current joint design requirements in the state of California produce conservative designs (i.e., joints with excessive amounts of reinforcement). The joints in these systems are capable of supporting the intended flexural mechanism, but at the cost of constructability. The goal of this report is to evaluate current methods, identify shortcomings, and develop methods or techniques for joint performance improvement.

The research was carried out in three phases. In the first, current design requirements, constructability improvement techniques, and joint force transfer mechanisms were experimentally investigated. This was accomplished with four large-scale experiments on cap beam to column subassemblies of typical geometry. Following analysis of the force transfer mechanisms and determination of the shortcomings, a second experimental phase was undertaken to evaluate joints subjected to high joint demands. This consisted of two subassemblies with reduced beam depths and increased column strengths. Furthermore, the effectiveness of the joint spiral reinforcement versus the use of lateral and vertical joint transverse reinforcement was evaluated. In the third phase, the effectiveness of the reinforcement in these designs was evaluated analytically using developed three-dimensional finite element models. The study strives to develop a set of joint design requirements based on damage criteria; two performance criteria are suggested. The first criterion determines a level of lateral reinforcement necessary to activate the joint width in shear resistance. The second criterion determines a level of vertical joint reinforcement necessary to limit crack formation in the joint.

The results of these phases show that the intended design mechanism does not completely occur, suggesting that the placement of reinforcement under current requirements may be ineffective. Furthermore, it is shown that the use of a joint spiral is not necessary for good joint performance and may be removed as a means of improving constructability. Headed reinforcement was shown effective when used as joint transverse reinforcement, thus providing additional means of construction improvement. Three-dimensional finite element models were found to provide a reliable estimation of global and local joint response. As a conclusion to this work, the results of parametric finite element analyses are used to develop possible damage-based joint design requirements.

17. Key Words Reinforced concrete, bridges, beam-column connections, joints, headed reinforcement, 3D finite element modeling, shear, tests, failure, experiments, modeling	18. Distribution Statement No restrictions		
19. Security Classif. (of this report) Unclassified	20. Security Classif. (of this page) Unclassified	21. No. of Pages 254	22. Price

Form DOT F 1700.7 (2-86)

ABSTRACT

Proper design of reinforced concrete bridge beam-column connections is imperative for the behavior of the bridge structure. While in the past this area was overlooked, resulting in bridge structure damage and in some cases collapse, current methods have overcompensated for these shortcomings. The presented research shows that current joint design requirements in the state of California produce conservative designs (i.e., joints with excessive amounts of reinforcement). The joints in these systems are capable of supporting the intended flexural mechanism, but at the cost of constructability. The goal of this report is to evaluate current methods, identify shortcomings, and develop methods or techniques for joint performance improvement.

The research was carried out in three phases. In the first, current design requirements, constructability improvement techniques, and joint force transfer mechanisms were experimentally investigated. This was accomplished with four large-scale experiments on cap beam to column subassemblies of typical geometry. Following analysis of the force transfer mechanisms and determination of the shortcomings, a second experimental phase was undertaken to evaluate joints subjected to high joint demands. This consisted of two subassemblies with reduced beam depths and increased column strengths. Furthermore, the effectiveness of the joint spiral reinforcement versus the use of lateral and vertical joint transverse reinforcement was evaluated. In the third phase, the effectiveness of the reinforcement in these designs was evaluated analytically using developed three-dimensional finite element models. The study strives to develop a set of joint design requirements based on damage criteria; two performance criteria are suggested. The first criterion determines a level of lateral reinforcement necessary to activate the joint width in shear resistance. The second criterion determines a level of vertical joint reinforcement necessary to limit crack formation in the joint.

The results of these phases show that the intended design mechanism does not completely occur, suggesting that the placement of reinforcement under current requirements may be ineffective. Furthermore, it is shown that the use of a joint spiral is not necessary for good joint performance and may be removed as a means of improving constructability. Headed reinforcement was shown effective when used as joint transverse reinforcement, thus providing additional means of construction improvement. Three-dimensional finite element models were found to provide a reliable estimation of global and local joint response. As a conclusion to this work, the results of parametric finite element analyses are used to develop possible damage-based joint design requirements.

ACKNOWLEDGMENTS

The research reported here served as the doctoral thesis of the first author, under the supervision of the other authors. The Structural Engineering Group of the California Department of Transportation deserves special thanks for their technical contributions to and their sponsorship of this project. In addition, much thanks to the Headed Reinforcement Corporation for their generous donation of material and technical support. Finally, this project could not have been completed without the tireless efforts of the numerous students and staff at the University of California, Berkeley, who spent evenings and weekends working toward the construction and testing of the specimens.

This work was supported in part by the Pacific Earthquake Engineering Research Center through the Earthquake Engineering Research Centers Program of the National Science Foundation under Award number EEC-9701568.

CONTENTS

LIST OF FIGURES

LIST OF TABLES

1 Introduction

Reinforced concrete bridges are used throughout the world as a means of transporting a large number of people and materials. These arteries make up one of the foundations of infrastructure, providing an economic link for urban communities and large metropolitan cities. Poorly designed bridges combined with large seismic events can effectively cripple a city, influencing both the short-term response and long-term recovery following an earthquake. As such, the proper performance of these systems is imperative.

Although much progress has been made in the design of reinforced concrete bridges, some questions remain. Shortcomings in many aspects of design have been identified as a result of damage sustained during large-magnitude seismic events. These issues, for the most part, have been identified and addressed by adopting changes in code requirements and executing retrofitting programs. Numerous research programs have been undertaken to examine many aspects of bridge response. One area in which ambiguity remains is the design and construction of reinforced concrete bridge beam-column connections.

Currently, there is no clear preferred procedure for bridge beam-column joint design. Several joint design recommendations exist throughout the world. Each has their own set of assumptions and goals. Some produce lightly reinforced joint systems, while others produce heavily reinforced joint systems. The question arises, how does performance relate to design? To answer this, the state of the art of beam-column joint design is investigated. This experimental and analytical study examines a variety of recommendations with a focus on California design techniques.

1.1 Beam-Column Joint Design Issues

Methods for beam-column joint design have undergone many changes in the past few decades and are still evolving. Interest in the behavior of bridge joints heightened as a result of the Loma Prieta earthquake when a number of reinforced concrete bridges in the San Francisco Bay Area sustained significant damage at their beam-column connections (Figure 1-1). Following the earthquake, new bridge connections were designed using theories developed in part from research into the behavior of building joints. Due to the difference between the desired response of bridge and building systems to earthquake loading, as well as a lack of consensus within the design community, these new designs tended to be overly conservative, making construction difficult (Figure 1-2). In the ensuing years, additional research has led to an improved understanding of joint behavior. However, this research has still not led to a consensus within the design and research communities as to a general mechanism to describe bridge joint behavior, nor has it led to a general procedure for bridge joint design. Furthermore, general design philosophy is evolving, with a trend toward performance-based criteria is being pursued in all aspects of structural engineering. Reinforced concrete bridge joint design concepts, however, are still firmly rooted in the idea of force transfer, with little concern for displacement or damage-based criteria.

Three areas of investigation remain important. First, the validity of the existing design concepts requires conceptual review to determine their usefulness in application to California bridge joint design. Second, California design methods should be studied using both experimental and analytical means to evaluate and improve the effectiveness and efficiency of the requirements. Third, a method to account for displacement and the expected level of damage in the joint is needed.

Figure 1-1: Damage to bridge joints resulting from large-magnitude earthquakes

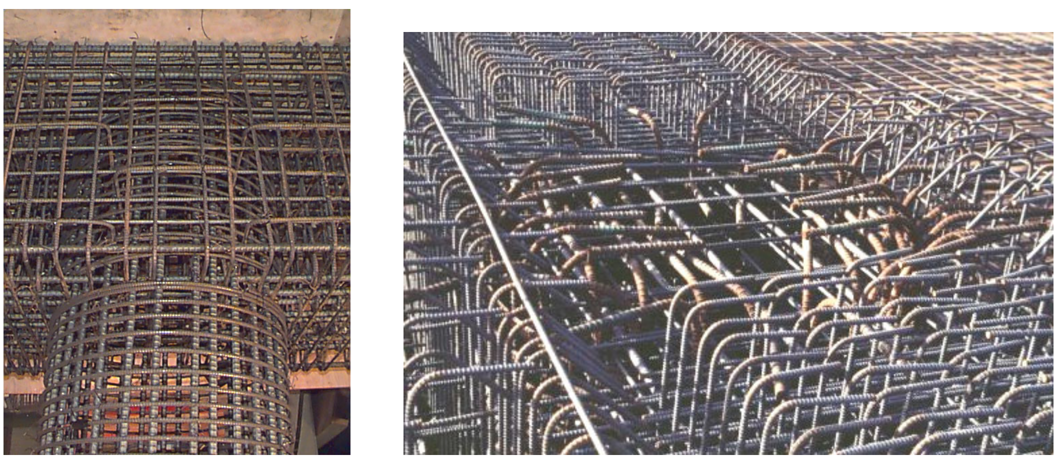

Figure 1-2: Reinforcement congestion of California bridge beam-column joints

1.2 Objectives of Research

The objective of this research is to show that California joint design requirements are conservative and can be made more efficient through the use of headed reinforcement and the adoption of a displacement-based design approach. Three areas are investigated in the development of this thesis: the evaluation of current bridge design requirements, the investigation of methods for improving constructability, and the development of a recommendation for joints based on limiting damage. These objectives were achieved through both large-scale experimental investigations of bridge components and three-dimensional finite element analysis. This section outlines the work conducted in each phase.

1.2.1 Experimental Program

A total of six 3/8-scale, beam-column subassemblies were built and tested under quasi-static lateral displacements. Boundary conditions and loading protocol were modeled from typical bridge conditions. In this presentation, the experimental program was divided into two phases: the first is based on current designs in California and the second aims toward higher joint shear demand to exaggerate damage within the joint region. The results were used to evaluate joint response, develop a force-transfer mechanism, and calibrate analytical models.

1.2.2 Finite Element Model Development

Three-dimensional finite element models were developed using trilinear concrete brick elements and embedded reinforcement. Appropriate constitutive relationships were selected based on material testing to correctly model the experimental response. Confidence in the analytical results allowed for the use of the finite element model in a parametric study.

1.2.3 Investigation of Parameters

The research culminates with a displacement-based recommendation developed from a parametric study of a typical joint configuration. The path for the parametric study was influenced by the information gained from both the experimental observations and results from the finite element studies. Appropriate quantities and arrangements of vertical and lateral joint reinforcement were determined.

1.3 Organization of Report

The work is organized as follows. A background of bridge joint design is presented in Chapter 2, including accepted joint force transfer concepts and codified recommendations. This is followed by the development of the experimental program, the determination of the subassembly boundary conditions and loading, and methods of experimental evaluation in Chapter 3. In Chapter 4, the development of the analytical program is presented. This includes the background and foundation for the finite element models used as well as justification of the selected constitutive models. With this basis, the results of the first and second phase of the experimental program are presented in chapters 5, 6, and 7. Finally, results from the parametric investigation are given in Chapter 8, followed by conclusions on the state of joint design and recommendations for future research in Chapter 9.

2 Joint Design Methods

The development of reliable reinforced concrete beam-column joint design procedures is an essential task for safer bridge systems. In the past, the importance of proper joint design had been overlooked, leading to serious consequences. From the 1971 San Fernando, California, earthquake to the 1994 Northridge earthquake, poor joint design has resulted in catastrophic structural failures. As a result, diverse and often complex joint design requirements have been adopted, but without a unified methodology. The following sections examine the widely accepted joint mechanisms and codified approaches used in the U.S. and abroad. In some cases, the approaches result in weak designs, while in other cases adequate strength is achieved at the expense of constructability. To address these issues, new joint design techniques are examined. In addition, possible directions for the development of effective joint design strategies are discussed.

2.1 Accepted Models of Joint Force Transfer Mechanisms

Dedicated experimental investigation of beam-column connections has been under way since the late 1960s when Hanson and Connor [1967] carried out a series of tests for the Portland Cement Association. Based on the experimental data generated since that time, several joint load transfer mechanisms have been suggested. The most common mechanism relies upon the compressive capacity of the joint concrete. This can be conceptualized in the following manner. Plastic hinging of beams or columns, or both, imparts a significant shear in the joint (i.e., $V = dM/dx = 2Mp/b_{joint}$), which may lead to the formation of diagonal shear cracks in the joint concrete (Figure 2-1). This, in turn, forces the joint to rely on concrete compression struts, running parallel to the cracks, for load transfer. Once the load in the strut exceeds the compressive strength of the cracked concrete, the joint resistance quickly degrades.

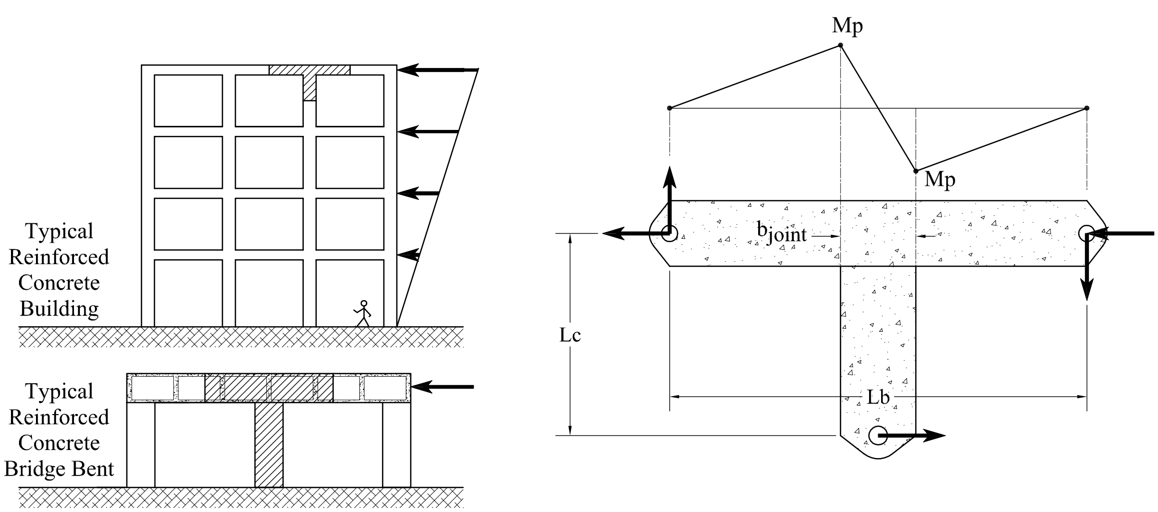

Figure 2-1: Joint moment gradient

2.1.1 Compression Strut and Truss Models

Two general methods of joint shear transfer were established using the compression strut concept: the principal compression strut model and the truss model. The compression strut model assumes that the tension forces in the longitudinal reinforcement of beam and column, ΔTb and $\Delta Tcol$, are anchored in the compression zone on the opposing faces of the joint. These tensile forces, combined with the compression forces acting on each face, result in two compression zones on opposing corners of the joint. The resultants of these forces are assumed to act toward each other, forming a principal compression strut, *Dc*, across the joint (Figure 2-2). This mechanism was first discussed by Paulay, et al. in the late 1970s [Paulay 1978].

In order for the longitudinal tension forces to be anchored only on the opposing faces of the joint, the bond loss must be significant. If this is the case, forces are transferred to the joint as compression forces acting in the joint corner. As a result, the model, used on its own, may be limited to systems that have undergone significant damage. To address this point, the model is often used in conjunction with a second joint model, the truss or shear panel model.

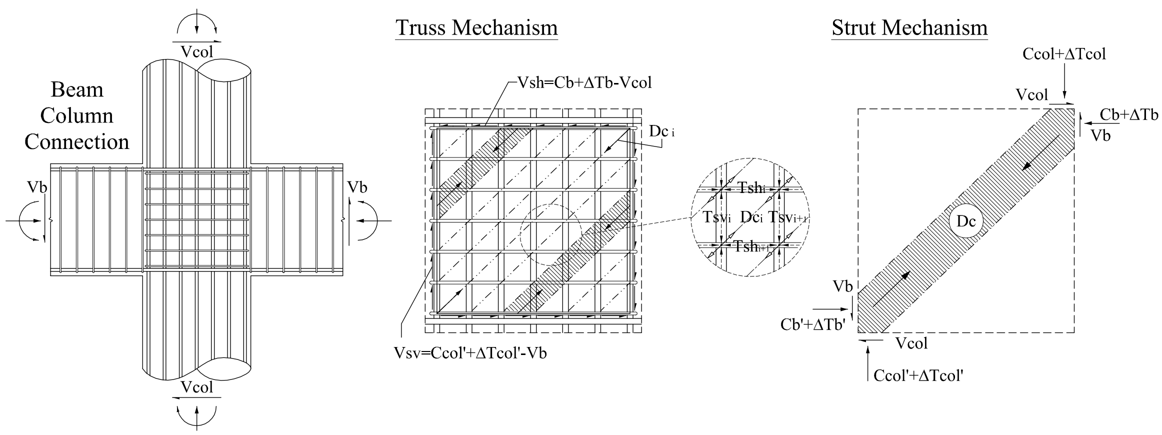

Figure 2-2: Truss and strut mechanisms

The truss analogy assumes that the forces developed in the beam and column reinforcement at the face of the joint are resolved within the joint through a panel of struts and ties. Assuming the existence of uniform bond, the development of the forces from the beams and columns imparts a uniform shearing force around the exterior of the joint, *Vsh* and *Vsv*. Resolution of these forces through the joint is accomplished using multiple tension and compression elements, (Tsh_i, Tsv_i and Dc_i), made up of reinforcing steel ties and concrete struts, respectively (Figure 2-2). This behavior has been extensively investigated for application on shear walls. Vecchio and Collins [1986] found that the response of shear panels could be predicted from the applied principal stresses, and compatibility, equilibrium and constitutive relationships. Direct extension of these models to beam-column joints subjected to in-plane stresses is conceptually straightforward. The downside, as mentioned previously, is that uniform bond must exist between the reinforcement and concrete for the mechanism to hold true. Joints subjected to cyclic inelastic loading often undergo significant bond degradation because of yield penetration and excessive shear cracking. Therefore, complete reliance on this mechanism may be unrealistic.

To create a joint mechanism that is applicable at all levels of loading, the truss model is often used in conjunction with the principal strut model. At lower levels of demand, the reinforcement is below yield and the system is in a virtually uncracked state. In this state, the joint can be evaluated as a shear panel, transferring forces through a series of compression struts and tensile ties. As the loads and cycling increase, the reinforcement making up the periphery of the shear panel yields. As yield progresses, bond is lost, resulting in a greater reliance upon a main strut running from the diagonally opposing compression zones of the joint. The strength of the strut mechanism in the end determines the strength of the joint. Transferring this concept to a design method, one could determine the size of the joint by the geometry needed to sustain the principal compression strut. The shear panel mechanism can then be used to determine the amount of transverse reinforcement required to develop bond through the joint. Varied combinations of these mechanisms have been recommended and are discussed in Section 2.2. In general, these methods seldom are applied directly to design. Instead, the methodology is often used implicitly within the code to determine both the levels of reinforcement and geometry required.

2.1.2 Strut and Tie Modeling

Extending the concept used in the strut and truss methods, one can envision various joint models composed of nonuniform arrangements and combinations of concrete struts and tension ties. This methodology, known as *strut and tie modeling,* has been used extensively for design of deep beams, corbels, and other discontinuity regions where standard design concepts fail [Schlaich 1987]. By means of this technique, the reinforced concrete system is replaced with an equivalent truss made of concrete compression struts and reinforcement tension ties. The layout of the equivalent truss then determines the layout of the reinforcement in the system. This provides the designer with more flexibility, allowing the formation of a variety of new load paths.

A shortcoming of the strut and tie method is that the design can be conducted without consideration for compatibility. As a result, a variety of strut and tie layouts can be developed for the same loading conditions, some of which may not be feasible considering compatibility. If the chosen strut and tie model varies significantly from the elastic stress distribution, the system must undergo a load redistribution to allow forces to be transferred along the intended paths. In reinforced concrete, load redistribution is accomplished by cracking and damage to the concrete. To limit this behavior, the chosen system should not only transfer the required loads, but do so in a manner approximately compatible with the elastic strain distribution. To meet serviceability conditions, deformation compatibility must be checked.

Due to the limited discussion of strut and tie models in the U.S. design codes, a brief presentation follows of the recommendations used for general development. It is generally accepted that compression is transferred through one of two mechanisms: the compression *fan* or the compression *strut*. The fan mechanism is used in regions where stress changes quickly (high stress gradient) creating a disturbed stress field, while the strut mechanism forms in regions where the stress field is essentially uniform. This mechanism is illustrated in an example of a cantilevered beam (Figure 2-3). As shown, the concentrated load is initially transferred through the system using a compression fan. These forces are quickly transferred through the system in a uniform pattern through individual struts.

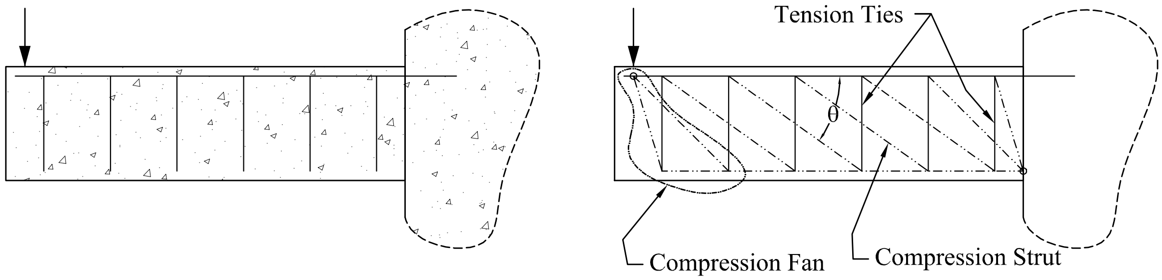

Figure 2-3: Strut and tie model of a cantilevered beam

The allowable angle along which these struts form is based upon matching the direction of the principal compressive stresses and by limiting crack widths. Some of the recommendations are presented in Table 2-1.

Table 2-1: Allowable strut angles	
Swiss Code, [MacGregor 1988]	$26^o \leq \theta \leq 64^o$
European Code [CEB-FIP 1990]	$31^o \leq \theta \leq 59^o$
American Design, [MacGregor 1988]	$25^o \leq \theta \leq 65^o$

The capacity of the struts should be checked to ensure that their compressive stress does not exceed the effective stress capacity, f_{ce}. In addition, the state of stress in the nodes where the struts and ties meet should also be checked. To ensure that the prescribed strut stress is less than the allowable compressive stress, the area of the strut must first be prescribed, with definition of both a width and depth for the strut. In beam-column connections, the width of the strut is assumed to equal the width of the joint. The depth of the strut can then be determined using tributary area assumptions. Knowing the strut force and the corresponding geometry, the strut stress can be found. Table 2-2 lists acceptable levels of allowable strut stress. Two suggestions are presented, one by MacGregor [1988] in which checks of the struts and nodes are required, and the other by the New Zealand Standards Association [NZS 1995] in which only a nodal check is necessary. Note that the NZS recommends a capacity reduction factor, $\phi = 0.80$.

Table 2-2: Strut and tie — nominal stresses			
Codes:	NZS	MacGregor	Comments
Nodes:	$f_{ce} = 0.65\ \phi f'c$	$f_{ce} = 0.85f'c$	Bounded by compression struts and bearing areas
	$f_{ce} = 0.55\ \phi f'c$	$f_{ce} = 0.65f'c$	Anchoring one tension tie
	$f_{ce} = 0.45\ \phi f'c$	$f_{ce} = 0.50f'c$	Anchoring tension ties in more than one direction
Struts:	Not Applicable	$f_{ce} = 0.50f'c$	In discontinuity regions
		$f_{ce} = 0.45f'c$	When severe cracking is expected at angles ~ 45^{o}
		$f_{ce} = 0.25f'c$	When severe cracking is expected at angles ~ 30^{o}
Where f′c is equal to the uniaxial concrete compressive strength.			

Tension resistance in a strut and tie model is provided by properly anchored reinforcement. The magnitude of this force contribution is equal to the yield stress multiplied by the area of the reinforcement. As seen in the beam example (Figure 2-3), these tension ties can consist of both transverse and longitudinal reinforcement. Putting all of these components together, one can develop a variety of strut and tie models representing force transfer in a joint. To assist in developing the load paths two rules should be followed: first, the load path should follow the most direct route, and second, the compressive paths should not cross one another.

Joint Strut and Tie Design Application

A codified application of the strut and tie method for joint application can be found in the 1996 bridge design recommendation, ATC 32: Improved Seismic Design Criteria for California Bridges. Based upon a series of tests conducted at the University of California at San Diego, Priestley developed a model for joint transfer using strut and tie techniques (Figure 2-4) [Priestley 1993]. The resulting recommendation uses the model implicitly to prescribe quantities of joint reinforcement. The strut and tie model resolves the forces generated by plastic hinging of the column, across the joint and to an area outside the joint region. By way of a series of diagonal struts, the force is transmitted to areas on each side of the joint. These forces are then resolved into tension ties, and corresponding levels of joint reinforcement are selected.

The ATC 32 model begins by the assumption that half of the column reinforcement is in tension. To further simplify the problem, the tension force is split into two discrete tension ties. The interior tie is anchored at the rear of the joint along the principal compression strut; the exterior tie is anchored closer to the beam-column interface. This exterior tie is anchored with two diagonal struts and one horizontal tie. The exterior column tension tie generates three regions of tensile forces. This, in turn, requires three levels of reinforcement: additional longitudinal reinforcement in the bottom of the beam, vertical transverse reinforcement adjacent to the column, and horizontal transverse reinforcement in the joint. The corresponding tension forces are 0.125Tc, 0.25Tc, and 0.25Tc respectively, where Tc is the column tension force.

$$Tc = 1.3\ (0.50As_{column}f_y) = 0.65As_{column}f_y \tag{2-1}$$

Where As_{column} is the total area of column reinforcement and f_y is the yield strength of the column reinforcement. In the above expression, 30% overstrength is assumed. Assuming the joint and column longitudinal reinforcement has the same yield strength, the longitudinal, vertical, and horizontal reinforcement requirements become $0.08As_{column}$, $0.16As_{column}$, and $0.16As_{column}$, respectively.

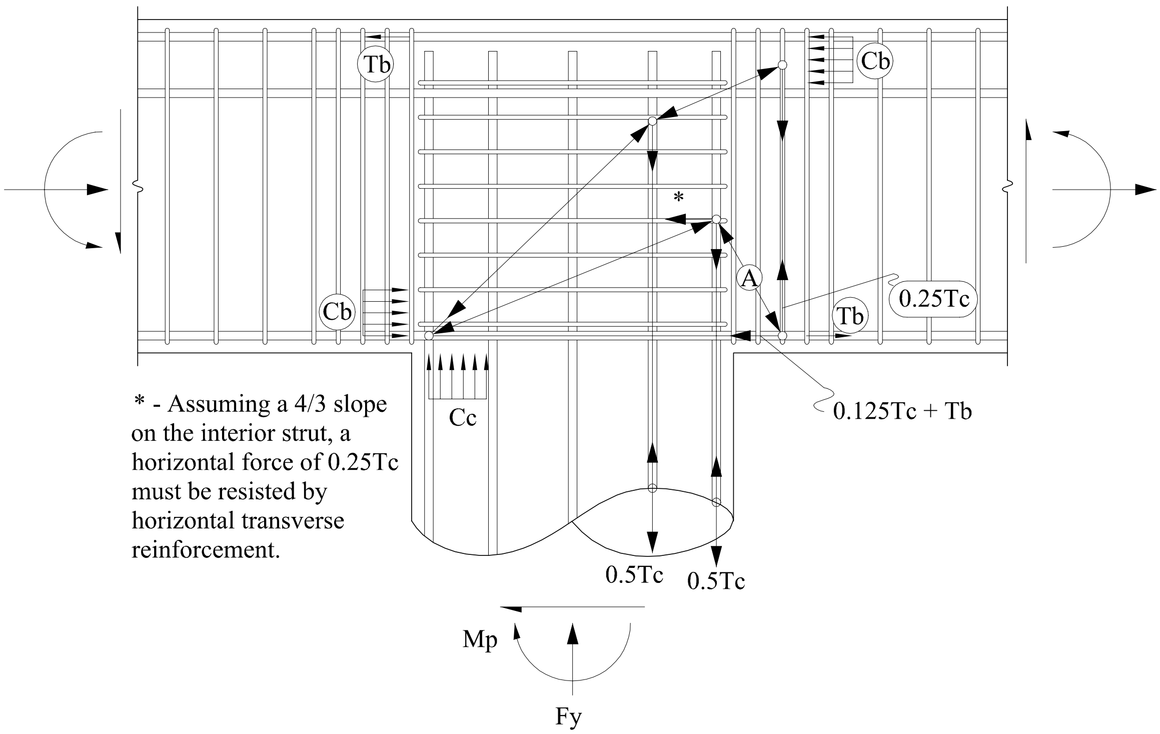

Figure 2-4: ATC 32 strut and tie model

In summary the following requirements are developed:

- To support the diagonal strut labeled A, additional longitudinal reinforcement is required in the bottom portion of the cap beam equal to $0.08As_{column}$. In addition, vertical stirrups with a total area $Ajv > 0.16As_{column}$ are to be placed on each side of the joint region within a distance $0.5D_{col}$ from the face of the column, where D_{col} is the column depth.
- To balance the $0.25Tc$ horizontal strut, a minimum volumetric ratio of spiral/hoop reinforcing, ρ_s should be provided over the entire column bar embedment length, l_{ac}.

$$l_{ac} = \begin{Bmatrix} \text{As close as possible to opposite face of beam.} \\ \geq \dfrac{0.028 d_b fy}{\sqrt{f'c}} \end{Bmatrix} \tag{2-2}$$

$$\rho_s \geq \frac{0.4 As_{column}}{l_{ac}^{2}} \tag{2-3}$$

The ATC 32 model presents a load path and develops reinforcement requirements based upon the forces generated. It should be noted that this load path is not unique. Other load paths are equally possible.

2.2 Additional Issues in Joint Design

Although the previously discussed models do provide a rational means of joint load transfer, they are concerned only with transfer of *forces* in the joint system. To safely resist the demands, *deformations* should also be limited. Parameters such as joint size, bond strength, yield penetration, axial load, and the effect of confinement by members framing into the joint can be used to limit the amount of damage. The following sections provide background on some of these requirements.

2.2.1 Bond

Experimental and analytical investigations of joint response have shown that bond has a significant impact on joint response [Scott 1996 and Sritharan 1997]. To obtain the flexural capacity of a member at the face of a joint, the tensile reinforcement must be properly anchored in or through the joint region. This can be achieved by developing the reinforcement straight into the joint or by providing hooks in the joint core. In modern seismic design approaches, it is common to design for development of flexural plastic hinges at the joint face. As a result, tensile reinforcement anchored in the joint is expected to perform well into the inelastic range. As the reinforcing steel is loaded beyond the elastic range, the bond tends to degrade. This action begins at the face of the joint as the reinforcement undergoes localized yield. As the yield progresses from the face into the joint, an associated bond loss follows. If this action propagates, it is possible for bond to be completely lost in the joint. Consequently, large system deformations may occur.

Large structural deformations, resulting from loss of bond in the joint region, can be alleviated through improved design. Previous research [Ichinose 1991] into bond behavior indicates that bond strength and ductility can be improved by confining the concrete in the region where the bar is anchored and by increasing cover on anchored bars. To further reduce joint degradation, the bond demands can be limited. One method of accomplishing this is to limit the ratio of bar size relative to the joint depth through which it is passing [Kaku 1991, Leon 1991]. This allows the bond stresses, generated from the flexural deformation of the adjacent member, to be more widely distributed. As a result, localized bond stresses are reduced, minimizing the potential degradation of joint.

2.2.2 Joint Confinement

As a means of providing a more efficient joint design, the confining effects provided by adjacent members and axial loads are sometimes accounted for in design [NZS 3101]. The belief is that if a beam framing into a column covers a majority of the column face, then that face is considered effectively confined. For example, for shear cracking to extensively occur on a joint face, the beam covering that face must form compatible diagonal cracks across its section. For such behavior to occur, these adjacent beams must be heavily damaged. As such, the contributions of confining beams are only considered when they are not expected to form hinges. These effects are taken into account by either increasing the allowable shear stress in the joint or by reducing the required quantity of transverse joint reinforcement. In some codes [ACI 352], these reductions are allowed if only one face is confined, while in other provisions reductions are allowed only when all faces are adequately confined [NZS 3101 1995].

Column axial load affects the behavior of the joint shear capacity and bond capacity of bars passing through the joint. Studies performed on reinforced concrete connections have produced conflicting results. A study reported by Agbabian [1994] has shown that compressive axial loading can result in a joint capacity increase on the order of 30% and an improvement in deformation capability on the order of 50%. The test program, which evaluated three different levels of axial load (0, 5, and 10% of the column axial capacity), indicated that axial load has the beneficial effect of reducing shear deformation and cracking, and increasing strength and ductility of the joint zone. A study by Kitayama [1991], however, concluded that axial load does not seem to influence joint shear strength. Axial stresses greater than $0.3f'c$ were found to improve bond capacity; however, high levels of axial load were found to decrease joint shear capacity by accelerating compressive failure of the principal strut. This variation in experimental results has led to a variation in code recommendations. Some codes [NZS 3101] allow for an increase in joint shear capacity based on the level of applied load. As a result, the quantity of transverse reinforcement can be reduced, thus easing construction. The newer strategies [ATC 32] determine the level of joint reinforcement based upon the level of principal stresses acting on the joint. As such, compressive beam or column loads are automatically taken into account in the design. Some codes, however, do not consider the effect of axial compression and assume it to be unconservative. Unfortunately, such codes also commonly exhibit an inattention to the opposite case: tension. When a reinforced concrete joint is placed in tension its capacity to transfer inelastic loads is reduced [NZS 3101]. This can become a considerable issue when examining exterior joints located in the lower levels of tall, slender buildings. Such regions are often subjected to excessive tension due to the overturning effect generated by earthquake loading. In these cases, improper detailing or an inappropriate assumption of capacity can prove detrimental to the system strength.

2.3 Code Requirements for Joint Design

To evaluate the state-of-the-practice for beam-column joint design, six codes representing the United States, New Zealand, and Japan were investigated. They are

- United States (U.S.): ACI 352 (1983) — ASCE-ACI Joint Committee
- New Zealand Standard 3101 (NZS 1982) — Code Practice for the Design of Concrete Structures
- New Zealand Standard 3101 (NZS 1995) — Code Practice for the Design of Concrete Structures

- U.S.: California Department of Transportation (Caltrans 1994) — Bridge Design Specification
- Japan: Architectural Institute of Japan — Structural Design Guidelines for Reinforced Concrete Buildings (AIJ 1994)
- U.S.: Applied Technology Council (ATC) Recommendation ATC 32 (1996)

Instead of detailing the step-by-step requirements, the following discussion is limited to the methods used by each code to satisfy certain aspects of joint design. The recommendations used for limiting shear stresses and bond demands, the effect of confinement due to loading and geometry, and the levels and arrangements of reinforcement are presented and discussed. Note that two European codes were also evaluated, the British Standard 8101 [1985] — Structural Use of Concrete, and the CEB-FIP Model Code [1990]. Both the British Standard and the European code (CEB) do not directly address joint design but instead provide strut and tie models and other tools that can be utilized for the determination of joint design requirements. As a result, the following discussion of code requirements addresses only the U.S., Japanese, and New Zealand recommendations.

2.3.1 Shear Stress Limitation

To ensure that a joint is capable of supporting an adjacent plastic mechanism, limitations are placed on the allowable level of joint stress. With the exception of the ATC 32 recommendation, this stress limitation takes the form of a maximum allowable joint shear stress. The accepted level of shear stress ranges from an upper bound of $18\sqrt{f'c}$ to a lower bound of $12\sqrt{f'c}$ (Table 2-3). Limits on the shear stress, in turn, prescribe the allowable joint geometry. As shown in Figure 2-5, interior joints constructed of normal strength concrete would be larger under the requirements of AIJ than that of Caltrans. Variations between the current codes is minimal below 4000 psi; however, for systems constructed of high-strength concrete the requirements in the U.S., New Zealand, and Japan deviate considerably. For example, at a concrete strength of 8000 psi the allowable shear strength according to AIJ is approximately 50% higher than that of Caltrans. This deviation is directly related to the design philosophies used by each code committee. Research in Japan has shown that joint shear strength depends strongly on the concrete compressive strength and very little on the level of transverse joint reinforcement [Kitayama 1991]. As such, the strength compression strut is assumed to be the dominant component of joint shear strength. Consequently, AIJ assigns joint shear capacity proportional to concrete compressive strength. The U.S. codes, however, assume the opposite, i.e., the truss model is the dominant component of shear strength. Consequently, U.S. joint shear capacity is proportional to $\sqrt{f'c}$. As a result, joints designed to U.S. code requirements benefit less from the use of high-strength concrete.

Table 2-3: Shear stress limitations	
Design Code	*Requirements (f′c [psi])*
NZS 3101 1985	$18\sqrt{f'c}$
ACI 352	$20\sqrt{f'c}$, $15\sqrt{f'c}$, $12\sqrt{f'c}$ For interior, exterior and corner joints, respectively.
Caltrans BDS	$12\sqrt{f'c}$
AIJ	$0.30\,f'c$ for interior cross-shaped joints and $0.18\,f'c$ for all others.
NZS 3101 1995	$0.20\,f'c$
ATC 32	Limits principal stresses.

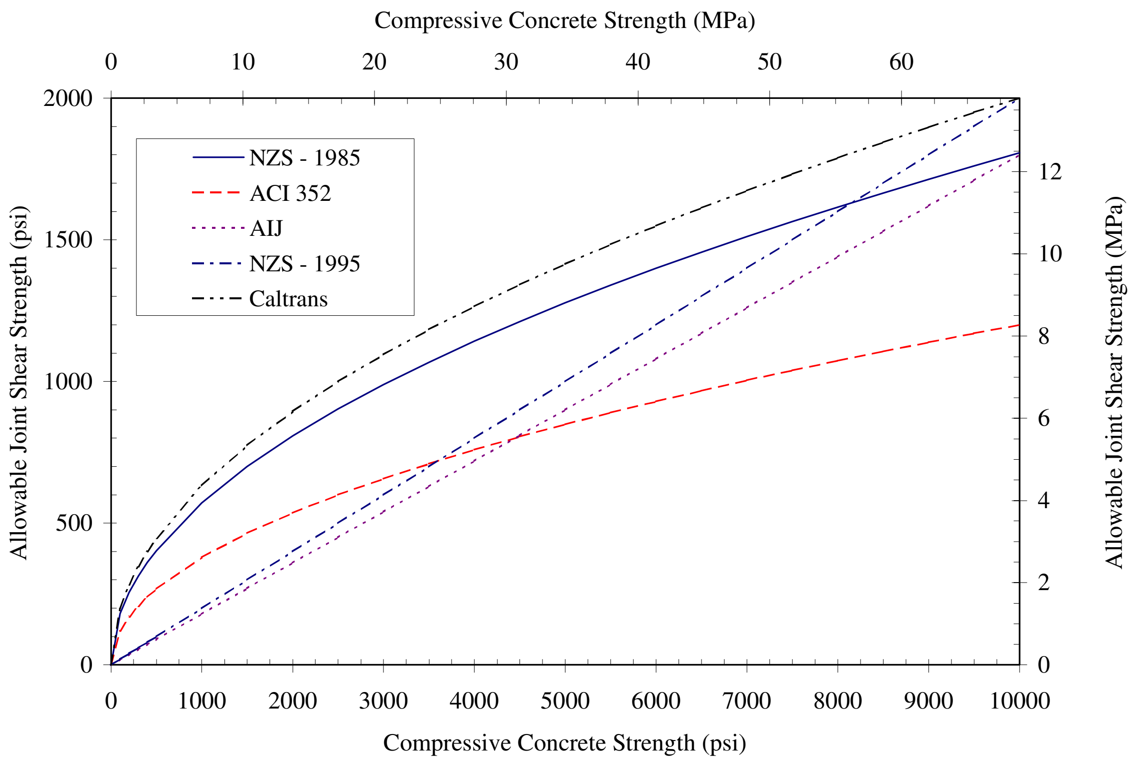

Figure 2-5: Shear stress limitations for interior joints

2.3.2 Limiting Bond Demands

In general, the effect of bond demand is directly considered in joint design requirements by limiting the diameter of the longitudinal reinforcement relative to the joint depth (Table 2-4). As discussed in Section 2.2.1, this is performed to limit excessive bond failure, which could lead to unexpected inelastic deformation in the joint and additional global displacements. A variety of different requirements are used (note stresses are assumed to be in psi). New Zealand assumes that the column axial load, P_{axial}, improves the bond capacity of the beam longitudinal reinforcement. Increasing levels of compressive axial load are assumed to produce additional confinement thus larger bar diameters are allowed. The 1995 revision of NZS 3101 adopted a similar design concept with the addition of a reliance on the concrete compressive strength, f'_c, and steel yield strength, f_y. This allows for a more direct relation to parameters of bond capacity. ACI 352 does not account for axial load, concrete compressive strength, or reinforcement yield strength in the determination of allowable bar diameter. Instead, a constant joint size to bar diameter ratio is used. This recommendation is based on work conducted in the U.S. and New Zealand up to 1982 [Kaku 1991, Zhu 1983]. The AIJ requirements curb bond demands relative to the bond strength. No limitations on bar size are recommended in either Caltrans Bridge Design Specification (BDS) or ATC 32.

Table 2-4: Bond limitations

Design Code	*Requirements (f'_c and f_y [psi])*
NZS 3101 1985	Beam longitudinal, $h_c/d_b \geq 35$ for $P_{axial}/f'_cA_g < 0.4$ $h_c/d_b \geq 25$ for $P_{axial}/f'_cA_g > 0.6$ linearly varying for $0.4 \leq P_{axial}/f'_cA_g \leq 0.6$ Column longitudinal, $h_b/d_b \geq 25$
ACI 352	Longitudinal bar diameter shall not exceed 1/20th of the depth through which they pass. See Eq. (2 – 5).
Caltrans BDS	Not addressed.
AIJ	Recommend curbing bond demands by limiting the ratio of the bar size to the joint depth. See Eq. (2 – 6).
NZS 3101 1995	Beam longitudinal, $h_c/d_b \geq 40\sqrt{f'c} / f_y$ for $P_{axial}/f'_cA_g < 0.1$ $h_c/d_b \geq 50\sqrt{f'c} / f_y$ for $P_{axial}/f'_cA_g > 0.6$ linearly varying for $0.1 \leq P_{axial}/f'_cA_g \leq 0.6$ Column longitudinal, $h_b/d_b \geq 38.5\sqrt{f'c} / f_y$
ATC 32	Not addressed.

Where,
h_c = column depth
P_{axial} = column axial load
A_g = column gross cross-sectional area
h_b = beam depth
d_b = diameter of longitudinal reinforcement

Figure 2-6 compares the minimum allowable joint depth, D_{jnt}, required for the development of longitudinal bars of a particular diameter, d_b. The recommendations of ACI 352 are compared with those of AIJ, NZS 3101, as well as the standard development length requirements of ACI 318-95. Note that the development length of Eq. (2-7) does not apply to development within the joint but instead applies to the development of bars past the critical cross section.

$$\text{ACI 352} \qquad D_{jnt} \geq d_b \cdot 20 \tag{2-4}$$

NZS 3101 1985 $$D_{jnt} \geq d_b \cdot 25 \tag{2-5}$$

AIJ $$D_{jnt} \geq \frac{d_b \cdot 1.25 f_y}{45\sqrt{f'c}} \tag{2-6}$$

ACI 318 $$D_{jnt} \geq l_d = \frac{3}{40} \cdot \frac{d_b \cdot f_y}{\sqrt{f'c}} \cdot \frac{\alpha \cdot \beta \cdot \gamma \cdot \lambda}{\left(\frac{c + K_{tr}}{d_b}\right)} \tag{2-7}$$

NZS 3101 1995 $$D_{jnt} \geq \frac{d_b f_y}{38.5\sqrt{f'c}} \tag{2-8}$$

In Figure 2-6, a concrete compressive strength, f'_c, of 4000 psi and a reinforcement yield strength, f_y, of 60 ksi is assumed for all cases. In Eq. (2-7), α, β, γ, and λ are bond parameters dependent upon the location, coating, size of reinforcement, and the type of concrete used. The parameters c and K_{tr} are dependent upon the cover and confinement, respectively. For a typical joint configuration, the parameters α, β, and λ are equal to unity, $\left(\frac{c + K_{tr}}{d_b}\right)$ is equal to 2.5, and γ is equal to 0.8 for bars smaller than #7 and 1.0 otherwise. If one applies the expression to the development within the joint, although that is not the intent of ACI 318, the resulting joint depth requirements can be found.

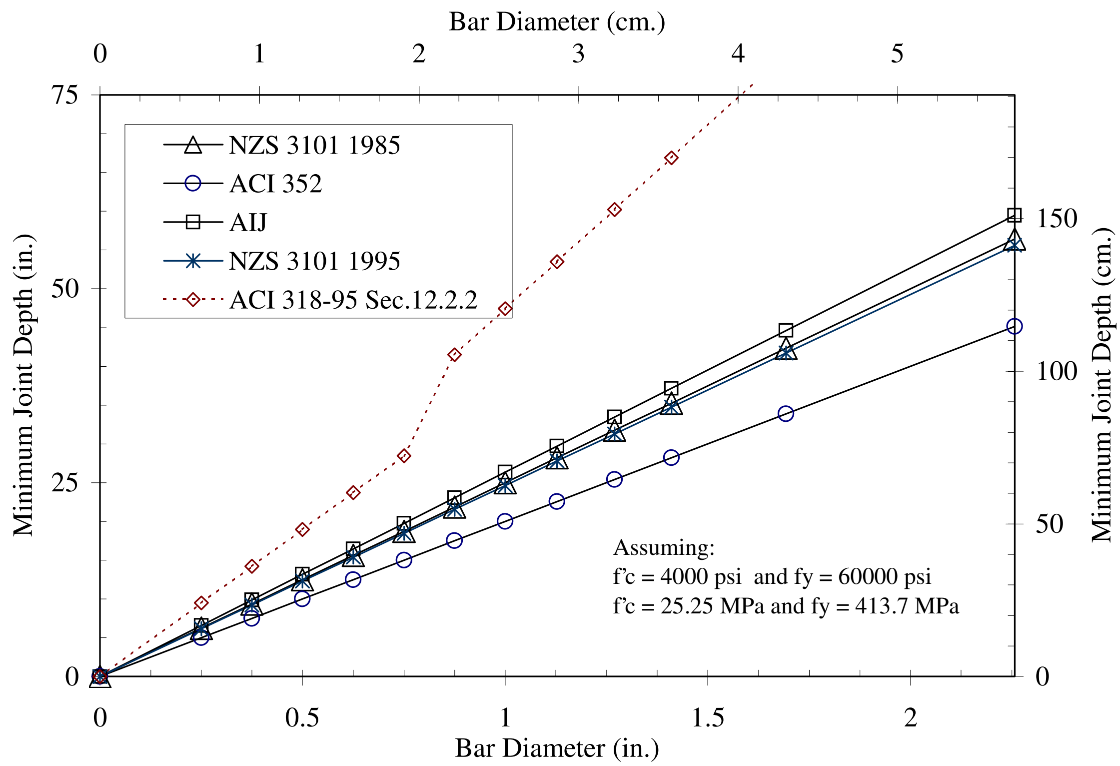

Figure 2-6: Bond requirements

ACI 352 has the lowest bond requirements, followed by NZS in the middle, and AIJ with the highest. A comparison with ACI 318 straight development length requirements illustrates that under these bond requirements, the longitudinal reinforcement may not be fully developed within the joint core. Thus, the state of practice assumes that bond degradation is allowed on the longitudinal bars passing through the joint.

2.3.3 Joint Reinforcement Requirements

Joint reinforcement is often, though not always, prescribed in terms of the level of demand placed on the connection. The codes that use this method quantify the demand in one of two ways: (1) in terms of the level of shear force applied to the joint and (2) in terms of the amount of tensile force applied to the joint by the yielding member. In the first method, the shear force demand is equated to the joint shear capacity. The demand is evaluated from the level of shear force acting on the joint in one or both directions (horizontal and vertical). The capacity of the joint is dependent on the joint reinforcement strength. From these relationships, the required shear strength and the quantity of shear reinforcement can be computed. The second method, used in Caltrans BDS and ATC 32, determines the level of joint transverse reinforcement from the tensile forces generated by the formation of a column plastic hinge. The requirements are based on an assumed strut and tie model of force transfer and are prescribed implicitly, as shown in Section 2.1.2. The resulting requirement defines the level of horizontal and vertical reinforcement as a function of the area of longitudinal reinforcement in the yielding member. A combination of these two methods is used in NZS 3101 [1995]. In some cases, additional reinforcement is added to provide confinement of the joint. To be conservative, these levels are often specified to be *in excess* of the required joint shear reinforcement.

Note that the ATC 32 and Caltrans codes assume that plastic hinges form in the column, while the other codes assume that beam hinges form. To compare the two, the horizontal and vertical terms can be switched. The following table provides a summary of the techniques used in each code to determine the level and arrangement of reinforcement in the joint.

Table 2-5: Joint reinforcement requirements	
Design Code	*Requirements*
NZS 3101 1985	Horizontal and vertical joint reinforcement is required. Area of horizontal reinforcement, *Ajh*, is determined from the level of horizontal design shear force, *Vsh*. Reinforcement consists of ties or spiral placed between the outermost layers of beam longitudinal reinforcement. Area of vertical reinforcement, *Ajv*, is determined from the vertical design shear force, *Vsv*. Vertical reinforcement can consist of the column bars or additional vertical stirrups hooked into the section. $Ajh = Vsh / f_y$ $Ajv = Vsv / f_y$
ACI 352	Horizontal transverse reinforcement consists of column ties or spiral and is required for joint confinement regardless of the level of joint shear. Vertical transverse reinforcement consists of an even arrangement of the existing column bars around the periphery of the joint. No actual requirements are placed on the amount of vertical reinforcement needed.
Caltrans BDS	Quantities of horizontal and vertical transverse reinforcement are required in the joint. The amount is based on the level of longitudinal reinforcement, A_s, developed from the column (the inelastic element). The minimum vertical and horizontal reinforcement shall be $0.2A_s$ and $0.1A_s$, respectively. Vertical transverse reinforcement shall consist of cap stirrups and added bars hooked around the longitudinal reinforcement. Horizontal reinforcement consists of hairpins stitched into the beam in two or more layers with a greater density outside the column core. These requirements are in addition to the continuation of the beam stirrups and column spiral through the joint. $Ajh = 0.1\ A_s$ $Ajv = 0.2\ A_s$
AIJ	Horizontal transverse reinforcement is required if a beam plastic hinge forms. Vertical transverse reinforcement required if a column plastic hinge forms. In both cases, the quantity required is dependent on the shear applied. Transverse reinforcement is required in only one direction. The assumption is made that resistance in the orthogonal direction is supported by the longitudinal bars.
NZS 3101 1995	Reductions are made in the quantity of horizontal transverse reinforcement based upon new information related to the effect of concrete and steel strength to bond capacity in the joint core. Consequently, greater reliance is placed on the concrete principal strut capacity. Requirements for the joint reinforcement parallel to the yielding member are a function of both the joint shear stress, v_j, and the tensile area of reinforcement in the yielding member, A_{ST}. Joint reinforcement in the secondary direction is a function of the first direction. Assuming that the transverse and longitudinal reinforcement has the same yield strength, a plastic hinge forms in the column and no axial load in the beam exists, the requirements become: $Ajv = 8.4 v_{jh} A_{ST} / f'_c$ $Ajh = 0.7 h_c Ajv / h_b$
ATC 32	Vertical transverse reinforcement is required based on the quantity of column longitudinal reinforcement developed into the joint. A minimum volumetric ratio of horizontal transverse reinforcement, ρ_s, is required based on the development length of the column bars, *lac*. Worst case: $\rho_s \geq 0.4\ A_s / lac^2$ $Ajv = 0.16\ A_s$

As noted in Table 2-5, varieties of techniques are used for determining an appropriate level of joint reinforcement. To illustrate the outcome of these techniques, each will be applied to a joint design, and the results will be compared in Section 2.4.

2.3.4 Accounting for Geometric and Applied Confinement

To reduce the required amount of reinforcement, the confining effects of adjacent members and axial load are often considered. As discussed in Section 2.2.2, the presence of adjacent members, i.e., lateral beams, increases the joint strength. To account for this effect, code requirements allow for an increase in the shear capacity of the joint or a reduction in the required transverse reinforcement (Table 2-6). The ATC 32 and Caltrans BDS do not allow for any reductions. This is due in part to the fact that both codes are used exclusively for the design of bridge joint systems, which do not commonly have large confining members.

Table 2-6: Confining action of adjacent members

Design Code	*Requirements*
NZS 3101 1985	Reduction in required shear reinforcement if beams are elastic.
ACI 352	Conditional reduction in horizontal confinement reinforcement allowed.
Caltrans BDS	Not accounted for.
AIJ	Conditional increase in shear capacity allowed.
NZS 3101 1995	Reduction in required shear reinforcement if beams are elastic.
ATC 32	Not accounted for.

In general, both axial tension and compression forces are taken into account when designing the joint. Depending on the level and action (tensile or compression) of the force, the joint reinforcement is decreased or increased appropriately (Table 2-7).

Table 2-7: Effect of axial load

Design Code	*Requirements*
NZS 3101 1985	Tensile and compressive axial loads increase and reduce the required level of shear reinforcement, respectively. Axial loads generated by prestressing also allow for the reduction of shear reinforcement.
ACI 352	Not accounted for.
Caltrans BDS	Compression and tension taken into account in determination of the quantity of reinforcement in the column spiral that passes into the joint.
AIJ	Not accounted for.
NZS 3101 1995	Tension and compression loads are considered in the determination of shear forces. As a result, the level of shear reinforcement is increased or decreased, respectively.
ATC 32	Directly taken into consideration in calculation of joint principal stresses.

2.3.5 Issues Related to Code Recommendations for Bridge Joints

In most cases of building beam-column joint design, joint demand is controlled by the formation of plastic hinges in adjacent beams. In bridges, however, plastic hinging in adjacent beams is either undesirable or unobtainable. In single-column bents, for example, plastic hinges form only within the base of the column under transverse loading. In multi-column bridge bents with integral box girders, plastic hinges can be developed within the beam. However, in general, limited access to the beam region and the corresponding bridge deck damage make post-earthquake inspection and repair of this mechanism uneconomical. In multi-column bridge bents supporting steel or concrete girders, formation of a beam plastic mechanism may result in unseating of the girders and considerable bridge deck deformation. Because of the negative economic and safety aspects of this behavior, plastic hinge formation is targeted in the columns where inspection and repair are easily conducted.

In building systems, column plastic hinging is undesirable due to the possible formation of a weak-story collapse mechanism in a single level of the building. In such a system, column plastic hinging may lead to relatively large drift of the column in that story. This deflection, combined with the significant weight of the supported structure, can lead to excessive column damage and collapse of the floor (P-Δ effects). Single-level bridge systems are not subjected to the same risk. Since the relative weight of the superstructure is low, P-Δ effects usually are not significant enough to cause progressive collapse. In addition, column deformability is relatively high. As a result, the typical design strategy is to provide reinforcement detailing of the bridge system such that hinges form in the column directly below the cap beam and sometimes above the footing.

These concepts are in most cases addressed in the design codes. For example, NZS and AIJ recommend levels of joint reinforcement relative to the hinging member; while ACI and Caltrans implicitly assume that hinging will occur in the beam and column, respectively. In general, codes remove any ambiguity as to their appropriate application.

2.4 Evaluation of Bridge Joint Designs by Different Code Requirements

The incentive for improving the design recommendations for bridge joints is best illustrated by a comparative design using current code design requirements. The designs were conducted on a prototype joint subassembly modeling the center portion of a three-column bridge bent (details are provided in Chapter 3 and Appendix A). To ensure compatible designs, the following assumptions are made:

- Joint design is based on plastic hinge formation in the column at the beam-column interface.
- Axial load in the column is $0.08A_{gcol}f'_c$, where A_{gcol} is equal to the gross cross-sectional area of the column and f'_c is equal to the concrete compressive strength.
- Concrete compressive strength, f'_c, is 4500 psi.
- Reinforcement yield strength is 60,000 psi.

- Joint design is controlled by loading transverse to the bridge span.
- Loads parallel to the bridge span are resisted by the box girder.
- Cover is 2.0 in.
- All flexural reinforcement consists of #14 reinforcement.
- All transverse reinforcement consists of #6 reinforcement.

Table 2-8 summarizes the volumetric reinforcement ratios required by the preceding design codes. To compare the different ratios, the same joint volume was assumed for all cases. The volume was chosen to be equal to the beam depth multiplied by the ATC 32 effective joint area. The resulting joint volume comprises the beam width, beam depth, and a length equal to twice the column diameter (80 in. x 104 in. x 160 in.).

Table 2-8: Joint reinforcement requirements

Specification	Vertical transverse reinforcement ratio	Horizontal transverse reinforcement ratio (spiral)	Horizontal transverse reinforcement ratio (straight bars)	Total volumetric transverse reinforcement ratio
ACI 352	0	0.203 %	0	0.203 %
AIJ	0.109 %	0	0.108 %	0.217 %
Caltrans BDS	0.129 %	0.085 %	0.125 %	0.339 %
NZS 3101 — 1982	0.316 %	0.092 %	0.125 %	0.533 %
NZS 3101 — 1995	0.102 %	0.095 %	0.125 %	0.322 %
ATC 32	0.473 %	2.500 %	0.092 %	3.065 %

Requirements for joints vary considerably. ACI, AIJ, Caltrans, and NZS require joint transverse reinforcement quantities from 0.2 to 0.5%. Note that ACI 352 recommends that column transverse reinforcement continue through the joint, while the Japanese code specifies that transverse joint reinforcement consist of the continuation of transverse reinforcement from the stronger member, in this case the beam. The resulting AIJ and ACI 352 joint reinforcement ratios are comparable. Caltrans and the revised 1995 NZS code require moderate amounts of reinforcement, both on the order of 0.3%. It is important to note that while Caltrans requirements are based on a strut and tie model, and the NZS 1995 is based on the combination of the truss and principal strut models, they both result in similar quantities of horizontal and vertical joint steel.

The ATC 32 design procedure requires a significantly different amount of joint reinforcement. For the preceding design example, ATC 32 requires 3.5% joint reinforcement versus an average of 0.4% for the other codified approaches. This difference can be attributed mainly to the requirements for joint spiral reinforcement. As discussed previously, Equation 2–3 presents the required joint transverse reinforcement ratio, ρ_s. The equation

$$\rho_s \geq \frac{0.4 As_{column}}{l_{ac}^{\,2}} \tag{2-3}$$

is based on the strut and tie model illustrated in Figure 2-4. This can be derived in the following manner. The strut and tie model requires that a total area of joint horizontal reinforcement equal to 0.16 As_{column} be used. Given that the joint reinforcement consists of a number, *n,* hoops or spiral with cross-section area, A_{sp}, the total area of horizontal reinforcement provided will equal $2nA_{sp}$. Assuming the reinforcement will be spread over the column longitudinal reinforcement length, l_{ac}, at a spacing s, the total area of horizontal reinforcement can be written as

$$2l_{ac}A_{sp}/s \geq 0.16\ As_{column} \tag{2-9}$$

The volumetric transverse reinforcement ratio is defined as

$$\rho_s = \pi DA_{sp}/\ (\pi D^2 s/4) = 4A_{sp}/Ds \tag{2-10}$$

where D is the column diameter. Eliminating A_{sp} between equations (2 – 9) and (2 – 10), one obtains

$$\rho_s \geq 0.32As_{column}\,/\,D\ l_{ac} \tag{2-11}$$

Making the assumption that the column diameter is equal to 0.8 times the column longitudinal development length results in the ATC 32 equation, (2-3). Thus, a well-founded basis can be derived for the requirement.

In this formulation, the reinforcement ratio is a function of the development length, l_{ac}, and the area of column longitudinal reinforcement, As_{column}. The required joint transverse reinforcement ratio is not dependent on the joint volume or column diameter. This, as shown in Table 2-8, can lead to conservative levels of joint reinforcement. For bridge columns, the area of longitudinal reinforcement often increases in proportion to the square of the column diameter. For columns of larger diameter (e.g., 9.0 feet), As_{column} becomes very large, resulting in a significant level of joint reinforcement. Under these conditions, the ATC 32 requirements produce considerable conflicts with constructability. Accordingly, the requirements may be too conservative for large bridge joint geometry.

Current code requirements for the design beam-column joints illustrate many differences. A lack of agreement upon an accepted mechanism produces considerable variation from one code to another. In some cases, such as Caltrans BDS, the resulting requirements prescribe continuation of both column and beam reinforcement through the joint. While in other cases, such as ACI 352, very low requirements are prescribed. Depending upon the assumed mechanism and the conservative nature of each code requirement, considerable variations in constructability are produced.

Whether through limits on allowable joint shear stress or through prescriptive levels of reinforcement relative to applied loads, the common thread in all the code requirements investigated is the reliance on force transfer. While force transfer provides a viable means of developing reinforcement requirements [Priestley 1996], it does not provide any indication of the expected deformation and accordingly damage to the joint. The designer typically assumes that the joint designed to these specifications will behave rigidly.

The expected performance however is not directly addressed in any of the codes. This issue is investigated further in the discussion of the experimental results in chapters 6 and 7, and is used as a motivation for the displacement-based design criteria developed in Chapter 8.

2.5 New Developments

Numerous alternative solutions to combat the issue of high congestion in joints have been posed and investigated. Ideas range from vendor-specific materials such as fiber-reinforced concrete and headed reinforcement, to the application of prestressing and the development of displacement-based design methods. The two most promising schemes involve the use of prestressing and the use of headed reinforcing bars. A brief background of each scheme follows.

2.5.1 Prestressed Joints

Prestressing has been used in the design and construction of bridges and building systems for more than 50 years. In concrete bridges, precast prestressed or post-tensioned girder systems are commonly used to increase the span length between adjacent bents. In buildings, it has been used to create long-span floor systems and to facilitate built-up construction by allowing post tensioning of prefabricated elements. Since the technology is well developed, the extension to use in the joint region is natural. One of the important aspects of this technology is that not only can it be applied to new construction but also to retrofit designs as well, by external post-tensioning. This has become a predominant means of increasing the capacity of poorly designed buildings and bridges.

Research has shown that prestressing can be used as an effective means of reducing the amount of joint reinforcement in new bridge designs and as a means of improving the strength and stiffness of existing designs. Sritharan and Priestley [1997] conducted a research program evaluating the behavior of bridge beam-column T-joints subjected to cyclic lateral loading. The test program investigated the effectiveness of prestressing in improving joint behavior. Subassemblies were constructed, modeling pre-1960 connection geometry. One as-built connection, one conventional design based upon a strut and tie model, and one partially prestressed joint design were tested. The program showed that prestressing the cap beam allows for a reduction in the amount of joint reinforcement without any decrease in the ductility of the joint system. Similar results were obtained by Lowes and Moehle [1995]. The test series investigated means of retrofitting pre-1960′s bridge beam-(square) column connections. The first test of an as-built 1960′s connection resulted in poor ductility and overall joint failure. To limit impact to the existing structure, the cap beam was widened to allow for the addition of post-tensioning. Sections were cast on each side of the cap beam and post-tensioning rods were installed. The final joint region contained no additional transverse reinforcement but was nevertheless effectively confined. Prestressing or post-tensioning of the cap beam is clearly a viable option for reducing the amount of reinforcement and improving the strength and stiffness of beam-column connections. As a result of the well-established work in this area, further investigation of joint prestressing is not conducted.

2.5.2 Utilization of Headed Reinforcement in Joint Design

Headed reinforcement has been shown to be effective in reducing congestion, improving bond, increasing confinement and assisting in the development of local strut and tie models. Application in joints is clearly appropriate and has been investigated. This section examines the load transfer mechanism for headed reinforcement, the types of headed reinforcement available, and the research conducted on its application in joint systems.

Headed reinforcement by definition is a reinforcing bar terminated with a head or end plate. The terminator is used to alter the principal force transfer mechanism between the reinforcement and concrete from bond to bearing. Depending upon the size of the plate, the connection between the bar and plate and the location in the structure, this can lead to a reduction of the required development length. This is equivalent to removal of both straight and hooked development lengths, and, in some cases, allows for a substantial reduction in reinforcement. The initial use of headed bars began in 1986 by Norwegian contractors for application in heavily reinforced offshore oil structures [Mitchell 1994]. Since then, it has demonstrated as being very beneficial in the reduction of congestion and improving constructability.

Varieties of head configurations are used (Figure 2-7). The shape of the plate is typically square or circular to provide the most effective use of the head. Rectangular or oval plates are sometimes used to assist in construction of heavily reinforced regions where construction access may be limited. An example of this use is illustrated in the construction of pressure vessels. When constructing the walls of these systems, the outer face is formed and a dense mat of longitudinal reinforcement is placed from the inside in two layers. Since access is limited to one side and the longitudinal reinforcement is very congested, the installation of stirrups becomes difficult. To accommodate the construction, headed bars with rectangular plates can be inserted through the closely spaced bars and turned to engage both the rear and front longitudinal reinforcement, thus greatly improving constructability [Mitchell 1994].

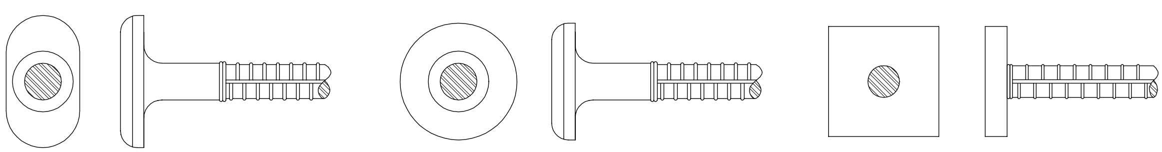

Figure 2-7: Headed reinforcement as provided by Headed Reinforcing Corporation

Two commercially available techniques are being used for the fabrication of the headed bars: the first consists of a screw-type terminator as provided by ERICO[1], and the second consists of a welded terminator provided by HRC[2]. The screw-type connector can be installed in the field or prefabricated to a given length. The bar end is reduced to a cone and threaded to match an available head plate (Figure 2-8(b)).

[1] ERICO, Inc. Concrete Reinforcement Products, 34600 Solon Road, Solon, Ohio 44139.

[2] Headed Reinforcement Corporation (HRC). 11200 Condor Ave., Fountain Valley, CA 92708.

This type of connection creates high compressive strength. The tension strength, however, is limited to the thread capacity, which may not allow for full development of the bar anchorage. ERICO terminators are therefore used to reduce but not eliminate the required development length. HRC bars are fabricated by friction-welding of the head to the end of the bar. This weld is created by rapidly turning the end plate (at a speed of approximately 1500 rpm) against the bar. The resulting friction causes the pieces to weld together. The friction technique results in a mushroom-shaped weld at the connection (Figure 2-8(a)). This shape creates a weld with a net section larger than the bar diameter, ensuring the development of the full capacity.

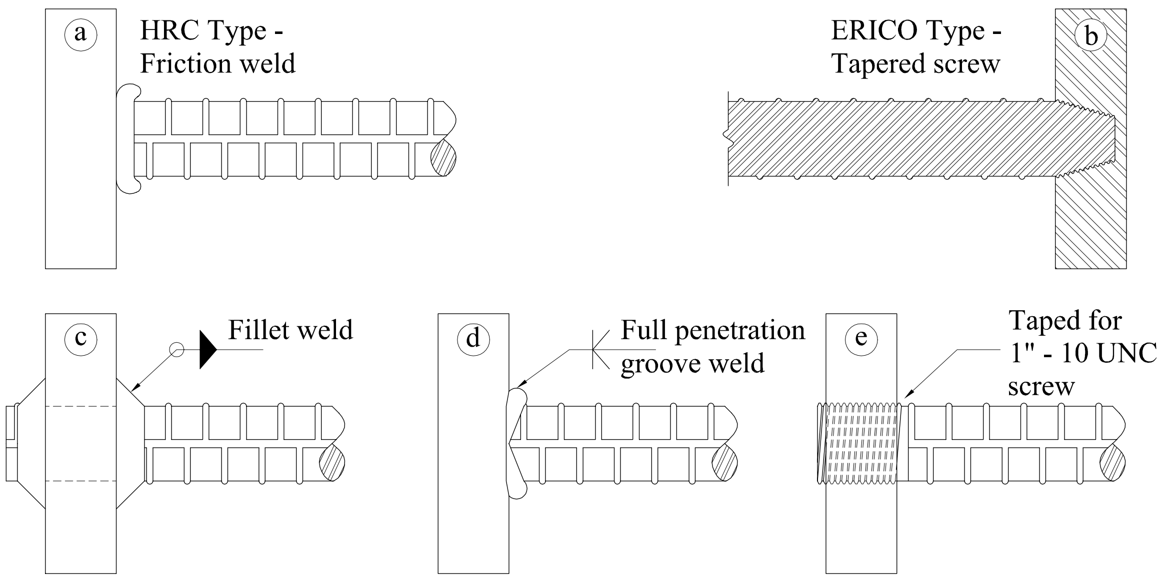

Figure 2-8: Terminator connections

In addition to the proprietary techniques available, standard fabrication methods can be used to create ″homemade″-type connections. The full tensile and compressive capacity can be sustained by at least two methods. In the first method, the bar can be passed through the terminator plate and fillet-welded on the interior and exterior faces (Figure 2-8(c)). This provides good compressive and tensile anchorage at the cost of a high fabrication expense. The bar end can also be threaded and attached to an end plate. Using a unified standard series UNC thread pattern (Figure 2-8(e)), good anchorage can be achieved, although at the cost of fabrication time. Additionally, a terminator can be formed by using a full-penetration groove weld between the head and the bar (Figure 2-8(d)). This technique produces good compressive anchorage with limited tensile anchorage due to the limited capacity of the weld. The comparative tensile strengths of these connections are calculated for a #8 bar (Table 2-9).

Table 2-9: Terminator capacities for a #8 reinforcement bar			
Type	*Terminator connection*	*% of bar tensile ultimate capacity*	*Comments*
a	Friction-welded HRC Type	100 %	Proprietary terminator proven to be reliable and capable of full bar development.
b	Threaded ERICO Type	Unavailable	Proprietary terminator, useful for reduction of reinforcement development. Allows for field placement.
c	Double fillet weld connection	100 %	Capable of full bar development. Requires significant fabrication: 3/8-in. fillets (for #8 bar) and drilled terminator plate.
d	Full-penetration groove weld	93 %	Significant reduction of development lengths. Requires high-strength terminator plate but otherwise, minimal fabrication.
e	Conventional threaded end	100 %	Capable of full bar development. Significant fabrication requirements: terminator plate drilled and taped, bar threaded.

The determination of the end plate size is critical. If the plate is too small, the development of yield forces in the bar will cause crushing of the concrete, which could lead to slipping or pullout. On the other hand, making the plate too large will reduce the constructability benefits by increasing congestion. The determination of the head area and thickness is ultimately controlled by the prevention of shear and flexural yielding and crushing of the concrete under the head at the yield strength of the bar [ASTM A970]. Assuming values for yield strength of the bar and plate, and a compressive strength of the concrete the minimum required plate geometry for a given bar size can be determined.

The yield strength of the bar can be computed from the yield capacity

$$F_{bar} = A_b f_y \tag{2-12}$$

where A_b is equal to the reinforcement bar cross-sectional area, and f_y is equal to the yield strength of the bar. The bearing strength of the plate, F_{plate}, can be determined from ACI 318, Sec. 10-17

$$F_{plate} \leq 0.85 f'_c \sqrt{A2 / A_h}\,(A_h - A_b) \tag{2-13}$$

where f'_c is equal to the compressive strength of the concrete, A_h is equal to the head area, and A2 is the area of the effective bearing cone (Figure 2-9). Assuming that the head has a clear distance of at least 1/2 times its width from any surface, the bearing capacity can be reduced to

$$F_{plate} \leq 1.7 f'_c\,(A_h - A_b) \tag{2-14}$$

Equating 2 – 12 and 2 – 14, the head area can be determined

$$A_h = A_b \left(1 + \frac{f_y}{1.7 f'_c}\right) \qquad (2\text{-}15)$$

With a concrete compressive strength of 4 ksi and a yield capacity of 60 ksi the required head area is 9.8 (approximately 10) times the bar area (refer to Table 2-10 for required terminator size).

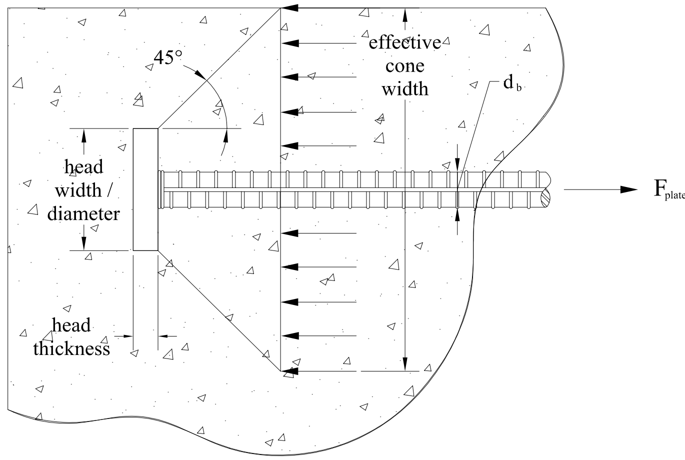

Figure 2-9: Stress distribution of headed reinforcement

Table 2-10: Required terminator size*

Bar Size	Minimum thickness (in.)**	Minimum Diameter Circular Head (in.)	Minimum Width Square Head (in.)
#3	0.375	1.250	1.125
#4	0.4375	1.625	1.500
#5	0.500	2.000	1.875
#6	0.5628	2.375	2.125
#7	0.625	2.875	2.500
#8	0.625	3.250	2.875
#9	0.6875	3.625	3.250
#10	0.750	4.125	3.625
#11	0.8125	4.500	4.000
#14	1.250	5.375	4.750
#18	1.625	7.250	6.375

* Assuming a reinforcement yield strength of 60 ksi and a concrete compressive strength of 4 ksi.
** From ASTM A970 Standard Specification for welded headed bars for concrete reinforcement

Headed reinforcement is commonly used in three applications: anchorage of longitudinal reinforcing bars, transverse shear reinforcement of beams and columns, and as lateral restraining reinforcement. Experimental investigations have shown that headed reinforcement can be safely used in a number of anchorage applications. Pullout tests conducted by DeVries [1996] on shallow and deep embedment of headed bars illustrated both the effectiveness and shortcomings of its use as anchorage. Shallow embedment capacity was shown to be dependent on embedment depth, edge distance, and concrete strength. For bars with low embedment depth and low edge distance, pullout-cone failure often occurs. Transverse reinforcement had no beneficial effect on the anchorage strength and in some cases even reduced the capacity. Deep embedment tests showed that side blowout failures could occur if the bar is placed too close to the concrete surface. In these cases, transverse reinforcement placed around the head was shown to improve pullout capacity. The tests also revealed that a significant portion of the pullout capacity is resisted by the head. In most cases, the additional strength gained by bond along the bar can be ignored. Further studies by Bashandy [1996] showed that the head provides the majority of the bar capacity. Cyclic load application from 5 to 80% of the bar ultimate capacity resulted in minimal reduction of anchorage capacity. Slip occurred only during inelastic deformation of the bar and was thus traced to elongation of the bar and not the head. Use of headed bars for anchorage has been further promoted by a series of structural application tests. Tests performed by Lehman [1998] have shown that they can be applied to the column-footing connections in bridges. Separate investigations by Priestley [1993], and McConnell and Wallace [1994] have shown that headed bars can be safely used to replace hooks in both bridge and building beam-column joints. Finally, tests performed by Haroun [1993] on wall panels have shown that headed bars can be effectively used to provide passive lateral confinement.

In summary, headed reinforcement improves anchorage capacity by providing a bearing mechanism in addition to bond along the bar length. The bearing mechanism allows for a reduction of anchorage length and, in turn, reduces the amount of reinforcement. This eases construction and reduces the costs in both material and labor. Headed bars can also be used in strut and tie designs to provide local anchorage zones. The possibility for accurate placement allows for a greater reliance on the formation of a particular mechanism. Application of headed reinforcement in wall systems has also been established. Tests showed that the lateral confinement provided by headed reinforcement could effectively improve capacity. This lateral confinement has also been shown to improve the capacity of beam-column joints. Prior to use, headed reinforcement should be evaluated to ensure that the proper head geometry and head-to-bar connection is used to meet the needs of the intended application. In addition, the effect of shallow embedment depth and limited coverage should be considered to eliminate pullout-cone and side-blowout failures. With proper consideration of possible failure modes, headed reinforcement can be safely used in joints for the development of longitudinal bars, design of particular strut and tie mechanisms, transverse reinforcement, and lateral confinement.

2.6 Bridge Joint Research Issues

The review of current practice for the design of beam-column connections has shown that a definitive joint design method does not exist. A variety of methods are being used, each based on a different concept resulting in different arrangements and quantities of joint reinforcement. Of these methods, bridge codes produce the most stringent requirements. While each method has a valid foundation, further research needs to be conducted with a focus on improving the current level of understanding. This can be used to advance the design practice by improving constructability and the ability to predict joint deformation response. These tasks can be accomplished through an experimental evaluation of joint performance, further investigation of strut and tie modeling methods, investigation of nonconventional designs, and development of a displacement-based approach to joint design.

Although some code requirements specify significant overstrength for the joint, it is not clear whether the joint will respond in an elastic or inelastic manner. An approach suggested by the New Zealand Standards Association is to allow the structure to resist inelastic loading by the formation of ductile energy-dissipating mechanisms outside of the joint core. The assumption is then made that the inelastic loads are transferred through the joint via a shear panel mechanism, a primary strut mechanism, or a series of struts and ties. While this may provide a rational approach for load transfer, the amount of damage and stiffness degradation that the joint undergoes as a result is unclear. It is necessary to develop tools or techniques that allow for estimating joint stiffness degradation relative to the applied loads. Creation of displacement-based recommendations and evaluation techniques would allow for both a comprehensive estimate of inelastic system deformation and a tool for evaluating potential weak zones in existing structures.

Another important aspect of joint behavior that warrants further study is how to best provide joint confinement. From the code investigation, it appears that the current design practice views continuation of the column transverse reinforcement as acceptable. This, theoretically, should produce the most benefit, since the spiral is in close proximity to the dilating core and the yielding reinforcement. The required continuation of the column transverse reinforcement, however, is generally prescribed in addition to an amount of horizontal and vertical joint shear reinforcement. The designs produced are very congested and difficult to construct. If one could show that lateral confinement, in the form of hairpins or headed bars external to the column core, could adequately confine the yielding column bars, then one could redefine the current practice. For example, one would be able to eliminate the column spiral and instead increase the amount of horizontal joint shear reinforcement such that it is able to support both the shear transfer and the required confinement. This would eliminate the difficulty of threading the horizontal joint shear reinforcement through the joint spiral. This issue is one of the motivations for the research presented in this report.

Another issue, reflected in the newest code, ATC 32, is the application of strut and tie modeling to a joint system. Although strut and tie modeling represents a rational means of transferring forces, it nevertheless relies on the formation of struts in a unique arrangement. The original mechanisms used as a basis for older codes such as the New Zealand Standard relied upon the formation of a primary strut and truss mechanism running diagonally across the joint from one compression zone to the other. The mechanism matches the behavior of the joint system both physically and analytically in that cracks formed as expected and load transfer was justified in a rational manner. The application of a particular series of struts and ties, however, is based upon many assumptions. Foremost, it does not directly or indirectly consider the issue of displacement compatibility. It assumes that the forces will be transferred through the predetermined struts regardless of whether the deformation of the joint causes cracks to form across these regions. Additionally, one can reason that this model may lead to excessive damage. Even if the assumed load paths are achieved and the forces properly transferred, the associated damage may be quite elevated since the suggested method places the majority of reinforcement outside of the joint. The lack of joint reinforcement imparts more of a reliance on a principal compression strut over that of the truss-type mechanism, thus leading to more damage. When considering that the local design community view ideal joint behavior as rigid response to load transfer, this level of damage may be unacceptable. Therefore, until more experimental and analytical evaluation is performed, the application of a unique combination of struts and ties remains questionable.

Joint design has been complicated by the fact that most design methods do not directly link the amount of reinforcement with the level of performance achieved. Currently, there is a tendency in the American practice toward achieving a high level of joint performance (i.e., rigid response). Because design philosophies do not clearly present a method of achieving this, this trend has resulted in extremely conservative joint designs. This is illustrated in the ATC 32 design strategy, which results in excessive levels of reinforcement. Though this aims toward a stronger and more damage-resistant joint, construction in this case becomes a significant issue.

Clearly current practice of reinforced concrete joint design leaves much to be desired. As a solution to the issues presented, three strategies should be implemented. First, a better understanding of joints must be obtained so that a method of practice can be developed that accounts for both equilibrium and compatibility. This will allow the designer to have an improved grasp of what damage will be expected for a given design. As a result, design objectives can be directly met. Secondly, research should be undertaken toward the development of a joint design method that provides a lower bound on the level of reinforcement, while still providing adequate strength and damage resistance. This will provide an alternative to the current strategy of overdesigning the joint to ensure safety. Finally, the use of new materials (e.g., headed reinforcement) should be thoroughly investigated as a means of solving the problem of joint congestion. These issues represent the focus of the research presented in this report.

3 Development of Experimental Program

A research project was undertaken to investigate methods of improving constructability of bridge beam-column joints subjected to equivalent earthquake loading. This chapter discusses the development of the experimental program. The determination of the prototype bridge configuration, the design of the experimental subassembly, and the instrumentation techniques used for evaluation are presented.

3.1 Bridge Terminology

A typical California bridge system is illustrated in Figure 3-1. This system consists of a single-level, long-span, elevated highway supported on multiple *columns*. These columns terminate in a solid reinforced concrete beam, referred to as the *cap beam*, which spans the entire bridge width. Together, the cap beam and columns make up a *bridge bent*. These bents, in turn, support the highway bridge span. Many different types of structural systems may be used to span the distance between bents. They range from prestressed concrete and steel plate girders, which rest on top of the cap beam, to *integral post-tensioned concrete box-girder* systems, commonly constructed monolithically with the cap beam. Long-span bridges are often divided into segments or *frames* to allow for shrinkage and expansion due to temperature variations. In monolithic construction, each frame typically consists of two to three bridge bents and their adjoining spans. Connection between adjacent frames is accomplished through the use of a *simple seat connection* capable of transmitting vertical (and possibly transverse) forces but allowing for longitudinal expansion and rotation. To limit the effects of pounding between frames and unseating during seismic events, longitudinal restrainers, often consisting of steel cables, are usually installed across the seats [DesRoches 1998].

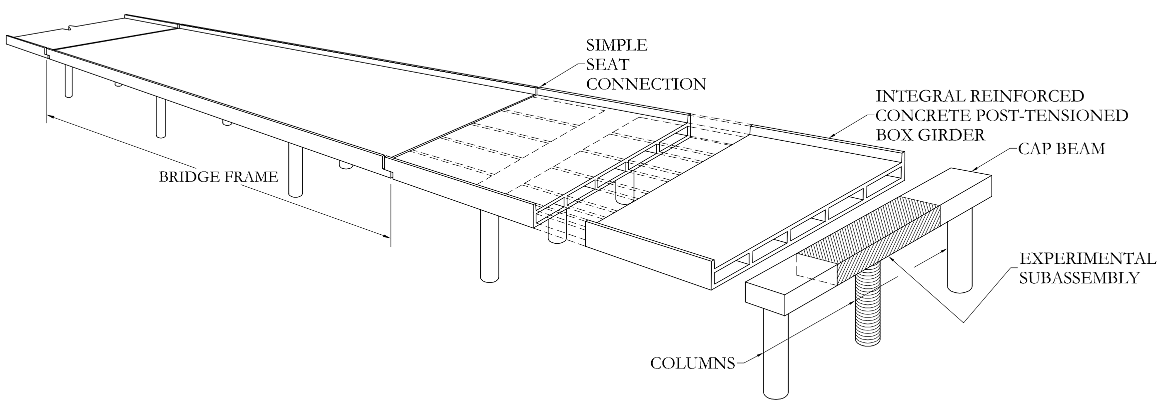

Figure 3-1: Components of a reinforced concrete post-tensioned bridge

3.2 Database Evaluation

To determine an appropriate geometry and structural configuration for the test series, typical California bridge construction was studied. The investigation examined bridge geometry, focusing particularly on reinforced concrete bridges built in California between 1985 and 1995. Sixteen bridges, including both new and reconstructed systems, were evaluated. These bridges represent a range of configurations, from single-column to four-column bents and long-span viaducts to one-bent overpasses. Pertinent aspects of the design, from the bridge geometry to the quantity and arrangement of reinforcement are summarized in Appendix A. This study resulted in the selection of a representative prototype, which is presented in the following paragraph.

The prototype structural system consists of a three-column bridge bent with an integral box girder and pinned column-to-footing connections (Figure 3-2). The bridge supports four lanes of traffic in one direction, representing half of a principal arterial. To support the 150-ft span, a longitudinal post-tensioning system is used. This involves a series of post-tensioning ducts draped appropriately in the webs of the box-girder. The cap beam is rectangular with a width larger than depth. The depth is comparable to the column diameter. Due to the almost exclusive use of spiral column reinforcement in California construction, a circular column cross section is used. The dimensions and geometry summarized in Table 3-1 and Figure 3-2, were found to be representative of a typical bridge constructed in California.

Table 3-1: Prototype (full-scale) bridge geometry			
Bridge type: Reinforced concrete post-tensioned cast-in-place, long-span, box-girder bridge			
Number of lanes	4	Column diameter, *Dc*	6 ft-3 in.
Bent-to-bent span, *S*	150 ft	Clear span beam length, *Lb*	26 ft-4 in.
Clear column height, *Lc*	25 ft-4 in.	Cap beam depth, *hb*	5 ft-2 in.
Top slab thickness, *st*	8.3 in.	Cap beam width, *wb*	8 ft-3 in.
Bottom slab thickness, *sb*	6.9 in.	Clear box width, *wbox*	9 ft-10 in.
Box web thickness, *tw*	1 ft	Frame height, *H*	27 ft-11 in.

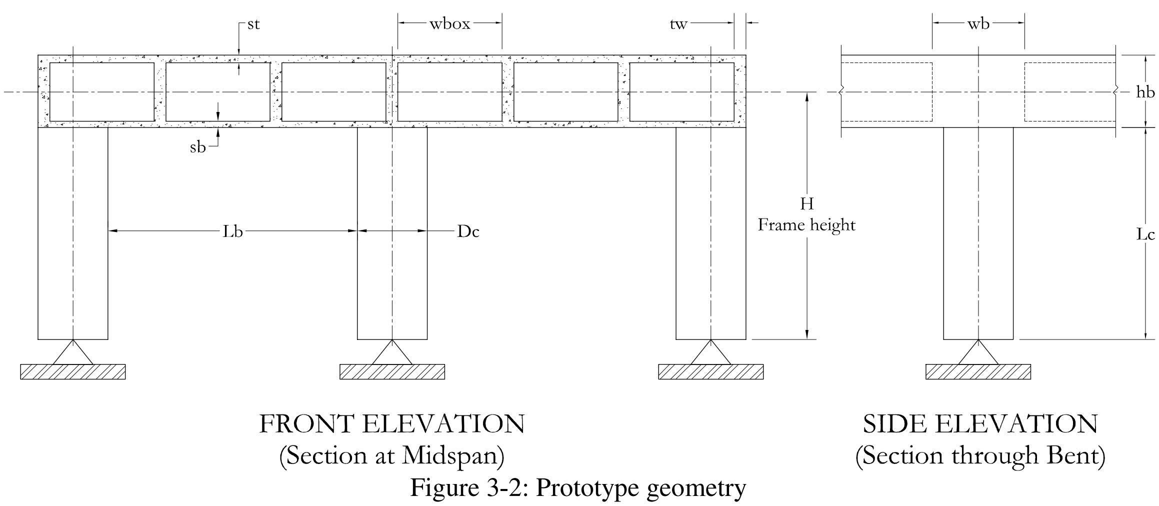

Figure 3-2: Prototype geometry

Representative reinforcement details, material properties, and loading are summarized in Table 3-2.

Table 3-2: Prototype (full-scale) bridge reinforcement and materials			
Column reinforcement ratio, ρ_{col}	0.0218	Concrete compressive strength, f'_c	4000 psi
Beam negative reinforcement ratio, ρ_{bmn}	0.00936	Reinforcement yield strength, f_y	60 ksi
Beam positive reinforcement ratio, ρ_{bmp}	0.00421	Column axial gravity load, D	$0.085A_g f'_c$
Column plastic hinge transverse reinforcement ratio			0.00979

3.3 Subassembly Development

The experimental investigation focuses on the behavior of an interior beam-column joint in a bridge system subjected to constant gravity loading and varying transverse loading. The test series focuses upon the actions and behavior of the joint when the bridge system is subjected to lateral loading. A T-shaped subassembly was chosen for this study. The assumption was made that the integral box-girder span would not contribute significantly to the lateral strength. Therefore, the subassembly was composed of only the cap beam and column. The lengths of the beam and column were chosen to coincide with the expected inflection points (i.e., points of zero moment) that occur when the bent is subjected to only lateral loading. The resulting subassembly consisted of the full column height and half the beam span on each side of the center column (the locations of inflection points in the prototype and subassembly are discussed later in this section). The subassemblies were loaded in the plane of the cap beam (i.e., the bridge transverse direction). Consequently, it was assumed that the box-girder longitudinal post-tensioning would not significantly affect the transverse response. Thus no post-tensioning was used.

To allow for the use of normal concrete aggregate and standard reinforcement sizes, the test scale was chosen to be 3/8. A schematic of the subassembly is shown in Figure 3-3. To simplify testing and construction the subassembly was oriented upside-down with the cap beam against the floor and the column in the air.

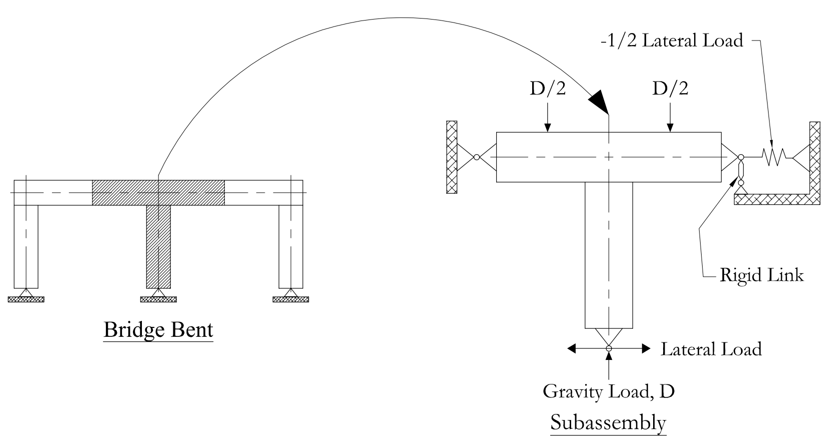

Figure 3-3: Experimental subassembly development

3.3.1 Gravity Load Simulation

The magnitude of the column axial load was chosen to be consistent with Caltrans standard design practice. A gravity load of $0.05A_g f'_c$ was recommended and used, where A_g is the column gross cross-sectional area and f'_c is the 28-day concrete compressive strength. It should be noted that the applied load was lower than the mean value of $0.085A_g f'_c$ estimated from the database investigation (see Table 3-2 and Appendix A).

The gravity load was applied axially at the base of the column and reacted against the beam at two points, one on each side of the joint (Figure 3-3). The locations of the beam reactions were chosen so that the beam moment at the joint face due to gravity load would be the same as the scaled value in the prototype. Figure 3-4 compares the bending moment diagram obtained from the scaled distributed gravity load on the prototype with that from the point loads applied on the subassembly.

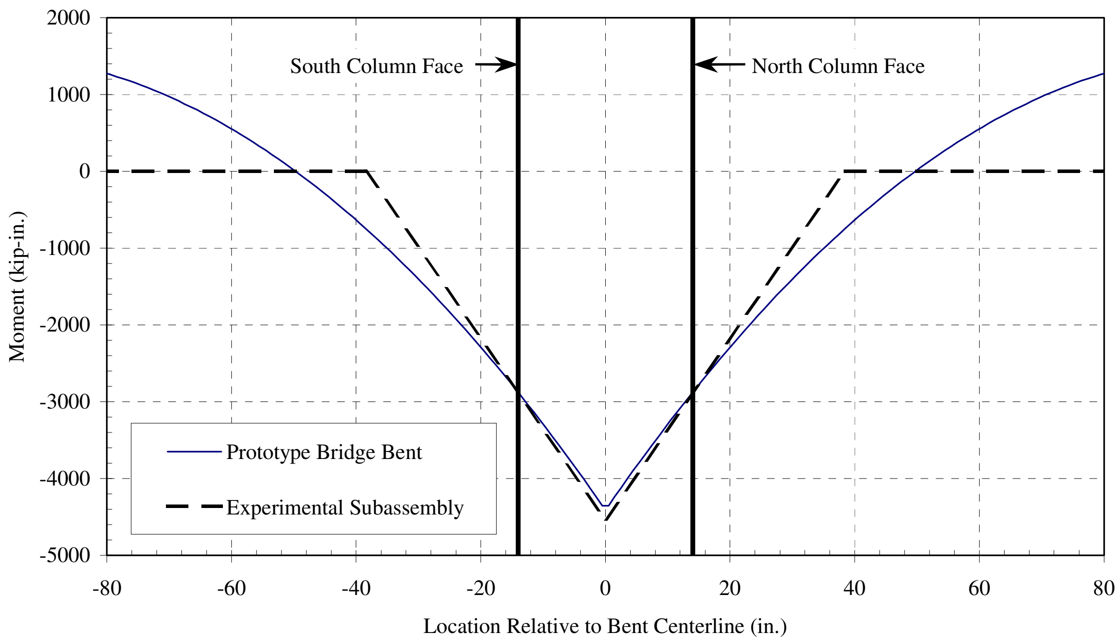

Figure 3-4: Cap beam gravity load bending moment distributions

3.3.2 Lateral Load Simulation

Two seismic loading conditions control the lateral load design:

- Ultimate level earthquake load (using Caltrans ductility and risk adjustment factor, Z = 8) with service level gravity load
- Plastic frame response (i.e., plastic hinge formation in the top of all columns) with service level gravity load

Bending moment and shear force distributions in the bent and the subassembly are shown in Figure 3-5 and Figure 3-6, respectively. In these distributions, gross member cross sections were used and the joint was assumed to be rigid. Considering the more critical load combination of gravity load and plastic frame response, the prototype and subassembly moments compare favorably at the column face. The negative moment distribution is modeled in the subassembly; however, the corresponding positive moment distribution is not accurately modeled. The resulting distribution is considered acceptable since it overestimates the load applied, thus placing higher demands on the joint system. For the same case (i.e., gravity load and plastic moment), the shear due to lateral loading is underestimated at the south face and overestimated at the north face of the joint. Because of the boundary conditions, the prescribed axial load, and the moment required at the face of the joint, the shear is not accurately modeled. It should be noted that the subassembly shears at the face of the column represent the average of the two cases shown in Figure 3-6 for the bent. It was expected that the underestimation of the subassembly shear at the south face would produce a small change in the nominal vertical joint shear stress of $0.7\sqrt{f'c}$, which is too small to alter the joint response.

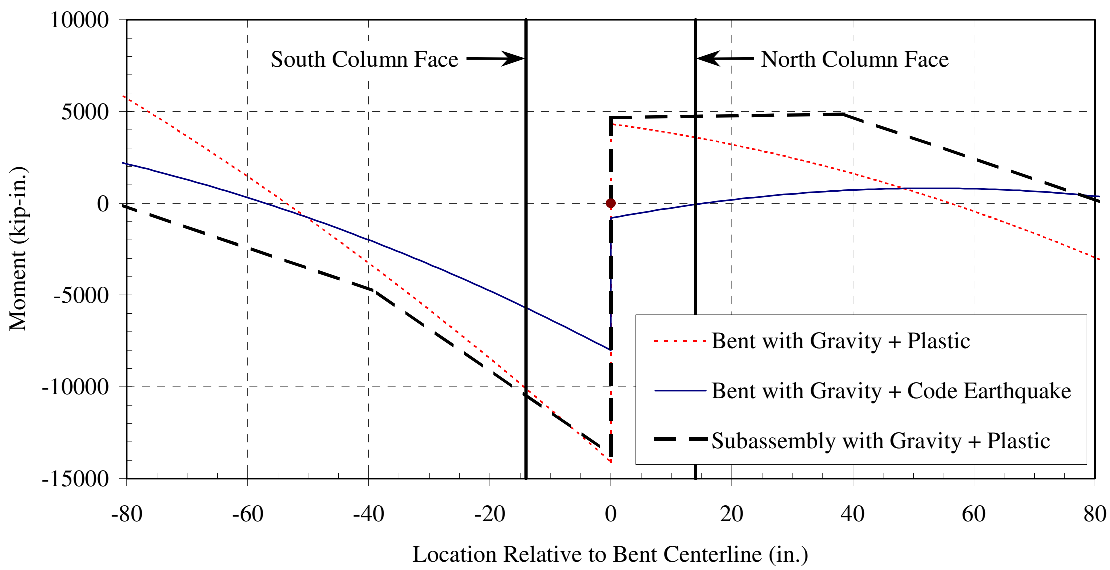

Figure 3-5: Cap beam lateral load bending moment distributions

Lateral loading of the prototype system results in an axial tension force on one beam segment and a compression force on the other. To account for this effect in the subassembly, a pin-pin system was initially considered. This, however, would have imposed an unrealistic fixity in the cap beam, creating a passive restraining action on the joint. To avoid this behavior, a pin and roller system was used to model the cap beam boundary conditions (Figure 3-3). To account for the tension-compression axial load distribution of the cap beam, a force corresponding to half the column lateral load was applied to the beam at the roller end in the opposite direction. This allowed the axial force in the beam, generated by the shear input from the column, to be split equally in tension and compression between both beam segments without an undesirable restraint to the joint.

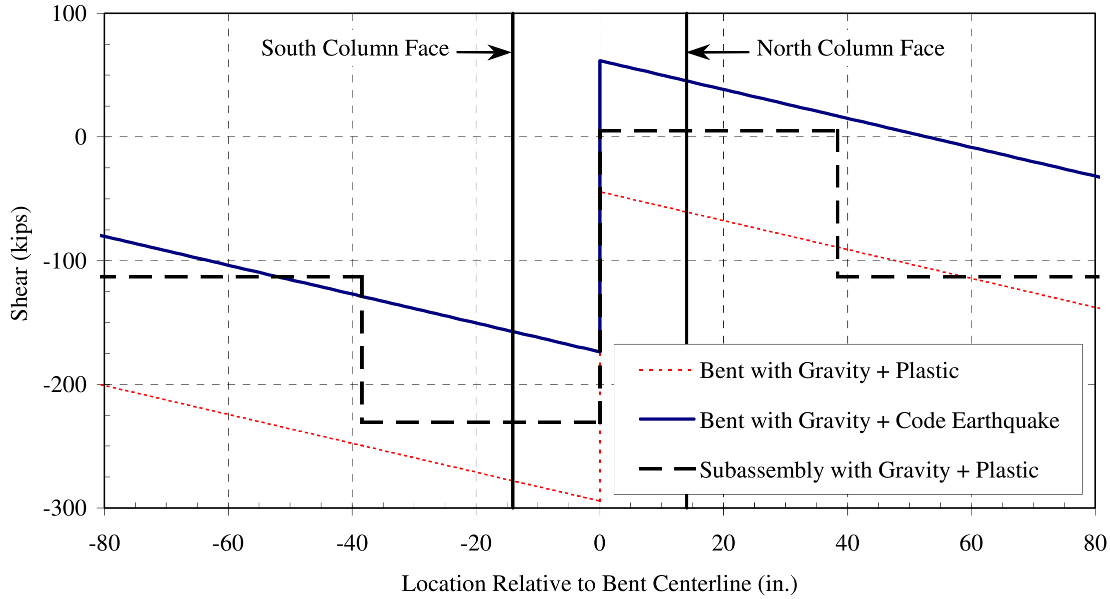

Figure 3-6: Cap beam lateral load shear force distributions

3.4 Experimental Setup

To facilitate the experimental program, the specimens were constructed and tested upside down. An exploded isometric view of the final layout, the elevation and plan of the testing system, and a photo of the test setup are shown in Figure 3-7 through 3-10. The gravity load was applied through the use of a vertical actuator, a spreader beam, axial rods, and a cap beam reaction frame. The vertical actuator applied half of the required axial load, *D/2*, to one end of the spreader and cap beam frame. Since the spreader was pinned in the center and vertically fixed on the other end, a lever was created, magnifying the actuator load by a factor of two. This resulted in the full gravity load, *D,* being applied to the column. The axial rods transferred this force to the cap beam frame, which reacted against the cap beam in bearing. The bearing forces were equal to *D/2* and were applied at a distance of 32 in. from each side of the column centerline. To reduce stress concentration, the cap beam reaction points were spread over an area having a width of 9 in. and a length equal to the full width of the cap beam. In addition, elastomeric pads in conjunction with Teflon sheets were used between the concrete and steel frame. This limited the localized crushing of the concrete due to inconsistencies in the surface and minimized longitudinal restraint, thus allowing free dilation of the joint.

The lateral load was applied at the base of the column (top of the column in the inverted test configuration). To ensure stability of the subassembly, two out-of-plane actuators were used for load application. The same displacement increment was prescribed to the two actuators, thus forcing the actuators to move along a straight path. As a result, out-of-plane displacement is minimized. The lateral loads were reacted against a steel reaction frame, which was monitored for deformation. To connect the actuators to the column base, a square footing block was cast monolithically with the column. Plates were installed on the front and rear faces of the block and prestressed together. The actuators were then bolted to the front plate. By using this configuration, compressive load transfer between the actuator and column was always achieved. When the actuators extended, the force was transferred to the column as bearing on the front face. When the actuator was retracted, the force was transferred through the prestressing to the rear of the reaction block where it was applied as compression.

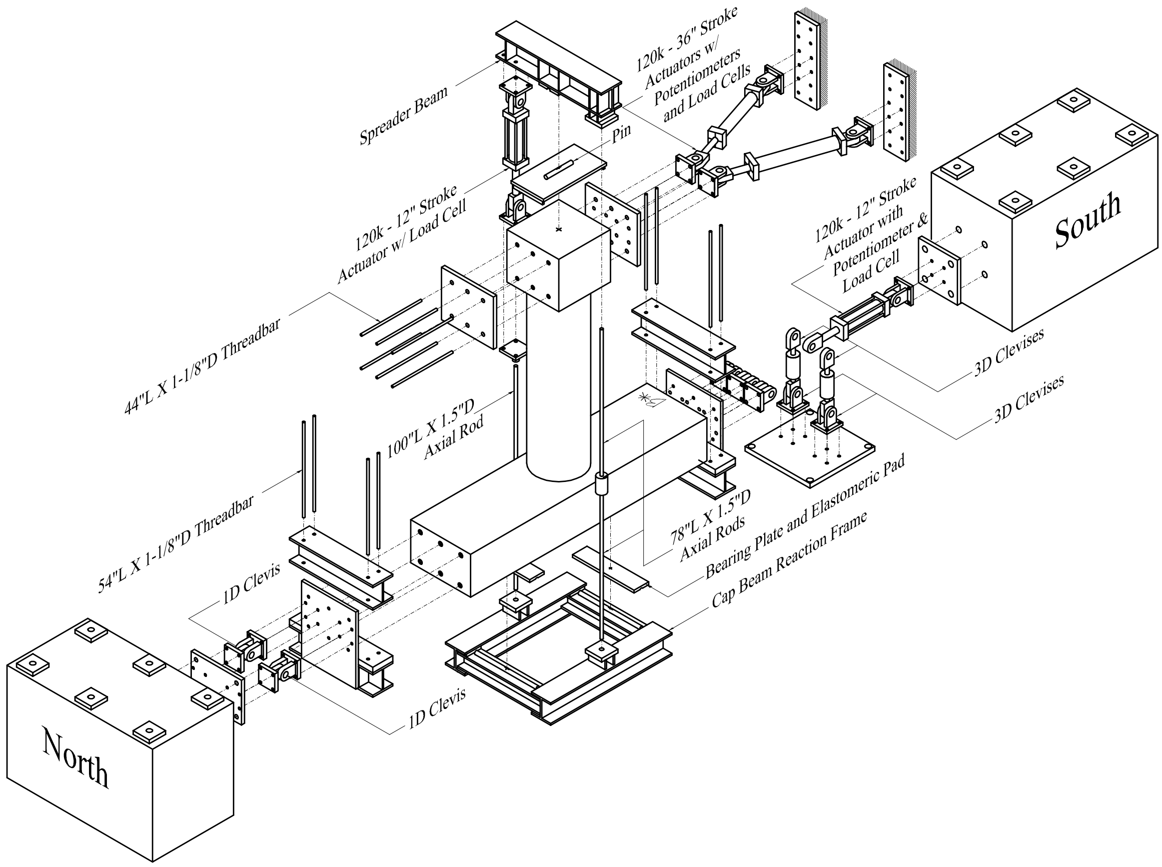

Figure 3-7: Exploded isometric view of the test setup

The cap beam boundary conditions were modeled using one-dimensional (1D) clevises in combination with multiple struts. The pinned end of the beam was connected to a rigid concrete reaction block using two 1D pins in parallel. This arrangement was chosen to provide stability against torsional action. The roller end was modeled with two struts connected in parallel. These struts were oriented vertically and were connected to the beam and floor through clevises. This arrangement allowed free axial deformation of the cap beam, thus creating a pseudo-roller boundary condition. It should be noted that this axial deformation does not occur horizontally but through an arc with a radial distance defined by the distance between the pinned ends of the struts. Since the beam extension due to joint dilation and beam damage was relatively small, any forces generated through the use of a curved roller path were negligible.

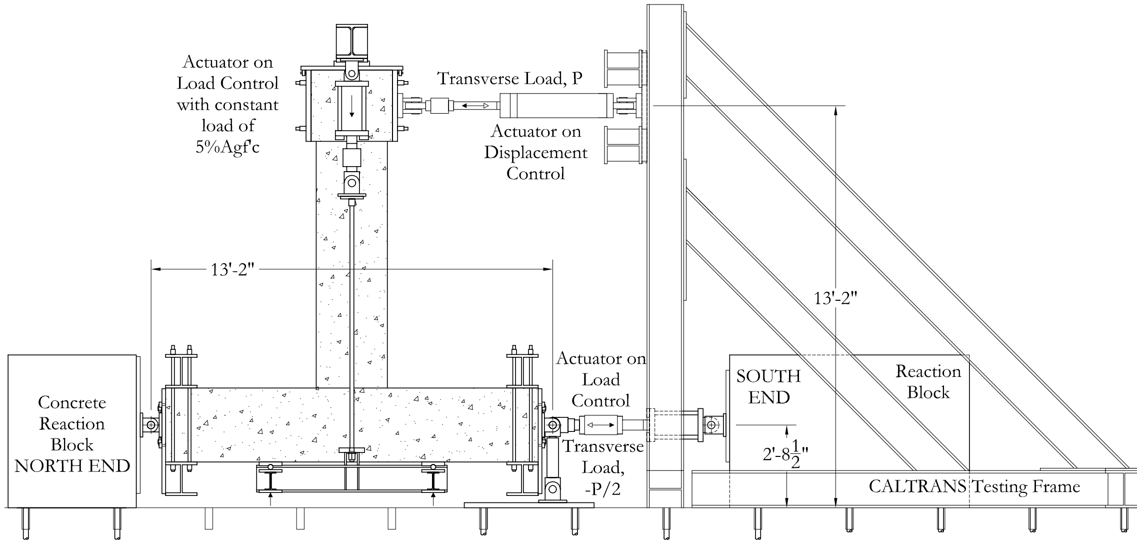

Figure 3-8: Elevation of experimental setup

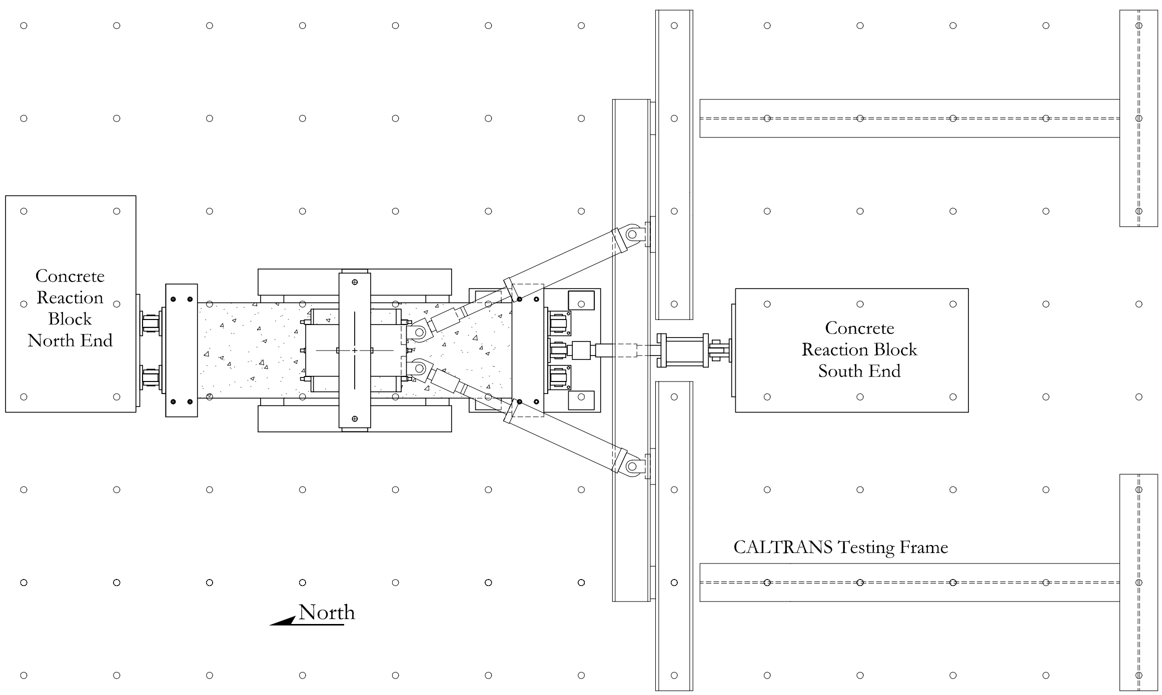

Figure 3-9: Plan of experimental setup

Figure 3-10: Experimental subassembly setup (Photo at end of testing)

3.5 Load Application and Control

Load application consisted of a cyclic unidirectional lateral load and a constant gravity load. The gravity load was statically applied under force control at the beginning of the test, prior to lateral load application. This gravity load was kept constant throughout the test. The lateral load was then applied through displacement control at the column tip (column base, in the real system). The force corresponding to the lateral displacement was calculated, in real time, through a feedback routine, which accounts for the original geometry, the change in displacement, and the measured load in each column actuator. This value was then halved and applied in the opposite direction along the beam to an actuator under force control. An outline of the load control protocol is presented in Figure 3-11.

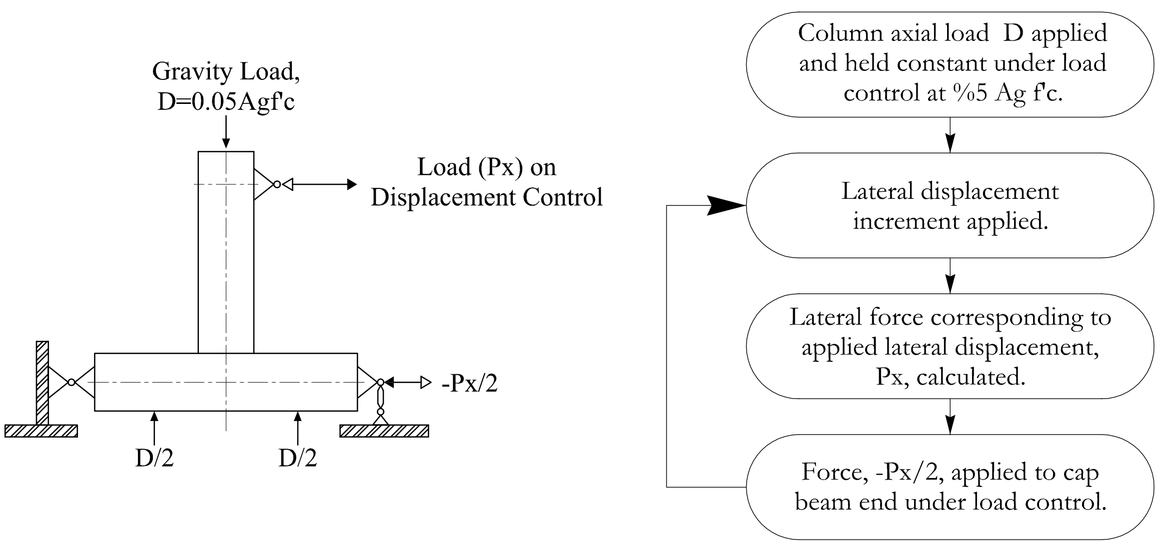

Figure 3-11: Control program

Lateral load application was conducted in a quasi-static manner with a loading rate between 0.01–0.03 in./sec. Data were recorded relative to the maximum displacement command for each cycle with approximately 200 points recorded per cycle with the exception of the first test specimen designated A1 for which 100 data points per cycle were recorded. Two cycles were performed at each displacement level prior to the estimated yield displacement. Once the yield displacement was reached, three cycles were performed at each displacement level followed by a low-level cycle (Figure 3-12). The low-level cycle, equal to 1/3 of the previous displacement, was applied after each post-yield cycle group to investigate stiffness degradation. Yield displacement was defined as the displacement corresponding to the first yield of the exterior column reinforcement at the beam-column interface. This value, estimated to be approximately 1.0 in. of displacement at the column tip, was used as the basis for the displacement history. The history consisted of three phases: low-level displacement to 0.10 in. (to ensure that all instruments and gages are operating correctly), elastic displacement cycles to 0.25, 0.50, and 1.00 in., and inelastic cycles to 2.00, 4.00, 7.00, and 10.00 in. Note that the load was not applied in uniform steps (i.e., 1, 2, 3, 4, 5…). Instead, an increasing step size was chosen (i.e., 1, 2, 4, 7, 10). This allowed for the early inelastic behavior to be investigated in detail while the ultimate response was approached in larger increments to avoid extensive low-cycle fatigue.

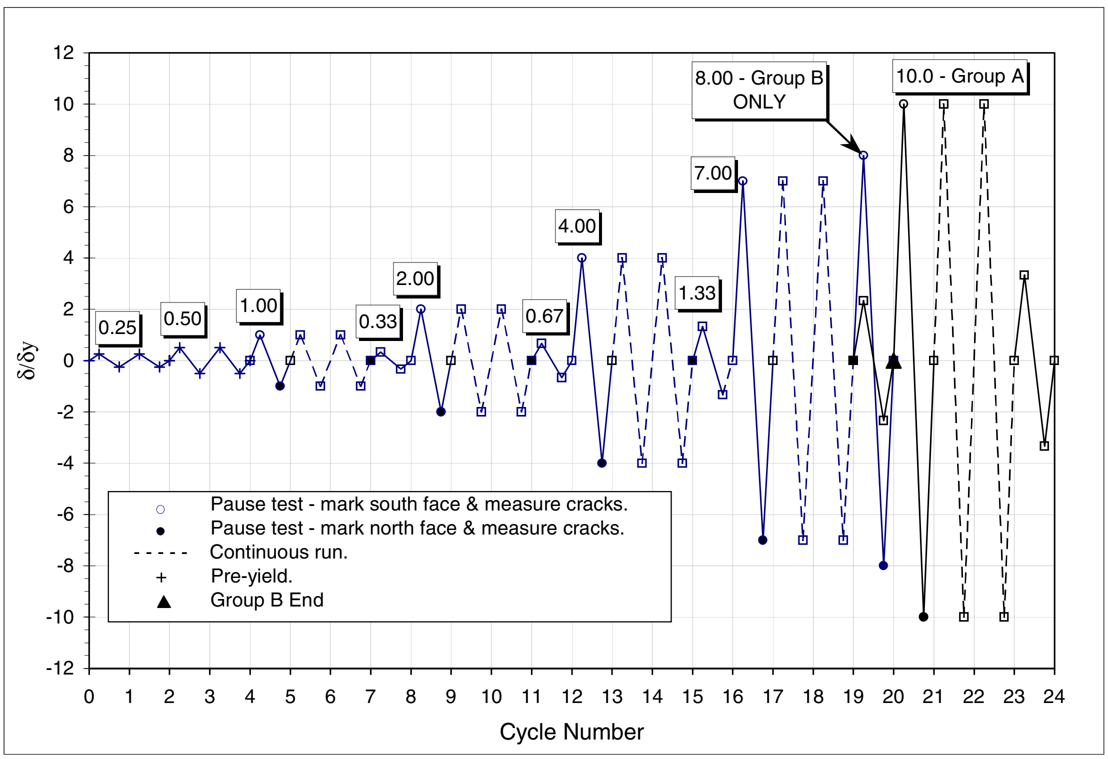

Figure 3-12: Lateral displacement pattern

The test was paused at the first peak of every cycle group, cracks were marked and measured and the test was continued. The peak displacement for each group was increased until the system lost significant strength. This loss in strength referred to either a significant decrease in the lateral load capacity of the displacement group (i.e., a drop > 20% of the ultimate measured force) or an amount of system damage such that continuation of the test would be hazardous. In the first test series, designated Group A, this occurs during the 10-in. displacement group and in the second series, designated Group B, this occurred in the 8-in. displacement group.

3.6 Instrumentation

Three categories of measurements were taken during each test: force, displacement, and strain. A summary of the methods used for these measurements is presented in the following sections.

3.6.1 Load Measurement

Load was measured to assist in the control of the lateral displacement history and to evaluate the force distribution in the subassembly. Load cells were used to measure the vertical forces on the south beam end and the horizontal and vertical loads being applied by the actuators. All load cells were calibrated in compression using a universal testing machine. The same calibration factor was assumed to apply in tension.

3.6.2 Displacement Measurement

External deformations were measured using displacement transducers (wire potentiometers) and linear-motion potentiometers. Three ranges of displacement transducers were used to measure large deformations: ±5 in., ±7.5 in., and ±15 in. The ±5 in.- and ±7.5 in.-range transducers were used for beam displacements and lower-level column displacements. The ±15 in. transducers were used to measure the larger displacements such as the column tip deflection. The wire potentiometers have an accuracy of 0.10% of full scale, i.e., ±0.03-in. resolution for a range of ±15 in. Wire potentiometers were connected directly to the concrete face through a glued tab or by attachment to an embedded threaded bar. Linear-motion potentiometers (LMP) were used to measure smaller-order displacements. Two strokes were used: ±0.5 in. and ±1.0 in., both capable of resolving displacements of ±0.001 in. The LMPs were used primarily on the face of the column and beam to measure shear deformations and curvatures. Local displacement instruments were mounted on embedded thread-bars. A wire was then used to bridge the distance to the next bar. This allowed for the measurement of relative deformation between two points on the subassembly. This connection requires the use of a balancing plate to ensure that only axial deformation is measured between points. Figure 3-13 illustrates the method of attachment to the subassembly [Lehman 1998].

The layout of external instrumentation for Group A is presented in Figure 3-14. The system consisted of a combination of shear and flexure deformation arrays (i.e., small-displacement), denoted by potentiometers G1 to G31, and a series of global displacement transducers. The location and number of potentiometers vary between groups A and B.

Displacement measurements allowed for the evaluation of many different aspects of system response. The techniques used are described in the following sections.

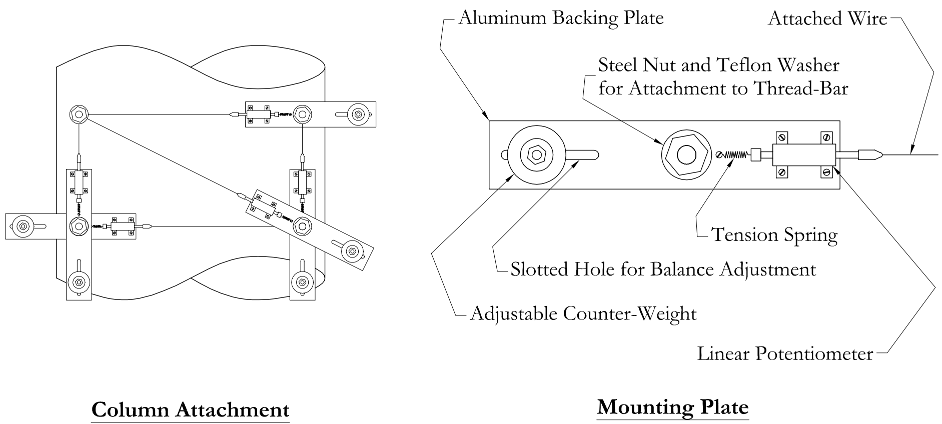

Figure 3-13: Mounting of external "small-displacement" potentiometers

Determination of Displacement Components

Global displacement of the beam-column subassembly consists of six primary components: (1) column flexure, (2) column shear, (3) beam flexure, (4) beam shear, (5) joint shear, and (6) slip / yield penetration of column longitudinal reinforcement. To evaluate the contribution of each component to the total displacement, an array of potentiometers was used (Figure 3-14). To accomplish this resolution, the potentiometer array can be visualized as a virtual truss system (Figure 3-15).

Using the method of virtual forces on a truss, the tip displacement can be computed from the geometry of the truss and the measured deformation of each member. Using the same technique on the virtual truss, the contribution of each component to the total displacement can be resolved.

Applying the virtual work principle, which states that total work of internal and external forces must vanish for any admissible infinitesimal displacement from an equilibrium configuration, i.e.,

$$\text{External Work} = \text{Internal Work} \tag{3-1}$$

$$\partial F \cdot \Delta = \sum_i \int_0^{\ell_i} \partial f_i \cdot \varepsilon(x)_i \, dx \tag{3-2}$$

Where ∂F is the virtual force, Δ is the real displacement, ∂f_i is the virtual force in each member i and $\varepsilon(x)_i$ is the strain at x in member i with length l_i. Assuming that the force does not vary along the member length, the equation can be reduced to

$$\partial F \cdot \Delta = \sum_i \partial f_i \cdot u_i \tag{3-3}$$

Where u_i is the displacement in member i. Since the virtual force in each member can be computed from the known original geometry of the truss system and applied virtual force ∂F, the tip displacement Δ can be calculated at any point in the loading cycle given u_i for each member at the same point in the loading cycle.

As a first step, the total displacements were calculated from the truss model and compared with the measured tip displacement. An average error of ±10% was found with a maximum of ±20% at the peaks.

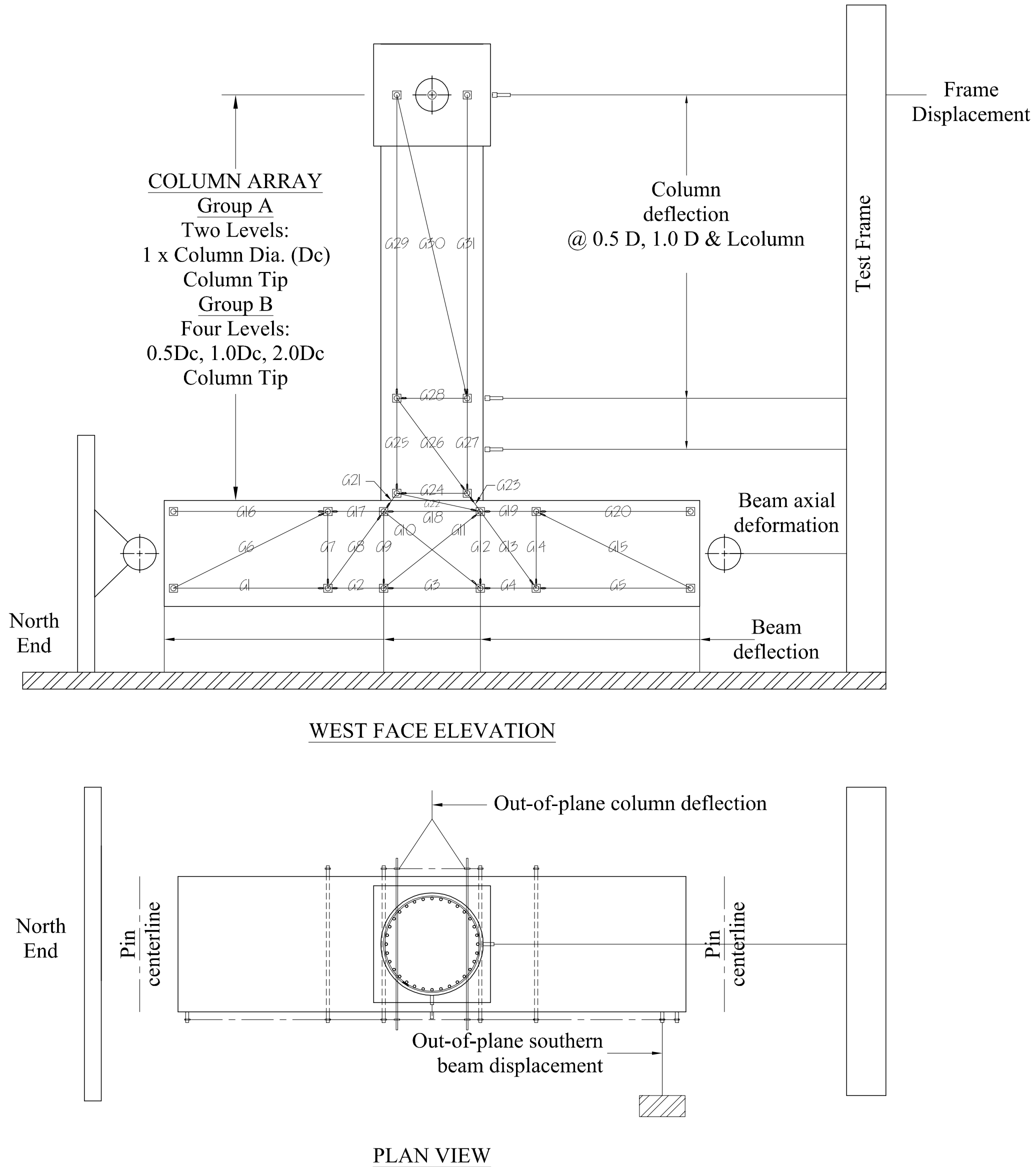

Figure 3-14: External instrumentation

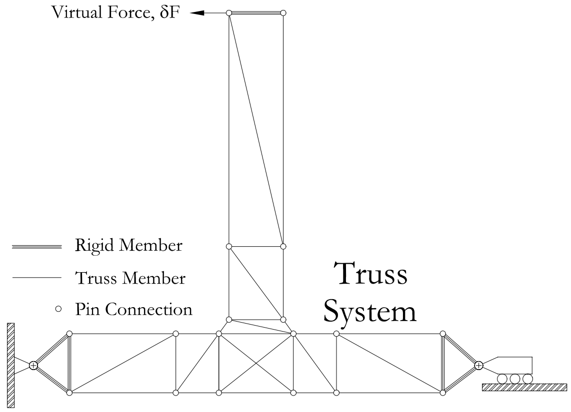

Figure 3-15: Modeled truss system

Two methods can be used to calculate the component displacements from the measurements obtained on the potentiometer array. The first method involves converting all the measured displacements to engineering strains and approximating the component displacement by the shear and flexural deformation at each level of the array. For this purpose, the strain is computed by dividing the displacement of each member by its original length. Flexural deformation is approximated by converting the strains to curvatures and integrating the curvature diagram over the specimen length. Similar methods can be used to estimate the shear and slip contributions to the total displacement. While this method allows one to convert the array displacements to strains and curvatures, it introduces strong assumptions, which may lead to additional errors. For example, using the curvature approximation, the entire column flexural displacement is estimated, in some cases, using only two points. The curvature can be assumed to be linear between the points or piecewise constant. The assumption of a linear distribution is appropriate for the elastic levels. However, when yielding and plastic hinging of the column begins, the curvature distribution is highly nonlinear. If the curvature distribution is assumed to be piecewise constant, the flexural displacement may be overestimated for elastic levels and underestimated for inelastic levels. To overcome these shortcomings, displacements can be computed using a second method that is based on the local member displacements obtained from the virtual truss technique. Flexural deformation results in elongation and contraction at opposing fibers of the cross section. The assumption is made that flexural displacements are captured in the deformation of the horizontal measurements of the beam array and the vertical members of the column array. The flexural contribution to the total tip displacement can thus be calculated with equation (3-3) by setting the displacement of all other array members to zero. Likewise, assuming that shear deformation is captured in the diagonal column and beam measurements, joint deformation in the diagonal joint measurements, and slip is captured in the interface measurements, the component contributions to the total displacement can be found at any point in the displacement history. Application of these techniques is presented in Chapter 5.

Determination of Joint Shear Stress-Strain

Joint performance is best evaluated by an examination of its shear stress-strain behavior. The techniques used to determine these quantities are discussed in the following section. Joint shear strain was extracted from the displacement measurements recorded on the potentiometer array located on the exterior face of the joint (Figure 3-16). The array was then divided into four triangles: ABD, BDC, DCA, and CAB. Using the Cosine Law and the change in length of each leg of the triangle, the change of the angle of each corner, dt_i-t_i, where t_i is equal to the original corner angle, was calculated at each step. The change in angle of each corner of the *array* was then calculated and averaged, thus providing the overall joint shear strain γ at each step.

$$\gamma = \frac{1}{4}\left[\left(\left(dt_1 - t_1\right) + \left(dt_8 - t_8\right)\right) - \left(\left(dt_2 - t_2\right) + \left(dt_3 - t_3\right)\right) + \left(\left(dt_4 - t_4\right) + \left(dt_5 - t_5\right)\right) - \left(\left(dt_6 - t_6\right) + \left(dt_7 - t_7\right)\right)\right] \tag{3-4}$$

Nominal joint shear stress was calculated by evaluating the vertical loads applied to the joint system from the column longitudinal reinforcement. A relationship between the column moment and tension force was derived. From this the vertical tensile load (or joint vertical shear force) was directly resolved from the applied column shear. The following example for the first test specimen, designated A1, is typical of all specimens. It is assumed that the load is monotonically increasing. Thus cyclic effects such as kinematic hardening and accumulation of damage are ignored. As a result, this method presents an upper bound on the vertical joint shear stress.

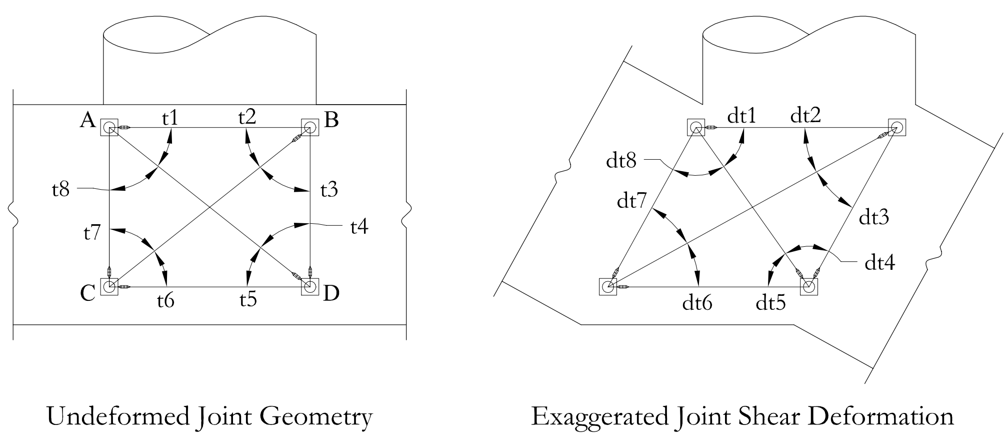

Figure 3-16: Joint instrumentation for shear deformation

A section analysis was conducted on the column cross section at the beam-column interface. As-built properties were used for section geometry and bar locations. Constitutive models were based upon material testing. Concrete modeling was conducted using Mander′s confined and unconfined concrete models for compressive behavior [Mander 1988] and elastic-brittle fracture behavior for tension. Reinforcement was modeled after the material stress-strain results. The relationship between column moment, *M*, and column tension force, *T,* is shown in Figure 3-17.

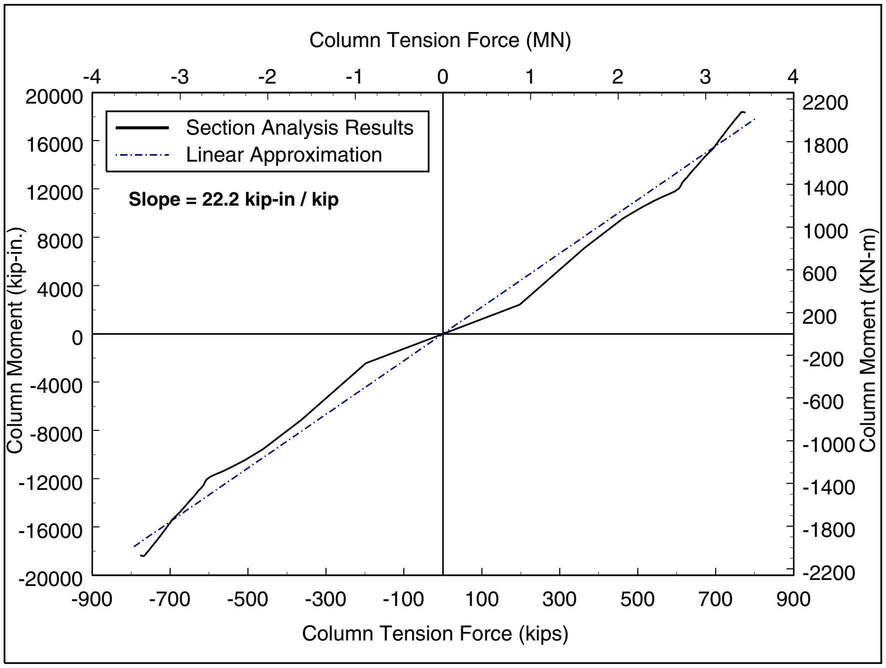

Figure 3-17: Typical moment-tension relationship (A1 behavior shown)

Assuming a linear relation between the moment and tension force, the following relationship was determined:

$$s_m = \frac{M}{T} = 22.2 \frac{kip - in}{kip} \tag{3-5}$$

Using this relation the tensile column force was equated to the applied column shear.

$$M = Vc\ L_{column} \tag{3-6}$$

$$T = M / s_m \tag{3-7}$$

Where M equals the column moment at beam-column interface, Vc equals the measured column tip load, T equals the tension force acting on beam from column, and s_m equals the slope of column moment-tension force relationship. The vertical joint shear stress, V_j, was then determined at section A (Figure 3-18).

$$Vj = \frac{T - Vb}{Aj} = \frac{T - Vb}{b_{bm} \cdot d_{bm}} = \frac{Vc \cdot L_{column} / s_m - Vb}{b_{bm} \cdot d_{bm}} \tag{3-8}$$

Where,

Vj = Vertical joint shear stress.
Vb = Beam shear force.
L_{column} = Column height.
Aj = Joint shear area.
b_{bm} = Beam width.
d_{bm} = Beam depth.

Joint shear stress-strain relations are presented and discussed in chapters 6 and 7. Note three-dimensional finite element analysis conducted in later chapters indicates that the use of the beam width in the calculation of shear stress may be unconservative. Depending upon the joint reinforcement and geometry the column diameter might be used in place of the beam width to provide a mode representative estimation of the effective joint size.

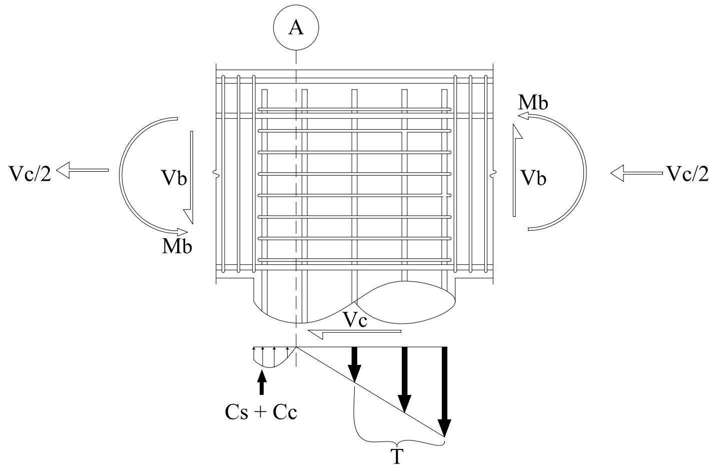

Figure 3-18: Joint forces

3.6.3 Strain Measurement

Strains were measured locally on the reinforcement and at points in the concrete matrix. Reinforcement strains were measured using foil gages mounted on the surface of the reinforcement. Two sizes of foil gages were used, one with a gage size of 0.08 in. by 0.07 in. (2 mm by 1.8 mm) and another with gage size of 0.20 in. by 0.08 in. (5 mm by 2 mm). Both were ″post-yield″ gages with a deformation capability of 10–15% strain. The bar surface deformations in the region surrounding the gage location were removed and the surface was polished. The strain gage was glued to the surface and covered by four protective coatings: air-drying polyurethane, wax, polysulfide liquid polymer compound (providing a tough flexible barrier), and vinyl mastic tape. A Teflon-coated wire was attached to the gages to minimize bonding to the concrete. Steel strains were measured to examine curvature, bond development and shear behavior, as well as other local behavior in the subassembly.

Concrete strain was measured using embedded concrete gages. Two types were investigated. The first type is composed of an instrumented plastic stick, 3.9-in. (100-mm) long with a rectangular cross section 0.08 in. by 0.39 in. (2 mm by 10 mm). Bond is achieved through an array of circular divots on the face of the stick. Testing, however, revealed a loss of bond between the concrete and the gage [Lowes 1996]. Due to the small size of the divots, the concrete mortar filled the voids and sheared during the loading history. A second type of gage consisted also of a plastic resin stick. Various lengths are available: 30 mm, 60 mm, and 120 mm. Unlike the first type, bond was achieved by providing an “Emory-board”-type surface on the plastic. Although some loss of bond occurred in the second type as portions of the gage surface were abraded during cyclic loading, the overall behavior was more desirable. Due to the availability of smaller lengths and cross sections, the second type (60 mm) was used in this investigation. Concrete gages were used primarily for evaluation of bond.

A typical arrangement of strain gages is shown in Figure 3-19. The layout corresponds to the arrangement used on Specimen A1. Longitudinal, transverse, and spiral reinforcement was instrumented. Combinations of concrete rosettes and linear gages were used in the joint region. Variation in number and layout occurred from one specimen to the other. The exact dimensions and arrangement are discussed in relevant subsequent sections.

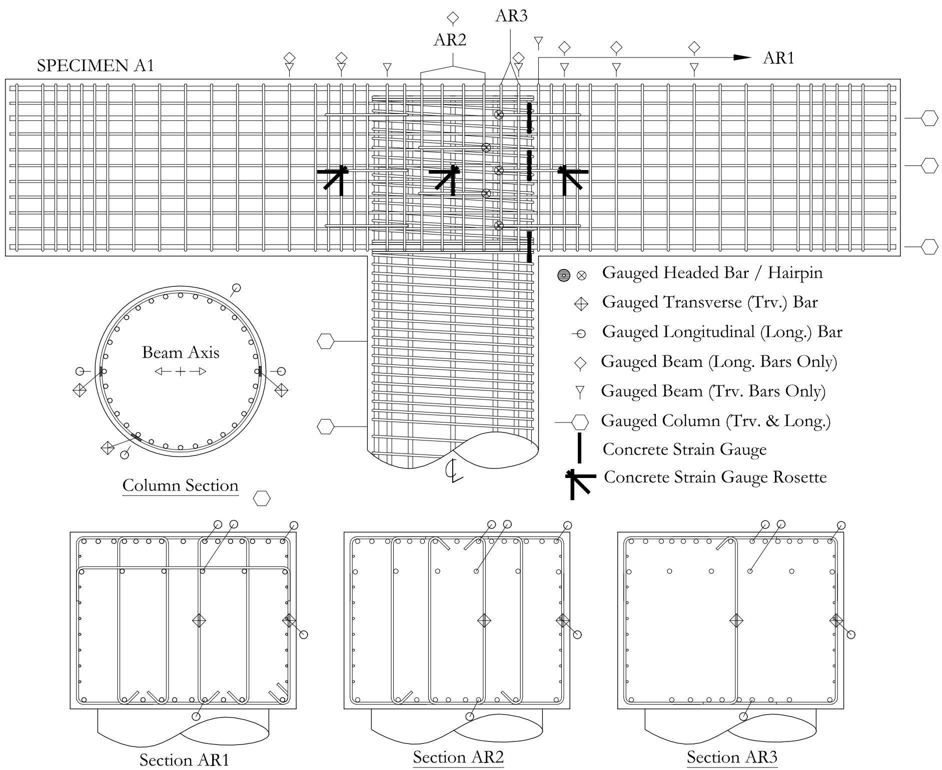

Figure 3-19: Arrangement of strain gages (Specimen A1)

3.7 Experimental Program

The experimental investigation of joint behavior was divided into two groups. The first group (Group A) investigated existing design strategies and the effectiveness of headed reinforcement for use as transverse joint reinforcement. Following testing and a preliminary evaluation of the behavior of the first group, a second group of specimens (Group B) was constructed and tested to failure. The focus of Group B was to investigate joint behavior under high demands. This was achieved by reducing the beam depth and increasing the column capacity. A brief summary of the specimens tested within each experimental group follows.

3.7.1 Group A

In Group A, current California bridge design methodologies as represented in the Bridge Design Specifications [Caltrans BDS 1995] and Memos to Designers [Zelinski 1995] were investigated. This test series consisted of four test specimens, designated A1 through A4. Specimens A1 and A2 are of a circular column configuration (typical of California construction) and A3 and A4 of a square column configuration. As required by Caltrans standards, all the specimens are designed to have an ultimate capacity limited by the flexural strength of the column. Specimens A1 and A3 were designed according to the 1995 Caltrans BDS and constructed using conventional steel reinforcement. Specimens A2 and A4 were designed to the same requirements; however, all transverse reinforcement in the vicinity of the joint was replaced with headed reinforcement. The focus of this series was threefold: first, the effectiveness of joint design requirements was evaluated in specimens A1 and A3; second, the application of headed reinforcement for use as transverse joint reinforcement was quantified in Specimens A2 and A4; and third, the behavior of square column-rectangular beam configurations was evaluated for the development of simplified analytical models. Details of the design methods and joint configurations are presented in Chapter 5 and Appendix C.

3.7.2 Group B

Upon the completion of Group A, two specimens were constructed and tested to evaluate the behavior of the joint under greater joint demands. Both specimens consisted of a circular column and a rectangular beam. The specimens were chosen to model tall bridge structures that typically have a beam depth to column depth ratio on the order of 0.8. As a result, the beam depth was reduced from that used for Group A. In addition, the quantity of column longitudinal reinforcement was increased and the quantity of transverse joint reinforcement was decreased. As a result the joint demands from shear and bond development were elevated (from $11\sqrt{f'_c}$ in Group A to $18\sqrt{f'c}$ in Group B), while the resistance was reduced. Unlike Group A, joint damage and possible failure was expected, providing additional information on the inelastic behavior of the joint. Specimen B1 investigated the effectiveness of overall joint confinement and the use of headed reinforcement. Specimen B2 investigated the effectiveness of spiral reinforcement on joint confinement. The design strategy and final details of Group B are discussed in Chapter 7.

4 Development of Three-Dimensional Nonlinear Finite Element Models

Most current methods of reinforced concrete beam-column joint design are based on a two-dimensional evaluation of the flow of stresses within the joint or using strut and tie methods or nominal stress methods. In general, reinforced concrete bridges are subjected to multi-directional ground motions. Therefore, response of bridge beam-column joints is three-dimensional (3D). Evaluation of existing bridges and development of design requirements for beam-column joints can be improved with 3D models that take into account compatibility, equilibrium, and the constitutive properties of the different materials. Many computational methods exist for modeling systems in three dimensions; how well these models reflect the actual behavior of reinforced concrete bridges, particularly systems subjected to seismic loading, is not clear. This chapter investigates 3D finite element methods for application to reinforced concrete bridges using available techniques and solution strategies. An effective procedure for modeling these systems in three dimensions is presented. The results of these modeling techniques are adopted and discussed in the following chapters.

The present research aims toward complementing the experimental program presented in Chapter 3 with the goal of improving the understanding of the structural response of reinforced concrete bridge beam-column joints. The 3D finite element analysis is intended to provide detailed results of the stress state, damage (cracking and plastification of concrete and yielding of reinforcement) initiation and propagation, and deformation experienced by the different components of the tested subassemblage. The developed 3D model will be used in Chapter 8 to conduct parametric studies aiming toward providing guidelines for joint design, particularly joint transverse reinforcement requirements.

4.1 Development of Models

4.1.1 Modeling Concrete in Three Dimensions

To limit the computational cost of the model, the concrete is discretized using trilinear eight-node isoparametric brick elements. A 2 x 2 x 2 Gaussian integration scheme is used over the brick elements (Figure 4-1).

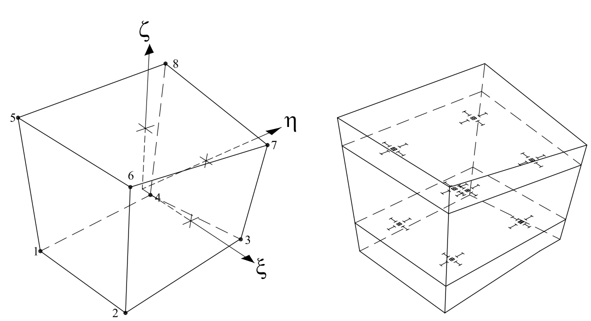

Figure 4-1: Trilinear brick element: node and Gaussian point locations using a 2x2x2 integration scheme

A standard finite element displacement formulation is used in this investigation. Displacement vector, $\{u\}$, within each element is interpolated from the vector of nodal degrees of freedom, $\{d\}$, using trilinear shape functions for the element, $[N]$, i.e.,

$$\{u\} = [N]\{d\} \tag{4-1}$$

The strain tensor within the element, $\{\varepsilon\}$, is then obtained from the displacement by differentiation, i.e.,

$$\{\varepsilon\} = \partial\{u\} \tag{4-2}$$

where ∂ is the usual differential operator used in the case of small deformation. Combining equations (4-1) and (4-2), the strain can be evaluated directly from the nodal displacements.

$$\{\varepsilon\} = \partial[N]\{d\} = [B]\{d\} \tag{4-3}$$

Using the principle of virtual work, the element stiffness matrix can be computed such that

$$\text{External Work} = \text{Internal Work} \;\Rightarrow\; \delta\{u\}^T\{r\} = \int_V \delta\{\varepsilon\}^T\{\sigma\}\; dV \tag{4-4}$$

where $\{r\}$ is the vector of element external loads, δ indicates a virtual quantity, $\{\sigma\}$ is the stress tensor within the element, and V represents the element volume. From equations (4-3) and (4-4), the following element stiffness matrix, $[k]$, can be derived as

$$[k] = \int_V [\mathrm{B}]^T[E][\mathrm{B}]\; dV \tag{4-5}$$

where $[E]$ is the constitutive matrix. In this study, the nonlinear behavior due to material damage is reflected in the matrix $[E]$. The global system of equations, in terms of the global stiffness, $[K]$, global nodal loads, $\{R\}$, and the global nodal displacements, $\{D\}$, becomes

$$[K]\{D\}=\{R\} \tag{4-6}$$

It is worth mentioning that $[K]$, $\{D\}$, and $\{R\}$ are obtained from $[k]$, $\{d\}$, and $\{r\}$ using standard assembly procedures. The theory of finite elements for linear and nonlinear problems is well documented in many textbooks, e.g., Cook 1989, Zienkiewicz and Taylor 1989, Zienkiewicz and Taylor 1991.

4.1.2 Modeling Reinforcement in Three Dimensions

Reinforcement is often modeled by one of two methods. The first method, which is less computationally demanding, involves the use of embedded or smeared reinforcement. The second method, more computationally expensive, involves separate discretization of the reinforcement. The second model allows for the investigation of bond-slip behavior of reinforcement with respect to the surrounding concrete. In this case, the reinforcement can be modeled as a discrete truss element attached to the adjacent concrete element through a series of interface elements. This technique carried out over the entire system becomes computationally expensive because of the need to introduce double nodes at the location of the reinforcement (one node on the concrete and another on the steel). These nodes are then connected by the interface elements.

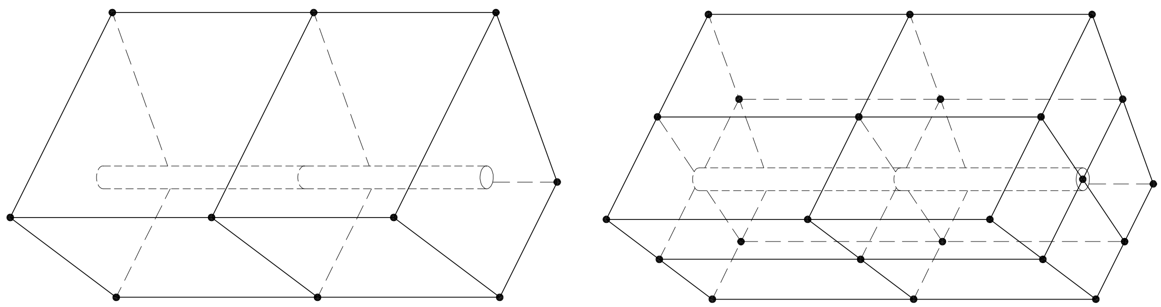

Figure 4-2: Reinforcement elements

Figure 4-2 illustrates the modeling of a 3D reinforced concrete component using both techniques. It is clear that when embedded reinforcement is adopted, two brick elements with 36 degrees of freedom can be used. On the other hand, discrete representation of reinforcement requires the use of eight brick elements for concrete and two truss (or beam) elements for the reinforcement in addition to interface elements between the steel and the concrete to represent the possible slip and dowel actions. This latter modeling technique will require solving for 90 degrees of freedom.

To limit the cost of the more accurate discrete modeling, combined modeling approaches can be followed, using embedded reinforcement for the majority of the bars and discrete reinforcement with interface elements at locations where potential slip exists. For example, in a bridge beam-column connection, the developed portion of the extreme column reinforcement in the joint should be modeled as discrete bars with interface elements. The remaining reinforcement can be modeled as embedded. The evaluation presented in this work is limited to the use of embedded reinforcement only.

Embedded Reinforcement

Embedded reinforcement is introduced within the concrete element through which it passes (referred to as the parent element). The stiffness of this "parent element" is then modified based on the path of the reinforcement through the element. As a result, the assumption is made that there exits perfect bond between the concrete and the reinforcement.

For the simple case where a uniform quantity of reinforcement is distributed across the element at a certain angle from the element natural coordinate system, the additional stiffness terms are easily computed as follows. Given that the *element* displacements are computed from the nodal displacements, (see Eq. (4-1)), the *reinforcement* displacements, $\{u\}^{\mathrm{r}}$, can be found using the same interpolation.

$$\{u\}^{\mathrm{r}} = [N]\{d\} \tag{4-7}$$

The same shape function matrix, [N], is used. However, it is evaluated at the isoparametric coordinates of the reinforcement integration points (2-point Gaussian integration scheme is used in the present study). The strain vector of the reinforcement can now be evaluated by

$$\{\varepsilon\}^{\mathrm{r}} = [B]^{\mathrm{r}}\ \{d\} \tag{4-8}$$

where $[B]^r$ is the strain-displacement matrix evaluated at the *reinforcement* integration points.

Standard transformation techniques are used to obtain the reinforcement strain tensor in the same orientation as the element strain tensor. Making use of transformation, reinforcement constitutive equations, and usual finite element procedure, one can obtain the contribution of reinforcement to the stiffness of the parent element and the corresponding internal force vector of the reinforcement. For details, refer to Feenstra [1993].

If the reinforcement is introduced in a nonlinear trajectory through the concrete element, such as the case of spiral reinforcement in a circular column, a general transformation matrix can be developed dependent upon the location and curvature of the reinforcement. The finite element package DIANA7[1] is used in the present investigation. In DIANA [Witte 1998], each bar is divided into segments. Each segment consists of the portion of the bar passing through the parent element. Reinforcement location points are then determined for each segment. For a two-point integration scheme, three location points are defined: two at the element boundaries and a third at the center of the bar segment (Figure 4-3). These points are used to describe the path and the curvature of the bar segment within each element. Numerical integration of each segment is then conducted along the isoparametric axis, ξ, of the segment. At each integration point an axis, x', tangent to the bar is determined using the segment location points. By transformation and use of the nodal displacements, the bar stress, σ_{xx}, and strain, ε_{xx}, can be evaluated.

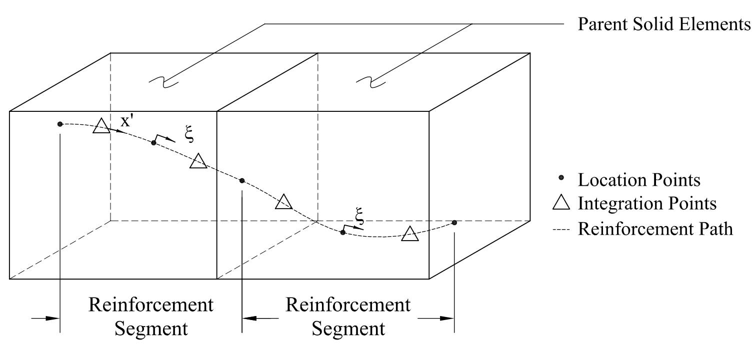

Figure 4-3: Reinforcement axes and discretization

In summary, embedded reinforcement is assumed to be perfectly bonded to the concrete element through which it passes. The strains and stresses in the reinforcement are coupled to the element nodal displacements. These values can be computed directly from the element shape functions and nodal displacements and are oriented tangent to the reinforcement path. The stiffness and internal force contributions of the reinforcement are accounted for in a similar manner as the element stiffness and internal forces with the exception that integration is performed at the *reinforcement* integration points and not the *element* integration points.

4.2 Constitutive Models

The constitutive models used in the finite element analysis are based on the mechanical properties of the concrete and reinforcement measured in the experimental investigation. Mechanical properties such as the moduli of elasticity and rupture, splitting tensile strength, compressive stress-strain relation, and the magnitude of fracture energy were determined through experimental testing by standard methods [ASTM and 50-FMC]. Extrapolation of these tests to a comprehensive model that provides not only the proper behavior but also a robust numerical formulation required the investigation of several available strategies. The development and justification of the constitutive relations used in this study are presented in this section.

4.2.1 Constitutive Modeling of Concrete

Concrete is a complex material; it is anisotropic and nonhomogeneous, and the tensile and compressive properties are dissimilar. Furthermore, concrete is a quasi-brittle material; it fails in compression through crushing and in tension through cracking. To establish a proper model, five areas of response must be evaluated: (1) the tensile yield surface, (2) the compressive yield surface, (3) tension-softening relationships, (4) compression hardening and softening relationships, and (5) cracking behavior (initiation, propagation, and closure).

Typically, a three-dimensional yield surface is created by combining the compressive yield surface of an established model with a tension cutoff. Another technique uses a total strain formulation as the basis for the rotating-crack approach. In this approach, a yield surface is not directly adopted. Instead, the constitutive relationship is defined in the principal strain state. The background and behavior of these two techniques are discussed in the following sections.

4.2.2 Modeling Concrete Compressive Response

Modeling plasticity of concrete in compression involves the use of a yield criterion, a flow rule, and hardening rules. The yield criterion is defined by setting the yield equation, f, equal to zero. The yield equation is dependent on the state of stress, σ, and the internal state variable, κ. The compressive behavior of concrete is often modeled with J_2 plasticity models, either the Von Mises or Drucker-Pager yield criterion. For J_2 plasticity, the following definitions for stress invariants (J_2 and I_1) are given by

$$J_2 = \frac{1}{6}\left[(\sigma_1 - \sigma_2)^2 + (\sigma_2 - \sigma_3)^2 + (\sigma_3 - \sigma_1)^2\right] \tag{4-9}$$

$$I_1 = \sigma_1 + \sigma_2 + \sigma_3 \tag{4-10}$$

where the principal stress tensor is defined by

$$\{\sigma\} = \{\sigma_1 \ \ \sigma_2 \ \ \sigma_3\}^{\mathrm{T}} \ ; \ \ \sigma_1 \geq \sigma_2 \geq \sigma_3 \tag{4-11}$$

---

[1] DIANA7 (DIsplacement ANAlyzer version 7) is a finite element code developed at TNO Building and Construction Research in the Netherlands.

The Von Mises yield criterion is defined as follows:

$$f(J_2, \kappa) = \sqrt{3J_2} - \bar{\sigma}(\kappa) \tag{4-12}$$

The term, $\bar{\sigma}(\kappa)$, represents the uniaxial hardening rule, which is discussed in the next section. Von Mises yield criterion is characterized by a circular yield surface perpendicular to the hydrostatic axis $\sigma_1 = \sigma_2 = \sigma_3$ (Figure 4-4(a)(b)).

When concrete is subjected to triaxial compressive stress, its capacity is increased. Compression tests performed on concrete with biaxial lateral confining stress (σ_3=0) have shown an increase in strength on the order of 16% over the uniaxial capacity [Kupfer 1973]. Therefore, the Drucker-Prager as a pressure-dependent yield criterion also is investigated. In this case, the expression for the yield surface, *f*, is

$$f(I_1, J_2, \kappa) = \sqrt{3J_2} - \alpha I_1 - \beta \bar{c}(\kappa) \tag{4-13}$$

The parameters α and β, and the cohesion, $\bar{c}$, are calculated using the following equations.

$$\alpha = \frac{2\sin\phi}{3 - \sin\phi} \tag{4-14}$$

$$\beta = \frac{6\cos\phi}{3 - \sin\phi} \tag{4-15}$$

$$\bar{c} = \sigma_3 \frac{1 - \sin\phi}{2\cos\phi} \tag{4-16}$$

Note that all parameters are dependent on the angle of internal friction, ϕ. σ_3 in Eq. (4-16) is taken as the uniaxial compressive stress which is a function of the plastic strain. The yield surface grows along the hydrostatic axis (Figure 4-4(c)). To properly account for this growth for concrete, the angle of internal friction is set to 10 degrees [Kupfer 1973].

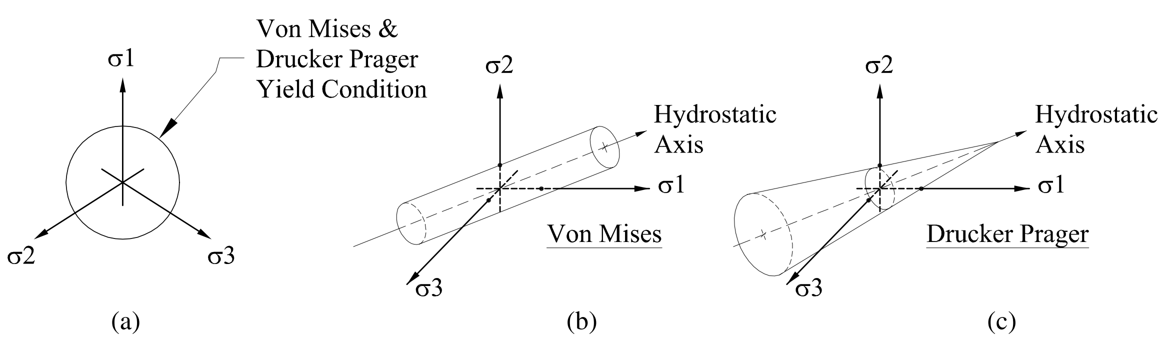

Figure 4-4: Von Mises and Drucker-Prager yield surfaces

For simplicity in the present investigation, exclusive use is made of the associated flow rule, (i.e., angle of internal friction is taken equal to the angle of dilatancy).

4.2.3 Uniaxial Compression Hardening / Softening Behavior

The uniaxial hardening and softening behavior of concrete is derived from experimental testing of concrete cylinders. Hardening behavior is extrapolated from compressive stress-strain evaluation of 6 in. by 12 in. concrete cylinders tested the day of the subassembly experiment. The softening branch was derived later from strain-control testing of additional cylinders (Appendix B). The average descending branch was normalized to the peak stress and the corresponding strain of the hardening branch. The resulting response is illustrated in Figure 4-5. The relationship between plastic uniaxial strain, ε_p, and the total uniaxial strain is also presented. The comparative cohesion for a 10-degree friction angle is also shown. Note that for incorporating the hardening-softening behavior of concrete for the Von Mises yield criterion the relation $\bar{\sigma} - \varepsilon_p$ of Figure 4-5 is discretized and directly used (i.e., $\kappa = \varepsilon_p$). On the other hand, the Drucker-Prager criterion utilizes the relation $\bar{c} - \kappa$. To obtain this relationship from the $\bar{c} - \varepsilon_p$ relation given by Figure 4-5, the following conversion is used [Witte 1998]:

$$\kappa = \frac{\sqrt{1+2\alpha^2}}{1-\alpha}\varepsilon_p \tag{4-17}$$

Accordingly, for a friction angle $\phi = 10$ and $\alpha = 0.123$, $\kappa = 1.157\varepsilon_p$.

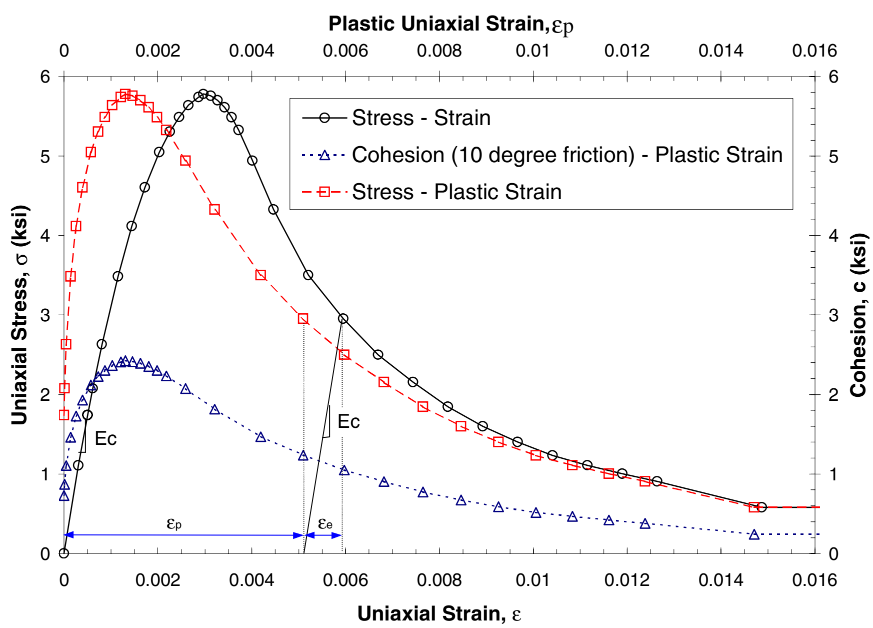

Figure 4-5: Typical uniaxial hardening / softening behavior used for concrete modeling

4.2.4 Concrete Tension Behavior

The tension yield surface typically consists of either a constant cutoff (Rankine yield surface) equal to the tensile concrete capacity or a bilinear envelope from the uniaxial tensile strength to the uniaxial compressive strength in the tension-compression regime combined with Rankine yield surface in the tension-tension regime (Figure 4-6). The bilinear yield surface is used in this investigation.

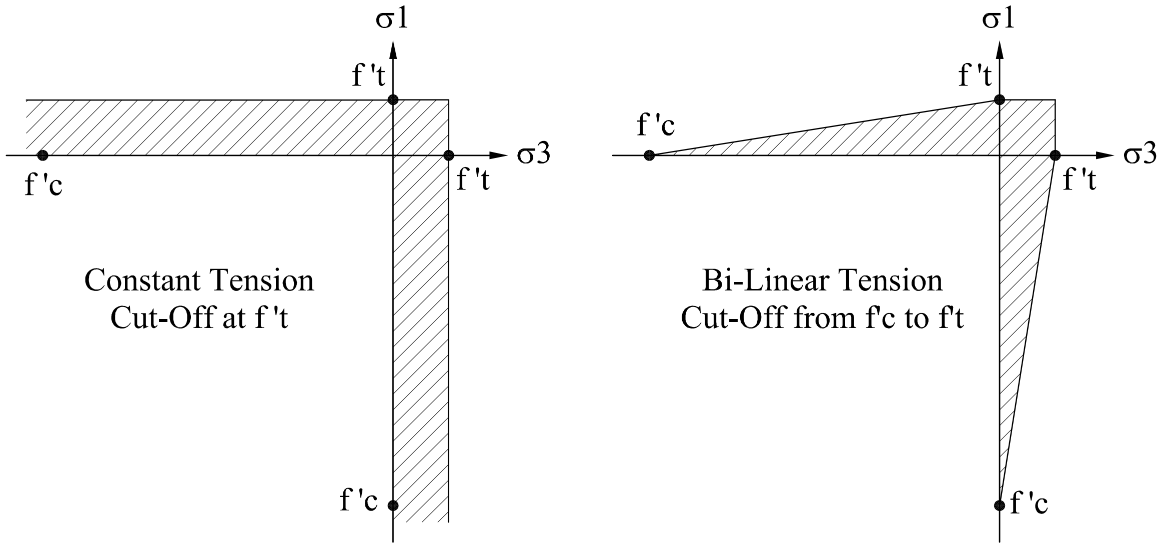

Figure 4-6: Tension cut-off models

The tensile stress-strain behavior consists of two phases: the hardening branch and the softening branch. The hardening branch is made up of a linear segment with a slope equal to the concrete elastic modulus. The softening branch may consist of a variety of functions. Four softening behaviors are investigated: brittle failure, linear tension softening, nonlinear softening, and bilinear softening (Figure 4-7(a)–(d)). There is some contention over the appropriate use of each model. Brittle failure assumes that when a crack occurs in an element, the concrete abruptly loses all tensile capacity perpendicular to the crack direction (Figure 4-7(a)). As shown in Figure 4-8, however, *unreinforced* concrete subjected to tension typically fails with a nonlinear decaying branch (Figure 4-7(c)). This decay is controlled by the fracture energy density of the concrete, g_f, (i.e., the amount of energy per unit volume of cracked concrete released in forming a crack with unit area). In the brittle model, the gradual dissipation of fracture energy is not accounted for. Consequently, the brittle model is considered conservative. One can argue that for reinforced concrete with a high volume of steel, the softening branch should be even greater than the unreinforced concrete behavior, and should be modeled as linear tension softening limited by the yield strain of steel, ε_y (Figure 4-7(b)). As cracks occur, the prevalence of reinforcement theoretically will restrain the crack. The restraint, in turn, limits the development of the crack opening and propagation in the element and the full loss of strength until the reinforcement loses a significant portion of its stiffness, i.e., it yields. To complete the evaluation, two additional models are investigated. One investigates the effect of using nonlinear softening. For that purpose Hordijk′s tension-softening model was used (Figure 4-7(c)). This model provides a good approximation of the measured unreinforced concrete tension-softening behavior (Figure 4-8). The final relationship uses a combination of brittle cracking (i.e., sudden drop to 10% of tensile capacity across the crack on crack formation) followed by linear tension softening to five times the cracking strain (Figure 4-7(d)).

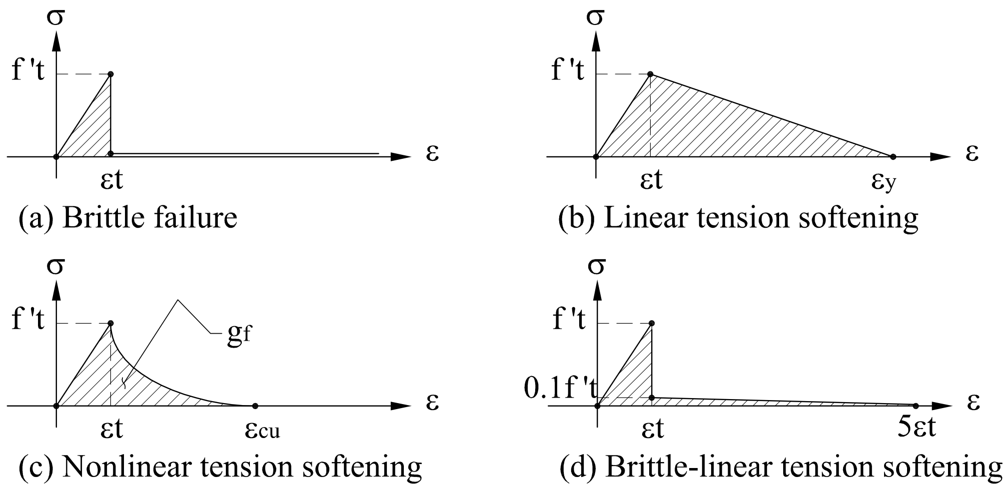

Figure 4-7: Uniaxial tension-softening models (Note: graphs not to scale)

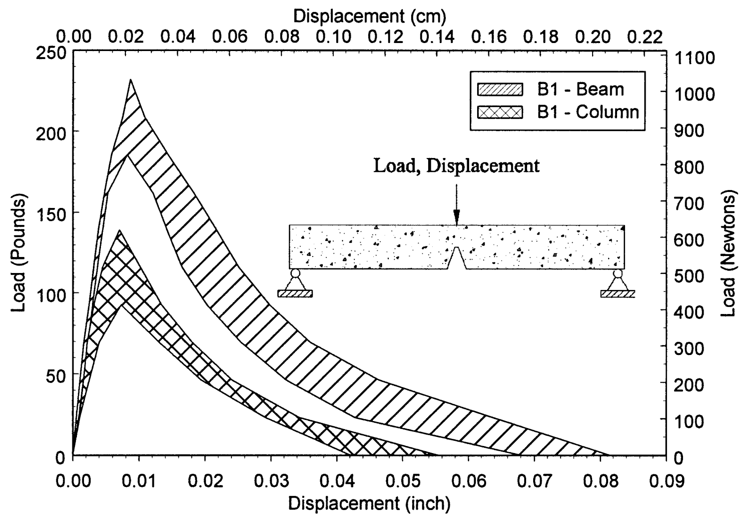

Figure 4-8: Envelopes of tensile failure response for unreinforced concrete

When using embedded reinforcement (i.e., without allowance for slip between reinforcement and the surrounding concrete), with stress-strain properties obtained from testing a bare bar, the stress-strain relation of the reinforcement should account for the tension-stiffening effects in reinforced concrete. In moderately or heavily reinforced elements, this effect may become more dominant than any material behavior [Farve 1985]. Accounting for this tension-stiffening is complicated when the reinforcement is aligned in three dimensions and when cracks intersect the reinforcement at different orientations. To evaluate the effect of tension softening (and stiffening) on the global system behavior, the response of the four softening σ-ε models are compared (Figure 4-7). In this investigation, fixed-crack formulation is utilized as will be discussed in Section 4.2.5.

For the Hordijk tension-softening model [Hordijk 1992], the fracture energy, G_f, calculated from fracture energy tests [50-FMC] shown in Figure 4-8. The crack bandwidth, *h,* was taken to be related to the element size as follows:

$$h = \sqrt[3]{finite\ element\ volume} \tag{4-18}$$

Note that

$$G_f = g_f\, h \tag{4-19}$$

The limit crack strain ε_{cu} and the shape of the descending branch are determined as follows:

$$\sigma_{cr}(\varepsilon_{cr}) = f'_t \cdot \begin{Bmatrix} \left(1 + \left(c1 \cdot \dfrac{\varepsilon_{cr}}{\varepsilon_{cu}}\right)^3\right) \exp\left(-c_2 \cdot \dfrac{\varepsilon_{cr}}{\varepsilon_{cu}}\right) - \dfrac{\varepsilon_{cr}}{\varepsilon_{cu}}\left(1 + c_1{}^3\right)\exp(-c_2) & \text{if } 0 < \varepsilon_{\mathrm{cr}} < \varepsilon_{cu} \\ 0 & \text{if } \varepsilon_{cu} < \varepsilon_{cr} < \infty \end{Bmatrix} \tag{4-20}$$

where parameters $c_1 = 3.00$, $c_2 = 6.93$, and

$$\varepsilon_{cu} = 5.136 \frac{G_f}{h \cdot f_t'} \tag{4-21}$$

In the above expression, the decomposition of the strain tensor into cracked $\{\varepsilon_{cr}\}$ and uncracked $\{\varepsilon_{co}\}$ as discussed in Section 4.2.5 is implied.

Performing the finite element analysis of the specimen designated A2 of the experimental program mentioned in Chapter 3, the analytical results are compared with the experimental results to select a proper model for the softening branch of the tensile σ-ε relation. The load-displacement responses are compared with the experimental envelope from the onset of cracking to initiation of column yielding. After this demand level, the behavior is controlled by the reinforcement constitutive relationship.

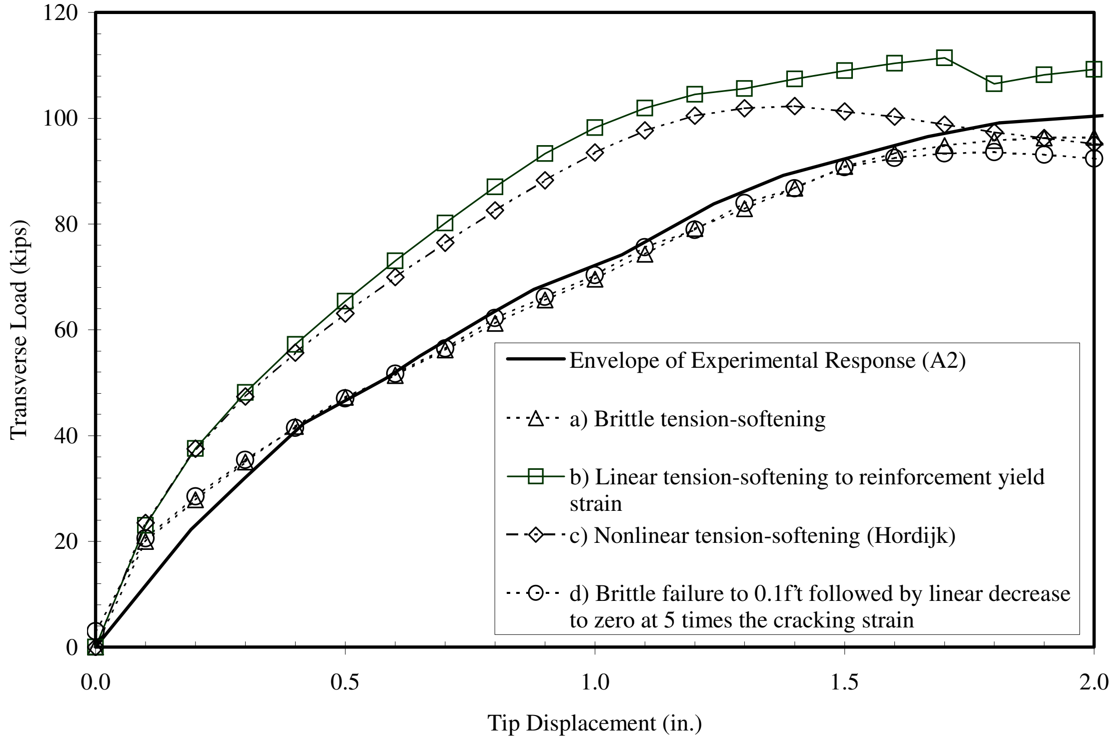

Figure 4-9: Effect of tension softening on the load-displacement relationship of a three-dimensional finite element beam-column model

Linear tension softening to the yield of the steel produces the highest stiffness, and the brittle failure results in the lowest (Figure 4-9). It is concluded that linear and nonlinear concrete tension softening overestimates the stiffness in 3D analyses when used in conjunction with embedded reinforcement and fixed-crack formulation. Nonlinear softening produces results comparable to that of linear softening. The assumption of brittle failure produces a good estimation of the experimental response. Use of a brittle model, however, requires that the reinforcement hardening properties be adjusted to account for tension stiffening. As a compromise to this argument, the fourth model, which combines a brittle failure with an unloading branch, was adopted for the remainder of this investigation. This model also avoids any numerical difficulty that may be encountered with the brittle model.

4.2.5 Modeling Cracking in Concrete

Once concrete reaches its tensile capacity it cracks and loses a large portion of its tensile strength. To properly model concrete in a finite element formulation, this behavior must be addressed. To accomplish this, a smeared crack formulation is used. Smeared cracking, also known as crack band theory [Bazant and Oh 1983], has been used extensively for modeling cracking of reinforced concrete. Consequently, many analysis packages include a predeveloped formulation within their options. In the present study, two methods of crack estimation are evaluated: the multi-directional fixed-crack model and the rotating-crack model.

Multi-Directional Fixed-Crack Model

If a concrete element is subjected to strains beyond its tensile capacity, one or more cracks may form. The total incremental strain in the element, $\{\Delta\varepsilon\}$, then becomes a combination of the uncracked concrete incremental strain (between the smeared cracks), $\{\Delta\varepsilon_{co}\}$, and the incremental strain occurring across the crack, $\{\Delta\varepsilon_{cr}\}$ [Rots 1988]; accordingly,

$$\{\Delta\varepsilon\} = \{\Delta\varepsilon_{co}\} + \{\Delta\varepsilon_{cr}\} \tag{4-22}$$

Assuming that the crack forms at a given angle, the local incremental crack strain, Δe_{cr}, can then be defined relative to the crack normal axis, *n,* and tangential axis, *t,* in two dimensions. In three dimensions, a second tangent axis, *s,* is used (Figure 4-10). Therefore, the crack will be subjected to increments of normal strain Δe_{cr}^{nn} and shear strains Δe_{cr}^{nt} and Δe_{cr}^{ns} (if used in 3D).

$$\{\Delta e_{cr}\} = \left[\Delta e_{cr}^{nn} \quad \Delta e_{cr}^{nt} \quad \Delta e_{cr}^{ns}\right]^T \tag{4-23}$$

The concept of fixed cracking assumes that the crack forms when the principal tension stress in the element reaches the tensile capacity of the material. At this level, a crack forms perpendicular to the principal tension axis. The crack orientation then becomes fixed. When shear retention is considered, i.e., shear stresses are transferred in the direction parallel to the fixed cracks, the principal stresses rotate relative to the fixed crack. Subsequently, crack strain continues to increase along the fixed orientation. The crack remains *fixed* until the principal tension reaches the tensile capacity at a threshold angle, α, from the current crack orientation. A threshold angle of 60 degrees is used in the present study. This eliminates the multiple formation of cracks at small angles from each other.

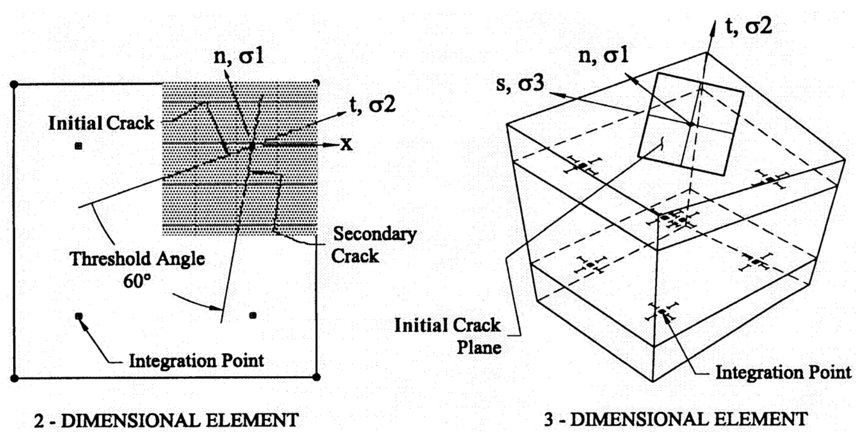

Figure 4-10: Crack orientation in an element (σ1, σ2, σ3 are principal stresses at initiation of first crack)

The incremental stress tensor, $\{\Delta s_{cr}\}$, in the crack direction contains the normal stress, Δs^{nn}, dependent on the amount of tension softening assumed, and the shear stresses, Δs^{nt} and Δs^{ns}, dependent on the shear retention model used, i.e.,

$$\{\Delta s_{cr}\} = [\ \Delta s^{nn} \quad \Delta s^{nt} \quad \Delta s^{ns}\ ]^{\mathrm{T}} \tag{4-24}$$

Using a transformation matrix, $[N_{cr}]$, dependent on the orientaion of the fixed crack, one may write

$$\{\Delta\varepsilon_{cr}\} = [N_{cr}]\,\{\Delta e_{cr}\} \quad \text{and} \quad \{\Delta s_{cr}\} = [N_{cr}]^{T}\,\{\Delta\sigma\} \tag{4-25}$$

where $\{\Delta\sigma\}$ is the global incremental stress tensor. The global relationship between the stress and strain increments for the element then becomes a combination of the constitutive relationship of the uncracked concrete, $[D_{co}]$, and the constitutive relationship of the cracked portion, $[D_{cr}]$. The uncracked material stiffness matrix is defined by the usual elasticity matrix in 3D. The cracked stiffness is specified independently for the three modes of failure: mode I normal crack opening D^{I}, and modes II and III crack shearing D^{II} and D^{III}. To simplify the formulation the assumption is made that the shear and normal behaviors are decoupled, i.e.,

$$[D_{cr}] = diag\,[\,D^{I}\;\; D^{II}\;\; D^{III}\,] \tag{4-26}$$

Mode I stiffness, D^{I}, is dependent on the tension-softening model used. Modes II and III stiffnesses, D^{II} and D^{III}, are dependent on the shear retention factor β as follows:

$$D^{II} = D^{III} = \frac{\beta}{1-\beta}\cdot G_c \tag{4-27}$$

G_c is the concrete elastic shear modulus = $E_c\,/\,(2(1+\nu_c))$, where E_c and ν_c are Young′s modulus and Poisson′s ratio of the uncracked concrete, respectively. The β term varies from 1 (0.999 in numerical implementation) for uncracked concrete to 0 for completely cracked concrete, and allows the control of shear resistance as a function of strain normal to the crack. Studies by Paulay and Loeber [1974] have shown that the shear stiffness across a cracked concrete section is dependent on the crack opening or strain, e_{cr}^{nn}. To accomplish this, β is made a function of the normal crack strain as follows [Frenray 1990]:

$$\beta = \frac{1}{1+\mu\varepsilon_{cr}^{nn}} \tag{4-28}$$

Where μ = 4447 is an empirical constant. A similar model was derived for use in the modified compression field theory [Vecchio and Collins 1998].

One of the disadvantages of the multi-directional fixed-crack model is the possible stress locking due to rotation of principal axes while the crack angle remains fixed. This is particularly significant for large values of shear retention [Rots 1988 and Mosalam 1998]. In this case, due to the nonzero values of D^{II} and D^{III}, shear stresses may occur in the orientations of the original principal stress directions at crack onset. As a result, the direction of the actual (current) principal stresses may be forced to rotate from the original directions leading to the formation of new cracks. To avoid this fictitious “stress chasing” behavior, a small shear retention value and a large threshold angle can be used. A sounder solution is to adopt the rotating-crack model as discussed in the following section.

Rotating-Crack Model

To account for the formation of multiple cracks at a point without the effect of stress locking, the rotating-crack model can be used. Formulation of the rotating model is based on the concept of the coaxial stress-strain relation, in which the stress-strain relationships are evaluated in the principal directions of the strain tensor. Unlike the fixed-crack model, the rotating model assumes that cracking strains can be generated by up to three orthogonal cracks that remain aligned with the principal directions of both stress and strain [Jirasek and Zimmerman 1997]. The incremental cracking strain can be written as

$$\{\Delta e_{cr}\} = \{\ \Delta e_{c1}\ \ \Delta e_{c2}\ \ \Delta e_{c3}\ \}^{T} \tag{4-29}$$

where Δe_{c1}, Δe_{c2}, and Δe_{c3} are the cracking strains normal to the crack planes and corresponding to the individual principal directions. Cracking initiates when the principal stresses reach the uniaxial tensile strength of the concrete. The relationship between the principal stress and the normal incremental crack strain is given by

$$\sigma_i = g(\Delta e_{cr\,i}), \quad i = 1, 2, 3 \tag{4-30}$$

If the element is subjected to triaxial tension, up to three orthogonal cracks can be present at the same point. This is different from the fixed-crack model, which allows the formation of only one crack at a given point and time. The function g depends on the current state of cracking. If the material is uncracked, the cracking strain is zero and remains so until the tensile strength is reached. Once this occurs, the function represents the softening law for the cracked concrete. This law is dependent on whether the crack is opening or closing. For crack opening, the brittle-linear tension-softening model is used (Figure 4-7(d)). A secant-unloading path is assumed.

Global incremental strain is calculated directly from the incremental cracking strains as follows:

$$\{\Delta\varepsilon_{cr}\} = [\ T\ ]\ \{\ \Delta e_{cr}\ \} \tag{4-31}$$

where T is the strain transformation matrix. In the rotating-crack concept, the transformation matrix is dependent on the current state of strain. Consequently, the transformation matrix rotates with the principal stresses. This provides a more accurate representation of crack formation. Using the multi-directional fixed-crack model, a crack can exist in a direction other than that of the principal tensile strain. In the rotating-crack model, the crack is always oriented normal to the principal tensile strain when it exceeds the cracking strain. Therefore, definition of the shear retention factor is not necessary. This technique was adopted for the joint evaluation studies presented in later chapters. Note that the adopted rotating-crack model is based on the concept of total strain. This technique does not make use of Von Mises or Rankine yield surfaces. Instead, the model is formulated along the same lines as the modified compression field theory first developed by Vecchio and Collins [1986].

To model rotating cracks the total strain model is adopted. For this model, a tension and compression relationship (Section 4.2.6) is used based on the appropriate constitutive properties. The relationship is then evaluated in the direction of the principal strains. This model can be used for both fixed and rotating-crack formulations.

4.2.6 Comparison of Concrete Compression Models

The effect of yield criteria was studied to determine which modeling technique best captures the measured response. Four concrete compression yield criteria were evaluated: (1) Von Mises yield criteria, (2) total strain formulation, (3) Drucker-Prager yield criteria using a friction angle of 10 degrees, and (4) elastic response. The study was conducted on a full subassembly using brittle concrete tensile response and multi-directional fixed-crack formulation. An experimentally determined stress-strain relation is adopted (Figure 4-5). The results are presented in Figure 4-11.

Elastic concrete compression provides an upper bound on the response. Under this condition, as the reinforcement yields, the concrete does not crush in compression but continues to increase, resulting in a divergence between the elastic and measured responses. The Drucker-Prager model produces a similar response due to an overestimation of the triaxial state of stress. When an element is subjected to triaxial compression, the Drucker-Prager yield surface infinitely increases. Thus, the column compressive strength continues to increase almost achieving an elastic compressive response. The Von Mises yield criteria provides a good estimation of the experimental response. As with Drucker-Prager, Von Mises yield criteria overestimates the response because of the triaxial state of compression; however, the yield surface does not increase in size along the hydrostatic axis. Consequently, the triaxial compression stress only marginally overestimates the response. The most accurate estimation of response was achieved using the total strain model. Concrete compressive capacity and overall response is accurately estimated. Consequently, the total strain model was adopted for the concrete compressive response in all investigations conducted in later chapters.

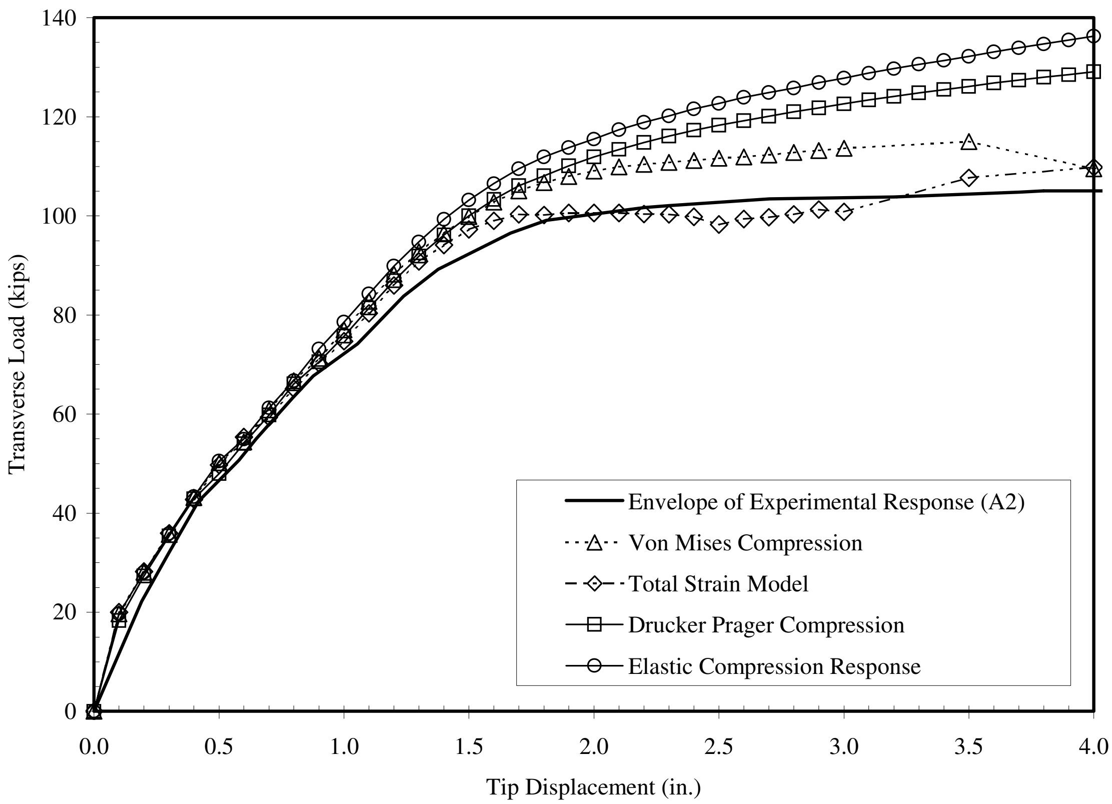

Figure 4-11: Effect of concrete compression relationship on overall system response

4.2.7 Comparison of Cracking Models

Two methods of modeling crack formation were evaluated: multi-directional fixed-crack formulation and rotating-crack formulation. Two cases of fixed-crack formulation were investigated. The first assumes a nominal shear retention (β = 0.2) and the second assumes that the shear retention along the crack is proportional to the crack strain according to Eq. (4-27). The study was conducted on the full subassembly using brittle concrete tensile response.

The rotating-crack model produces the lowest strength, slightly underestimating the experimental results (Figure 4-12). The fixed-crack models produce a stiffer response with higher strength. This can be attributed to the fixed-crack formulation, which assumes that a shear stress exists along the crack. Consequently, the formulation produces additional stiffness and strength compared with that of the rotating-crack model, which does not have any shear resistance along the crack (since the crack is always oriented along principal directions where shear stress is zero). Increasing the shear component in the fixed-crack formulation (i.e., accounting for higher β), further magnifies this effect. The rotating-crack model was adopted for all investigations since it provides a good estimate of response as well as a more rational formulation.

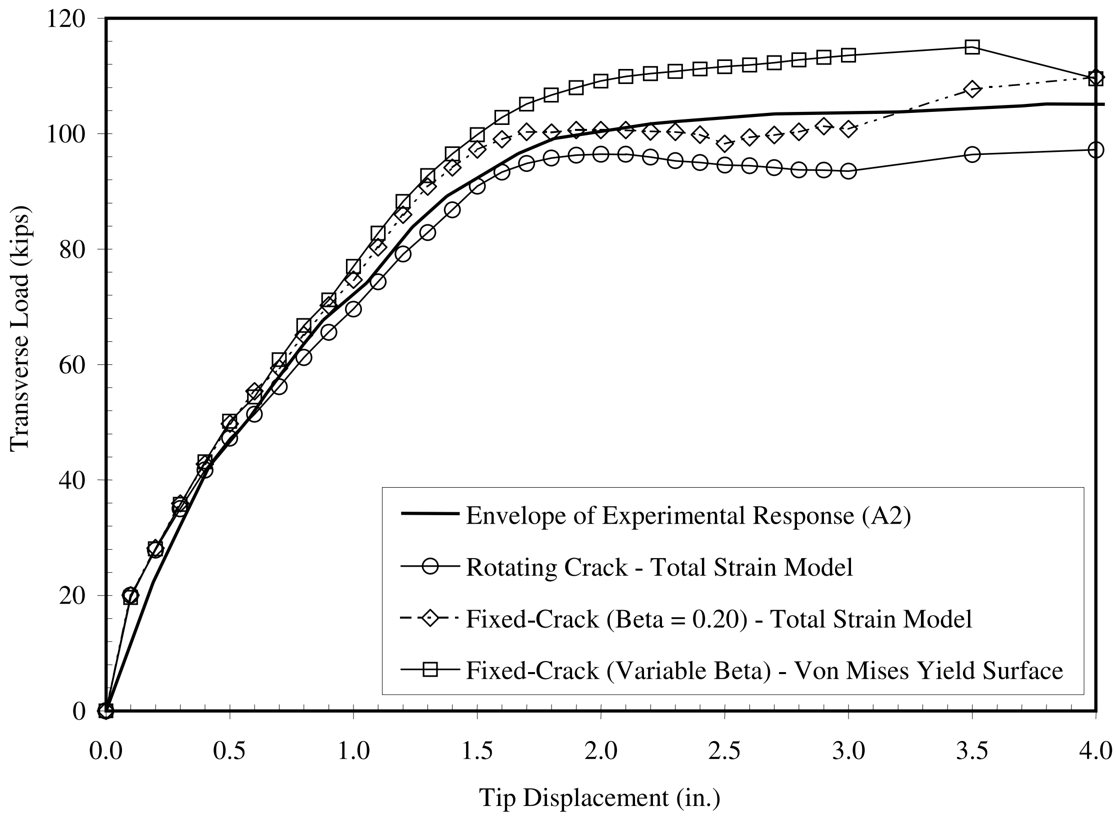

Figure 4-12: Analytical cracking models compared to experimental response of Subassembly A2

4.2.8 Constitutive Modeling of Reinforcement

Reinforcement is modeled using the Von Mises yield criterion discussed previously. The hardening rule is based on the uniaxial stress-strain response from material testing. The tension and compression responses are assumed identical (Figure 4-13). The behavior consists of elastic-hardening-fracture branches. To model fracture, the reinforcement stress is abruptly dropped after the rupture stress, f_u, is reached. It should be noted that if reinforcement is modeled by discrete elements, this abrupt drop of stress could lead to difficulty in convergence. However, since the reinforcement is embedded in the concrete elements, the reinforcement stiffness adds to that of the concrete parent element. Thus, modeling bar fracture in this way should not create any numerical problems when dealing with embedded reinforcement.

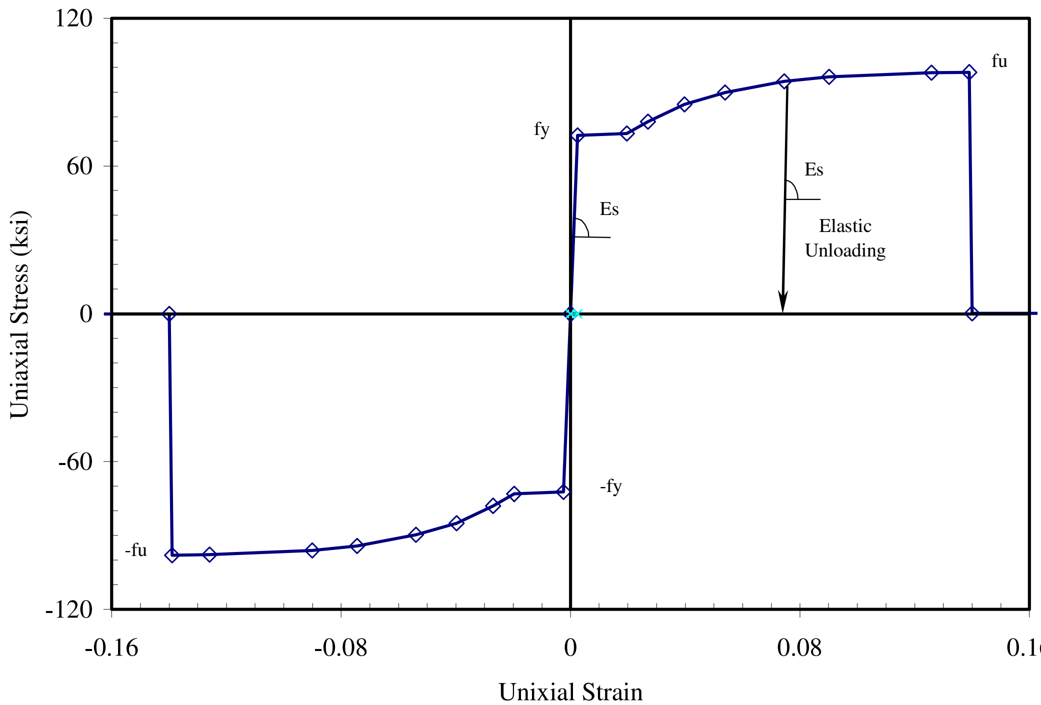

Figure 4-13: Typical hardening-softening model for reinforcement

4.3 Solution Strategy

Three solution strategies are used for the finite element investigation: regular Newton, modified Newton, and linear (Figure 4-14). For moderate nonlinear behavior where minimal damage (cracking or plasticity) in each increment is expected, regular Newton iteration is used for solving the system. Regular Newton recalculates the tangent stiffness matrix for each iteration of a given step; as a result the method converges with fewer number of iterations. If the system reaches moderate levels of damage, the stiffness recalculation at each iteration may lead to divergence in the solution. To avoid this problem, the modified Newton strategy is used. Modified Newton uses the initial tangent stiffness at the beginning of the loading step for all iterations of the solution in this step, thus minimizing the computation time for each step. For situations where high nonlinearity is encountered, the linear solution strategy is used. The initial elastic stiffness is adopted and kept constant for the entire analysis. This procedure requires many iterations to reach a converged solution; however, the cost of each iteration is low since the tangent stiffness matrix is formulated, assembled, and decomposed only once at the beginning of the analysis. In general, the linear formulation provides an unconditionally convergent solution [Argyris 1969] and therefore was used initially in all models. Regular Newton iteration, however, proved to be the most efficient when using embedded reinforcement and total strain formulation and was adopted for the majority of the subsequent analyses.

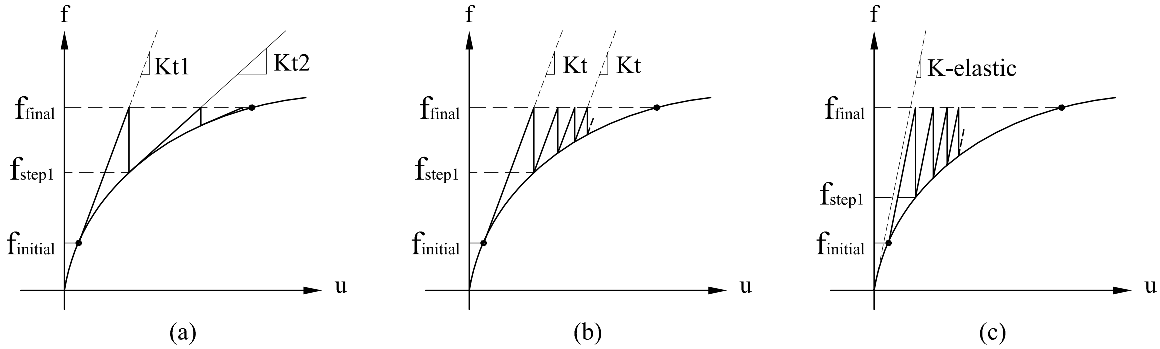

Figure 4-14: Solution strategies: (a) regular Newton, (b) modified Newton, (c) Linear (f: load, u: displacement)

4.4 Evaluation of the Finite Element Model

As a demonstration of the effectiveness of the proceeding formulation, results from the finite element models are compared with a series of bridge subassembly tests. A background of the experimental setup is given in Chapter 3. Selection of the finite element mesh and comparisons to the experimental results are given in the following sections.

4.4.1 Mesh Development

The finite element models are discretized to match the boundary conditions and geometry of the tested specimens. The finite element discretization and reinforcement layouts are shown in Figure 4-15 and Figure 4-16, respectively. The gross dimensions and material properties are chosen to coincide with those of the as-built subassembly. The only deviation is the discretization of the top block (column base), which is modeled as elastic material to reduce computational time. As a result, discretization of the actual square cap block, shown in Figure 3-8, is not necessary. Dead load is applied as a uniform load on the top of the column and reacted against the beam. The location and magnitude of the reactions are chosen to match the loads applied during the tests. Transverse loading is applied as a nodal displacement at the center of the top reaction block in the x-direction (parallel to the beam axis). Both ends of the beam are modeled as pin supports. It should be noted that the pin supports of the beam are modeled using space truss elements to reduce the stress concentrations at the supports and to have similar conditions to the experimental setup. The stiffness of these truss elements was chosen to be similar to the pins used in the test setup. In the experiment the axial load of the beam is maintained under load control to be *P/2* in each span, where *P* is the lateral load corresponding to the applied lateral displacement. The loading could be modeled using pin-pin supports; however, this did not allow free expansion of the joint. To address this a comparison of the behavior using pin-pin and pin-roller was conducted. The variation in joint response was found negligible. Accordingly, pin-pin support conditions were adopted for all analytical models.

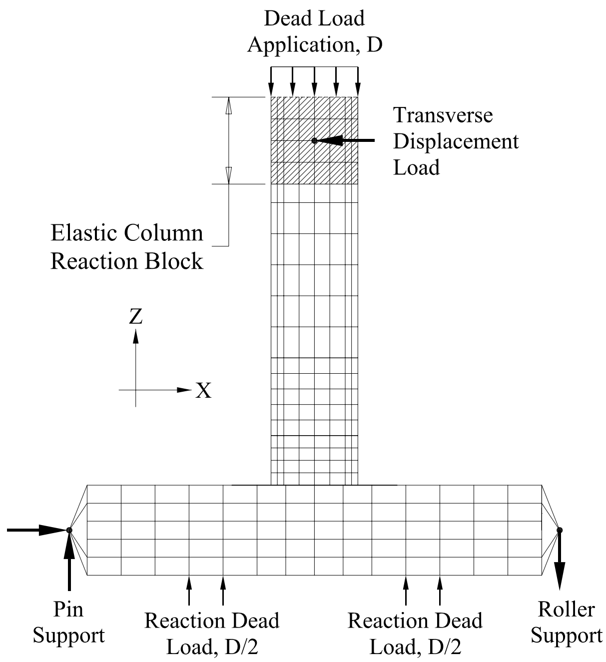

Figure 4-15: Finite element discretization for Subassembly (A2)

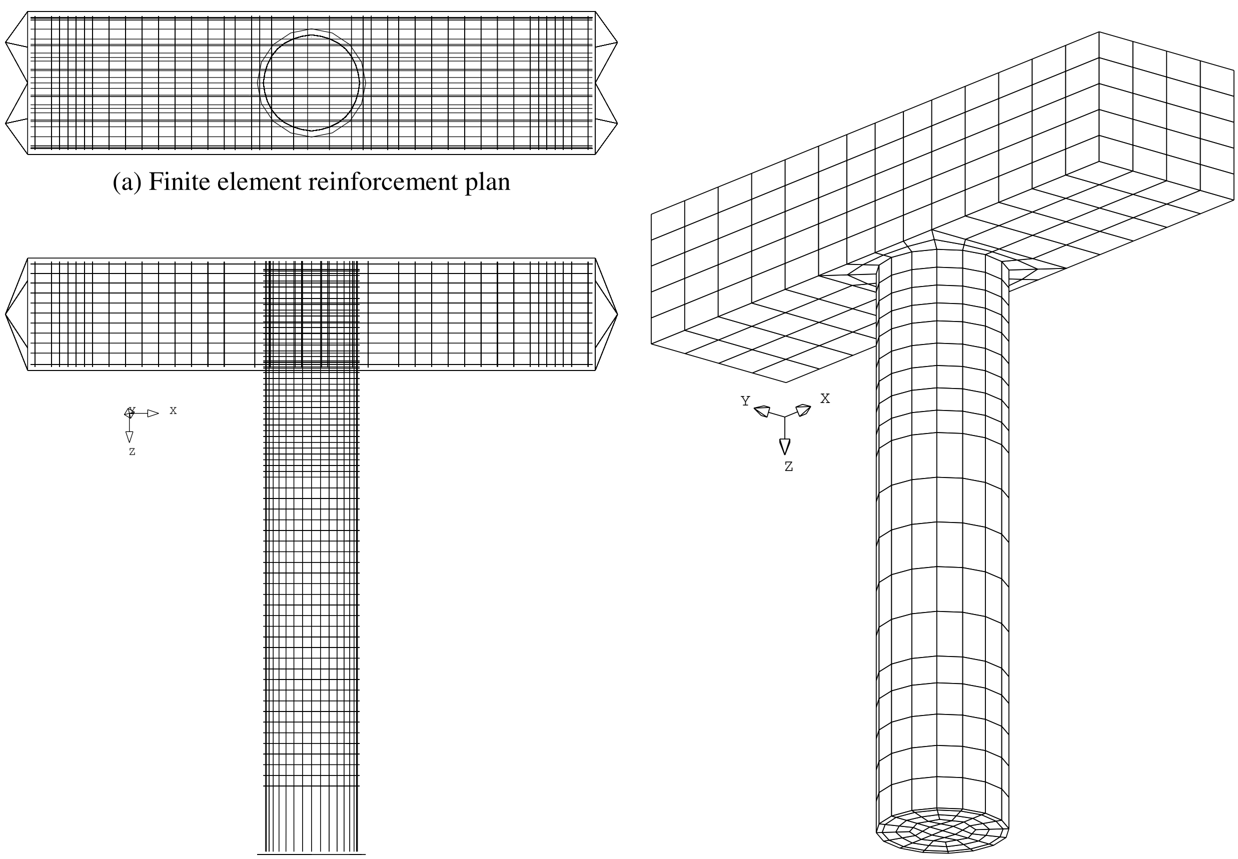

(a) Finite element reinforcement plan

(b) Finite element reinforcement elevation

(c) Isometric view of concrete mesh

Figure 4-16: Model discretization

4.4.2 Parameters of the Constitutive Models

In the present study, the following material parameters (as defined in previous sections) are used.

Table 4-1: Specimen A2 material parameters				
Material Parameter		*Beam Properties*	*Column Properties*	*Units*
Concrete tensile strength	$f't$	0.43	0.54	ksi
Concrete compressive strength	$f'c$	5.81	5.53	ksi
Concrete elastic modulus	Ec	3470	3480	ksi
Concrete Poisson ratio	ν_c	0.15	0.15	-
Fracture energy	Gf	0.77	0.99	kip-in. / in.^{2}
Crack bandwidth	h	3.8	6.1	inch
Steel elastic modulus	Es	28800	27500	ksi
Steel Poisson ratio	ν_s	0.3	0.3	-
Steel tensile yield strength	fy	72.4	67.1	ksi

The data for Specimen A2 are presented to illustrate typical values determined by experimental testing. Material properties vary between specimens; a full description of testing procedures and a summary of the properties measured for the test series are presented in Appendix B.

4.4.3 Finite Element Model Verification

The finite element modeling is conducted using a total strain model with compression hardening-softening and brittle-linear softening tensile response with rotating-crack formulation for the concrete. Reinforcement is modeled as embedded with Von Mises yield criteria augmented with elastic-hardening-fracture behavior in tension and compression. A regular Newton numerical solution strategy is adopted. A comparison of the global load-displacement behavior is shown in Figure 4-17. The finite element model marginally underestimates the experimental resistance. This behavior consistently appears in all analytical subassembly models. The underestimation can be attributed to the analytical concrete constitutive relationship particularly in relation to the rotating-crack formation. In this formulation, cracks in concrete always coincide with principal strain directions. These cracks are treated as smooth cracks without explicit accounting for shear transfer mechanisms such as aggregate interlocking or dowel actions. Accordingly, underestimation of capacity is anticipated. Since response of the beam-column joint was comparable to measured experimental response (as will be discussed later), the constitutive relationships were not modified to exactly match the experimental load-displacement relation.

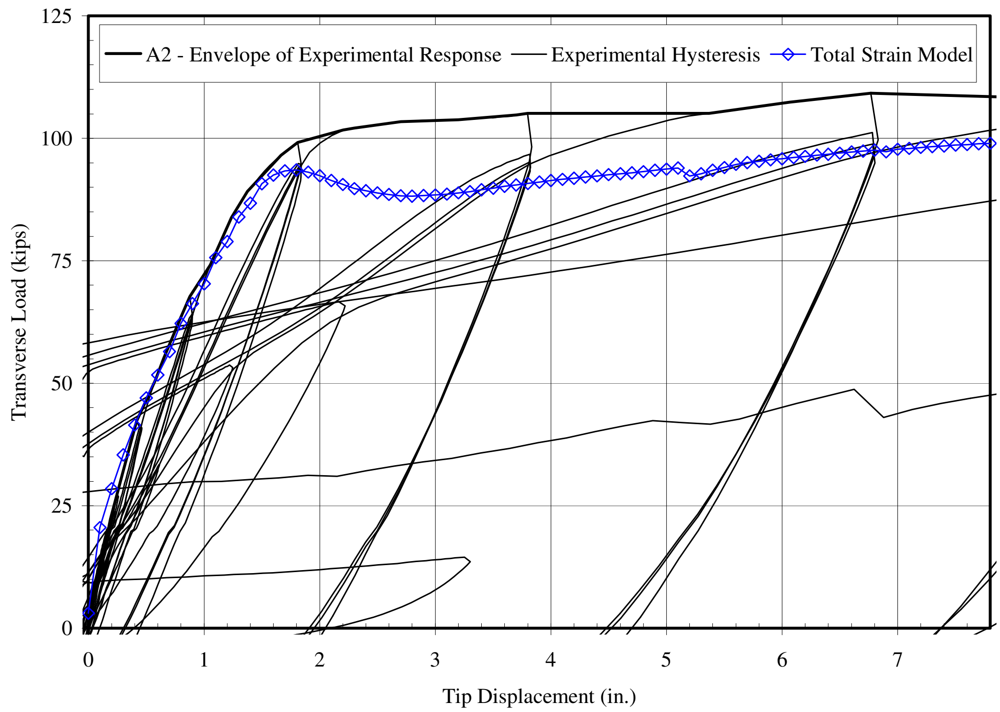

Figure 4-17: Comparative load-displacement behavior

To further evaluate the accuracy of the finite element model, the contribution to the total system drift is evaluated at each level of applied total drift. In the experimental evaluation, the contributions are computed using an array of external displacement transducers (see Section 3.6.2). The comparison between the analytical and the experimental results is shown in Figure 4-18 where good agreement is apparent. For small levels of drift, 0% to 0.5%, inherent errors in the transducer measurements lead to an overestimation of the total displacement (Figure 4-18(a)). Nevertheless, the trends of the displacement contributions agree with the observed behavior. Initially, column flexure is the predominant contributor to the displacement as initial cracks form in the column. This is followed by cracking of the beam section at 1% drift. Following this level, the inelastic column yielding and spalling takes place, leading again to a predominance of column flexural response. Using the computed nodal displacements from the finite element analysis, the component contributions to the total drift from the analytical model can be determined. As shown in Figure 4-18(b), the analytical model appropriately replicates the behavior recorded from the experimental subassembly. The largest error is the underestimation of column flexure. As discussed earlier, to create a model that is computationally practical for further parametric studies, trilinear brick elements were used. Linear elements are inherently stiff in modeling flexure. Therefore, it is reasonable that the column flexure is underestimated on the order of only 5%.

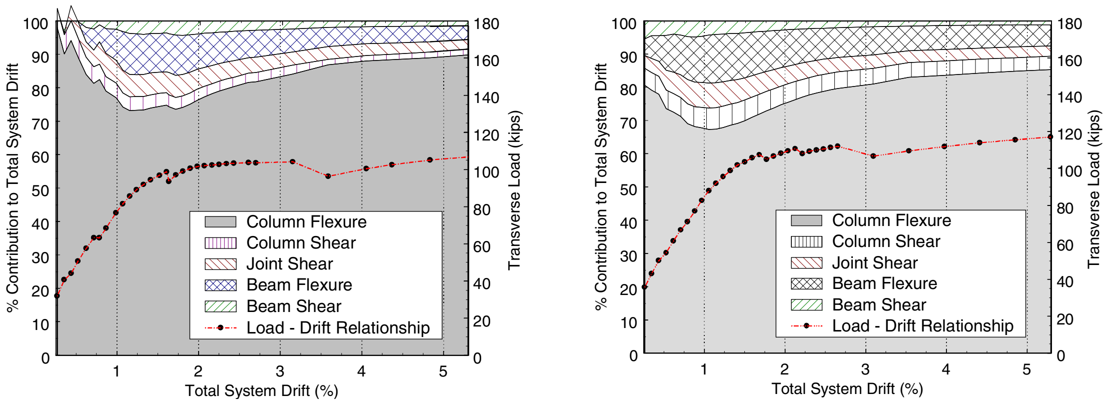

(a) Experimental subassembly

(b) Finite element model

Figure 4-18: Different contributions to total system drift

4.4.4 Reinforcement Behavior

The analytical model shows that the use of embedded reinforcement provides a good estimation of reinforcement strains for the analyzed experimental model (A2). As shown in Figure 4-19, strain values at levels beyond yield are properly estimated both in the column region as well as within the beam-column joint region. Note that, due to loss of a few strain gages during the experiment, only four strain measurements are presented.

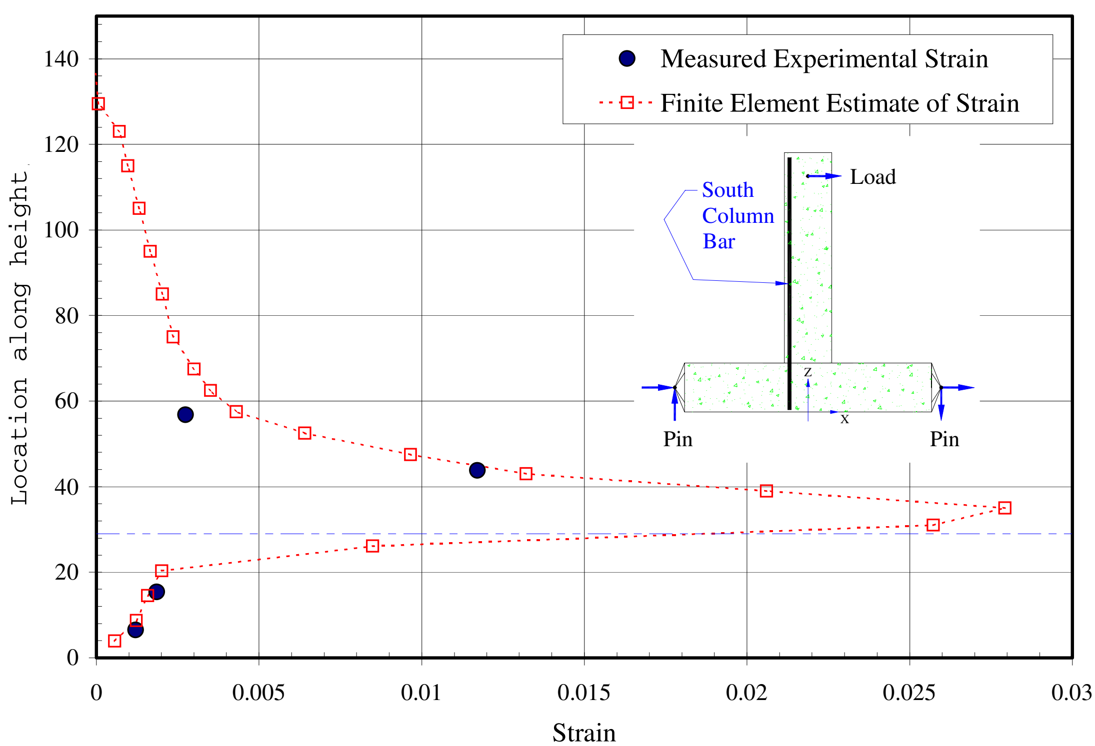

Figure 4-19: Strain in southern exterior column longitudinal reinforcement (3.6% drift)

Typically, modeling reinforcement as being embedded may not be appropriate for the straight development of column bars into a joint. The amount of yield penetration that occurs at the beam-column interface creates local pullout, which cannot be captured properly without directly accounting for bond-slip in the model. Nevertheless, as shown here for moderate levels of development (i.e., satisfying code requirements), strain development in the joint region is reasonably represented.

4.4.5 Cracking Estimation by Rotating-Crack Formulation

A comparison of experimental and analytical results shows that the rotating-crack formulation provides a good estimation of crack formation in a three-dimensional model. Figure 4-20 illustrates the crack behavior in the beam at 4.0-in. displacement (3.6% drift). This level corresponds to a displacement ductility of approximately 4.0, which is approximately half of the ultimate displacement capacity. Figure 4-20(a), represents the extent of beam cracking present on the east face of the experimental subassembly. The estimated orientation of cracks in the analytical model is shown in Figure 4-20(b) where length of the line represents the amount of crack strain. The diagonal joint cracking pattern observed in the experiment is reproduced by the analytical model. Furthermore, the crack strain is largest along the central diagonal joint crack (Figure 4-20(b)), as observed in the experimental subassembly.

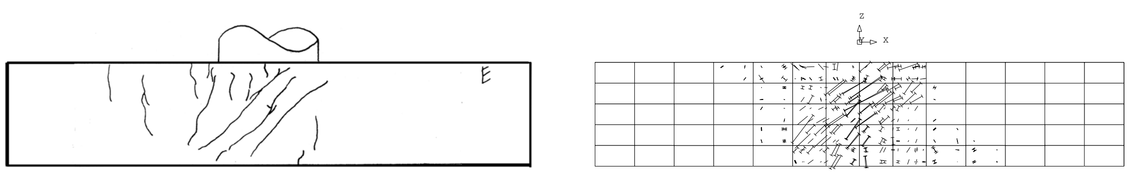

(a) Experimental subassembly (b) Crack orientation in finite element model

Figure 4-20: Joint cracking at 3.6% drift

The cracking behavior of the column is also represented by the analytical model (Figure 4-21). Figure 4-21(a) represents the crack pattern recorded during the experiment at 4.0 in. of column displacement (3.6% drift). Figure 4-21(b) represents the estimate of cracking produced by the finite element analysis. The lengths of the crack marks in Figure 4-21(b) indicate the magnitude of the crack strain. Both the experimental and analytical crack illustrations are presented as a projection of the column onto the *x-z* plane. The cracking on the column from the beam-column interface to 55% of the column height is presented. As shown, the base crack and the array of flexural cracks on the south column face are appropriately estimated. The high amount of vertical cracking illustrated on the north face (compression side according to the loading direction) of the finite element model illustrates the initiation of column spalling within the column cross section. This behavior is not noted in the experimental observations until further in the loading sequence when the spalled section visibly buckled outward on the north column face. Nevertheless, it is possible that similar cracks occurred internally prior to visible spalling.

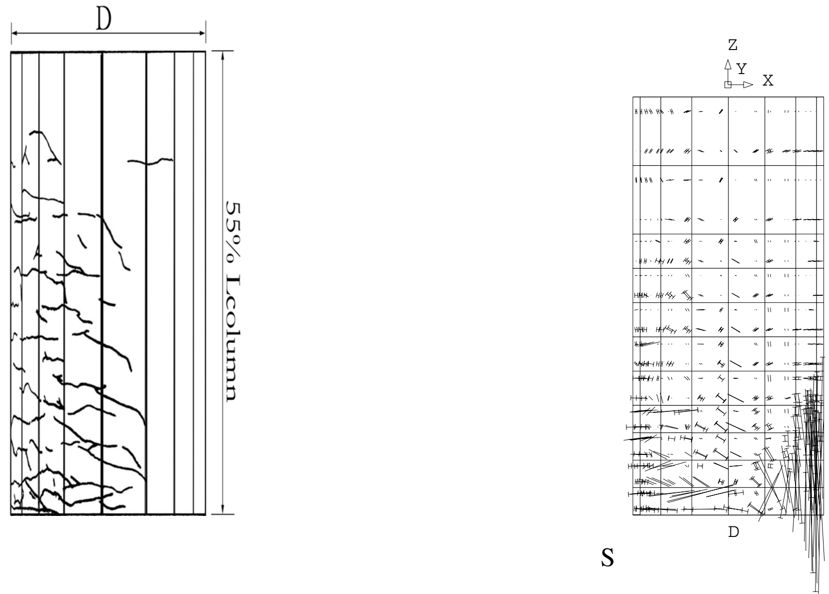

(a) Projected map of crack pattern on experimental subassembly

(b) Measured crack pattern on finite element model

Figure 4-21: Column crack patterns at 3.6% drift

Figure 4-22 demonstrates the importance of 3D finite element modeling. This figure shows a contour plot of the calculated transverse strains within the joint region. These results are given at an applied lateral drift of 4%. It is observed that regions of high tension occur close to the cap beam longitudinal faces. These regions of high transverse tension indicate potential location of splitting cracks in the longitudinal direction of the cap beam; this behavior was observed in Group B specimens where larger demand is placed on the joint region. From these preliminary results, one can infer the importance of 3D modeling for further understanding of failure of beam-column joints.

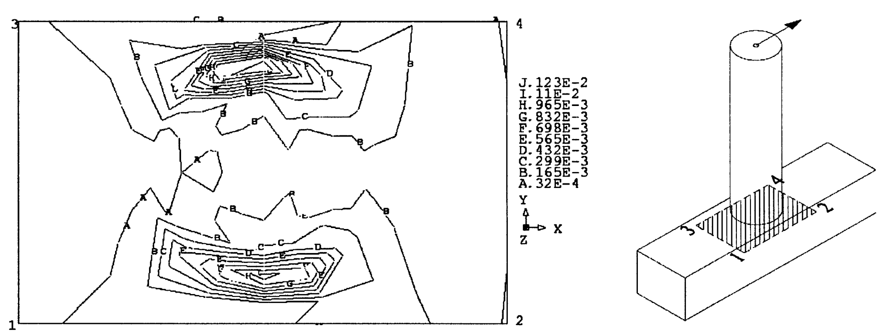

Figure 4-22: Contour plot of strains in the transverse direction (Y-axis) within the joint region
[Note: ε_{cr} = 0.12E-3 and ε_{cu} = 0.60E-3]

4.5 Concluding Remarks

The formulation developed in this chapter is used as the basis for all finite element analyses carried out in the remainder of this report. As shown, the modeling techniques accurately reproduce the experimental behavior. In the later chapters, these techniques will be used for the evaluation of joint transfer mechanisms and parameter studies. Unless noted, all following finite element analyses are conducted using the following parameters: embedded reinforcement with Von Mises yield criterion with hardening fracture model, trilinear concrete brick elements with total strain formulation, rotating-crack model, nonlinear compression hardening-softening, and multi-linear tensile response with brittle failure at cracking. All material parameters are based on the experimental results reported in Appendix B.

5 Design of California Beam-Column Joints with and without Headed Bar Reinforcement

The first phase of the experimental investigation consists of four test specimens, designated Group A. In this phase, design recommendations used in 1996 for bridge joint construction in the state of California are evaluated. In addition, the effectiveness of headed reinforcement for use as joint transverse reinforcement and the behavior of square column configurations is studied. The design assumptions and details for this first experimental phase of subassemblies are presented.

5.1 Subassembly Geometry

The specimens model a bridge bent typical of 1996 California construction (Figure 3-2). As discussed in Chapter 3, the prototype structure consists of three circular columns with pinned column to footing connections. Gross member dimensions are based on the average values taken from a survey of 16 RC bridges built in California between 1982 and 1994 (Appendix A).

The beam width was altered from the database study to meet the most recent requirements of Caltrans Bridge Design Specification. As noted in Caltrans Seismic Design Memo [Caltrans 1994], the width of the cap beam, b_{bm}, is defined as a minimum of 2 feet greater than the column diameter, a scaled width of 104 inches was used. To facilitate laboratory testing and to ensure that standard construction materials could be used in building the experimental test models, lengths in the laboratory test models were scaled by a factor of 3/8 from the original size.

Performance of present design recommendations and new design strategies were evaluated through the investigation of the interior joint assembly. The subassembly configuration consists of the interior column and half the beam span on each side of the column (Figure 5-1). The first two specimens, which model current construction, are composed of a circular column and rectangular beam. To assist in the development of an analytical joint model, two specimens with square columns were also built and tested. To be consistent, the square column geometry and reinforcement were designed so that the flexural capacity would be approximately equal to that of the circular column configuration. The following dimensions were used for Group A specimens.

Table 5-1: Group A subassembly dimensions

Model scale	3/8	Clear column height	Lc = 111.0 in.
Column diameter, A1 & A2	Dc = 28.0 in.	Square column depth, A3 & A4	h_c = 25.0 in.
Clear beam length, A1 & A2	$Lb1$ = 130.0 in.	Clear beam length, A3 & A4	$Lb2$ = 133.0 in.
Clear beam height	h_b = 29.0 in.	Cap beam width	w_b = 37.0 in.

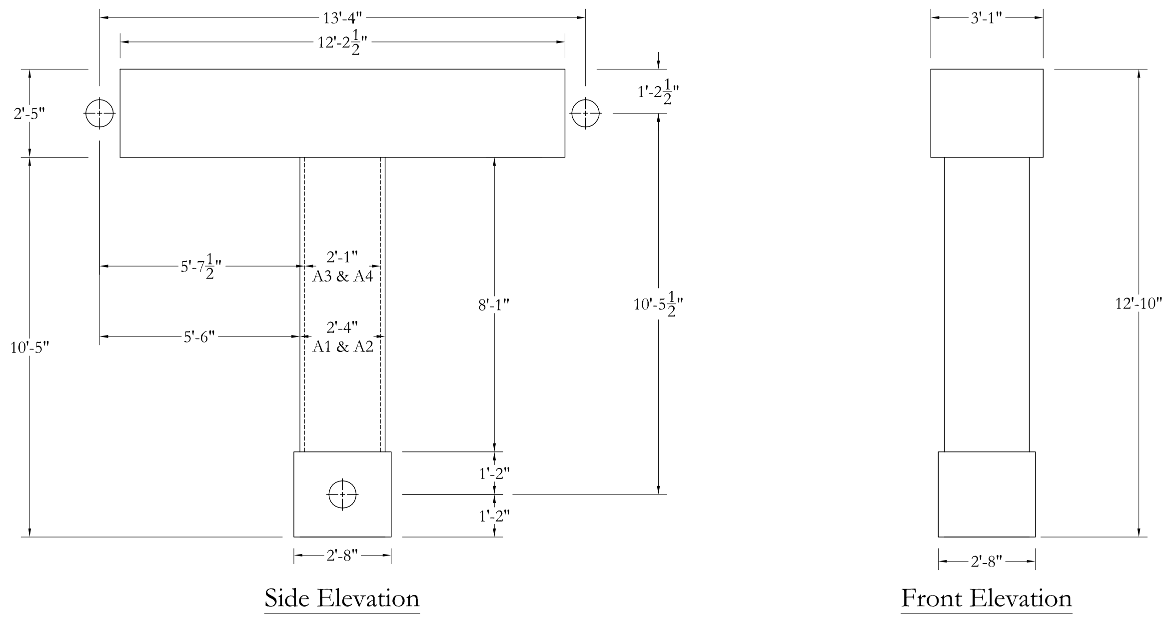

Figure 5-1: Group A test specimen configuration

5.2 Flexural and Shear Design

The analysis of the system was performed using both linear elastic and plastic analysis of the bridge bent assuming

- The joint region is rigid.
- Axial deformation is negligible.
- There is uniform stiffness along the length of the columns and along the length of the beams.

Design of the system was conducted using the geometry and column reinforcement ratio computed from the database investigation. With these values, the remaining reinforcement was designed according to Caltrans Bridge Design Specification. The following three loading conditions were investigated:

(1) Dead + Live + Impact

(2) Dead + Earthquake (Acceleration Response Spectrum with $Z = 8.0$)

(3) Dead load applied to system with plastic hinges at each column

Design requirements were predominantly controlled by plastic hinge formation in the columns. To ensure that a stable column mechanism would occur, an overstrength was applied to the design of the beam. Using these requirements, the test specimens were evaluated as a part of the full prototype bridge bent and checked in the subassembly configuration (Chapter 3). Since the forces in the prototype system were not perfectly modeled, the subassembly demands often controlled the design of the bridge bent.

The subassembly configuration controlled the flexural design of the system and the shear design of the column. The following load factors were used in the subassembly design.

- $Mu(Column) = 1.2Mp(Column)$

- $Mn(Beam) = \frac{1}{2}Mu(Column) / \phi_{flexure} = Mu(Column)/1.8$

- $Vn(Column) = (Mu(Column) / L_{column}) / \phi_{shear}$ with $Vc = 0$ kips within plastic hinge length.

Where ($\phi_{flexure}$ = 0.9) and (ϕ_{shear} = 0.85) are strength reduction factors for flexure and shear, respectively. Beam shear design was controlled by the prototype structure behavior.

- *Vn(Beam)* = Function of column plastic capacity and dead load on real system.

In addition to the load factors and overstrengths, the techniques used in California Bridge construction place special flexural requirements on the design of the cap beam. During construction of a cast-in-place box-girder bridge system, the superstructure is built in a well-defined sequence (Figure 5-2). The columns are cast to a height approximately 4.0 in. (full-scale) higher than the beam soffit (A). False work is installed to support the construction of the superstructure. The bridge soffit and box-girder webs are then formed and the superstructure reinforcement is installed (B). To allow for early removal of cap bent false work, the BDS requires that the negative flexural capacity of this partially completed cap beam resist the dead load of the remaining section. As a result, the negative flexural reinforcement is placed in two layers. The bridge is cast to the first layer of cap beam negative flexural reinforcement, approximately 3/4 of the depth (C). Once adequate strength is attained, the cap beam becomes self-supporting allowing for the removal and relocation of the false work to a different portion of the bridge (D). The construction is completed by inverting the box-girder forms, installing the deck reinforcement and placing the final lift of concrete (E). As a result, the box-girder forms remain inside the completed bridge. To model this as-built behavior, the beam-column cold joint was properly replicated in the subassembly. The cap beam cold joint, however, was eliminated in the subassembly construction due to the expected limited effect on behavior.

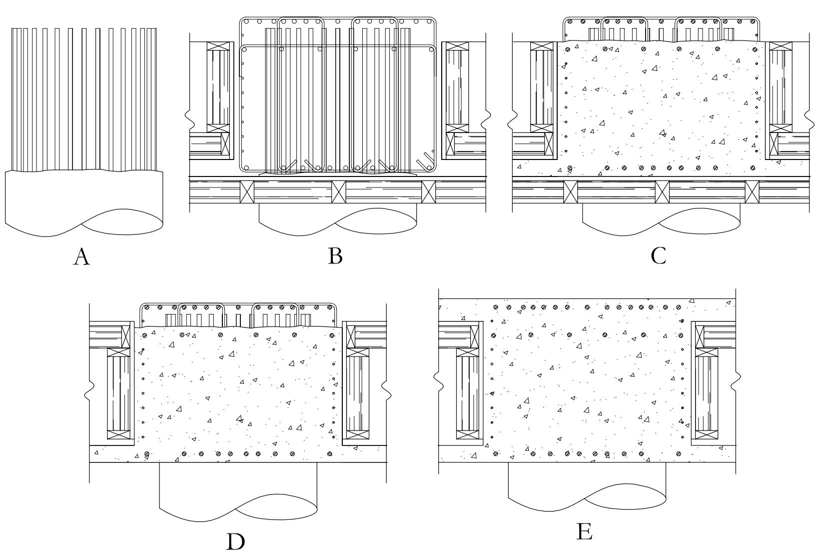

Figure 5-2: Cap beam construction

Table 5-2: Group A reinforcement quantities						
Specimen	Column Flexural Reinforcement A_{steel} / A_{gross}	Column Shear Reinforcement Within Plastic Hinge Region V_{steel} / V_{gross}	Column Shear Reinforcement Outside of Plastic Hinge Region V_{steel} / V_{gross}	Beam Positive Flexural Reinforcement A_{steel} / A_{gross}	Beam Total Negative Flexural Reinforcement A_{steel} / A_{gross}	Beam Shear Reinforcement Av_{steel} / s (in.^{2} / in.)
A1 & A2	2.29 %	0.98 %	0.53 %	0.41 %	0.86 %	0.16
A3 & A4	2.25 %	1.22 %	0.81 %	0.49 %	0.90 %	0.16

Table 5-2 summarize the flexural and shear reinforcement ratios used in Group A specimens. The flexural reinforcement ratio is the area of longitudinal reinforcement to the gross cross-sectional area of concrete. Column shear reinforcement ratios are presented as the volumetric ratio of transverse reinforcement within a spacing, *s*, to the gross cross-sectional area, A_{gross}, multiplied by *s*. Beam shear reinforcement is presented as the area of vertical transverse reinforcement, Av_{steel}, per spacing *s*.

5.3 Joint Design

The joint design was based upon Caltrans 1995 Seismic Design Memo [Zelinski 1995]. As discussed in Chapter 2, this document specifies all requirements for sizing and reinforcing of the beam-column joint shear zone. In summary, the following is required:

5.3.1 Joint Geometry

- The joint shear zone width shall be a minimum of 2.0 feet wider than the column diameter.
- The joint shear zone length shall be a minimum of the lesser of (2 x column width) and (column width + 2 x beam depth).
- The joint geometry shall then be sized such that the shear stress in the joint shear zone shall be less than $12\sqrt{f'c}$.

5.3.2 Joint Reinforcement

- The column longitudinal reinforcement shall be anchored into the far end of the joint.
- The column spiral shall be continued into the joint to the end of the longitudinal reinforcement.
- An additional quantity of vertical transverse reinforcement equal to 20% of the column reinforcement area, As_{column}, is required in the joint shear zone.

- An additional quantity of horizontal transverse reinforcement equal to 10% of the column reinforcement area, As_{column}, is required in the joint shear zone. The reinforcement shall consist of hairpin-shaped ties.

- Side face (i.e., longitudinal skin) reinforcement equal to 10% of the main cap negative reinforcement shall be equally distributed to each face of the cap beam.

As prescribed by the preceding requirements, the following reinforcement quantities were used for each specimen (Table 5-3). The orientation and arrangement of reinforcement is illustrated in Figure 5-4 through Figure 5-9.

Table 5-3: Group A joint reinforcement

Specimen	*A1*	*A2*	*A3*	*A4*
Effective joint volume** Width x height x length (in.)	37 x 29 x 56	37 x 29 x 56	37 x 29 x 50	37 x 29 x 50
Volumetric vertical transverse joint reinforcement ratio, ρ_{jv}	0.171 %	0.149 %	0.170 %	0.157 %
Volumetric horizontal transverse joint reinforcement ratio, ρ_{jh}	0.223 %	0.212 %	0.258 %	0.269 %

**Joint shear stress was checked to ensure that the joint geometry produced allowable values.

5.4 Materials

The reinforcement and concrete used in the construction of the test specimens were chosen to match the materials used in California bridge construction. Longitudinal reinforcement consists of Grade 60 steel meeting the requirements of ASTM A706 Standard Specification for Low-Alloy Steel Deformed Bars for Concrete Reinforcement. This specification has been adopted by the California Department of Transportation due to its improved characteristics over that of traditional reinforcement meeting the requirements of ASTM A615 Specification for Deformed and Plain and Billet Steel Bars for Concrete Reinforcement. The A706 specification prescribes that the reinforcement

- Have good ductility by limiting the minimum elongation;
- Be weldable by requiring a carbon equivalence of 0.55% and providing limits on chemical composition; and
- Have a bounded tensile and yield strength.

The improved tensile behavior is illustrated in a comparison of their stress-strain response (Figure 5-3). Due to the scaled size of the transverse reinforcement (#3 bars were used), material meeting the requirements of ASTM A706 was unavailable. Considering that no welding was required and the transverse reinforcement was expected to experience only limited inelastic deformations, ASTM A615 bars were used for transverse reinforcement. To ensure that proper strength was obtained, the bars were preselected according to their mill certified strength.

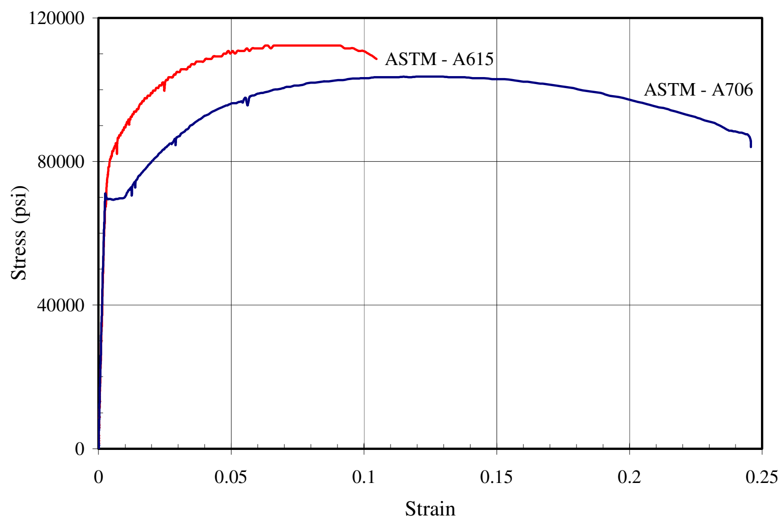

Figure 5-3: Stress-strain behavior of reinforcing steel

Normal weight concrete was used, the mix consisted of Portland cement, coarse and fine aggregate, water, and water reducing and retarding admixtures. A water-cement ratio of 0.53 was used. To account for the testing scale, the aggregate size was reduced from the typical max aggregate size of 3/4 in. to a size of 3/8 inch. As is common in field construction, ready-mix concrete was supplied with a slump of 5 +/- 1 in. The concrete was placed by pump and consolidated using hand vibrators. Descriptions of all material-related information can be found in Appendix B. Included in this summary are the testing procedures used, summaries of all measured properties and concrete mix proportions. The properties measured for the reinforcement and concrete used for Group A specimens are presented in Table 5-4 and Table 5-5, respectively.

Table 5-4: Group A reinforcement properties

Bar Use	*Column Ties A3 and A4*	*Ties, Skin and Spiral*	*Headed Transverse*	*Anchor Block Transverse*	*Headed Longitudinal*	*Conventional Longitudinal*
Bar size	#2	#3	#4	#4	#6	#6
ASTM specification	Unknown	A615	A706	A706	A706	A706
Elastic modulus E_s	29200	28500	28500	29000	29000	27200
Yield stress σ_y	76.0	77.0	74.0	71.0	72.5	68.0
Yield strain ε_y	0.00260	0.00270	0.00260	0.00245	0.00250	0.00250
Plateau strain ε_{yp}	0.032	N.A.	0.013	0.011	0.020	0.012
Ultimate stress σ_u	104.0	122.5	109.0	113.0	98.5	102.0
Ultimate strain ε_u	0.111	0.192	0.131	0.117	0.140	0.139
Fracture strain ε_f	0.165	0.250	0.220	0.210	0.240	0.240

Note: All stresses and elastic moduli are in ksi. N.A.: Not Applicable

Table 5-5: Group A concrete properties						
Test Subassembly			*A1*	*A2*	*A3*	*A4*
Column	Compressive strength	f'_c	5.51	5.81	5.34	5.54
	Corresponding strain	ε_c	0.00295	0.00297	0.00280	0.00295
	Splitting tensile strength	f'_t	0.540	0.425	0.503	0.465
	Young's modulus	E_c	3.36	3.47	3.28	3.29
	Fracture energy	G_f	0.000984	0.000774	0.000916	0.000848
Beam	Compressive strength	f'_c	5.29	5.53	5.97	5.99
	Corresponding strain	ε_c	0.00296	0.00295	0.00279	0.00289
	Tensile strength	f'_t	0.563	0.544	0.578	0.432
	Young's modulus	E_c	3307	3476	3796	3676
	Fracture energy	G_f	0.00103	0.000992	0.00105	0.000788

Note: All forces are in kips and lengths in inches. Poisson's ratio, ν_c, of 0.15 is assumed.

5.5 Group A: Details

5.5.1 Specimen A1: Caltrans Standard Design Details for Circular Column Configuration

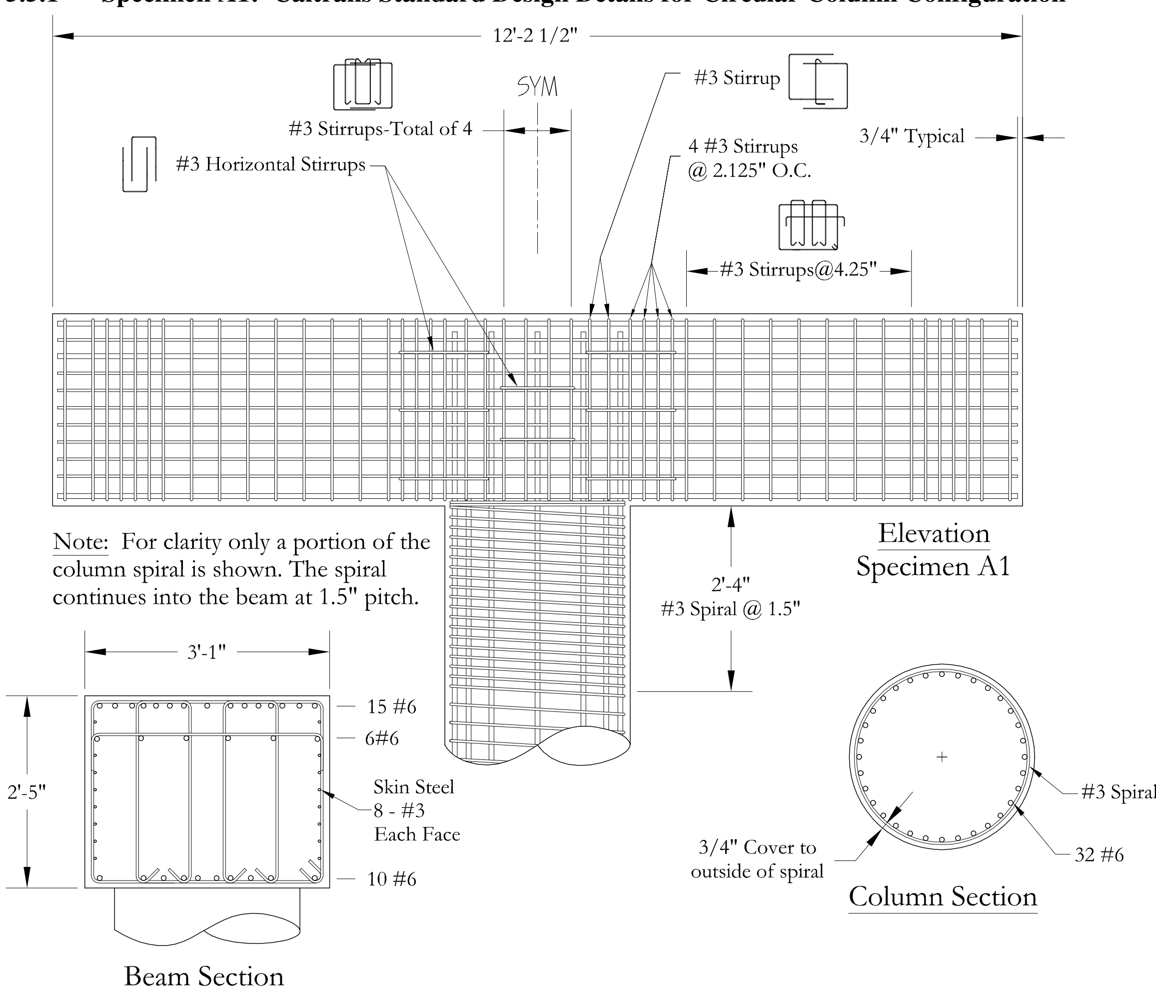

Figure 5-4: Specimen A1 elevation and sections

The first specimen, A1, consists of a circular column and rectangular beam. Reinforcement is conventional and standard materials and details are used. All design requirements meet the 1995 Caltrans Bridge Design Specification [Caltrans 1995]. Figure 5-4 presents the used arrangement of reinforcement.

5.5.2 Specimen A2: Headed Reinforcement Prototype with Circular Column Configuration

The second specimen, A2, consists of a circular column and rectangular beam, identical to Specimen A1. Reinforcement consists of both conventional and headed reinforcement. To investigate the effectiveness of headed reinforcement in beam-column applications, the column longitudinal reinforcement is terminated with heads. The bars are anchored deep into the cap beam to take advantage of the large compression forces developed in the rear of the joint. To assist in development of the beam longitudinal bars passing through the joint, the headed column bars engage the cap beam negative flexural reinforcement (Figure 5-6). In addition, the vertical and horizontal joint transverse reinforcement used in Specimen A1 was replaced with an equal area of headed reinforcement. Due to the unavailability of #3 headed reinforcement, #4 bars were used for the joint transverse reinforcement. An arrangement similar to A1 was chosen. This results in a comparable but sparser layout. The final details are shown in Figure 5-5.

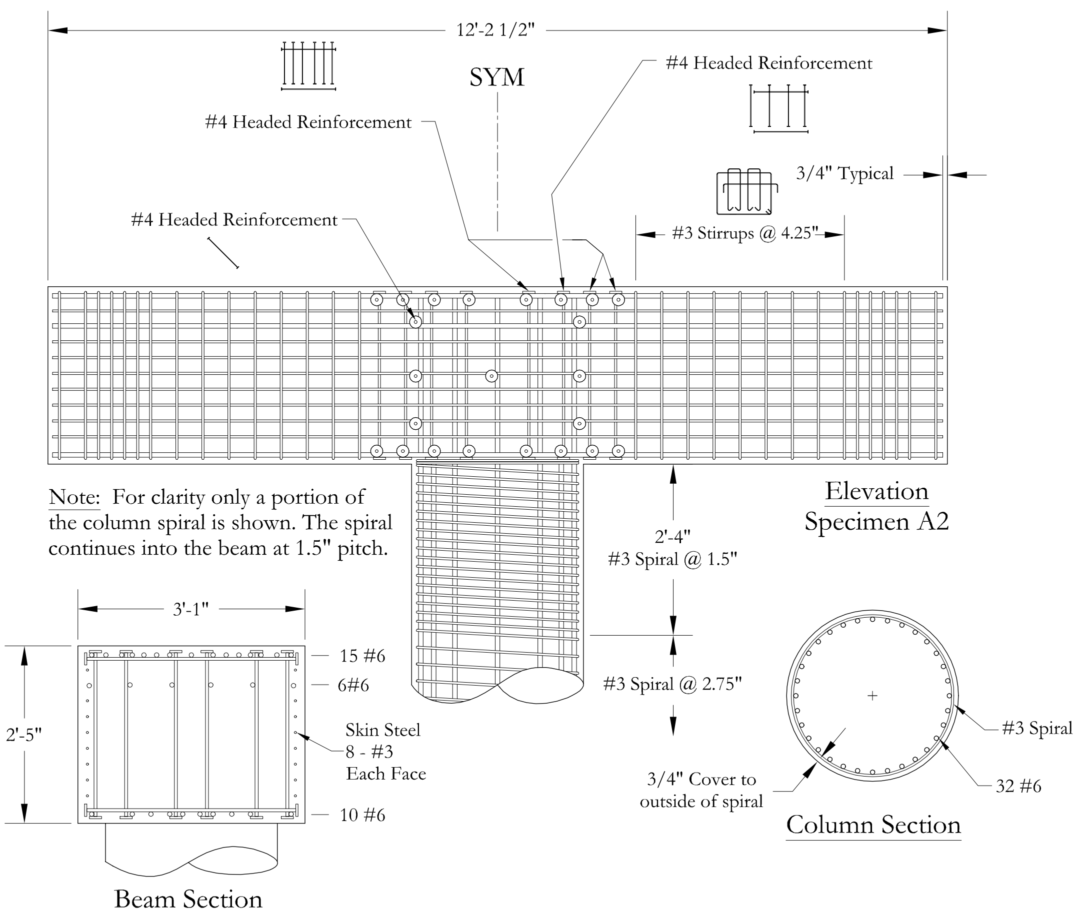

Figure 5-5: Specimen A2 elevation and sections

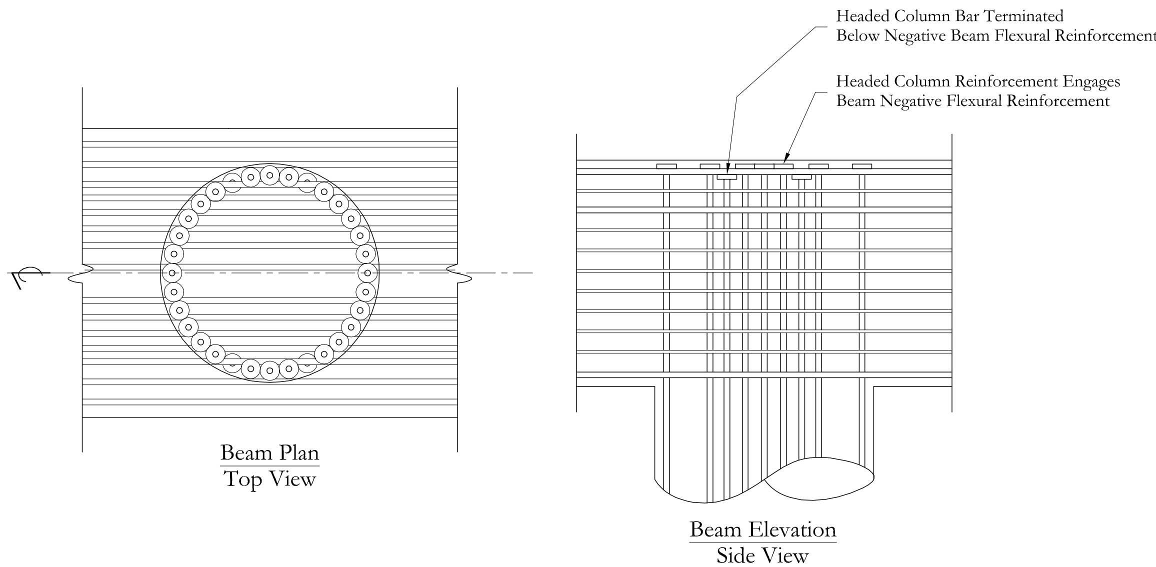

Figure 5-6: Anchorage of column reinforcement, A2

5.5.3 Specimen A3: Caltrans Standard Design Details with Square Column Configuration

The third specimen, A3, was designed to the same requirements as Specimen A1 with one exception. To assist with calibration of a two-dimensional finite element model and to evaluate the effectiveness of different column cross sections, square column geometry was chosen. Conventional reinforcement and standard materials were used. The column depth and the quantity of longitudinal reinforcement were chosen to match the flexural capacity of the circular column specimens. A 25-in. cross section with 32 #6 bars was used. In California, to ensure considerable ductility Caltrans requires that every other longitudinal bar be hooked. Cross-ties were altered using both 135 and 90 degree hooks. The final details are shown in Figure 5-7.

5.5.4 Specimen A4: Headed Reinforcement Prototype with Square Column Configuration

The fourth specimen, A4, consists of a square column, rectangular beam, and a combination of conventional and headed reinforcement. The quantity of column longitudinal reinforcement is equal to the amount used for Specimen A3. The conventional column bars are replaced with headed bars anchored beyond the extreme beam reinforcement to assist in anchoring the negative beam flexural reinforcement (Figure 5-8). As with Specimen A2, all #3 transverse reinforcement in the vicinity of the joint was replaced with #4 headed reinforcement. The details are shown in Figure 5-9.

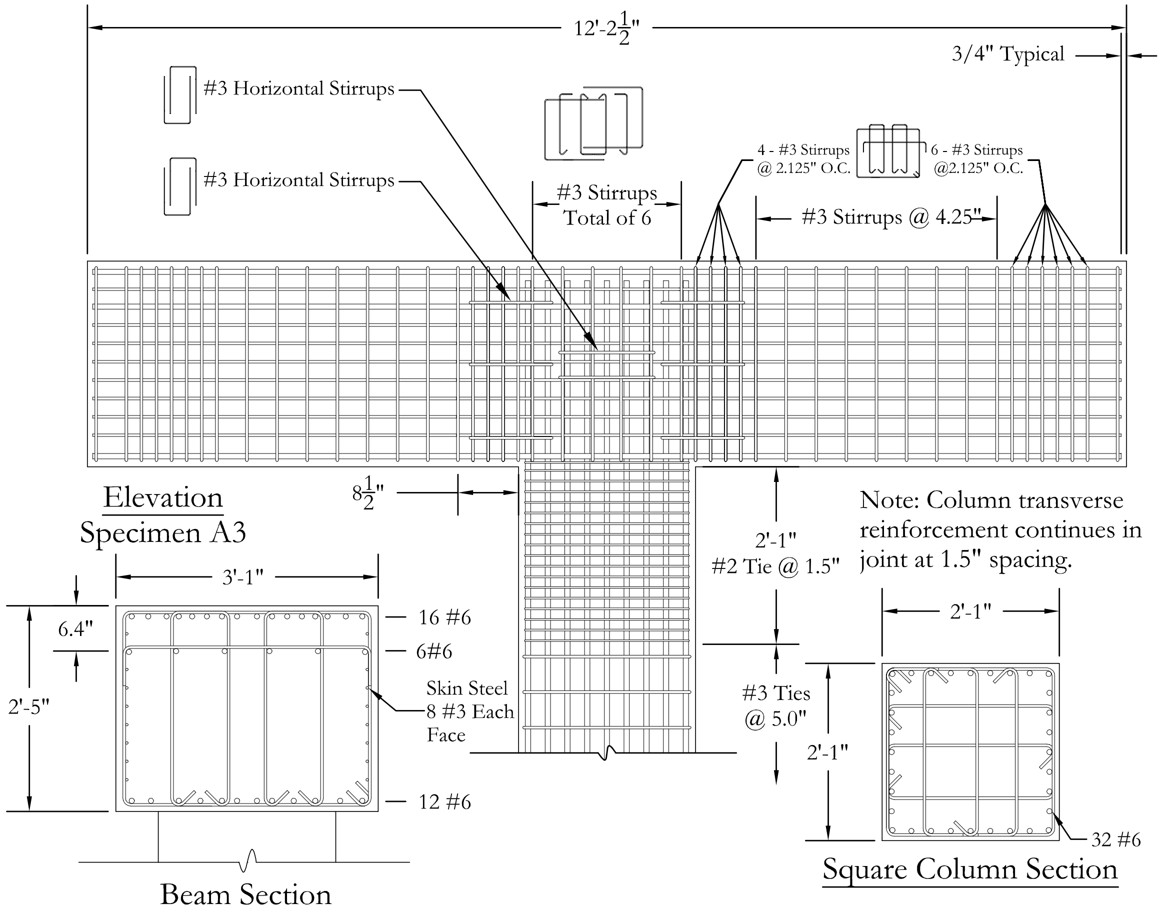

Figure 5-7: Specimen A3 elevation and sections

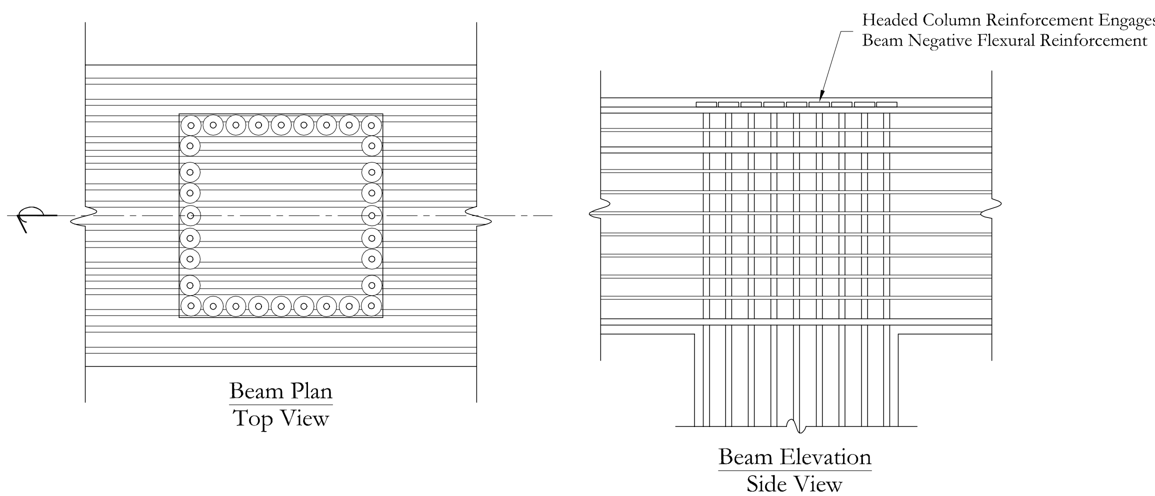

Figure 5-8: Anchorage of column reinforcement, A4

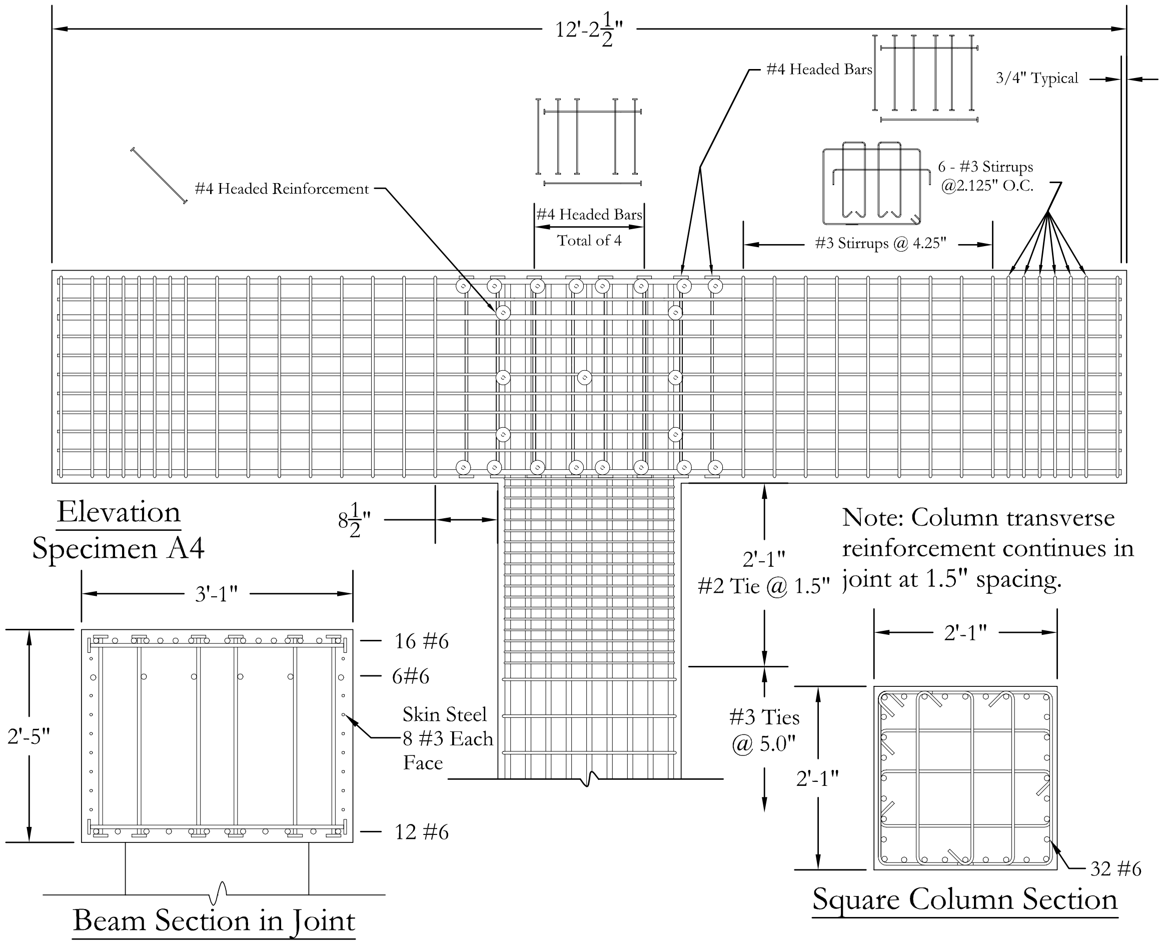

Figure 5-9: Specimen A4 elevation and sections

5.6 Summary of Design

Group A specimens evaluated the methods used in the state of California for the design of bridge joints. Four subassemblies were developed: two evaluating the effectiveness of circular column configurations and two evaluating the effectiveness of square column configurations. One square and one circular column subassembly evaluated current conventional reinforcement construction techniques (Figure 5-10). The remaining two subassemblies evaluated the effectiveness of headed reinforcement for use as both transverse joint and longitudinal column reinforcement (Figure 5-11). The effectiveness of these requirements and design techniques are investigated in the next chapter.

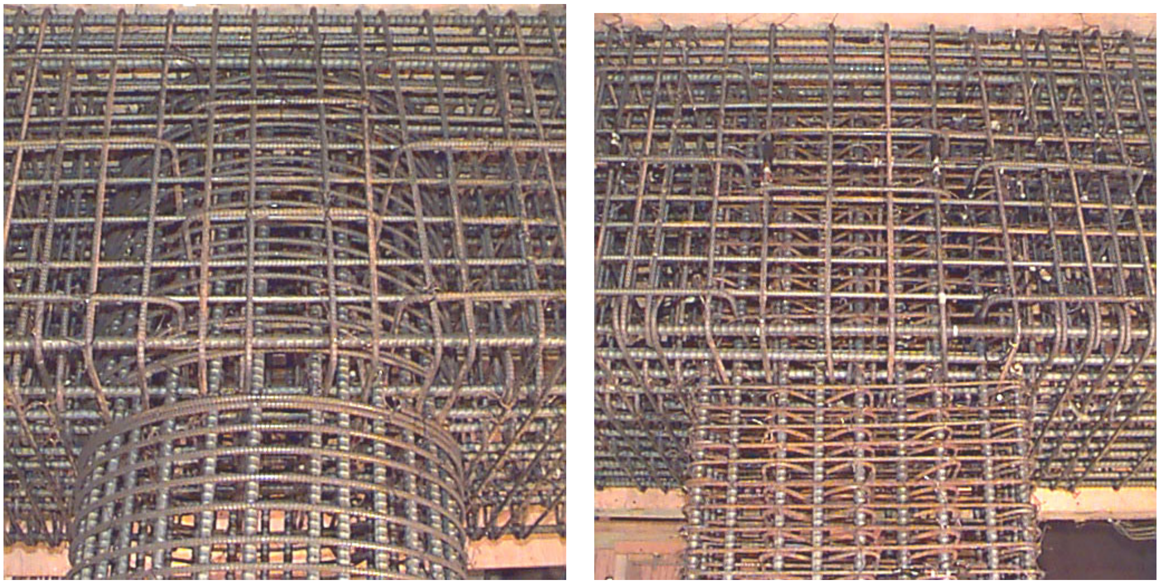

Figure 5-10: Final reinforcement layout, subassemblies A1 and A3

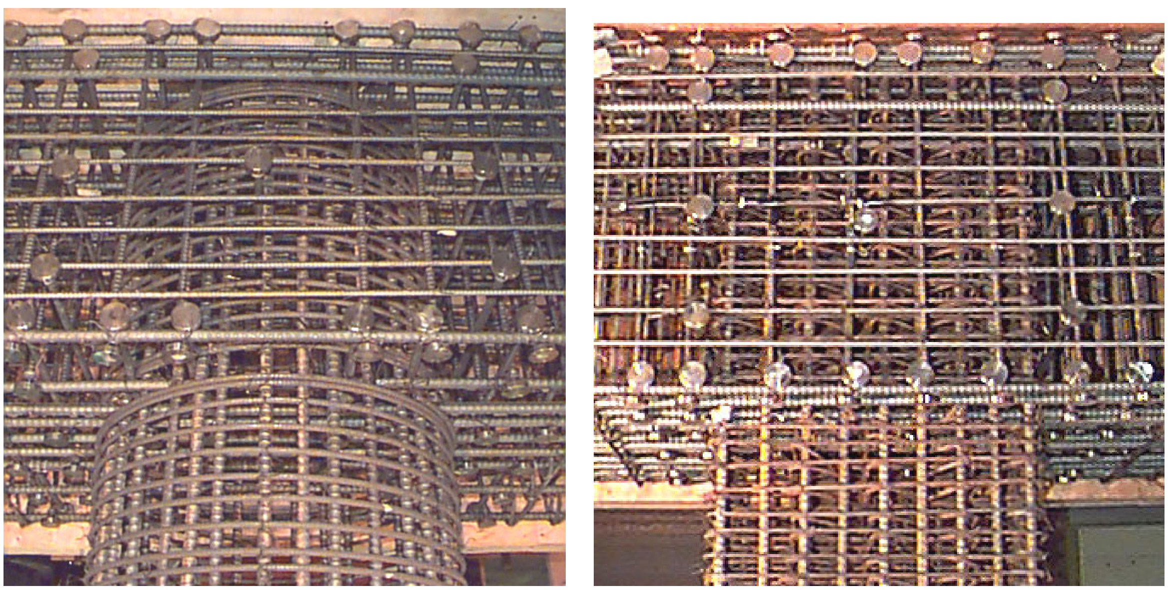

Figure 5-11: Final reinforcement layout, subassemblies A2 and A4

6 Behavior of California Joint Design Requirements

This chapter evaluates the experimentally observed behavior of Group A specimens. The effect of the use of headed reinforcement as column longitudinal and joint transverse reinforcement and the effectiveness of the California Department of Transportation joint design recommendations are discussed. The global behavior of the subassemblies is discussed in terms of the observed progression of damage, the hysteretic response, and the strength and stiffness degradation. The responses of the different joint designs are evaluated on a global level through a comparison of the contributions of component deformations (i.e., joint shear, beam flexure, column flexure, beam shear, and column shear) to the total subassembly displacement, and through an evaluation of the joint shear strength and /stiffness. Local response of the joint is investigated through a comparison of the measured strains on the column longitudinal reinforcement, the beam longitudinal reinforcement, and on the joint spiral and transverse reinforcement within the joint region. In addition, a joint strut and tie force transfer mechanism is evaluated using the experimental results and further expanded on using three-dimensional finite element modeling.

6.1 Global Experimental Behavior

The results from Group A showed that beam-column subassemblies, designed according to the Caltrans Bridge Design Specification [Caltrans 1994] and using conventional reinforcement, follow a predictable, stable path of behavior when subjected to seismic forces. Furthermore, the use of headed reinforcement in place of traditional transverse reinforcement was demonstrated to be similarly effective in providing a stable joint transfer mechanism. The geometry of the column, square or circular, did not significantly affect the global behavior.

The progression of damage was comparable in all specimens (Figure 6-1). Damage initiated with column flexural cracking at low levels of lateral loading. Beam flexural cracking and joint shear cracking followed closely thereafter. At the same level of demand, splitting cracks formed on the cap beam soffit, radiating away from the column face. Column longitudinal reinforcement yielding occurred subsequently, followed by inclined cracking along the column height, and later followed by spalling on the north and south column faces. Continued propagation of spalling along the column height, coupled with strain hardening and increasing demand, eventually led to buckling of the column longitudinal reinforcement. This was closely followed by fracture of the longitudinal bars and a rapid decrease in strength.

The damage of each Group A specimen following failure was comparable (Figure 6-2). In all cases the specimens developed the desired plastic hinge mechanism in the column. Drifts on the order of 8% were achieved prior to strength loss. Joint damage was limited to inclined cracking with maximum width of 0.02 in.

Table 6-1 summarizes events recorded during each experiment. Close visual inspection was limited to observations taken at the end of each cycle. As a result, physical quantities such as cracking and spalling are noted only with respect to the displacement cycle. Events obtained from the recorded data such as yield and maximum load include the displacement cycle and the corresponding measured deflection.

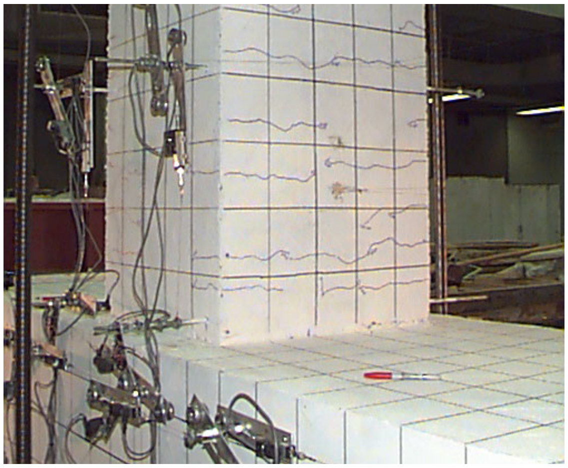

(a) Column cracking

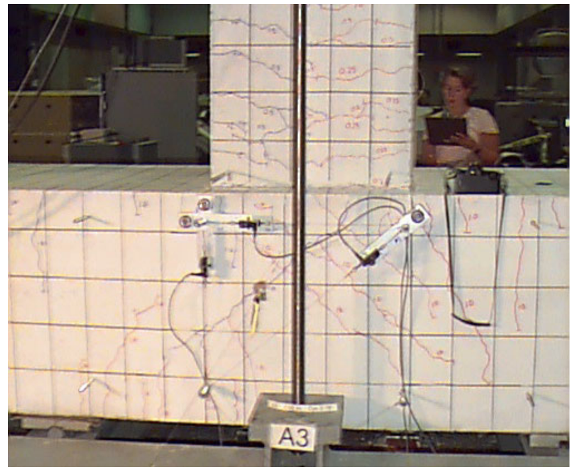

(b) Joint cracking and beam flexural cracking

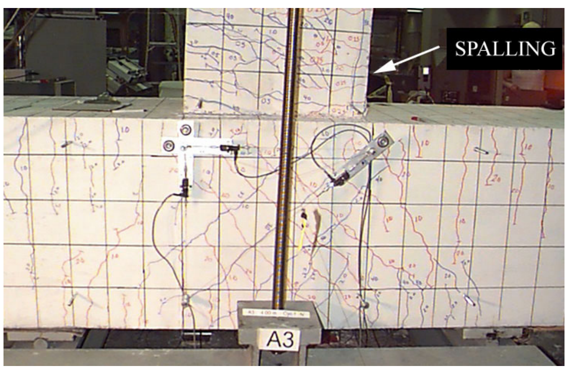

(c) Column inclined cracking and initialization of spalling

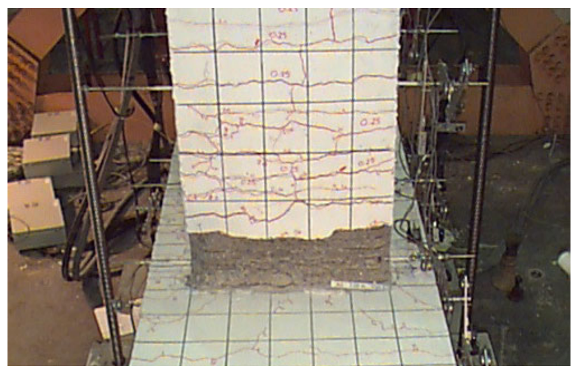

(d) Significant spalling

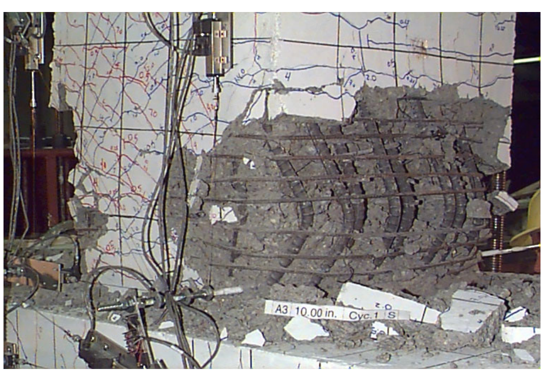

(e) Buckling of column longitudinal reinforcement

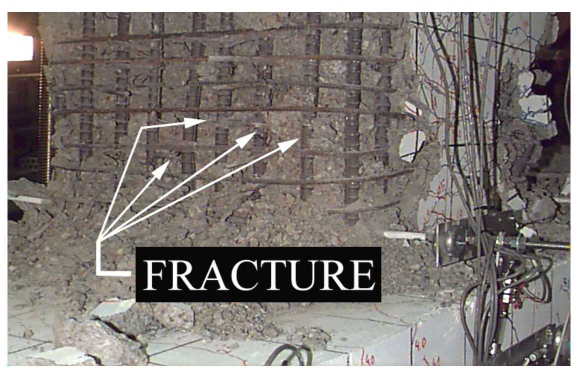

(f) Fracture of column longitudinal reinforcement

Figure 6-1: Progression of typical damage (Specimen A3)

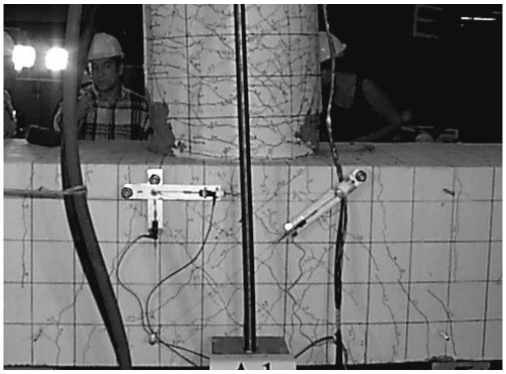

(a) Specimen A1
(at ultimate load level and 7.0 in. tip displacement)

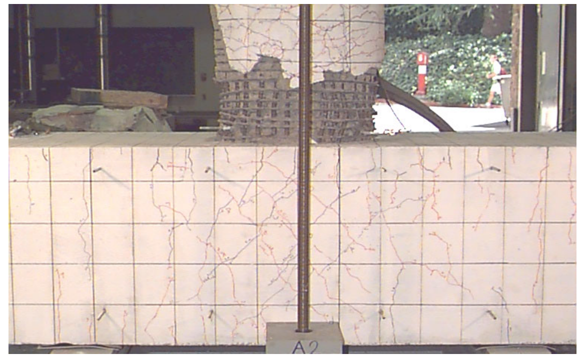

(b) Specimen A2
(at end of test)

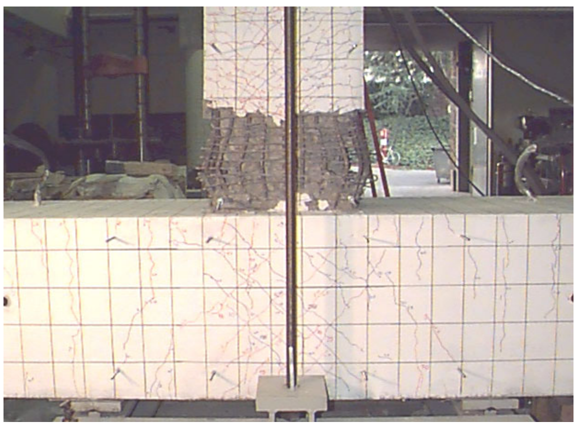

(c) Specimen A3
(at end of test)

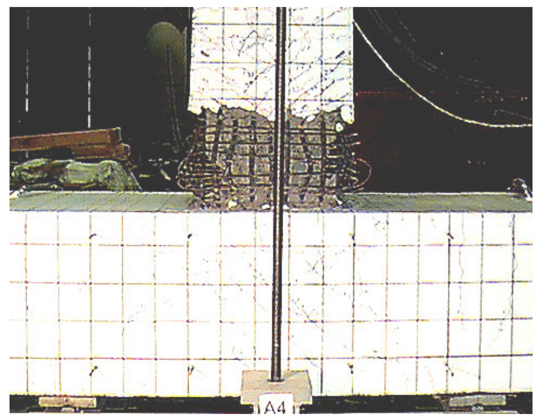

(d) Specimen A4
(at end of test)

Figure 6-2: Damage near ultimate stage for all specimens in Group A

Note that with the exception of A1, all specimens were tested according to the loading protocol and displacement history described in Chapter 3. Two errors occurred during the testing of Specimen A1, which affected the displacement history. First, the control system was improperly zeroed, and second, the specimen support slipped. Specimen A1 was tested with an initial 0.24-in. northern displacement. Unfortunately, the error was not noticed until late in the test. At this point the system had begun to yield; thus zeroing the load was not feasible. As the magnitude of the applied displacements increased, the effect of the initial displacement on the overall history became less pronounced. Nevertheless, the non-symmetric displacement history resulted in non-symmetric cracking and may have contributed to premature column yielding. Secondly, halfway through the test, during the 1.0-in. and 2.0-in. displacement levels, an anomaly was noted on the load-displacement curves. Near the end of the 2.0-in. displacement level, a slip of the northern pin support was identified. At this point, the test was paused and plates were welded in place to prevent any further movement. The slip of the northern end resulted in a rigid body rotation of the whole specimen about the southern support. Readings from displacement transducers placed on both the northern and southern end of the subassembly allowed for the removal of the rigid body displacement from the measured tip displacement during data reduction. To check the stiffness of the repaired support, an extra half cycle of displacement (2.0 in. to the north) was added to the displacement history. These adjustments are noticeable between events 4 and 5 (Figure 6-3).

Table 6-1: Group A test observations

Event #	*Event Description*	*Column Tip Displacement (in.)*			
		A1[*]	*A2*	*A3*	*A4*
1	Column Cracking	(0.10″ – N)** Cycle 1	(0.10″ – N) Cycle 1	(0.25″ – N) Cycle 1	(0.25″ – N) Cycle 1
2	Joint Cracking & Beam Flexural Cracking	(0.25″ – N) Cycle 1	(0.50″ – N) Cycle 1	(1″ – N) Cycle 1	(1″ – N) Cycle 1
3	South Column Reinforcement Yield	1.28″ North: (1" – N) Cycle 1	N.A. Strain Gage Failure	1.57″ North: (2" – N) Cycle 1	1.41″ North: (2″ – N) Cycle 1
4	North Column Reinforcement Yield	1.04″ South: (2" – S) Cycle 1	1.40″ South: (2" – S) Cycle 1	1.95″ South: (2" – S) Cycle 1	N.A. Strain Gage Failure
5	Onset of Column Spalling	(4″ – N) Cycle 1	(4″ – N) Cycle 1	(4″ – N) Cycle 1	(4″– N) Cycle 1
6	Peak North Lateral Load	7.82″ North: (7" – N) Cycle 1	7.60" North: (7" – N) Cycle 1	7.67" North: (7" – N) Cycle 1	7.76" North: (7" – N) Cycle 1
7	Peak South Lateral Load	7.39" South: (7" – S) Cycle 1	7.64" South: (7" – S) Cycle 1	7.87" South: (7" – S) Cycle 1	7.85" South: (7" – S) Cycle 1
8	1st Buckling of Column Reinforcement	(7" – N) Cycle 1	(10" – S) Cycle 1	(7" – N) Cycle 2	(7" – N) Cycle 1
9	1st Fracture of Column Reinforcement	(10" – S) Cycle 1	(10" – S) Cycle 3	(10" – S) Cycle 1	(10" – N) Cycle 1
End	Failure	Column Longitudinal Reinforcement Buckling and Fracture at Beam-Column Interface			

[*]A1 was cycled with an initial north displacement of 0.24 in..
[**]( ) denotes the displacement group and direction for the event listed.

The observed behavior of the headed and conventionally reinforced systems was similar. The only significant exception was the occurrence of buckling for specimens A1 and A2. This variation is most likely due to either construction variances or the unsymmetrical displacement history used for A1, and not attributed to reinforcement type. This issue is investigated further in the section on local behavior. The compatibility between the subassemblies can be further illustrated in a comparison of the displacement history of each subassembly. Figure 6-3 presents the column tip displacements for each Group A specimen as a function of the data history. The numbers on the graphs correspond to the event numbers in Table 6-1.

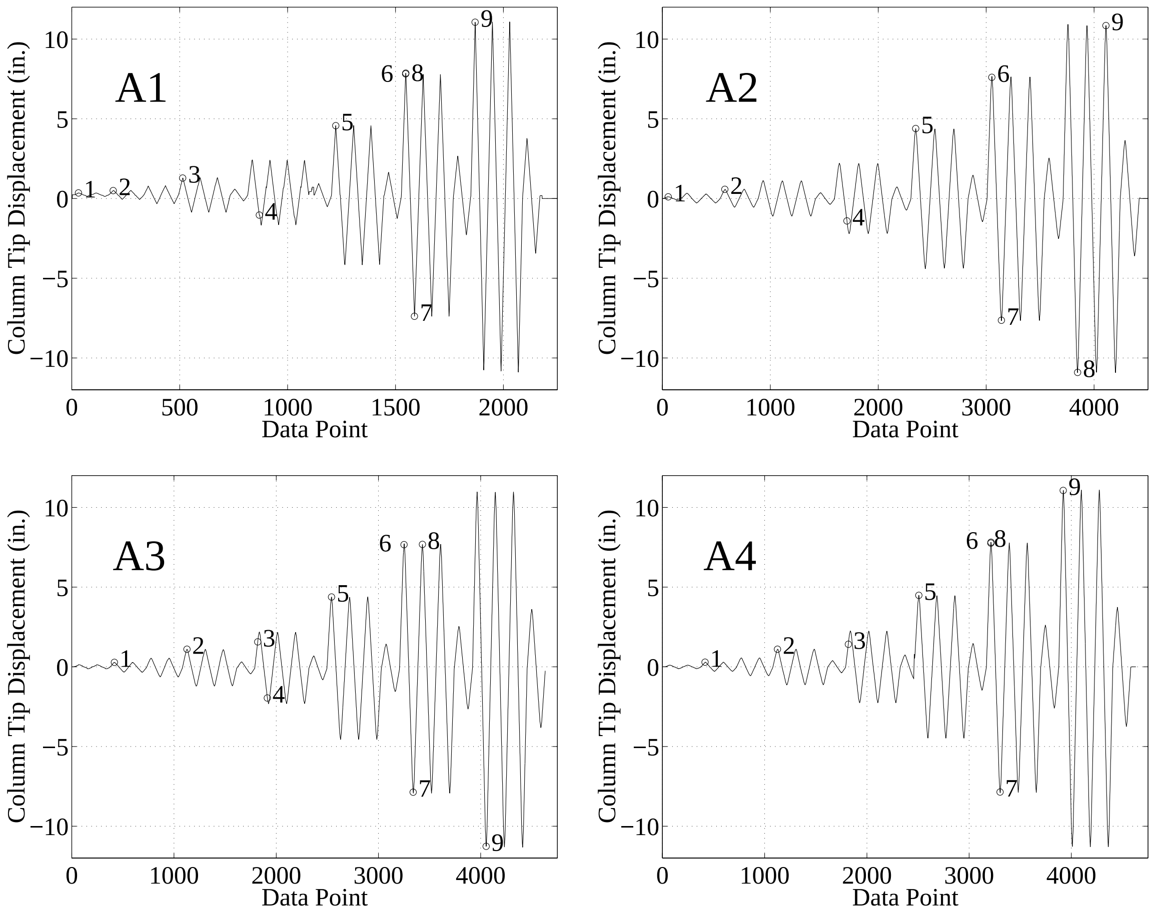

Note: The number of data points were doubled after Specimen A1.

Figure 6-3: Displacement histories

The significant load and displacement events and boundary conditions for each specimen are presented in Table 6-2. This includes the level of axial load applied, the occurrence of first yield, the maximum load capacity, the maximum displacement capacity calculated using two different techniques, the maximum joint crack opening, and the height of column spalling. First yield corresponds to the point at which the measured strain of the column reinforcement, at the beam-column interface, reached the yield strain. Column strain was measured by an array of strain gages on the north and south column reinforcement and compared with the yield strain determined by material testing (Appendix B). The ultimate load refers to the maximum lateral load that the subassembly was able to resist. Ultimate displacement corresponds to a predetermined level of system degradation. Two common definitions are used to describe this condition. In the first definition, ultimate displacement corresponds to the point where the descending branch of the global hysteresis envelope intercepts the yield force. In the second definition, ultimate displacement corresponds to the point where the descending branch of the global hysteresis envelope intercepts 80% of the ultimate load [FEMA 273 BSSC 1997]. Due to the sudden drop in capacity during the 10-in. displacement groups, the tests were halted for safety. As a result, larger displacement cycles were not performed, leaving some ambiguity to the actual system capacity loss. The assumption is made that the hysteresis envelope drops rapidly at the final 10-in. displacement group.

Table 6-2: Group A experimental results					
Experimental Item		*Measured Values*			
		A1	*A2*	*A3*	*A4*
Column axial load (Constant value — under load control)		149.2	145.1	146.6	146.4
1st yield of column longitudinal reinforcement, column tip force	Fy	71.5	77.0	91.2	89.0
1st yield, column moment (at beam-column interface)	My	7937	8547	10123	9879
1st yield, column tip displacement	Dy	1.3	1.4	1.6	1.4
Ultimate load, column tip force	Fm	110.4	109.2	116.5	113.6
Ultimate load, column moment (at beam-column interface)	Mm	12250	12120	12930	12610
Ultimate load, tip displacement	Dm	7.82 $\mu = 6.0$	7.60 $\mu = 5.4$	7.67 $\mu = 4.8$	7.76 $\mu = 5.5$
Ultimate displacement 1	$Fu = F_y$	≥ 10.0 $\mu \geq 7.7$	≥ 9.8 $\mu \geq 7.0$	≥ 9.8 $\mu \geq 6.1$	≥ 8.4 $\mu \geq 6.0$
Ultimate displacement 2	Fu = 80%Fm	≥ 10.0 $\mu \geq 7.7$	≥ 9.8 $\mu = 7.0$	≥ 9.8 $\mu \geq 6.1$	≥ 8.3 $\mu \geq 5.9$
Maximum joint crack opening		0.016	0.020	0.013	0.016
Height of spalling on column		16	20	18	18

Note: All units are in kips and inches.

In Table 6-2, the displacement ductility, μ, is given in terms of tip displacements normalized by column tip displacement at 1st yield, *Dy*.

Variation in the joint design from conventional to headed reinforcement had little apparent effect on the global load and displacement behavior. The measured yield and ultimate strength and deformation for each configuration are comparable, varying at most by 8%. The variation in load and displacement, at yield and ultimate, correlates to the measured strengths of the longitudinal reinforcement. The longitudinal reinforcement used in the headed specimens has a higher yield strength and lower ultimate strength than the conventional reinforcement. As a result, the headed circular column system had a higher strength at yield than its conventional counterpart, while at ultimate, the conventional system was stronger. The strengths of the square conventional assembly are consistently higher than the headed system. However, the corresponding displacements for the conventional assembly are greater than those for the headed system at yield and less at ultimate. These variations may be due to slight inconsistencies in construction rather than a result of joint behavior or reinforcement behavior.

Joint damage in the form of concrete cracking was observed in all subassemblies. Joint crack openings were manually measured on representative cracks. The crack openings were very small, up to 0.020 in., and did not continue to grow after the occurrence of column yielding. The observed joint damage for the different subassemblies was similar. This is illustrated by the crack pattern recorded during testing of specimens A1 and A2 (Figure 6-4).

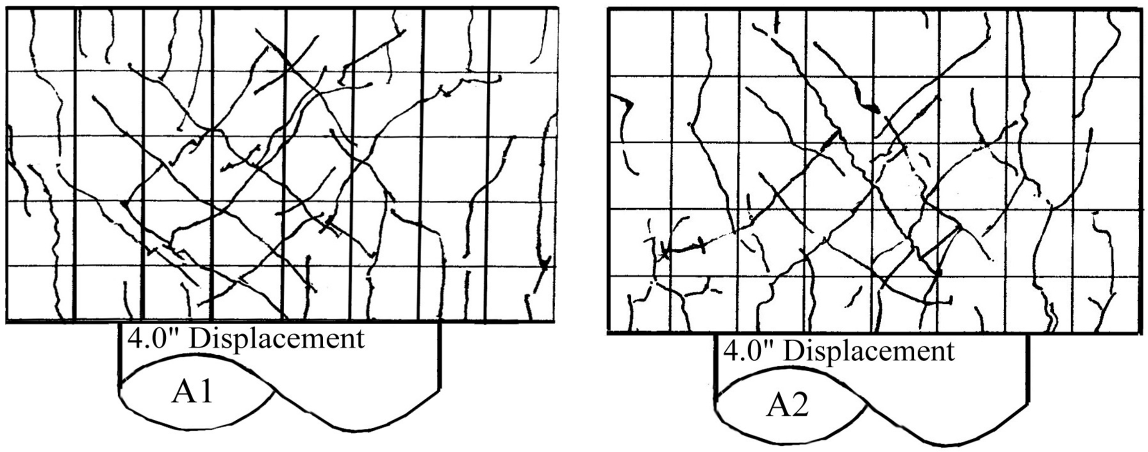

Figure 6-4: Crack pattern in joints after the 4.0-in. displacement cycle group for specimens A1 and A2

At the ultimate stage, spalling extended to an average length of 18 in. on both the circular and square column configurations. This corresponds to 64% of the circular column diameter and 72% of the square column depth.

As shown, all four subassemblies designed according to Caltrans bridge design code had comparable global behavior. The headed reinforcement did not noticeably change the global response. Damage progressed in the same sequence: column flexural cracking, joint shear and beam flexural cracking, column shear cracking, column concrete cover spalling, column longitudinal bar buckling, and fracture. In all cases, column plastic hinging controlled the ultimate response.

6.1.1 Hysteretic Response

The global behavior of the beam-column system can be best illustrated by the load-displacement behavior measured at the column tip. The measured relations for each subassembly are presented in Figure 6-5 through Figure 6-8. These quantities were measured directly at the column, through load cells and linear potentiometers (Chapter 3). In the following discussion, observed global events are correlated to the load-displacement hysteresis curves.

The circular column subassemblies respond in a ductile manner. The hysteretic curves, shown in Figure 6-5 and Figure 6-6, are almost identical. Both have a significant yield plateau initiating at a tip displacement of approximately 2.0 in. and continuing to the ultimate displacement level of 10 in. The hysteretic loops show relatively little pinching. This is indicative of three issues: (1) adequate reinforcement anchorage, (2) proper joint shear strength, and (3) adequate beam and column shear strength. As noted by Sozen [1974], significant slip of column reinforcement or low joint shear strength leads to a "slackness" in the load-displacement history (i.e., pinching) which is not present. Accordingly, the observed hysteresis loops represent behavior of systems controlled by flexural response of the column and beam.

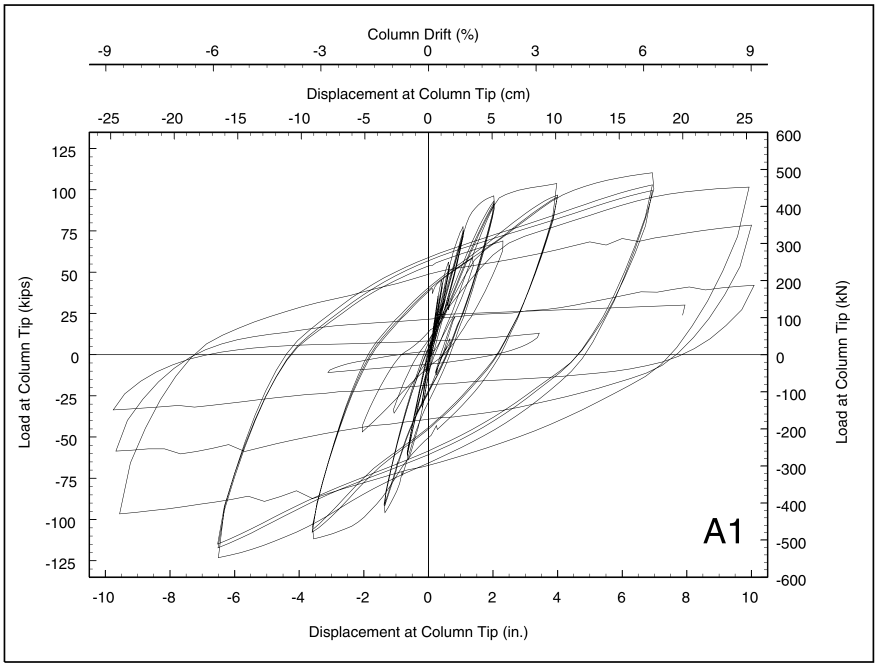

Figure 6-5: A1 load-displacement behavior

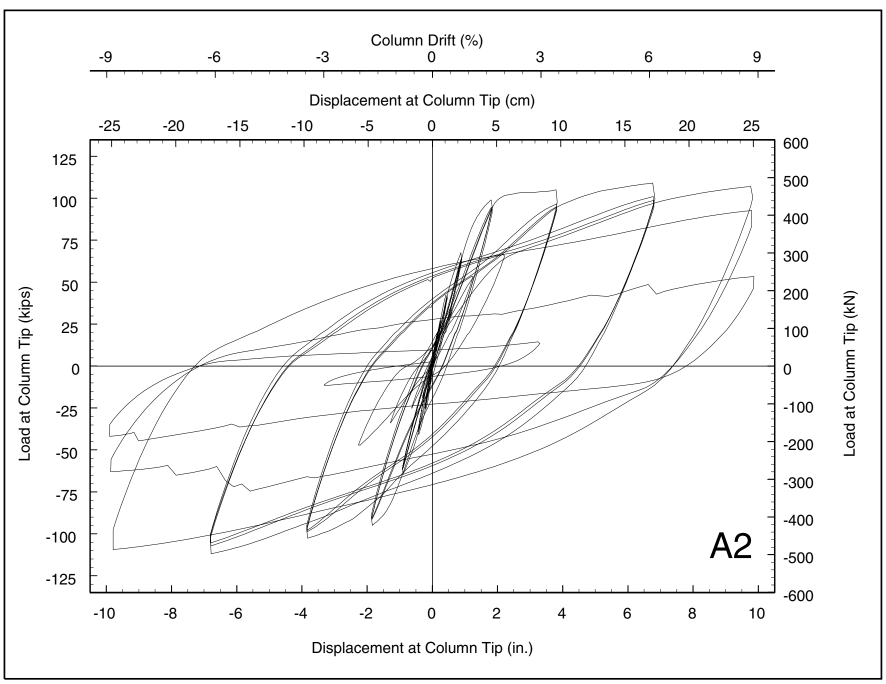

Figure 6-6: A2 load-displacement behavior

Fracture of the column longitudinal reinforcement of specimens A1 and A2 manifests itself as an abrupt change in stiffness. In Subassembly A1, this change can be observed on the first southern (negative) 10-in. cycle. This corresponds to tensile fracture of the north column longitudinal reinforcement. The initial stiffness decrease is closely followed by a sharp increase in stiffness. This can be explained as the result of rapid load redistribution to the adjacent tensile reinforcement. As another bar fractures, the lateral stiffness once again drops. Subassembly A2 responds in a similar manner to A1. On the second southern (negative) excursion, a successive degradation in stiffness can be observed. This corresponds to multiple fractures of column longitudinal reinforcing bars. From this point on, the system rapidly loses strength and stiffness. Note that the occurrence of buckling has little immediate effect on the overall system response. This is evident in the response of A2, which underwent buckling during the 7-in. displacement level. At this demand, the strength remained stable. These buckled bars eventually fractured during the 10-in. displacement cycles leading to notable strength degradation.

The square column subassemblies A3 and A4 exhibited a stable yield plateau from approximately 2.0 in. to 7.0 in. of column displacement (Figure 6-7 and Figure 6-8). For Subassembly A3, pinching of the hysteresis became apparent during the second 4.0-in. displacement cycle. At this demand level, significant yielding of the column longitudinal reinforcement was recorded. This coincided with the relatively wide flexural crack openings observed along the column height. One explanation for the measured pinching is as follows. Notable tensile yielding of the south longitudinal column reinforcement occurs during the first southern displacement to 4.0 in. This results in large crack openings along the column height. Load reversal to 4.0 in. results in a decrease in stiffness that continued until the cracks fully closed, at which time the stiffness once again increased. During the first southern 4.0-in. displacement, the north longitudinal column reinforcement yields considerably. This again results in large crack openings. The occurrence of this effect on both faces exacerbates pinching of the load-displacement response. This effect is notable in a comparison of the first and second load reversals toward the north during the 4.0-in. displacement level. On the following displacement excursion to 7.0 in., buckling of the column longitudinal reinforcement occurred. This buckling manifests itself once again as noticeable pinching of the hysteresis. Upon load reversal, the buckled reinforcement is pulled in tension, thus straightening the bars. This leads to a decrease in stiffness from the preceding cycle since the straightening action takes less force. Once the buckled shape is removed, the stiffness increases once again, thus creating the pinching effect in the recorded hysteresis. This pinching response is more prevalent in the square column subassemblies than the circular ones because the majority of the column longitudinal reinforcement lies on extremities of the section. As a result, many bars buckle and straighten at the same time, thus significantly altering the system stiffness. In the circular column subassemblies, the longitudinal bars are evenly spaced around the periphery and depth of the column. As a result, bars buckle and straighten at different demand levels, leading to a gradual decrease and increase in stiffness, which is not apparent in the hysteretic curves.

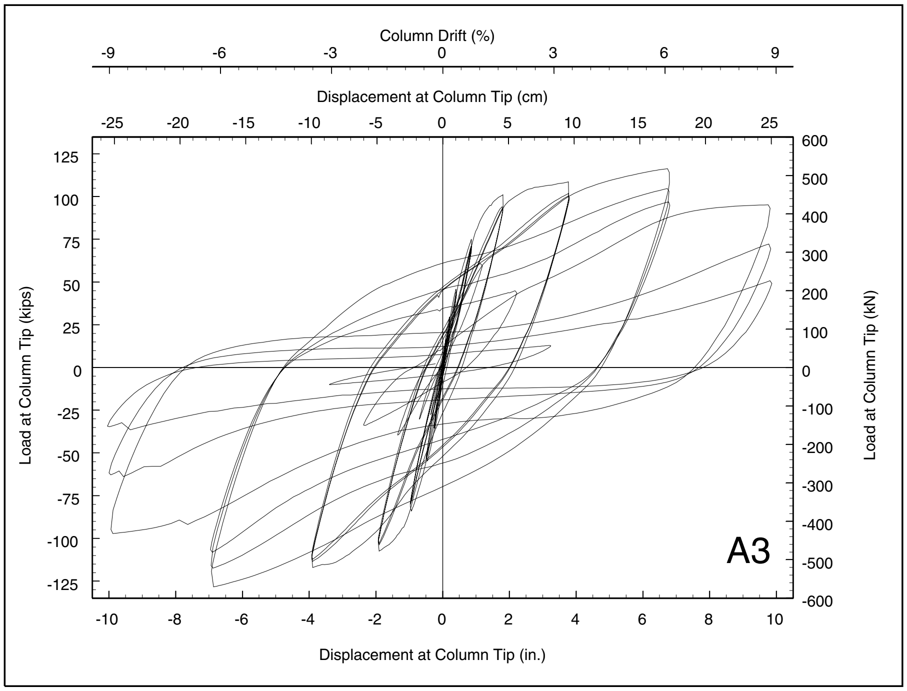

Figure 6-7: A3 load-displacement behavior

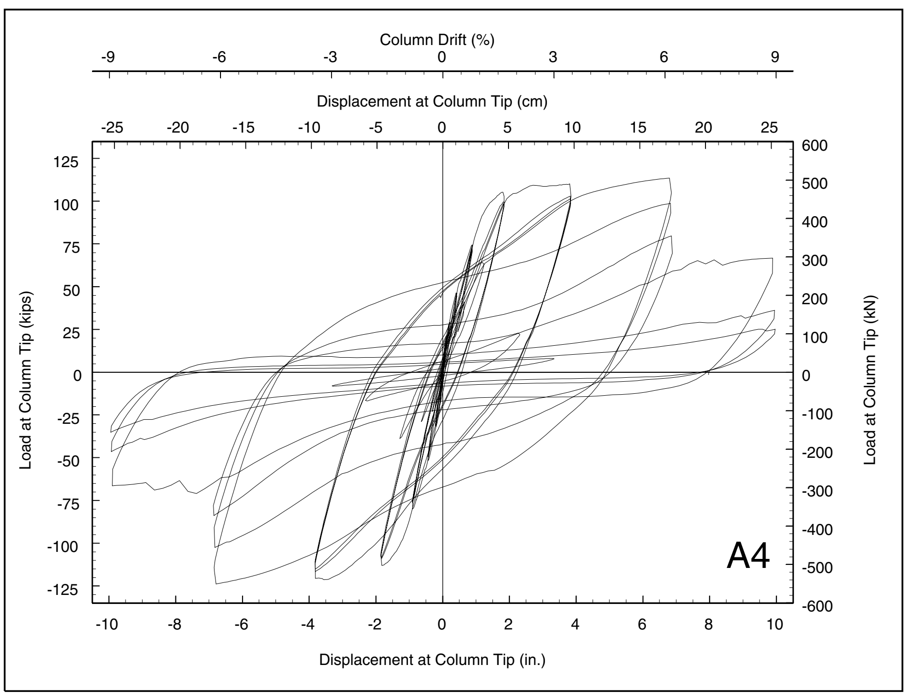

Figure 6-8: A4 load-displacement behavior

The measured load-displacement behavior of Specimen A4 is essentially the same as that of Specimen A3. The degree of pinching and the overall shape of the hysteresis are comparable. The exception is the strength decrease that occurred between the 7-in. and 10-in. displacement cycles. In Specimen A3, a 20% decrease in strength was noted between the first 7-in. cycle and the first 10-in. cycle. In Specimen A4, a 40% decrease was noted over the same range. This may be a result of the earlier initiation of longitudinal reinforcement buckling in Specimen A4 (Table 6-1). As a result, stiffness degradation started earlier in A4 than A3, leading to a greater decrease in strength at the same level of displacement demand.

In general, the global load-deflection responses of the four specimens were very ductile. With the exception of the pinching noted previously, the circular column specimens and the square column specimens had comparable hysteretic loops. The replacement of headed reinforcement did not noticeably change the global hysteretic response. While the square column specimens had a higher capacity than the circular column specimens, the strength degradation occurred at a lower level of drift. In addition, the square specimens exhibited a greater amount of pinching as a result of the arrangement of the column reinforcement.

6.1.2 Strength Degradation

To assist in the development of nonlinear models, the following section evaluates the system strength degradation associated with reversed cyclic loading. Strength degradation is defined as the loss of resistance between subsequent cycles at the same displacement level. The percentage decrease in load capacity is defined as the difference between load resisted in the two cycles divided by the load resisted in the first cycle of that pair of cycles for that displacement amplitude. The strength degradation is organized with respect to displacement ductility, where the displacement ductility is defined as the displacement divided by the displacement resulting in first yield of the column reinforcement.

Up to a displacement ductility of 4.0, a 5% to 8% decrease in resistance was measured between the first and second cycles at a particular displacement amplitude (Figure 6-9). This behavior occurred for both the square and circular column specimens. At this same level of demand, the decrease in strength between the second and third cycles is almost negligible (approximately 2%). Since the behavior is consistent in both the elastic and inelastic levels, this decrease may be attributed to crack formation or bond-slip.

After a ductility of 4.0, the strength degradation of the beam-column specimens is more noticeably affected by cyclic loading. At this level of demand, spalling of the column cover, and buckling and fracture of column longitudinal reinforcement were observed near the beam-column interface. Each of these actions is likely to have had a significant effect on the strength degradation of the subassemblies. Before and during the initiation of spalling, the compression face may still be able to bear on the cover concrete. As spalling develops, the compression face is reduced, leading to a notable decrease in resistance. Buckling has a similar effect on the strength degradation. Prior to buckling, the reinforcement is capable of providing a relatively high stiffness against compressive loading. After buckling, the bar is deformed, leading to a notable decrease in stiffness on excursions to the same displacement. Likewise, the occurrence of fracture leads to significant strength degradation. The combination of these failure mechanisms affects the overall strength degradation of the subassemblies. After a displacement ductility of 4.0, strength degradation between the first and second cycles increases from 5% to as high as 45% (Figure 6-9). Unlike the lower demand levels, the strength degradation did not stabilize after the second cycle but continued in subsequent cycles (Figure 6-10).

Specimen A4 has the largest capacity reduction from the first to second cycle between ductility 6 and 9. This led to constant capacity reduction from the second to third cycles in the same ductility range. This shows the effect of fracture on strength loss. In Specimen A3, fracture of longitudinal reinforcement commenced on the first northern displacement to a μ of 9.0. Consequently, strength loss was significant between the first and second cycles and minimal between the second and third.

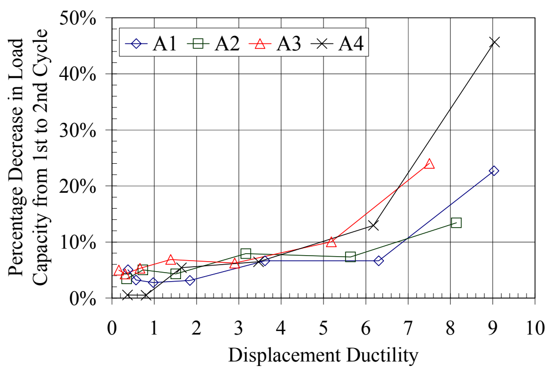

Figure 6-9: Capacity decrease from first cycle to second cycle

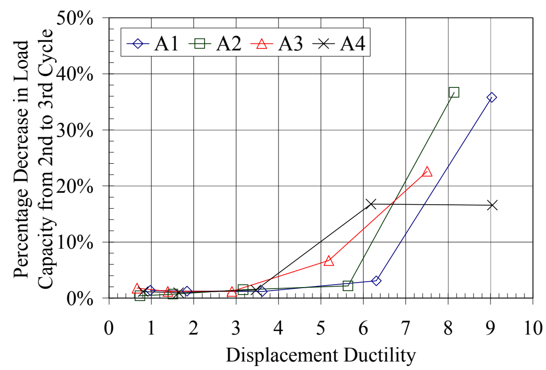

Figure 6-10: Capacity decrease from second cycle to third cycle

Some approaches for evaluation of reinforced concrete construction [FEMA 273] recommend that strength degradation be accounted for in the load-deformation envelope by constructing a backbone curve drawn through the intersection of the first cycle curve for the $(i)^{th}$ deformation step with the second cycle curve of the $(i\text{ -}1)^{th}$ deformation step (Figure 6-11). Backbone curves were developed using this approach for Group A subassemblies (Figure 6-12).

The backbone curves show that the square and circular column beam-column configurations with headed and conventional reinforcement produce similar global responses. The initial stiffness and the initiation of the yield plateau are similar. The only notable difference is the strength decrease measured in Specimen A4, which can be attributed to an early occurrence of buckling in the column longitudinal reinforcement. Since the square column configuration has a tendency for rapid strength degradation after the initiation of buckling, the envelope obtained for A3 may overestimate the yield plateau. Slight construction changes could lead to earlier buckling and reduced strengths thus altering the capacity after a ductility of 4 as the case for A4.

In summary, cyclic effects on strength degradation were not significant prior to a ductility of 4. At this level of demand the decrease in the capacity as a result of cyclic loading were a maximum of 8% between the first and second cycles and a maximum of 5% between the second and third cycles. A reasonable conclusion is that the experimental behavior can be adequately modeled by a monotonic analysis as will be the case for the finite element analyses of Chapter 8.

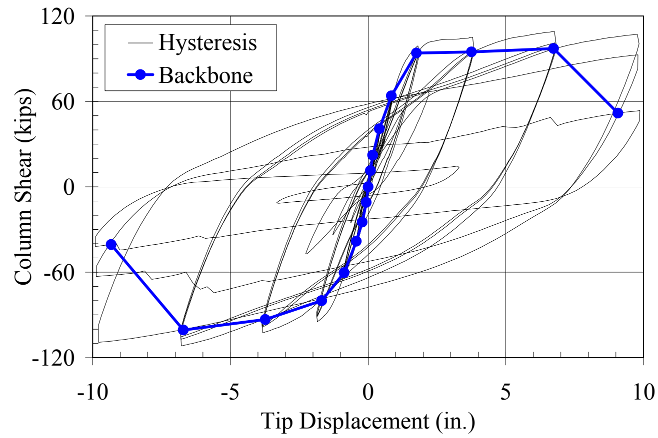

Figure 6-11: Backbone development per FEMA 273

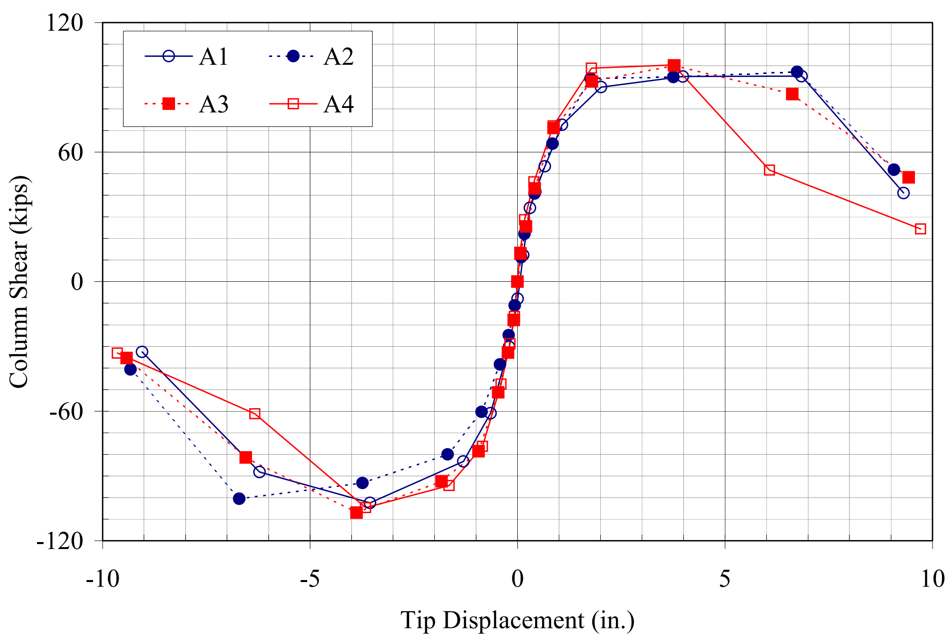

Figure 6-12: Global load-displacement backbone curves for Group A

6.1.3 System Stiffness

As a means of evaluating the rigidity of the subassembly over the life of the structure, the system stiffness was calculated at different levels of displacement demand. Using data from the pre-yield cycles and the low-level cycles that follow each post-yield group, the system tangent stiffness was computed throughout the displacement history. Figure 6-13 compares this stiffness at various phases of the experiment with the maximum ductility that the system has undergone. Note that under low levels of displacement, the resolution and inherent friction in the displacement transducers result in measured load increases without appropriate displacement changes. This produces a very high artificial stiffness under low displacement (or ductility) levels. As a frame of reference, the stiffness history is compared with an initial stiffness computed with the measured material properties and the as-built gross cross sections (shown as filled symbols on the global stiffness axis).

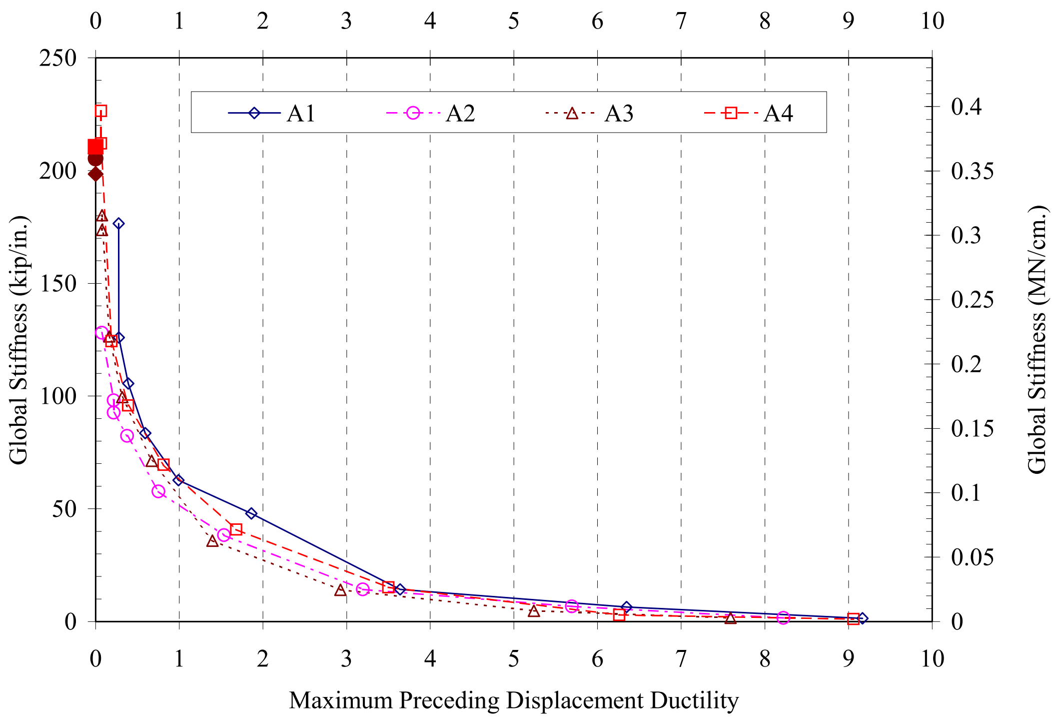

Figure 6-13: Tangent global stiffness

In general, all four subassemblies behaved in a similar manner. The system stiffness rapidly decreases, dropping to approximately 25% of its uncracked stiffness by the onset of yielding. This decreases further, to less than 10% by a displacement ductility of 3.0. After this point the stiffness drops linearly to approximately 1% at the end of the test. The only significant deviation between the subassemblies occurred with A1. As a result of the loading error discussed in Section 6.1.1, the column damage is unsymmetrical, producing higher system stiffness at a displacement ductility of 2.0 than that measured for Specimen A2.

To isolate the source of degradation, the subassembly stiffness was computed analytically and compared to the experimental behavior measured at various states of system damage (Figure 6-14). Subassembly A1 is used for this comparison. Using the as-built dimensions and the measured material properties, three levels are evaluated: (1) uncracked system stiffness using the gross moment of inertia, (2) cracked-column stiffness using the cracked transformed inertia over the column height, and (3) cracked system stiffness using the column and beam cracked moment of inertia over their respective lengths. In all cases, the joint is assumed to be rigid.

The comparison with the measured stiffness shows that the initial stiffness is slightly overestimated by the analytical solution. This can be attributed to initial cracking prior to testing, or to the limited resolution of the instrumentation. In each case, the analytical estimation is comparable to the experimentally measured system stiffness giving validity to the analytical estimation. Analytically, column cracking accounts for a 50% decrease in system stiffness. In the experiment, column cracking initiated at a displacement ductility of 0.1. Cracks, however, were not well distributed until a ductility of 0.5. This corresponds with the analytical estimation of column cracking which intercepts the experimental stiffness at a ductility of 0.5. Experimentally, beam cracking occurred just prior to a ductility of 0.5. This again correlates with the stiffness predicted by the analytical model.

In summary, the use of the gross cross-sectional properties overestimates the initial stiffness of the beam-column subassemblies. Both the square and circular column configurations had a significant decrease in the global tangent stiffness prior to yielding (on the order of 75%). This continues to decrease to approximately 10% of the system elastic stiffness by a displacement ductility of 3.0. Both the square and circular configurations had similar stiffness degradation.

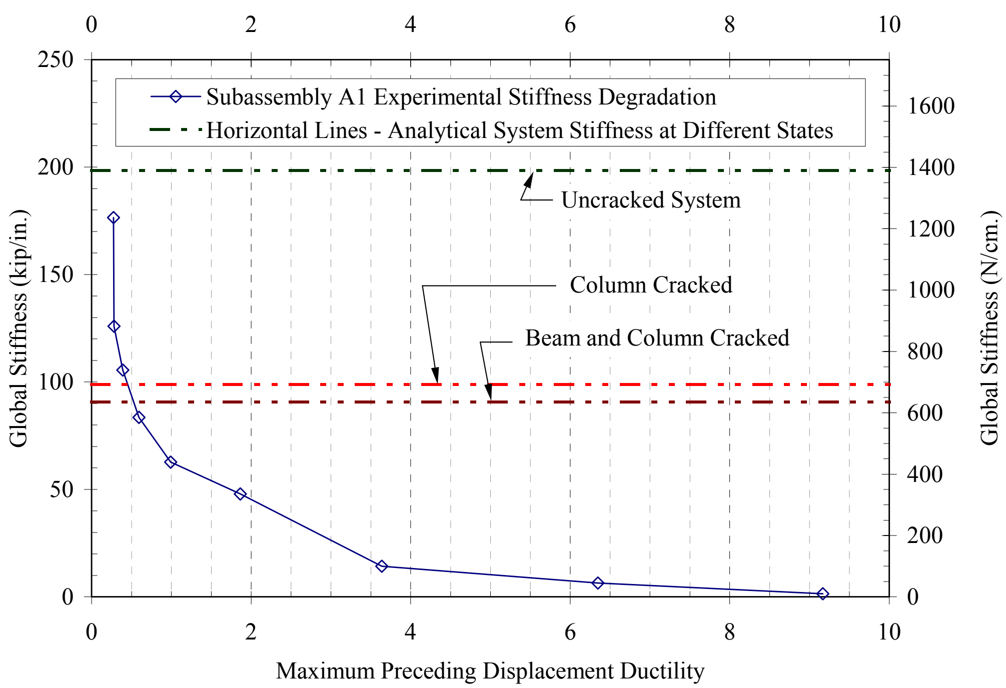

Figure 6-14: Typical system stiffness degradation

6.1.4 Energy Dissipation

The level of energy dissipation was calculated to provide an estimate of system damping. The energy dissipated is equal to the cumulative area enclosed within the load-displacement hysteresis loops. Figure 6-15 presents the energy dissipated as a function of system drift. Both circular column configurations dissipated the same level of energy at comparable levels of drift. Likewise, both square column specimen behaviors were similar. The circular specimens dissipated somewhat less energy than the square specimens, even though the square specimens had more pinching than the circular specimens (Figure 6-5 through Figure 6-8). The marginally higher energy dissipation in the square-column subassemblies results because they had a higher yield and ultimate strength than did the subassemblies with circular columns.

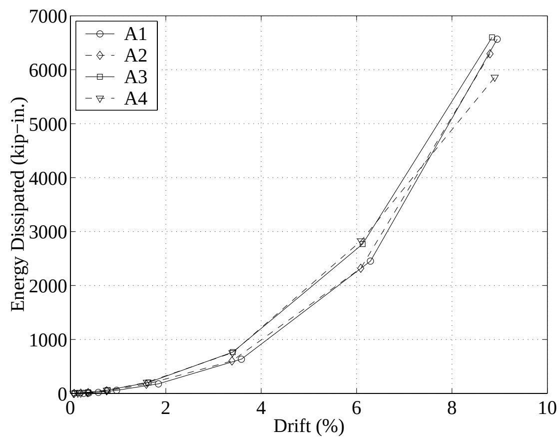

Figure 6-15: Cumulative energy dissipated at different levels of drift

6.1.5 Element Contributions to Global Displacement

Response of a reinforced concrete beam-column subassembly can be viewed in terms of several different components of deformation. In this section, six different components are evaluated. These are (1) flexural deformation of the column, (2) flexural deformation of the beam, (3) shear deformation of the column, (4) shear deformation of the beam, (5) shear deformation of the joint, and (6) slip of the column reinforcement from the joint. An external array of instrumentation was installed to capture the displacement contributions (Chapter 3). Results are presented for two levels of system damage: displacement ductility of 1.0 and 4.0. These levels represent the system behavior at the onset of significant damage and the behavior near the ultimate strength of the systems (note that ultimate load capacities were recorded at a ductility between 4.8 and 6.0), respectively.

At a displacement ductility of 1.0, the contribution of each component to the total drift is similar among subassemblies (Figure 6-16). The combined effect of beam and column flexure makes up 52–57% of the total displacement. Column shear is below 10% and beam shear is approximately 5%. The deformation associated with reinforcement slip makes up approximately 25% of the total tip displacement.

Two aspects of the data in Figure 6-16 are noted. First, note the difference in column flexural contribution between A1 and A2. This is believed to be due to the initial loading applied to A1 (Section 6.1.1). This offset resulted in longitudinal reinforcement yield occurring in the 1-in. displacement group for A1, whereas for A2, yielding did not occur until the 2-in. displacement group. As a result, at a ductility of 1.0, Column A1 was subjected to fewer cyclic load reversals than A2. Thus, the column stiffness is higher, producing a lower portion of the total displacement. A second aspect of Figure 6-16 is the difference in contribution of slip for a circular and square column. When a square column reaches yield, all bars on the tension face yield simultaneously. In the circular column configuration, the bars are distributed around the perimeter; as a result, only one bar yields at the onset of column yielding. Therefore, circular columns produce lower demand on the joint, less yield penetration, and less slip.

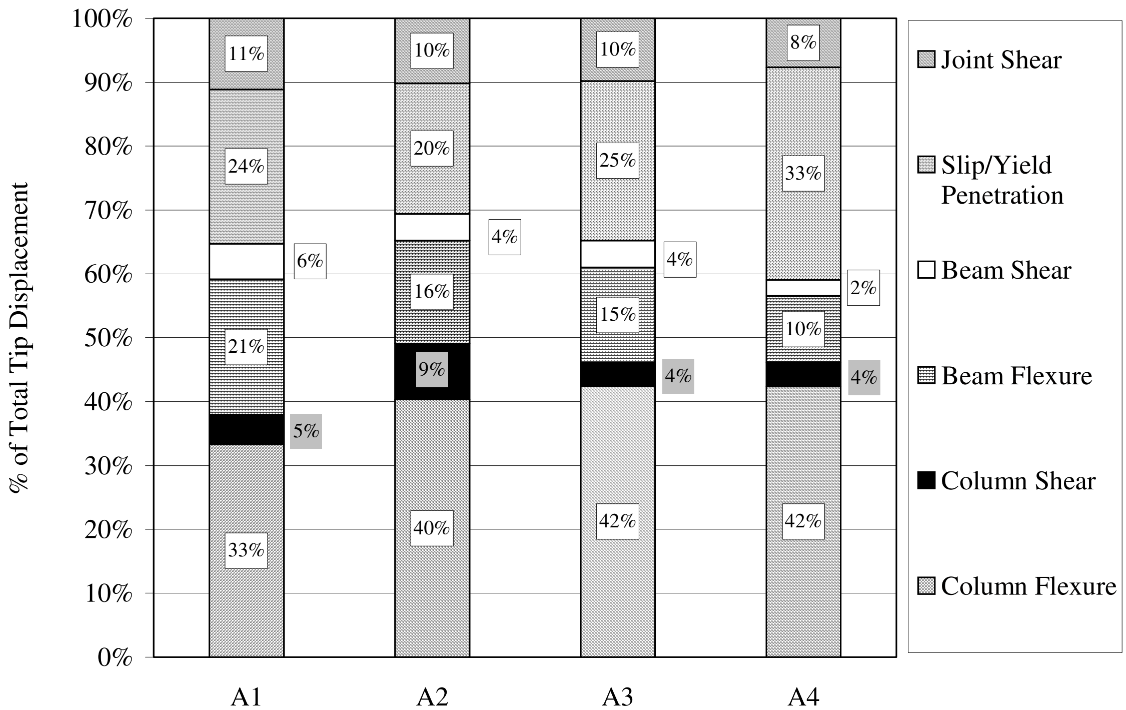

Figure 6-16: Contribution to total tip deflection at displacement ductility of 1.0

At a ductility of 4.0 the joint has experienced distributed cracking, and spalling of the column has begun. As a result, column flexure and slip of the column reinforcement from the cap beam control the system response (Figure 6-17). Beam flexure and shear, column shear, and joint shear make up less than 7% of the total displacement. The variation between A1 and A2 is most likely due to the early yield of A1 (as a result of the initial 0.24-in. displacement offset). Slip of Specimen A4 is greater than that of A3. This suggests that the headed column bars may have been less restrained than bars developed straight without a head. This hypothesis is counter-intuitive but could be a result of the sparse joint transverse reinforcement layout used in A4. Discussion of this issue is continued in the section on local behavior.

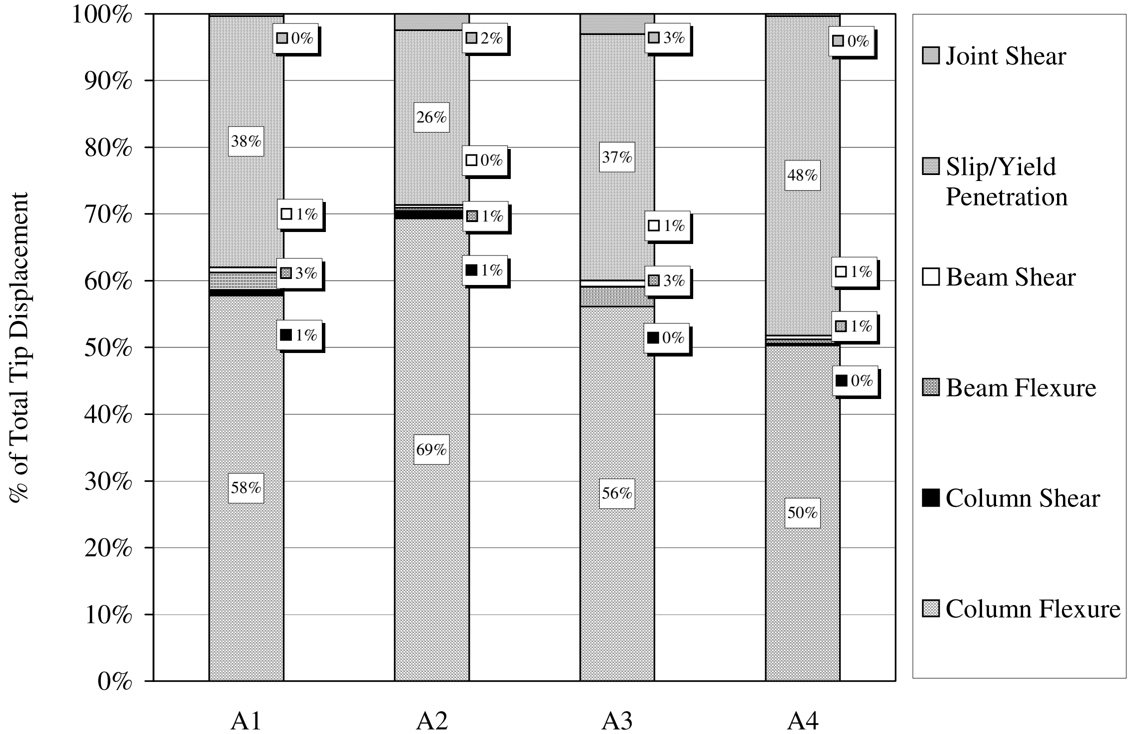

Figure 6-17: Contribution to total tip deflection at displacement ductility of 4.0

Inelastic response of the subassemblies is predominantly due to column inelastic response. At lower levels of demand the joint deformation represents up to 11% of the total tip displacement. After the column reaches its plastic capacity, however, the system behavior is dominated by column plasticity with relatively little contribution from the joint. This is consistent with the design intent.

6.1.6 Joint Behavior

Effectiveness of a joint design can be quantified by its ability to transfer loads with minimal deformation and damage. To examine this aspect, joint shear stiffness was calculated. Joint shear stiffness is defined as the nominal shear stress divided by the nominal joint shear strain. The assumptions used for computation of the shear stress and strain were discussed in Chapter 3.

The shear stress-strain responses measured for Group A specimens up to the peak load are presented in Figure 6-18 through Figure 6-21. Specimen A1 exhibits a skewed shear stress-strain behavior as a result of an error in the loading protocol. The circular column configuration produces a more flexible joint shear response than that of the square column configuration.

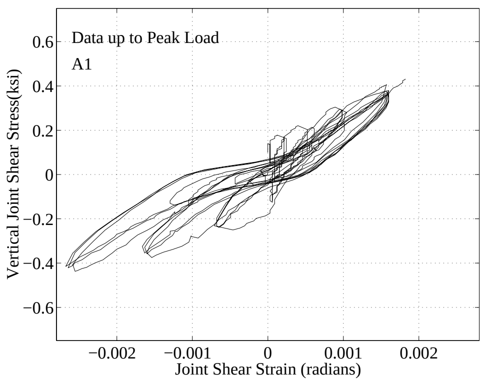

Figure 6-18: A1 joint shear response

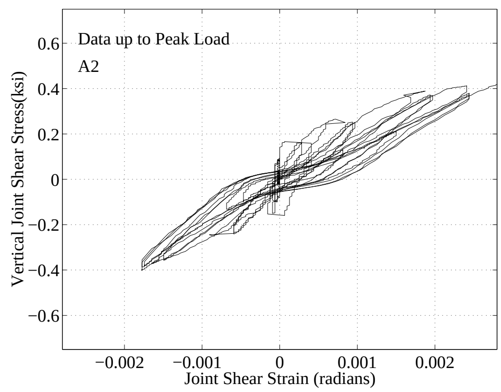

Figure 6-19: A2 joint shear response

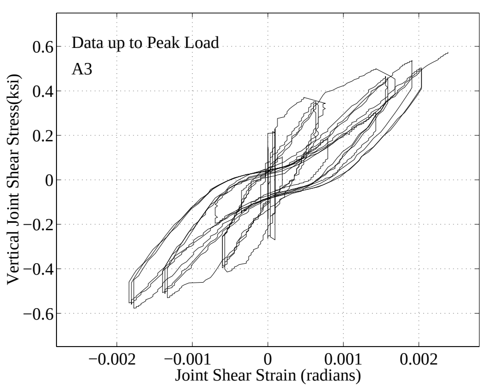

Figure 6-20: A3 joint shear response

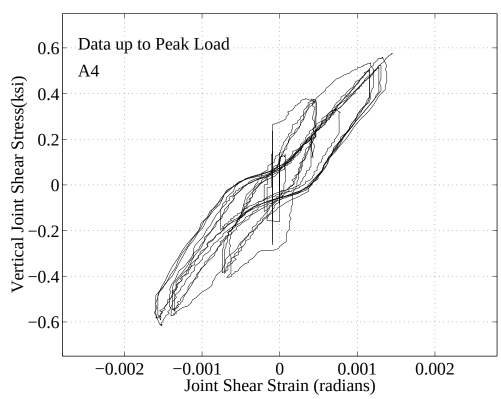

Figure 6-21: A4 joint shear response

Backbone curves were developed from the measured experimental responses using the recommendations of FEMA 273 (Figure 6-22). The results are plotted in Figure 6-23 for all specimens in Group A. These backbone curves show that the joints in the square column subassemblies, A3 and A4, have higher shear stiffness than the circular column subassemblies, A1 and A2. There is no significant difference in the behavior of the joints detailed with conventional reinforcement and those detailed with headed reinforcement.

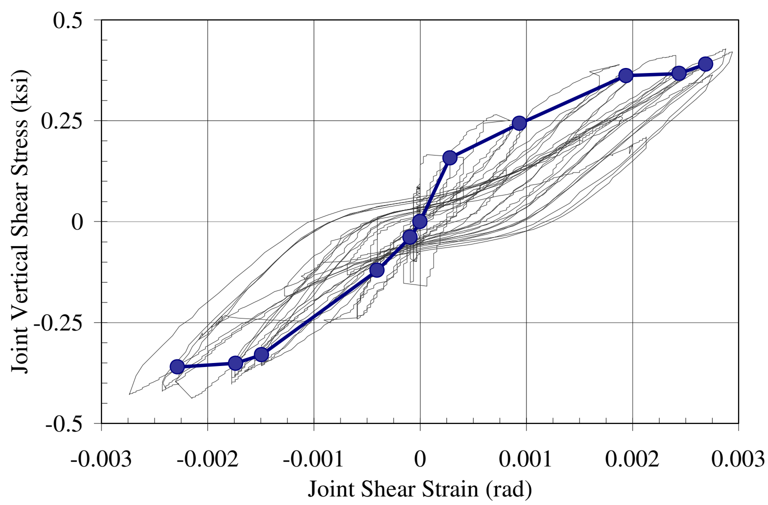

Figure 6-22: Joint shear backbone development

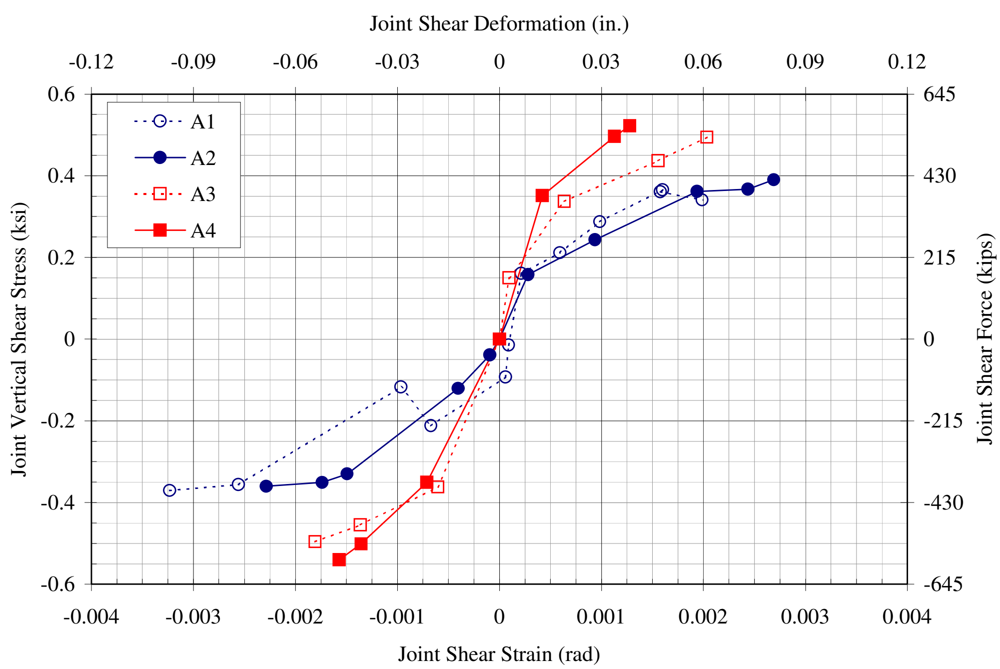

Figure 6-23: Joint shear stress-strain backbone curves for Group A

To evaluate the joint shear stiffness of Group A specimens, the tangent stiffnesses were calculated at different points throughout the load history. The stiffness degradation of each of the subassemblies is plotted against the maximum preceding column tip displacement (Figure 6-24). As discussed in Chapter 3, external linear potentiometers were used to measure the joint shear strains. Since these instruments had a finite resolution, the shear strain may not have been accurately measured until joint cracking began. An initial joint shear stiffness can be calculated from the shear modulus of concrete. Using a Poisson's ratio, ν, of 0.15 and the average elastic modulus, E_c, of Group A, this value is computed from Hooke′s law, $G_c = E_c / (2*(1+\nu))$. The resulting elastic joint stiffness is equal to 1550 ksi/radian.

The joint stiffness decreases to approximately 1/3 of its theoretical elastic stiffness prior to the onset of column yielding (Figure 6-24), which occurred at a tip displacement of 1.4 in. After this level of demand the joint stiffness decrease stabilizes. This can be attributed to the formation of the column plastic hinge.

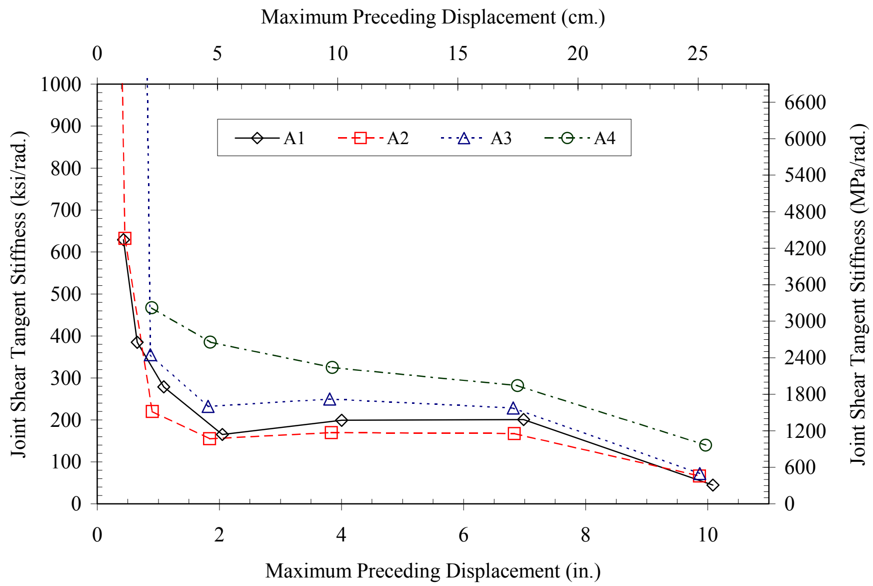

Figure 6-24: Joint shear tangent stiffness

6.2 Local Behavior

Investigation of local behavior consists primarily of the evaluation of strain at various locations and levels of loading. The investigation is divided into three components: column behavior, beam behavior, and joint behavior. The column behavior includes both the flexural response and the amount and source of slip. This is followed by an evaluation of the beam flexural response and a comparison with analytical models. An evaluation of joint behavior is conducted in which the levels of demand on the joint spiral and transverse joint reinforcement are investigated.

6.2.1 Behavior of Column Longitudinal Reinforcement

Column behavior is investigated in the following sections by an evaluation of the strains in the extreme tension and compression column longitudinal reinforcement. The behavior of the circular and square column subassemblies are compared under both compressive and tensile responses. Figure 6-25 presents the tensile strains in the circular columns A1 and A2. The strains (x-axis) are plotted along the northern column bar (y-axis); positive values on the y-axis represent the region within the beam depth, and negative values represent regions along the column height.

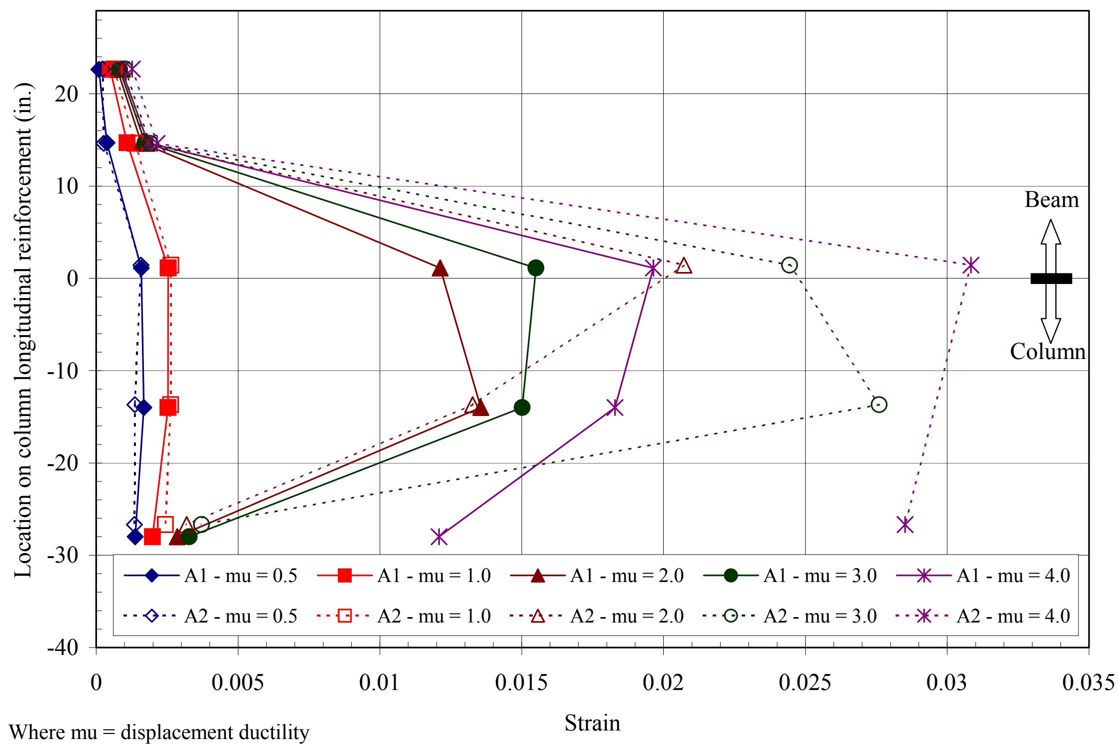

Figure 6-25: Longitudinal column reinforcement tensile strains, circular column specimens

At early stages of loading, the responses of the two circular column subassemblies are essentially identical. The strain decreases linearly within the joint and column, from a maximum at the interface to small values at each end. At a displacement ductility of 2.0 and greater, A2 recorded higher interface strains than A1. Since both columns and beams are identical, this increase in column strains at the same level of displacement demand could be attributed to a decrease in the stiffness of A1 due to a softer joint region or a higher degree of slip.

The headed reinforcement is subjected to higher strain demands than the conventional reinforcement. Within the joint, strains for specimens A1 and A2 showed a similar trend, decreasing quickly near the end of the bar. At the interface, however, the headed reinforcement was subjected to much higher strains under similar levels of demand. This could be an indication of reinforcement slip. Slip of the non-headed bars would decrease the demand on the system, allowing A1 to reach the same displacement as A2 with lower strain. This is consistent with the greater slip measured in Specimen A1 at a displacement ductility of 1.0 and 4.0 (Figure 6-16 and Figure 6-17). This indicates that the use of headed column longitudinal reinforcement can decrease the level of slip for fully developed bars at the cost of higher strain demands.

In the circular column specimens, longitudinal reinforcement yielding propagates into the column. Within the cap beam the longitudinal reinforcement strains abruptly decrease to a fraction of the beam-column interface strain. While in the column, both specimens consistently reach a level of equal tensile strain from the interface to a distance of approximately 14 in. away from the interface, half the column diameter.

Combining this behavior with the measured height of spalling (Table 6-2) one can infer that these subassemblies may develop a column flexural plastic hinge on the order of half the column diameter.

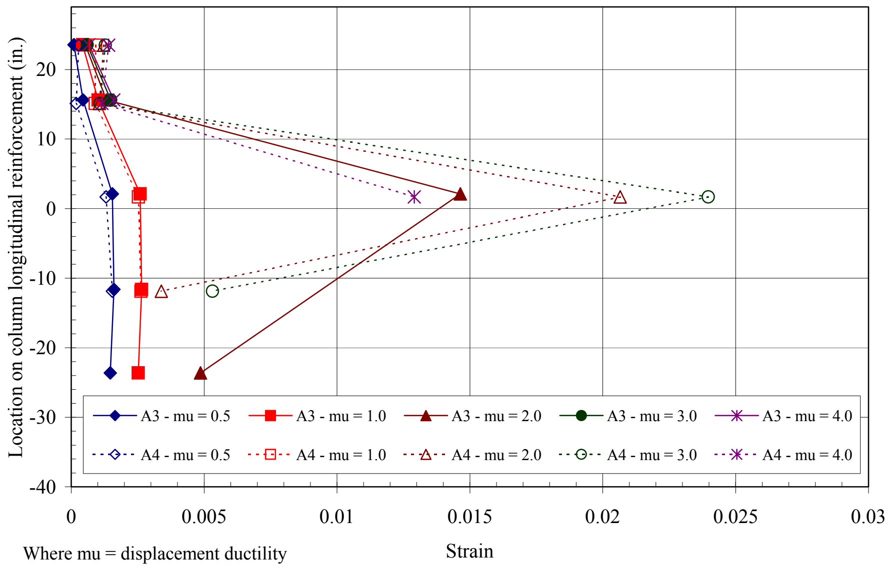

Figure 6-26: Longitudinal column reinforcement tensile strains, square column specimens

The tensile strains in the longitudinal reinforcement of the two square column assemblies are similar up to the onset of yielding (Figure 6-26). Beyond a ductility of 1.0, the headed bars were subjected to larger strains than the conventional bars in the column. After a ductility of 2.0, the column strain gages began to fail. The strain gages within the joint recorded similar levels of strain for both A3 and A4. The strains in A4, however, did not decrease to zero at the end of the bar, but instead remained constant or decreased only slightly. This behavior suggests that the headed reinforcement was developed partly through bearing on the heads.

In general, the compressive behavior of the column reinforcement was characterized by a maximum value at the beam-column interface and gradual decrease in the column and joint. In both the square and circular columns, the headed reinforcement tended to have a greater permanent tensile strain, often leading to tensile strains under compressive loading (Figure 6-27 and Figure 6-28).

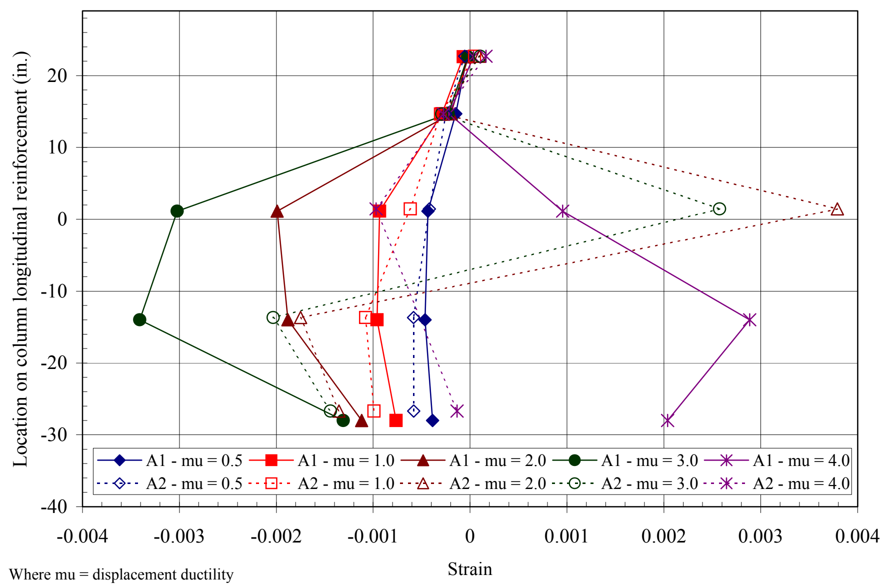

Figure 6-27: Longitudinal column reinforcement compression strains, circular column specimens

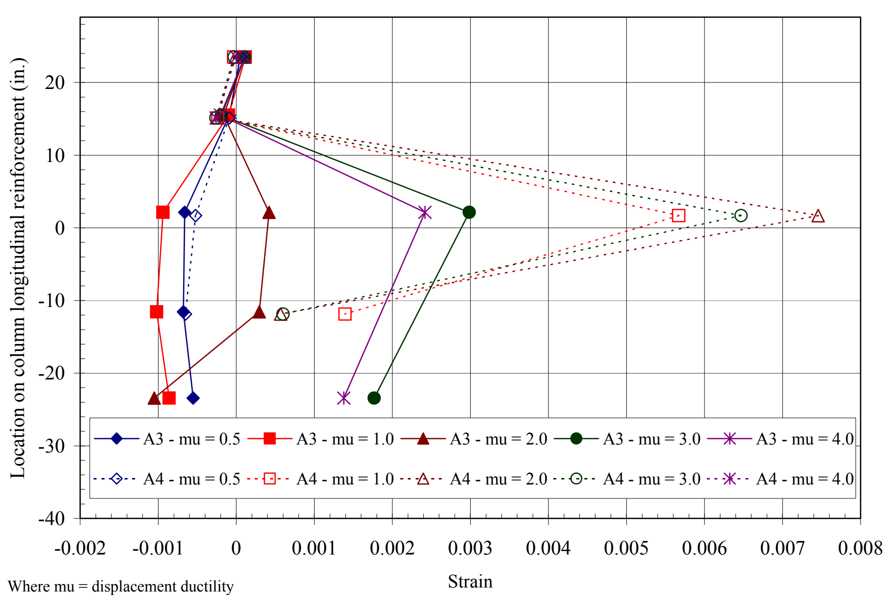

Figure 6-28: Longitudinal column reinforcement compression strains, square column specimens

The tensile column reinforcement strain distribution can be used to estimate the bond stress distribution in the joint. A typical bond stress distribution is shown in Figure 6-29. This average bond stress distribution was obtained from Specimen A1 and is typical for the behavior of Group A. To compute these values the stress in the bar was computed first. The strain history measured at each gage location was converted into a stress history using the Menegotto-Pinto model [Farve 1985], initially implemented by Filippou-Yassim and subsequently modified by Lowes [1999]. From this, the bond stress, μ_b, on the reinforcement was computed with the following relationship [MacGregor 1988]

$$\mu_b = \Delta\sigma \, d_b / 4\ell \tag{6-1}$$

Where $\Delta\sigma$ is equal to the change in stress between adjacent gages, d_b is equal to the bar diameter, and ℓ is equal to the distance between adjacent gages. As shown, the majority of the bond action takes place near the end of the bar. This region corresponds to the flexural compression zone of the beam and diagonal compression strut of the joint. It is likely that the high compressive stress improves bond in this region.

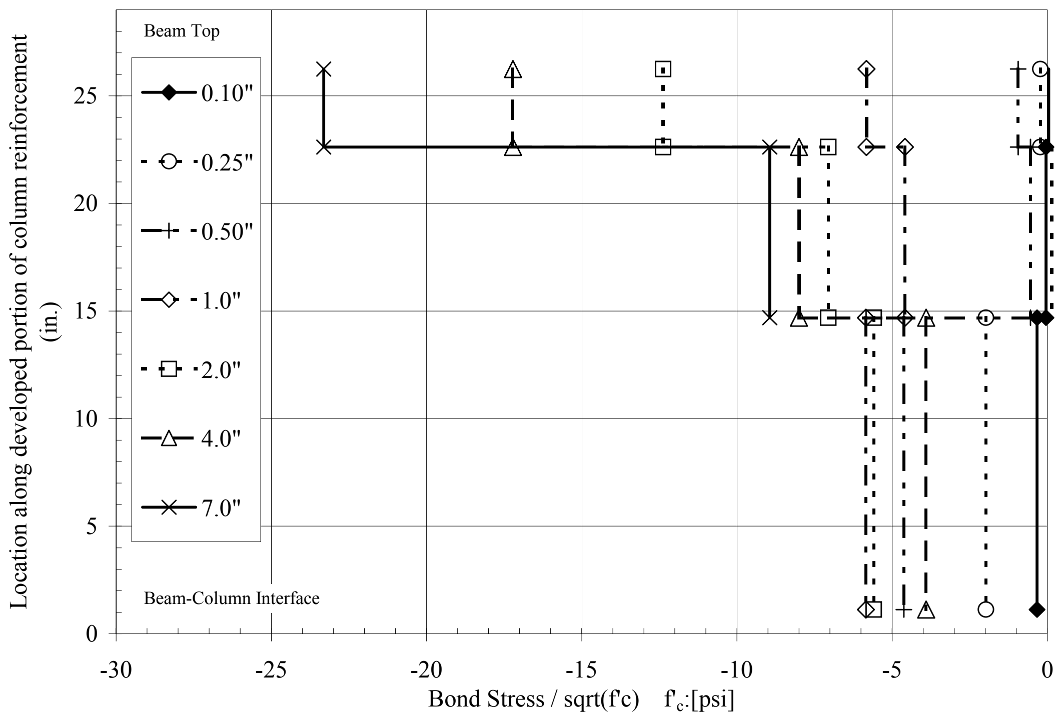

Figure 6-29: Typical bond stress demand, Specimen A1 north bar shown

Slip Components

Evaluation of the slip of the column reinforcement from the joint reveals that the use of headed reinforcement reduced pullout as expected. Slip of the column longitudinal reinforcement from the joint, Δ_T, can be defined as the combination of two actions: elongation from straining action along the bar, Δ_S, and pullout caused by loss of bond over the embedded length, Δ_P, producing the relation

$$\Delta_T = \Delta_S + \Delta_P \tag{6-2}$$

Pullout, in turn, can be decomposed into two components: pullout due to local bond-slip along the embedded bar, Δ_b, and complete dislocation of the bar from the concrete, Δ_d, with the relation

$$\Delta_P = \Delta_b + \Delta_d \tag{6-3}$$

The displacement components are illustrated in Figure 6-30.

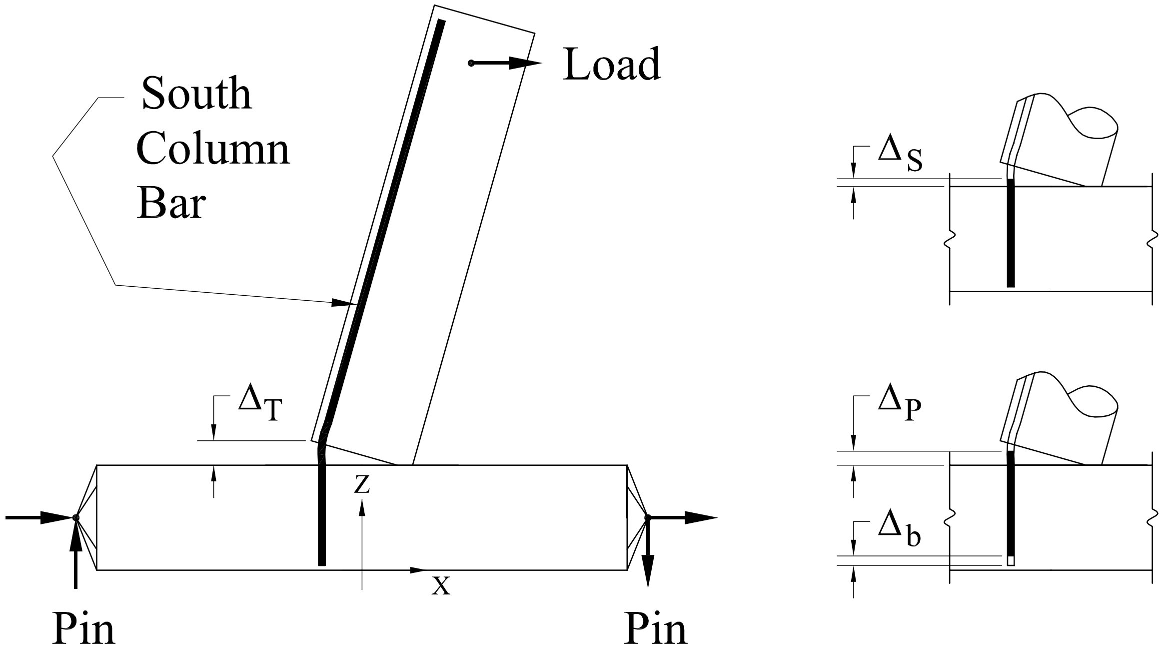

Figure 6-30: Slip components

Use of headed reinforcement essentially fixes the end of the bar against deformation. This decreases the amount of pullout since the bar is unable to globally pullout from the surrounding concrete matrix. As a result, deformation of the bar is limited to straining actions along the bar and local bond-slip along the bar length. Consequently, straining action is increased from that recorded for non-headed reinforcement (see Figure 6-25 and Figure 6-26 comparing A2 with A1, and A4 with A3). Overall slip however is greater in Specimen A1 than in Specimen A2 (Figure 6-16 and Figure 6-17). This indicates that the pullout has a larger component in the non-headed system.

To evaluate the pullout contribution, the total slip and elongation due to bar straining were determined and subtracted. The total slip was determined by direct external measurement at the interface. Elongation due to straining action was determined by integrating the strain measurements along the embedded column bar length. The resulting amount of pullout is greater in the non-headed system as expected (Figure 6-31). In summary, the use of headed column longitudinal reinforcement reduces the amount of pullout and increases the amount of straining action along the bar. This creates a slip mechanism, which is reliant upon ductile yielding as opposed to brittle global pullout, providing an improvement over that of conventional column longitudinal reinforcement.

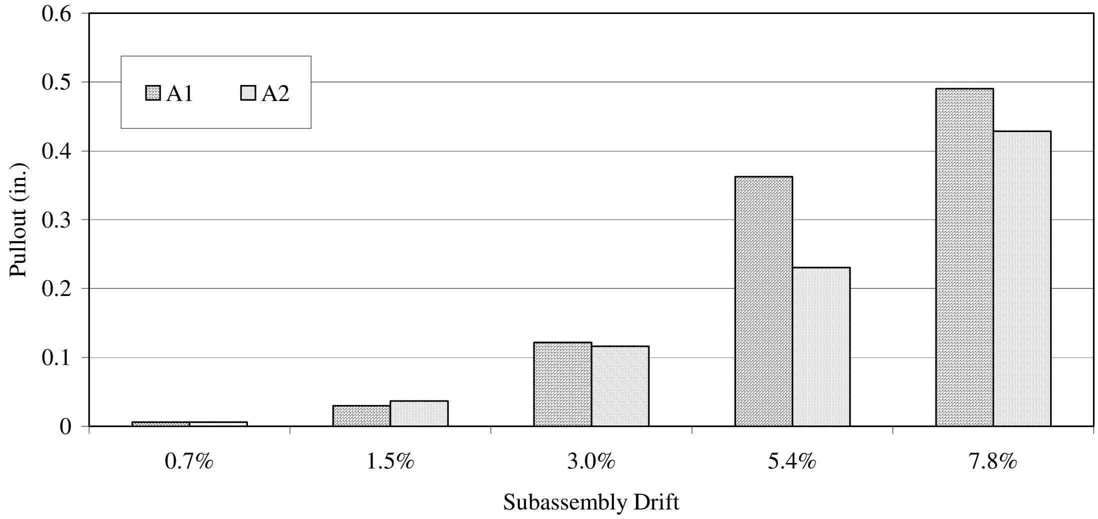

Figure 6-31: Column longitudinal reinforcement pullout at different drift levels

6.2.2 Cap Beam Flexural Behavior

To evaluate the flexural behavior of the cap beam of the subassemblies, the experimental results are compared with the expected flexural behavior computed using a simple analytical model. As discussed in Chapter 3, strain gages were installed on the beam longitudinal reinforcement. A number of bars were instrumented along their lengths. For comparative purposes, the data from the interface layer (positive flexural reinforcement), the top layer (primary negative reinforcement), and the middle layer (secondary negative reinforcement) are presented.

The analytical model consists of a two-dimensional (2D) cross-sectional analysis of the subassembly using the as-built dimensions and measured material properties. The following assumptions are made:

- Plane sections remain plane.
- Stress-strain relationship of concrete is determined from Mander′s confined and unconfined concrete models [Mander 1988].
- Stress-strain relationship of reinforcement is based on a multi-linear constitutive relationship determined from material testing. Hysteretic behavior is not considered (i.e., Baushinger effect on reinforcement is ignored).

For this evaluation, the subassemblies were evaluated under two load levels, corresponding to the onset of column yielding (μ = 1) and the ultimate load capacity (approximately μ = 5 to 6.5). In each case, the gravity load was applied in combination with a lateral load. These levels allow for an evaluation of the system under service level loads as well as the maximum demand level. The load cases used for each specimen are summarized in Table 6-3.

Table 6-3: Load levels used for beam strain investigation			
Subassembly	Gravity load D (kips)	Yield lateral load P_{yield} (kips)	Ultimate lateral load $P_{ultimate}$ (kips)
A1	149.2	71.5	110.4
A2	145.1	77.0	109.2
A3	146.6	91.2	116.5
A4	146.4	89.0	113.6

The analytical model is constructed to match the boundary conditions of the experimental subassembly (Figure 6-32). The concrete constitutive relationship is based on Mander's concrete model [Mander 1988] expressed as follows:

$$f_c(\varepsilon_c) = \frac{f_{cu} \cdot \left(\dfrac{\varepsilon_c}{\varepsilon_{cu}}\right) \cdot r}{r - 1 + \left(\dfrac{\varepsilon_c}{\varepsilon_{cu}}\right)^r} \qquad \text{for} \qquad 0 < \varepsilon_c \le \varepsilon_{max} \tag{6-4}$$

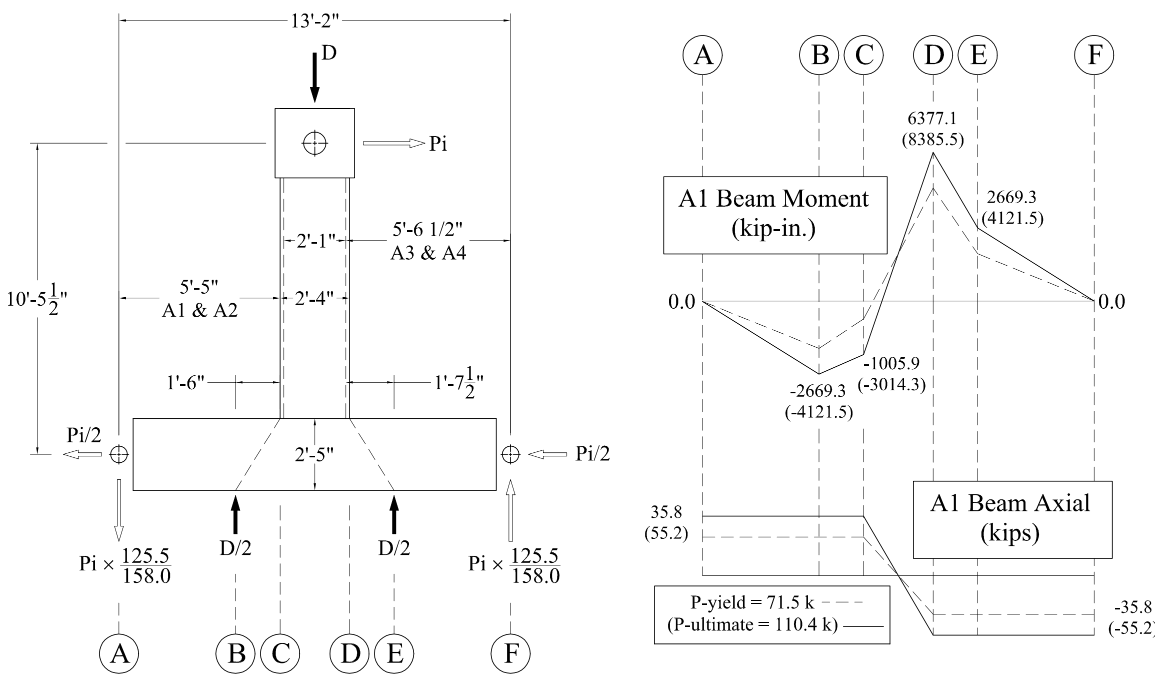

Figure 6-32: Model loading and cap beam demand

where f_{cu} is the compressive concrete strength, ε_{cu} is the corresponding strain, and the ratio r is given by

$$r = \frac{E_c}{E_c - E_{\sec}} \tag{6-5}$$

where E_c is the concrete elastic modulus and E_{sec} is the secant concrete modulus to f_{cu}. For unconfined concrete, f_{cu} is equal to the uniaxial compressive strength and ε_{max} is equal to the strain at which spalling begins, taken as 0.004. For confined concrete, f_{cu} accounts for the amount of confining reinforcement and ε_{max} is equal to the strain at which stirrups fracture [Scott 1982].

$$\varepsilon_{\max} = \left[0.004 + 0.9\min\left[\rho_y \quad \rho_x\right]\cdot\left(\frac{f_{yh}}{300}\right)\right] \tag{6-6}$$

Where ρ_x and ρ_y are the area transverse reinforcement ratios in the x and y direction, respectively of the cross section and f_{yh} is the corresponding yield strength in MPa. The concrete tensile behavior is assumed to be elastic-brittle. All material parameters are based upon experimental testing, unless noted. The material properties for each subassembly are summarized in Appendix B. The concrete and reinforcement constitutive relationships for all of the subassemblies were comparable. The models used for Subassembly A1 are presented in Figure 6-33 and Figure 6-34.

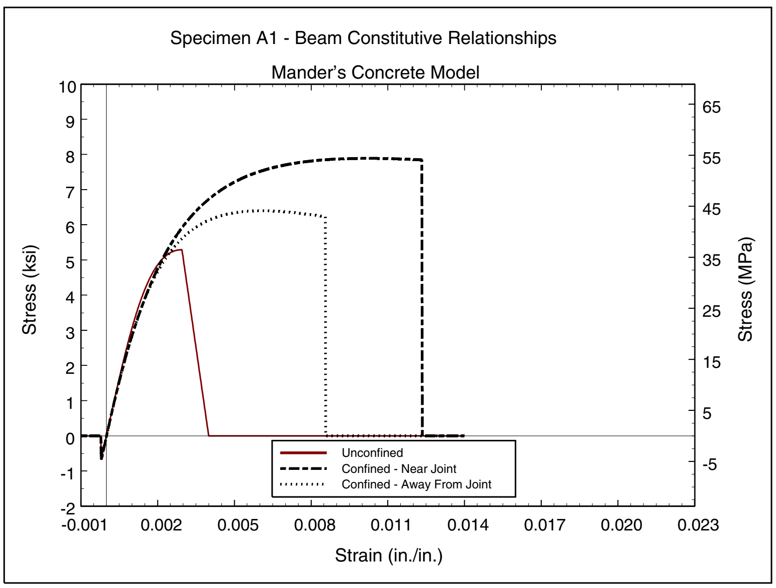

Figure 6-33: Typical concrete constitutive relationship

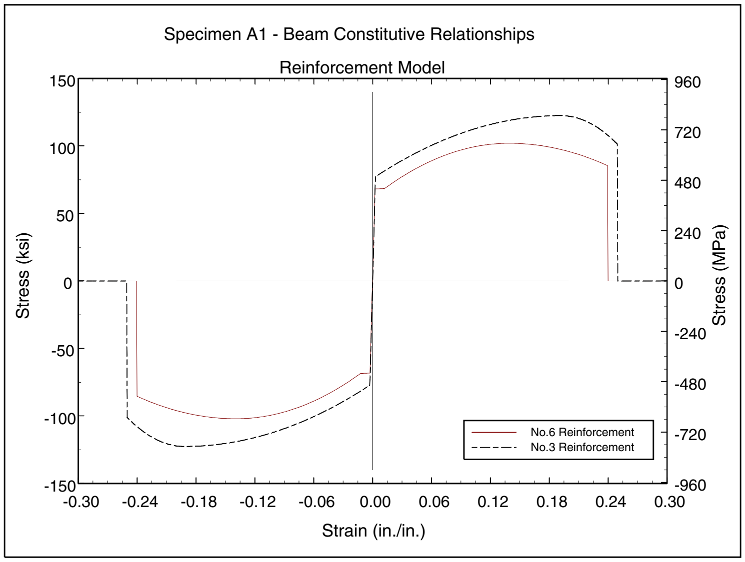

Figure 6-34: Typical reinforcement constitutive relationship

Since the stirrups are more closely spaced near the beam-column interface, the level of confinement varies along the length of the beam (Figure 5-4). As a result, the beam was evaluated at two cross sections: near the column face and away from the column face. Coupling this with the two previously mentioned load cases results in the analysis of the following eight load-section combinations for the cap beam:

Yield Load

1. Tension on section near joint with positive flexure
2. Tension on section away from joint with positive flexure
3. Compression on section near joint with negative flexure
4. Compression on section away from joint with negative flexure

Maximum Load

5. Tension on section near joint with positive flexure
6. Tension on section away from joint with positive flexure
7. Compression on section near joint with negative flexure
8. Compression on section away from joint with negative flexure

The moment-curvature relationships were developed using a fiber cross-sectional analysis software program *ARCS* [Thewalt 1993]. The following relationships were developed for Specimen A1 (Figure 6-35 and Figure 6-36). A small variation occurs in the beam moment-curvature response between the yield level and ultimate load levels. In the tension-positive flexure region, the moment-curvature envelope marginally *decreases* from yield level to ultimate level as a result of the increase in axial tension. In the compression-negative flexure region, the moment-curvature envelope marginally *increases* from yield level to ultimate level as a result of the increase in axial compression.

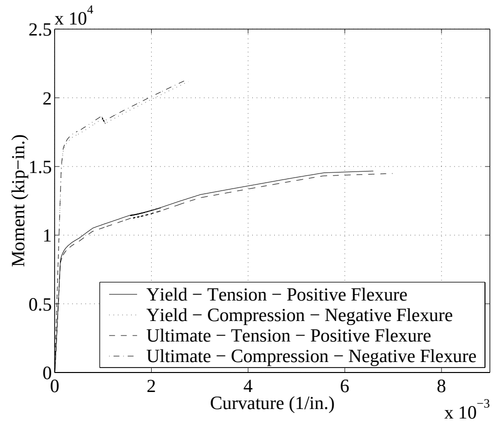

Figure 6-35: Analytical moment-curvature behavior away from column face

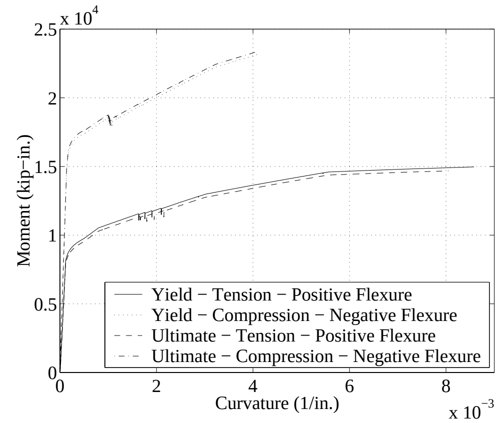

Figure 6-36: Analytical moment-curvature behavior near column face

To evaluate if the beam behaved according to standard flexural assumptions, the experimental strain distribution is compared with the preceding analytical distribution. Using statics, the moment distribution was derived for the two load cases (Figure 6-32). Knowing the moment-curvature relationships at the different locations in the beam, the corresponding strain values on the top, middle, and interface longitudinal bars could be estimated from the *ARCS* analysis. The following figures compare the analytical and experimental distributions on each layer of flexural reinforcement. The analytically obtained strain distribution is assumed to change linearly between the two column faces.

The measured and calculated strains for Group A are compared in Figure 6-37 through Figure 6-40. In general, the experimental results correlate very well with the analytical results; the deviations are discussed in the following paragraphs.

At yield, the strains in the top reinforcement correlate with the analytical results. At the ultimate load level, however, the strains in the top reinforcement on the compression face of the joint (left side) shifted in tension. This indicates that the tensile forces are not completely developed within the joint length but appear to be anchored on the compression side of the joint. This behavior is typical of the response of all four specimens.

The secondary layer of negative reinforcement compares well at yield. At ultimate, however, the experimental values are underestimated. For the circular column configurations the left side of the joint is estimated to lie on the beam neutral axis at yield and ultimate load levels. At yield, the measured strain correlated with the expected zero strain values. At ultimate, however, the reinforcement was in tension. This could be attributed to pull-through of tensile reinforcement from the tension face of the joint or anchorage from the tensile column longitudinal reinforcement. On the beam segment subjected to axial compression and negative flexure (the right side), the strains at ultimate load are elevated away from the joint face. This action could be attributed to the formation of a compressive strut mechanism arching from the gravity load toward the joint. This behavior is typical of all Group A specimens.

The most notable deviation between the predicted and measured response occurs on the interface reinforcement. This can be seen in the response of specimens A1, A2, and A4. Within the column depth a tensile spike was recorded at the ultimate load level (Note: a similar spike was measured on Specimen A3 at a higher displacement demand level). In all cases this sharp increase eventually exceeded the yield strain of the reinforcement. This can be attributed to the local development of the tensile column reinforcement. The high tensile forces developed at the face of joint from the column are anchored locally through compressive strut formation leading to tensile strains on the interface beam reinforcement crossing that strut. The greater increase measured by the circular column reinforcement could be attributed to the higher demand placed on the extreme tension bars. Since the circular column has one bar at its extremity versus the nine bars in the square column, the same flexural strength requires higher curvatures. As a result the extreme tensile bar in the circular column would be subjected to a higher strain and produce higher local anchorage forces. This in turn creates a higher local strut mechanism from the column longitudinal bars in the circular column subassemblies, resulting in the measured tensile strain increase on the interface reinforcement.

In addition to the increase within the joint, the compressive and tensile strains measured on each side of the joint were less than the analytical prediction. This can be attributed to compression strut formation from the gravity load. Because the load is applied to the top face of the beam close to the beam-column face, (18 in. for A1 and A2 and 19.5 in. for A3 and A4), strut action could result in reduced compression as compared with what is expected based solely on flexural theory. The bottom reinforcement does not see the corresponding increase in strain that accompanies the increase in flexure.

In summary, the strain distribution in the beam longitudinal reinforcement is not significantly affected by the details used in the joint. All specimens behaved in a similar manner; the strain levels exceeded those predicted by conventional flexure theory within the joint region. In the regions adjacent to the joint the measured strains exceeded the predicted values on the top reinforcement and were less for the strains on the interface reinforcement outside the joint region. The square or circular column configuration did not noticeably affect the distribution of the beam strain. In all cases, the development of the column tensile forces appears to have resulted in a localized increase in the beam strain on the interface longitudinal bars, often resulting in localized yielding.

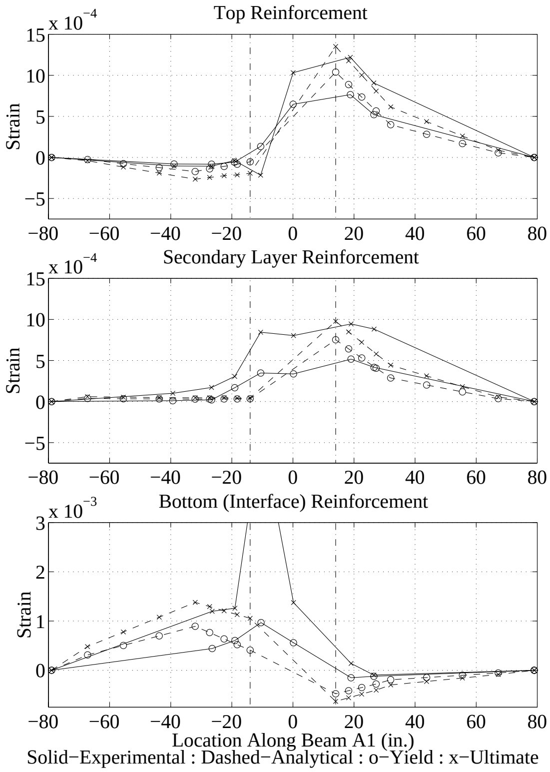

Figure 6-37: Beam strain distribution A1

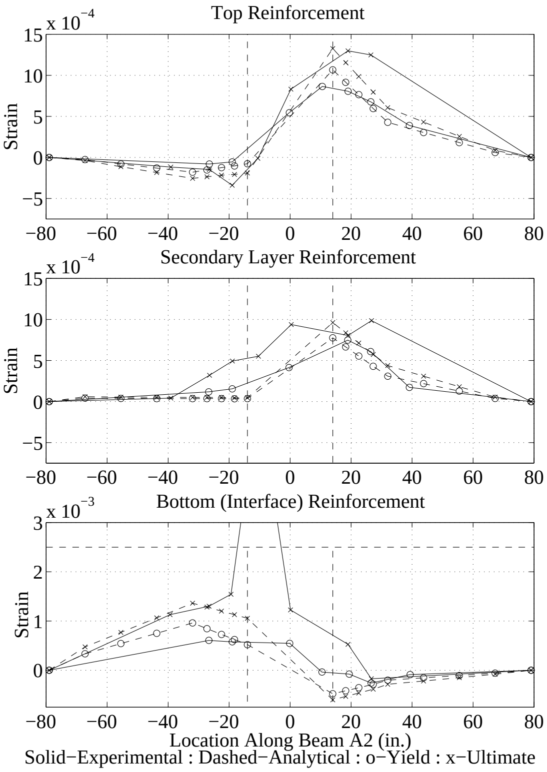

Figure 6-38: Beam strain distribution A2

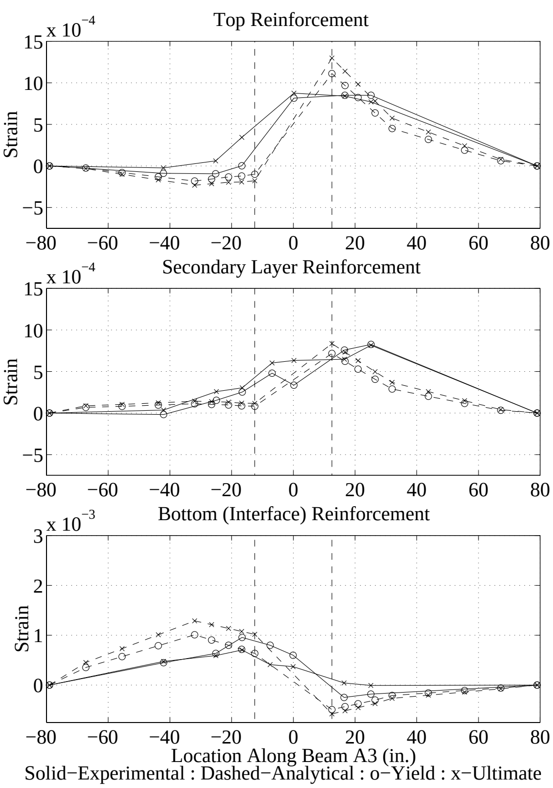

Figure 6-39: Beam strain distribution A3

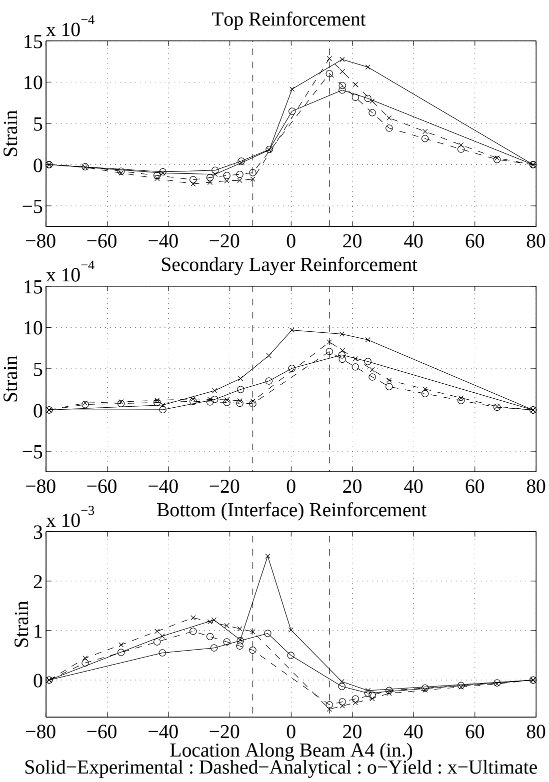

Figure 6-40: Beam strain distribution A4

6.2.3 Beam Transverse Reinforcement

To evaluate the force transfer mechanisms in the vicinity of the joint, strain gages were placed on the interior and exterior beam and joint vertical transverse reinforcement (Figure 6-41 and Figure 6-42). This section investigates the global behavior of Group A specimens, compares the response of A1 with A2 and A3 with A4, and draws conclusions on the activation of vertical transverse reinforcement.

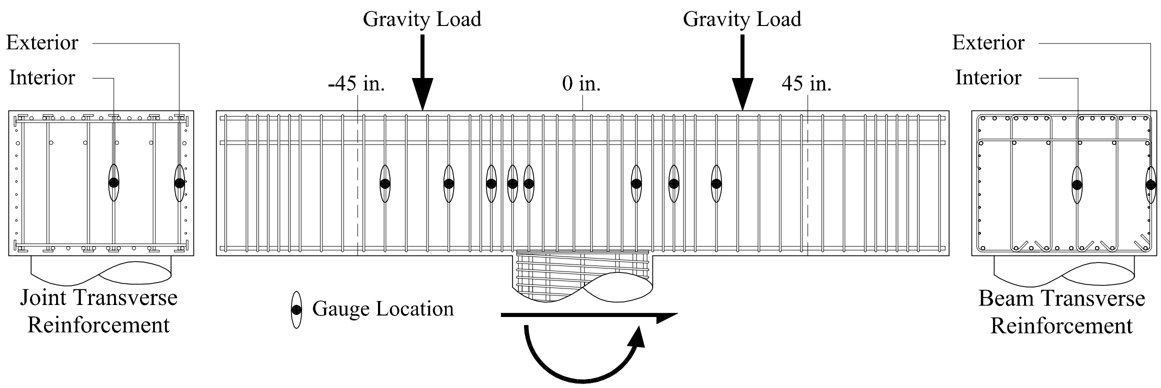

Figure 6-41: Specimens A1 and A2, location of transverse reinforcement strain gages

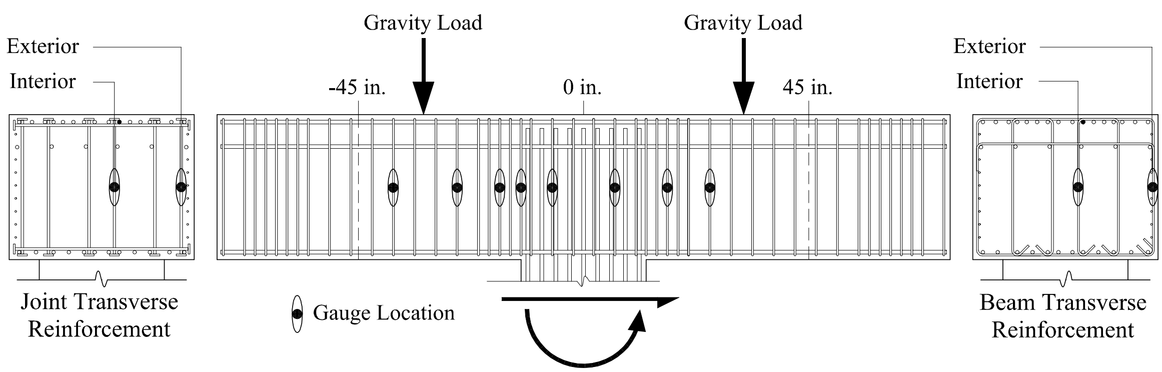

Figure 6-42: Specimens A3 and A4, location of transverse reinforcement strain gages

The global responses of Group A specimens were similar. The strain distribution is plotted relative to the beam length at a displacement ductility of 0.5, 1.0, 2.0, and 4.0 (Figure 6-43 through Figure 6-46).

Within the cap beam, small strain values were measured. This behavior is expected. At the peak load response for Specimen A1, the shear force at one beam depth away from the column face is equal to 87.7 kips. Assuming a concrete shear resistance of $2\sqrt{f'c}\, b_{bm}d_{bm}$, where $f'c$ is the concrete compressive strength in psi, b_{bm} is the beam width, and d_{bm} is the beam depth, the shear capacity of the concrete alone is 148 kips. As a result, the beam transverse reinforcement is not significantly activated by the shear load.

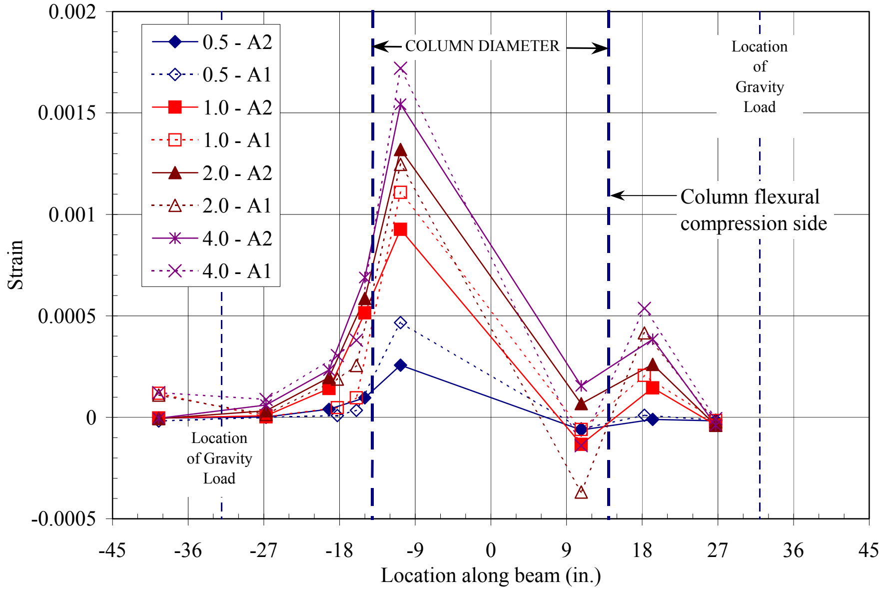

Figure 6-43: Specimens A1 – A2 interior beam transverse reinforcement strain distribution

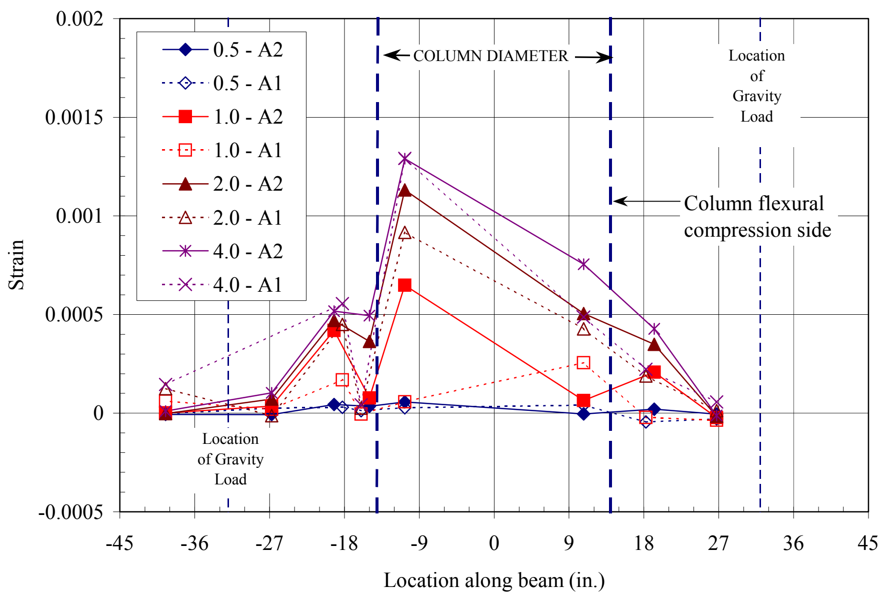

Figure 6-44: Specimens A1 – A2 exterior beam transverse reinforcement strain distribution

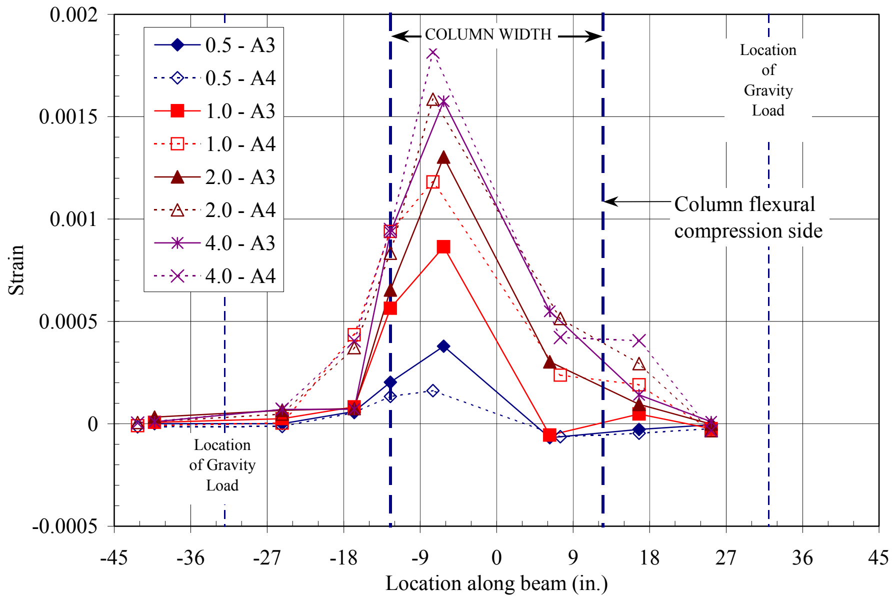

Figure 6-45: Specimens A3 – A4 interior beam transverse reinforcement strain distribution

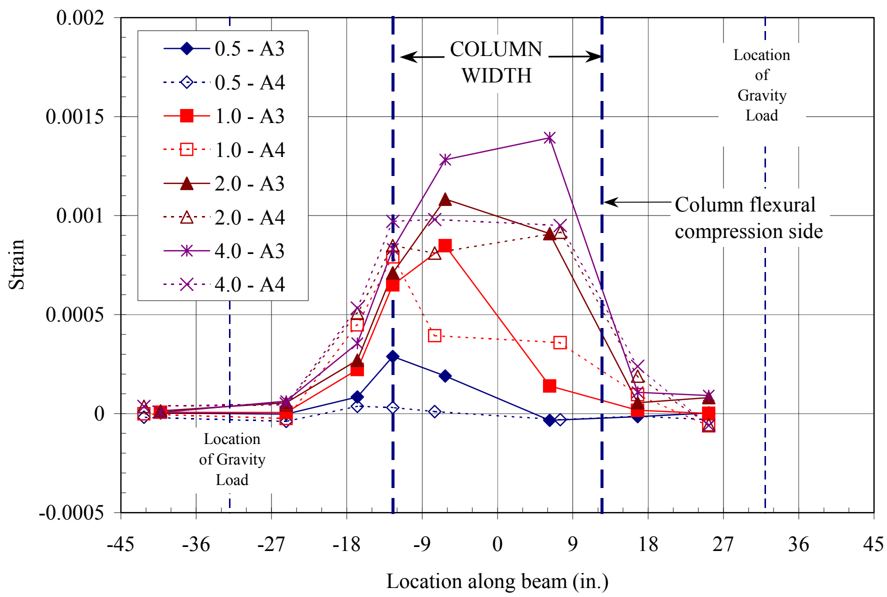

Figure 6-46: Specimens A3 – A4 exterior beam transverse reinforcement strain distribution

Within the joint and in the column flexural tension side, the vertically oriented transverse reinforcement experiences a sudden increase in strain (Figure 6-43 through Figure 6-46). On the inside of the joint (Figure 6-43 and Figure 6-45), the strain decreases rapidly (high strain gradient) toward the flexural compression side of the joint. In contrast, the strain gradient on the exterior face of the joint remains somewhat lower, i.e., low decrease of strain values toward the column flexural compression side (Figure 6-44 and Figure 6-46). These observations are consistent with the formation of a primary diagonal compression strut toward the center of the joint with more uniform shear strain at the joint face. Along the interior of the joint, the flexural compression strut would result in compressive strains in the transverse reinforcement, whereas on the flexural tension side the anchorage of column reinforcement in the strut would be manifest in high tensile strain, as shown.

This previously discussed observed joint behavior can be accounted for in the following manner: on the exterior of the joint, the concrete cracks ″uniformly″ in shear, resulting in a *shear panel* mechanism. On the interior of the joint, the concrete is confined as a result of the surrounding volume of concrete and the continuation of the column spiral reinforcement into the joint. This causes a compression strut mechanism to remain confined to the center of the joint, which in turn leads to concentration of tension and compression on each side of the joint. This produces the sharp decreases and increases measured on the interior joint transverse reinforcement. The square column configuration behaves similarly to the circular configuration except for the decrease in strain on the interior bars on the column flexural compression side of the joint. Since the column has a square cross section, the compressive column force is distributed over a larger proportion of the beam width. As a result, the localized compressive stress is decreased, thus preventing the notable drop measured on the circular configurations.

The behavior of the vertical joint transverse reinforcement on the interior and exterior of the joint illustrates the three-dimensional response of the joint system. This behavior indicates that a shear panel mechanism may occur on the exterior of the joint, while at the same time, a principal compression strut forms on the interior of the joint. This variation of the behavior through the joint depth supports the recommendation to use confining reinforcement within the joint core and vertical shear reinforcement outside of the core [ATC 32, 1996].

6.2.4 Effectiveness of Joint Confinement Techniques

The spiral reinforcement was instrumented within the joint depth to evaluate the effectiveness in confining the joint core. Figure 6-47 presents the strain values measured on specimens A1 and A2 on the north face of the joint region for northern displacement ductility. In general, the joint spiral was subjected to low demands, remaining elastic over the entire displacement history. The spiral had the highest tensile strains at the top and interface of the joint and the lowest tensile strains at mid-height. The interface strain increase could be associated with the dilation generated from the high column compression force. This compression effect should decrease as the distance from the top compression corner of the joint increases. The strain, however, increases again at the top of the joint. This could be a result of dilation caused by the tensile development of the top beam reinforcement.

For high levels of demand, Specimen A1 measured a greater amount of strain (compared to A2) in the spiral reinforcement particularly at the interface. This could indicate that Specimen A2 dilated less under similar levels of demand. If so, the use of headed reinforcement is more advantageous for out-of-plane joint confinement than conventional joint reinforcement (i.e., use of hairpins). The nonuniform strain distributions shown in Figure 6-47 indicate that core dilation confinement is less needed in the mid-depth of the joint.

The out-of-plane reinforcement strain distribution (Figure 6-48) has the opposite trend to the spiral. The strain is lowest at the top and interface (soffit) of the joint and highest in the center of the joint. The increased strain in the middle is indicative of greater global joint dilation at the mid-depth of the section. This behavior occurs on both the headed and conventionally reinforced joint configurations. This decrease in strain at the top and bottom hairpin and headed reinforcements, however, may be misleading. At the top and bottom of the joint, there exist a number of horizontal beam stirrup legs oriented in the out-of-plane direction. These bars were not instrumented, so their dilation resistance in the experiment is unknown. Therefore, it is likely that in these regions the hairpin/headed reinforcement strains are lower because the out-of-plane stirrup bars were providing dilation resistance. Somewhat higher strain measurements were recorded on the conventionally reinforced joint at lower levels of demand, but at higher levels of demand the strains for both specimens were similar. Note that two distributions are shown for Specimen A1 at each demand level. The first presents the strain on the bars labeled 1-3-5 (see inset picture); these hairpins are located in the same vicinity as the headed bars. The second distribution, labeled 2-4, presents the strain on the hairpins crossing the center of the joint. The strains were measured on the out-of-plane leg of the hairpin; however, the longitudinal leg of the hairpin affects the strain. Hairpins 2 and 4 provide a measure of the dilation at the center of the joint while hairpins 1, 3, and 5 provide a measure of dilation of the outer portion of the joint. Thus hairpins 2 and 4 provide a comparative measure to that of the headed bars.

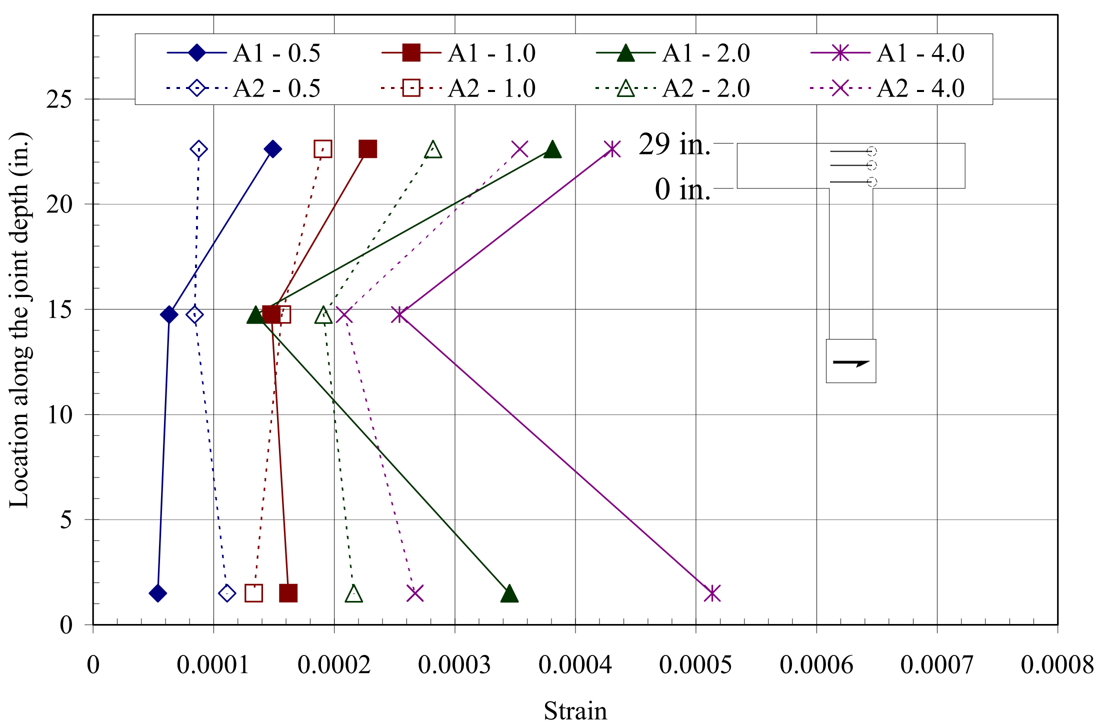

Figure 6-47: Specimens A1 and A2 strain distribution on joint spiral

The Caltrans design method, used in Group A, created a mechanism which is dependent upon both the spiral and out-of-plane transverse joint reinforcement. For the current details, dilation of the core occurs most significantly at the interface and top of the joint. The dilation of the entire joint width is greatest at the mid-depth. Note that the demands applied to the joints of Group A resulted in minimal joint damage. The elastic strain levels measured on the joint reinforcement indicate that for these joints the levels of reinforcement used may be overly conservative.

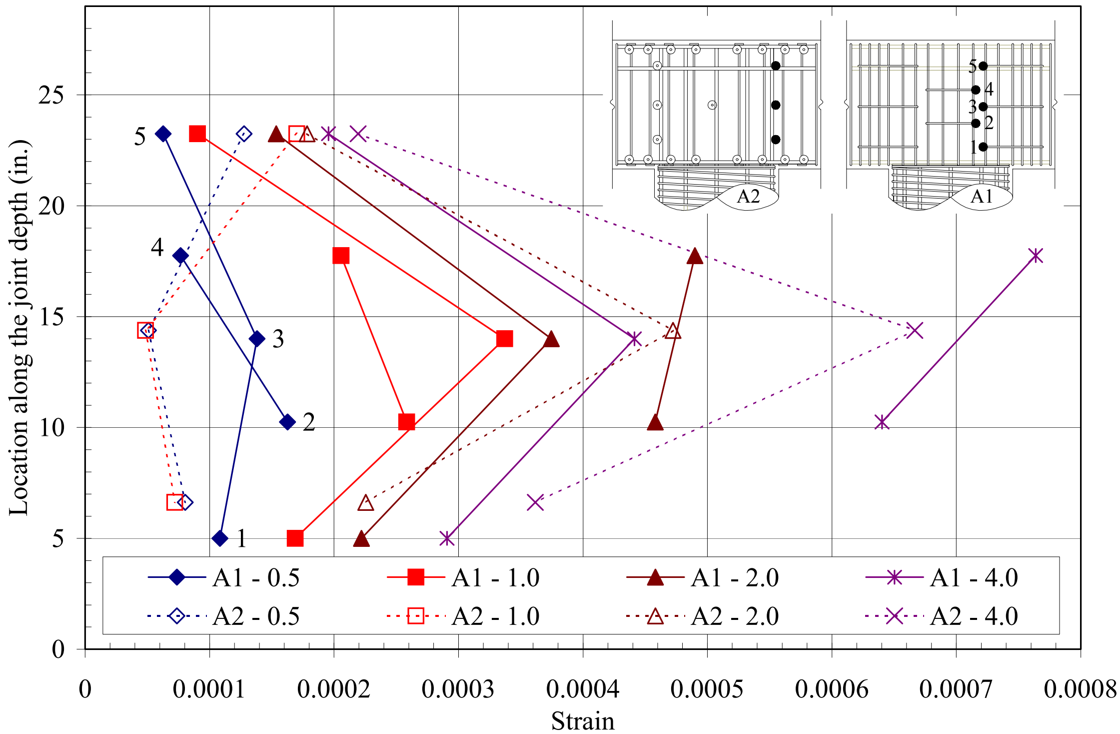

Figure 6-48: Specimens A1 and A2 strain distribution on out-of-plane joint reinforcement

6.3 Force Transfer in Joints Designed According to 1995 Caltrans BDS

Many questions remain to be answered: What mechanism of force transfer is being activated in the joint? Is the postulated mechanism used in the design procedure actually occurring? If so, how accurately does it model the measured behavior? If behavior does not follow the intended mechanism, why and what can be done to improve the design procedure? These questions are discussed and investigated in this section through an evaluation of the strain gradient in the joint region coupled with two-dimensional strut and tie modeling.

The active force transfer mechanism can be inferred from the strain distributions measured on the longitudinal reinforcement and transverse joint reinforcement. The preceding presentation of the reinforcement strain distribution indicates that the column and beam behaved according to conventional concrete analysis assumptions. This justifies the validity of the strain gage measurements, and, more important, allows for a determination of regions where high strain gradients took place. This can be used to isolate the location where high compression forces occur or high tension forces are anchored. The strain distribution on the anchored column reinforcement is a good example of this behavior. Figure 6-29 presents the bond stress distribution along the bar length. The high stress gradient at the tip of the bar indicates that the majority of the bar tensile force is anchored at the top of the joint as opposed to an even distribution along its length. This localized stress concentration can be attributed to a principal compression strut mechanism, which results in clamping action against the bars at that location, thereby improving bond. Knowing the stress distribution on a number of joint bars, the force transfer mechanism can be estimated.

To estimate the stress distribution along each bar, the strain history of each gage was transformed into a stress history using the tested monotonic material properties (as described in Section 6.2.1). Assuming the stress distribution does not change through the thickness of the joint, the force can be calculated at each gage location by multiplying the stress with the total bar area at each level. For example, if a stress of 10 ksi is estimated to act on the interface beam longitudinal bars at the center of the joint, the force would be equal to 10 ksi multiplied by the area of the 10 #6 interface bars, resulting in a total force of 44 kips. Knowing the stress at the face of the joint and the stresses at different locations within the joint, the change in stress of bond stress from one gage to the next can be determined. Thus using the strain measurements along a bar, the change in stress from one point to the next can be estimated. This can be used to develop a strut and tie mechanism that is consistent with the variation on the reinforcement forces.

Figure 6-49 presents a strut and tie model of joint force transfer for Specimen A1 at a displacement ductility of 4.0 (3.7% drift). The tensile loads act at the location of the longitudinal reinforcement. The column tensile loads are lumped into two discrete forces to simplify the model. The magnitudes of the two tensile column forces correspond to the strain distribution measured on the column longitudinal reinforcement. The magnitudes of the compressive loads are computed by equating the summation of normal forces (tension, axial, and compression) on each face equal to zero. The location of the compressive load is then computed by equating the summation of moments acting on each face to zero. The resulting exterior joint forces are transferred through the joint according to the reinforcement stress distribution determined along each bar. This allows for the development of a force path through the joint.

It is necessary to point out that the behavior is three dimensional in nature and that not all bars were instrumented. As a result the two-dimensional strut and tie model shown is only an *approximation* of the force transfer mechanism active in the joint. The determination of the explicit transfer mechanism would require a significant amount of additional information. Nevertheless, the 2-D transfer mechanism provides insight into the effectiveness of the reinforcement.

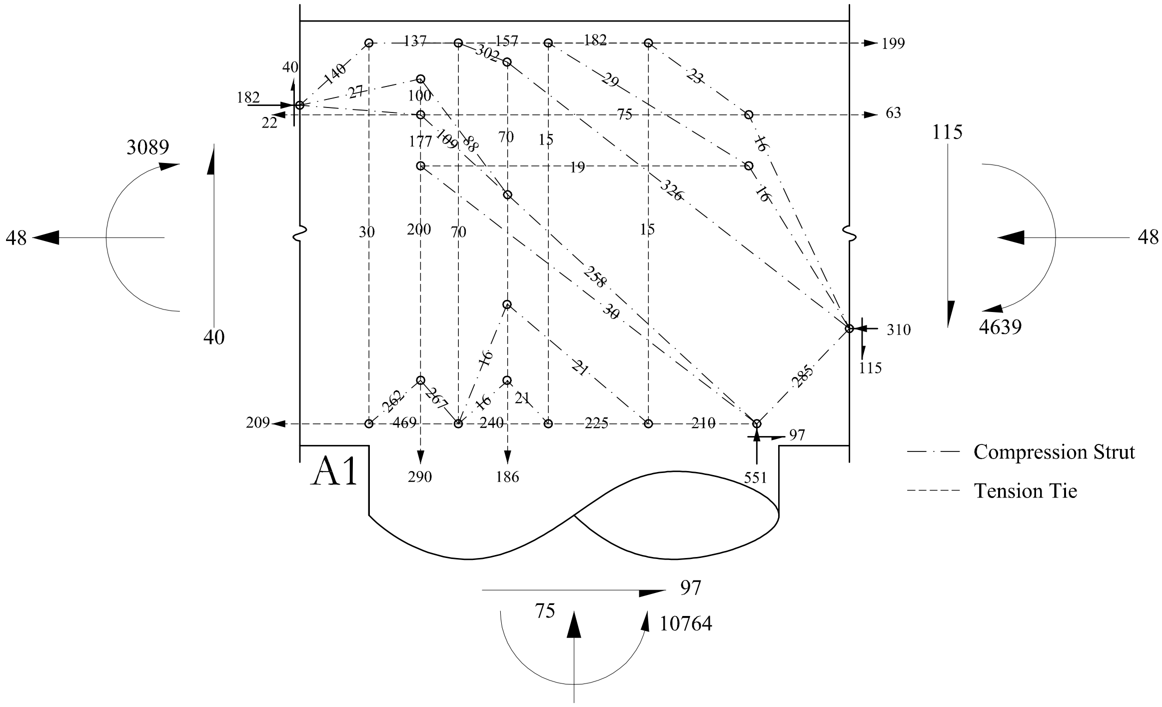

Figure 6-49: Two-dimensional strut and tie representation of force transfer at $\mu_\Delta = 4$ (Specimen A1)

The strut and tie model indicates that force transfer is accomplished primarily through a combination of a principal compression strut and a series of vertical tension ties. The tensile column reinforcement forces are anchored at four locations along its length. On the extreme tensile face, anchorage occurs primarily at the top of the joint near the beam compressive force. This behavior is intuitive in that the tensile force is anchored in the region where the highest confining stress exists. The secondary column tensile force anchorage is more uniformly distributed throughout its embedded length. The local pullout of the column reinforcement results in a sharp increase in the tensile force in the beam interface longitudinal bars and adjacent vertical stirrups. This behavior was noted in the distribution of strain in the beam longitudinal and transverse reinforcement in Figure 6-37 and Figure 6-43, respectively, and is modeled here using two small compression struts shown near the lower left-hand corner of the joint (Figure 6-49). To close the force transfer mechanism, vertical and horizontal reinforcement bars are activated throughout the joint.

The postulated strut mechanism implicit in design is based on a simplified load path as shown in Figure 6-50. The primary differences between the ″measured″ force transfer mechanism and the design model can be attributed to the anchorage of the column tensile reinforcement. The design model assumes that the extreme tensile forces will be anchored near mid-depth, producing demand in the transverse reinforcement exterior to the joint and in the interface beam reinforcement along the entire length of the joint. The mechanism for Specimen A1, however, indicates that the tensile column forces are anchored primarily at the top of the joint, not near the interface. In addition, shallow pullout cones develop on the tensile column bars near the face of the joint, not deep within the joint. This produces a localized increase of stress on the interface beam reinforcement directly below the tension column reinforcement as well as a uniform force distribution on vertical transverse reinforcement inside the joint length. The implication is that the assumed transfer model does not occur. Thus the reinforcement details are developed from a mechanism that differs somewhat from the one that actually occurs. This results in a joint that is inefficient in transferring forces. To evaluate the transfer mechanism on a finer scale, the joints are evaluated through the use of three-dimensional finite element models in the following section based on modeling techniques discussed in Chapter 4.

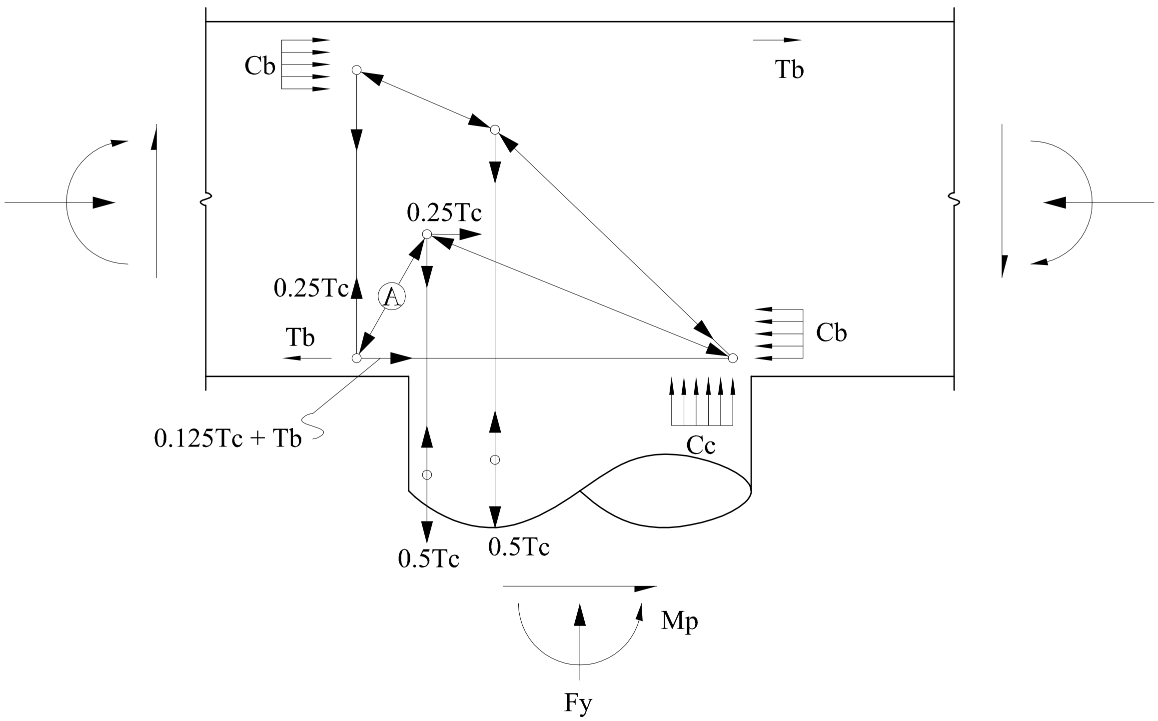

Figure 6-50: Proposed force transfer mechanism [Priestley 1993]

6.4 Three-Dimensional Finite Element Evaluation of Bridge Joint Response

As discussed in Chapter 2, the goal of bridge joint design requirements is to provide an effective joint force transfer mechanism with minimal damage and efficient usage of reinforcement. To accomplish this, design requirements are leaning to the use of two-dimensional strut and tie models. Inherent in the use of strut and tie modeling is the assumption of damage implied by the postulated failure mechanism unless the model clearly follows the elastic behavior. To achieve a particular strut and tie model, the joint must crack so that forces can redistribute to the intended load path. This may be contrary to the design criteria, which are attempting to minimize damage. In addition, the adopted strut and tie model is a two-dimensional representation of a three-dimensional transfer mechanism. Although this is not a significant issue in square column configurations, it is a concern in circular column configurations (the predominant configuration used in California bridge systems). The two-dimensional representation creates ambiguity as to where reinforcement should be placed to most efficiently transfer the forces. For example, are the tension ties more effective on the interior of the joint or the exterior face of the joint? Does the placement of tension ties on the exterior result in less damage? An appropriate joint design methodology should consider these three-dimensional effects to effectively and efficiently determine the reinforcement requirements. To provide additional insight to the joint behavior in three dimensions, finite element models can be used. These models have the potential to accurately capture the experimental behavior, thus allowing for the evaluation of additional information not measured in the experiment, and can be used to develop recommendations on a more appropriate placement of joint reinforcement. These models are limited by the accuracy of material models and solution strategies, both of which can be a severe limitation.

To assist in evaluating the joint performance, three-dimensional finite element analyses of the circular column configurations were conducted. The models were constructed to match the as-built dimensions (Figure 6-51) and material properties. Background and justification of the finite element methods used are presented in Chapter 4.

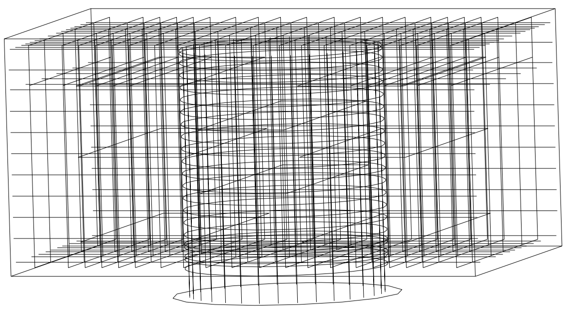

(a) Specimen A1

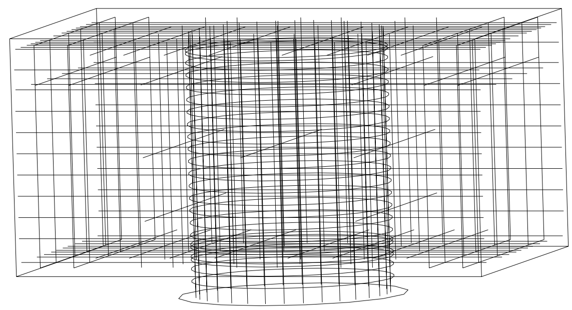

(b) Specimen A2

Figure 6-51: Finite element model of joint reinforcement (wire frame view)

Figure 6-52 compares the measured and calculated strain in the vertical joint reinforcement at the center and face of the joint, at a tip displacement of 4.0 in. The analytical and experimental results of Specimen A2 are presented; the behavior is comparable to that of Specimen A1. The high strain increase measured on the interior vertical bars in the tensile region of the column (north column face) is represented well by the model. The behavior of the exterior reinforcement, however, is underestimated. This is a result of the analytical modeling techniques, which evaluate the response under monotonic displacement application. As a result, effects such as crack reversal and cyclic dilation are not accounted for. Figure 6-53 presents the strain of the internal and external vertical transverse reinforcement located on the south end of the joint. At the initiation of joint cracking (Figure 6-53(a)) the strain in both the internal and external bars drift into tension on north load application. On the south load application the interior bar goes into compression and the exterior bar returns to zero but begins to drift in tension. The behavior of the interior bar is indicative of a reliance on the anchorage of the column reinforcement. When the column applies compression to the region, the interior vertical transverse reinforcement increases marginally in compression. When the column reinforcement is anchoring in tension the transverse bars go considerably into tension. Since this response is driven by column anchorage, the effect of bidirectional load application on the internal reinforcement is minimal. The external transverse reinforcement, however, is reliant on shear of the joint face. As the joint begins to form shear cracks, the strain in the bar begins to drift. This indicates that cracks formed during loading do not completely close on unloading. Once shear damage becomes significant, cracks open across the joint on both south and north displacements. As a result, the southern exterior transverse joint reinforcement goes into tension on both northern and southern displacements (Figure 6-53(b)). Bidirectional loading can thus produce crack reversal and additional demand on the exterior transverse joint reinforcement that is not seen in a monotonic model. An issue not presented in the finite element model.

The strain values measured on the spiral reinforcement for the southern face of the joint are compared with the analytical strains in Figure 6-54. The spiral strains are greatest at the top of the joint and at the beam-column interface. Between the two peaks the tensile strain decreases. The analytical models produce a similar distribution; however, the response is shifted in compression. This can again be attributed to cyclic load application, which produces crack openings that do not close upon load reversal.

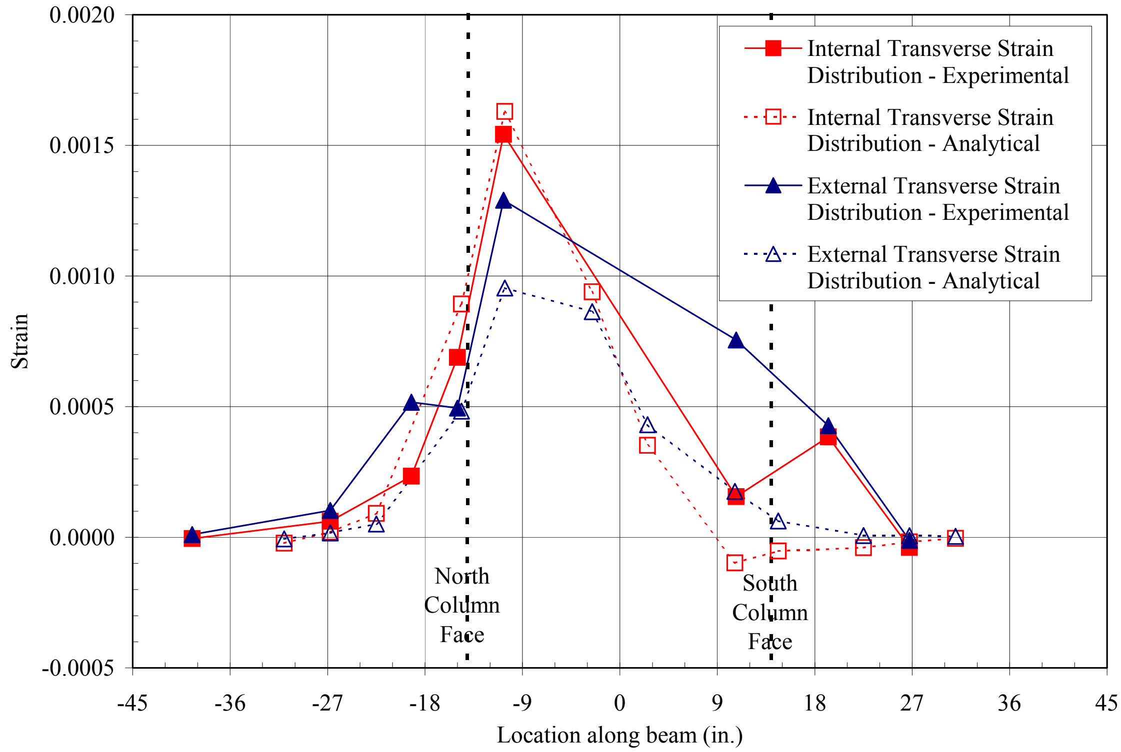

Figure 6-52: Measured and predicted strain distribution of beam external and internal vertical transverse reinforcement

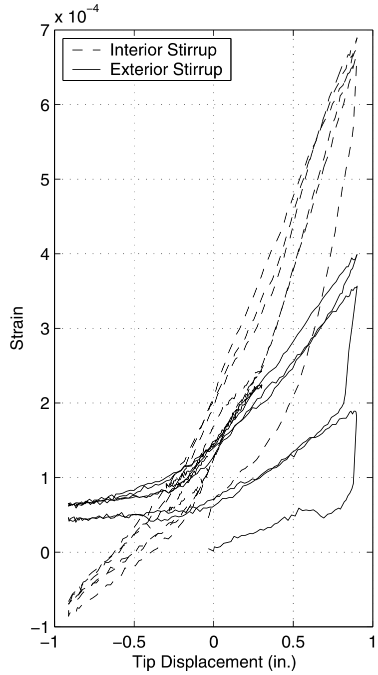

(a) Before significant joint cracking

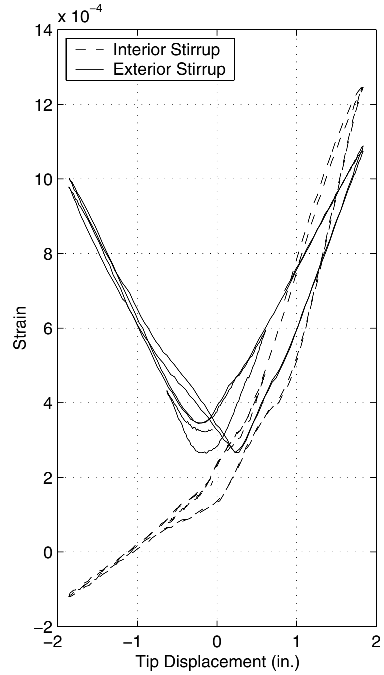

(b) After significant joint cracking

Figure 6-53: Strain of vertical transverse reinforcement at south end of the joint (A2)

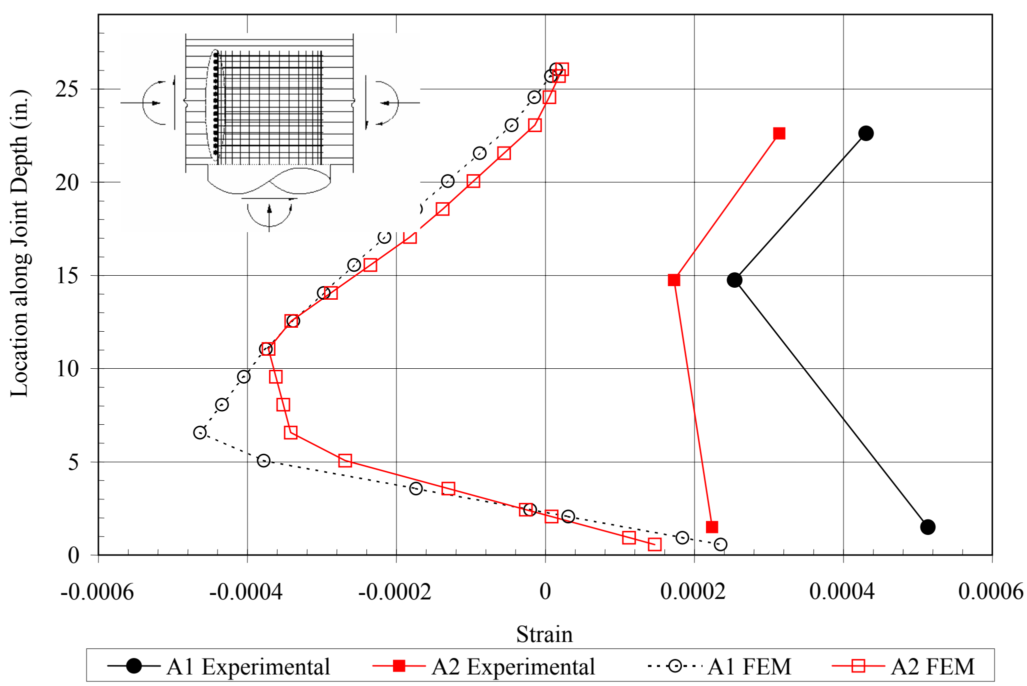

Figure 6-54: Measured and predicted joint spiral reinforcement strain distribution

The strain demand measured on the vertical exterior and interior reinforcement indicates that the internal bars were subjected to greater demand than the external bars (Figure 6-53). This is intuitive, since the maximum tensile forces from the circular column are transferred to the beam at the center of the joint. This behavior is indicated in the analytical models as well. Figure 6-55 presents the analytical principal compressive stress distribution at vertical longitudinal sections through the center and face of the joint for specimens A1 and A2 at a column tip displacement of 4.0 in. Note that compression is a negative. At the interior of the joint (Figure 6-55(a) and (c)), a notable increase in compression occurs from the column and adjacent beam compressive face to the diagonally opposing compressive beam face. This supports the assumption of a diagonal strut at the center of the joint. However, at the face of the joint (Figure 6-55(b) and (d)) the magnitude and variation of the principal compressive stress is significantly decreased, producing less variation. Thus the analytical model suggests that a greater proportion of the compressive strutting action occurs at the interior of the joints.

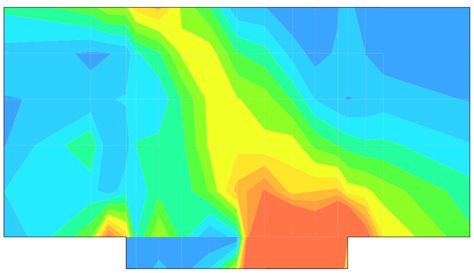
(a) Vertical section at center of joint A1

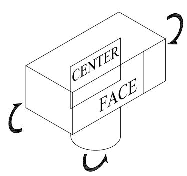

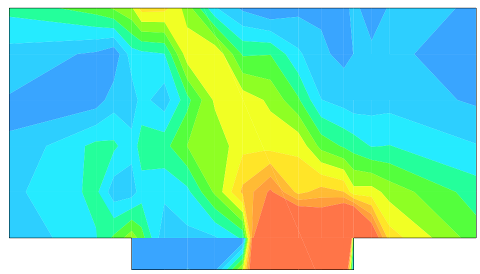
(c) Vertical section at center of joint A2

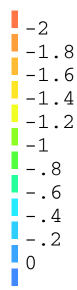

Contour legend (ksi)

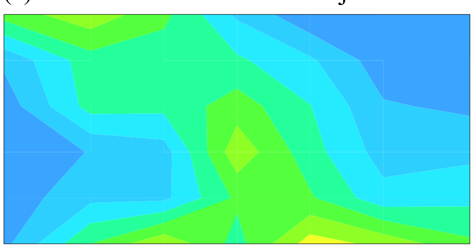
(b) Vertical section at face of joint A1

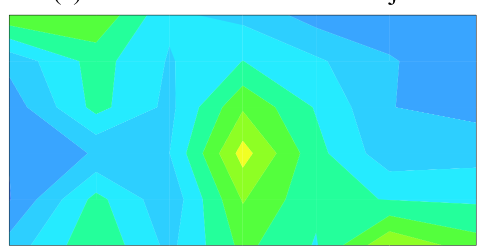
(d) Vertical section at face of joint A2

Figure 6-55: FEM approximations of principal compression stress in the joint region

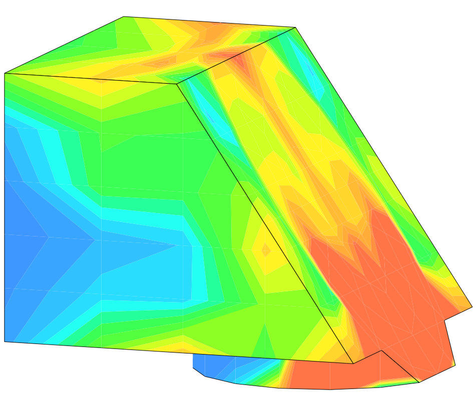
(a) Diagonal section through joint (A1)

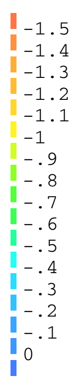

Legend (ksi)

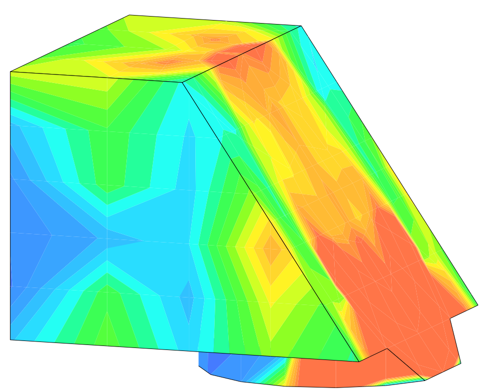
(b) Diagonal section through joint (A2)

Figure 6-56: FEM approximations of principal compression stress on diagonal cross sections through joint

The finite element models can be used to define the effective width of the principal compressive strut. The width of the compressive strut is primarily within the diameter of the anchored column (Figure 6-56). The placement of additional vertical reinforcement in the center of the joint (as in Specimen A2 compared to Specimen A1) produces a greater compressive strut width (Figure 6-56(b)). This results in lower principal compressive stresses on the face of the joint, producing more uniform shear damage on the exterior face. This is supported by the crack strain opening orientation (normal to the actual crack direction) and magnitudes estimated on the exterior of the joint (Figure 6-57). The figures corroborate the greater presence of a strut mechanism on the face of A1.

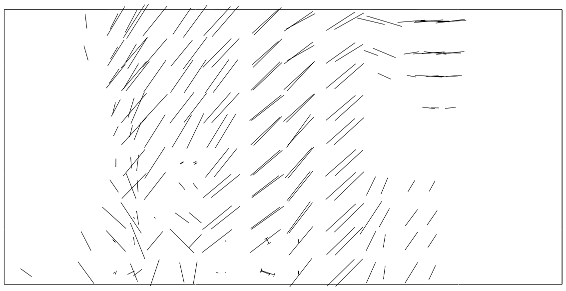

(a) Diagonal section through joint (A1)

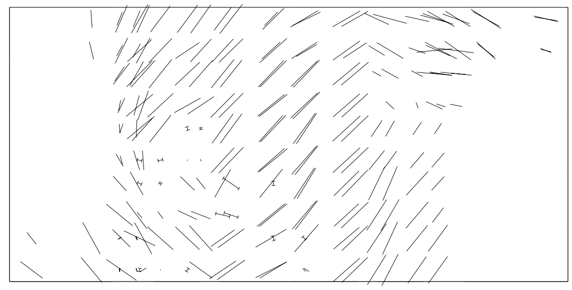

(b) Diagonal section through joint (A2)

Figure 6-57: FEM approximations of crack strain and orientation at the exterior face of the joint

In Figure 6-55(a) and (c), a localized compressive stress increase occurs around the tensile column reinforcement. This is indicative of a localized strut formation as a result of bond transfer at the point where the column bars enter the joint. This behavior occurs at the interior of the joint near the extreme tension reinforcement, thus supporting the strut and tie model developed for Specimen A1 (Figure 6-49). This localized demand should be accounted for in the design. This can be accomplished by additional factors of safety on the beam flexural design or through the addition of interface reinforcement at the development locations of the column longitudinal tensile bars.

Overall, the finite element models do well in representing primary actions in the joint. The predominant transfer mechanism is a compression strut in the center portion of the joint. The strut is confined primarily to the width of the column diameter; however, additional tension ties develop outside the joint to anchor the localized pullout of the column tensile reinforcement. The width of the strut indicates that the placement of vertical reinforcement would be most effective within the joint core and not on the face of the joint. The demand levels for these models, however, are low, with maximum principal compressive stresses on the order of 2.0 ksi at a displacement ductility of 4.0 and all reinforcement remaining linear elastic. Under these conditions the joint is well behaved. To determine the behavior of the joint under significantly higher demand an additional study, Group B, was conducted, as described in Chapter 7.

7 Studies of Alternative Joint Design Approaches

The experimental results presented in Chapter 6 suggest that current design recommendations for beam-column joint systems do not provide an efficient use of reinforcement. To gain further insights into the mechanisms active in joint force transfer, the results of tests on two additional specimens, designated Group B, are presented in this chapter. These tests investigate the behavior of joints subjected to severe demands. Using the results, methods of improving constructability, methods of limiting slip, and methods of optimizing reinforcement details for improvement of joint confinement are developed.

Several conclusions with regard to reinforcement schemes can be drawn from the results of Group B. The results presented in this chapter will show that joint hairpins are necessary to activate the large cap beam widths used in current recommendations. Without hairpins, the joint core can separate from the cap beam face, thus decreasing the effective joint width and increasing demand on the vertical transverse joint reinforcement. This in turn decreases the capacity of the joint. In addition, the vertical reinforcement is most highly activated within the core near the location of the extreme column tensile reinforcement. Consequently, vertical reinforcement should be concentrated in the center of the cap beam rather than at the face of the joint. Spiral joint reinforcement provides good resistance to slip of the column reinforcement. Nevertheless, a well-distributed array of horizontal transverse reinforcement will provide comparable levels of slip resistance. In addition, both horizontal transverse reinforcement and spiral reinforcement provide similar levels of shear resistance. Therefore, the joint system can be constructed without the use of the joint spiral, thus allowing for a decrease in the quantity of joint reinforcement and improved constructability.

This chapter begins with the development of the Group B specimens. This includes the design concepts as well as the details used. The subassembly configuration is presented along with the design capacities. The investigation then focuses on the global behavior of the specimens followed by local behavior and studies using finite element techniques.

7.1 Group B: Subassembly Development

This second phase of the investigation focuses on experimental evaluation of a reinforced concrete bridge system typical of California designs. The subassembly configuration, boundary conditions, and test scale are essentially the same as those used for Group A.

7.1.1 Specimen Global Geometry

To investigate the behavior of the joint over both elastic and inelastic ranges of response, the joint shear demand was significantly increased over that of Group A. To achieve this, the column longitudinal reinforcement ratio was increased by 46%, and the beam depth was decreased by 18%. These changes increase the joint demand in two ways, first by elevating the applied joint shear force generated from the column, and secondly, by decreasing the joint area over which the force is developed. Note that the resulting ratio of h_{beam}/D_{column} (82%) is still comparable to what is seen in taller bridge structures. The column longitudinal reinforcement ratio was elevated to 3.14%, representing an upper bound of typical California construction. The remaining portion of the system (i.e., cap beam and joint) transfers the load associated with the ultimate flexural response of the column. To decrease the joint area, the beam is made shallower than the beam in Group A. Nevertheless, the resulting ratio of h_{beam}/D_{column} (~ 82%) is still comparable to what is surveyed for bridges with high superstructures (refer to Appendix A). A summary of the global geometry is presented in Table 7-1.

Table 7-1: Group B subassembly dimensions

Subassembly scale	3/8	Clear column height	L_c = 114 in.
Column diameter	D_c = 28 in.	Clear beam length	L_{b1} = 130 in.
Cap beam height	h_b = 23 in.	Cap beam width	w_b = 37 in.

The beam flexural design is based on the following three load cases: (a) Dead + Live + Impact, (b) Dead + Earthquake and (c) a plastic load case in which all the columns are at ultimate flexural capacity with the dead load applied. Dead load was approximated from the average box-girder and span dimensions provided by the database investigation (Appendix A). The dead load was approximately equal to $5\% A_g f'_c$, where A_g is equal to the gross column area and f'_c is equal to the concrete compressive strength. Earthquake load was calculated using a maximum ground acceleration of 2.0 g (ARS=2.0) and a ductility / risk factor Z=8.0. The plastic load case (c) controlled the response and the design of the system.

7.1.2 Flexural and Shear Design

The specimens meet the requirements of ACI and Caltrans BDS for flexural and shear design with the following adjustments and conditions:

Column Requirements

$Mult_{column}$ = Moment capacity determined using the measured material properties and Mander's concrete model. Computed using ARCS section analysis program [Thewalt 1994].

Mn_{column} = Moment capacity determined using ACI defined material properties and limiting strain of 0.003. Computed using ARCS.

Nu_{column} = Axial load in column = $5\% A_g f'_c$

$Vu_{column} = Mult_{column} / L_c$

$Vs_{column} = (Vu_{column} / 0.85) - Vc_{column}$

Where, Vc_{column} = (0 in plastic hinge region, $2\sqrt{f'c} \cdot D_c^2$ outside the plastic hinge region)

Beam Requirements

$Mu_{beam} = f(Mult_{column}$, Specimen Geometry), No overstrengths applied.

$Vu_{beam} = f(Mult_{column}$, Specimen Geometry), No overstrengths applied.

Using the preceding requirements the beam and column were designed (distinction is made between positive Mn_{pos} and negative Mn_{neg} moment capacities) and the results are summarized in Table 7-2.

Table 7-2: Beam and column design summary	
Column Capacities	*Beam Capacities*
Mn_{column} = 12180 kip-in.	Mn_{neg} = 11550 kip-in.
$Mult_{column}$ = 17870 kip-in.	Mn_{pos} = 7896 kip-in.
Nu_{column} = 138 kip	Vn_{beam} = 286 kips
Vn_{column} = 193 kips	

7.2 Conceptual Joint Design Models

The joint details used in Group B investigate the effectiveness of different types of lateral reinforcement in providing anchorage of column reinforcement and resistance to shear deformation. Two design strategies were studied: the first, used in Specimen B1, included only lateral transverse headed joint reinforcement and the second, used in Specimen B2, included only joint circular hoops. These models evaluate whether joint confinement is better achieved through the continuation of the column spiral into the joint or beam transverse reinforcement. To determine the level of reinforcement to be used in each specimen, a conceptual design model based on anchorage of the column reinforcement was used. To resist the anchorage forces, the transverse reinforcement in Specimen B1 was oriented both parallel and transverse to the beam axis. In Specimen B2, column bar anchorage and joint confinement was achieved using only joint hoops around the anchored column reinforcement; no additional horizontal transverse joint bars are used. To provide comparable levels of shear resistance, the same quantity of vertical reinforcement is used in both specimens. To determine the required quantity of joint reinforcement, a level of bond demand was estimated. From these bond demands, a strut pattern was developed to transfer the forces to the horizontal reinforcement. Both B1 and B2 were designed to resist the same level of bond demand. The following section discusses the justification for the quantities of reinforcement used.

7.2.1 Bond Development

The distribution of bond stress in the joint region is highly nonlinear. Figure 7-1 presents the average bond stress distribution on the tensile column reinforcement in Specimen A1. The response is typical of the behavior of Group A. The majority of the bond action occurs near the end of the bar. This region corresponds to the flexural compression zone of the beam and the top of the diagonal compression zone (Figure 7-2). The high compressive stress provides a lateral confining pressure on the bar, thus improving bond in the region. From the magnitude of the compressive load and measured bond stress, a relationship can be developed (Figure 7-3). This allows for a less conservative determination of required development length, which is advantageous in Group B where a shallower cap beam-profile was used.

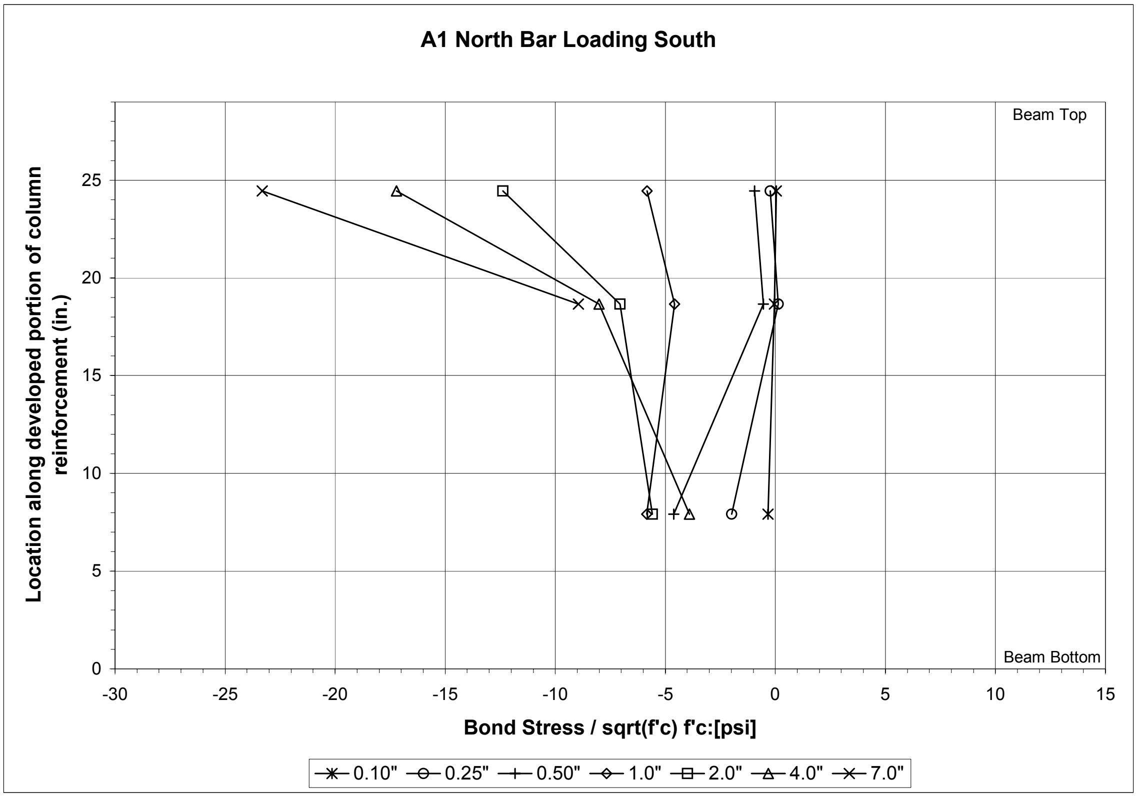

Figure 7-1: Typical bond stress distributions of Group A at increasing applied column tip displacements

Due to the reduced beam depth and increased column reinforcement, the peak compressive stress from the beam acting on the joint increases from ~20% *f'c* to ~68% *f'c* and the maximum nominal vertical joint shear stress increases from 12.0 to $19.0\sqrt{f'c}$. Based on studies performed by Eligehausen [1983] and Malvar [1992] on the effect of confining stress on the bond capacity and the measured response of Group A (Figure 7-3), the assumption was made that the peak bond stress allowed under these conditions be limited to $40\sqrt{f'c}$.

7.2.2 Bond Transfer Mechanisms

Anchorage of the column reinforcement was assumed to occur over a low and high capacity region of bond resistance. Since the high bond region lies within the diagonal compressive strut, the associated force is assumed to transfer along the strut, thus not requiring any additional transverse reinforcement. The low bond stress region, however, is conservatively assumed to have bond stress of $6\sqrt{f'c}$ distributed over the *full* development length of the bar. This stress requires development through additional transverse vertical and horizontal reinforcement as discussed in subsequent sections.

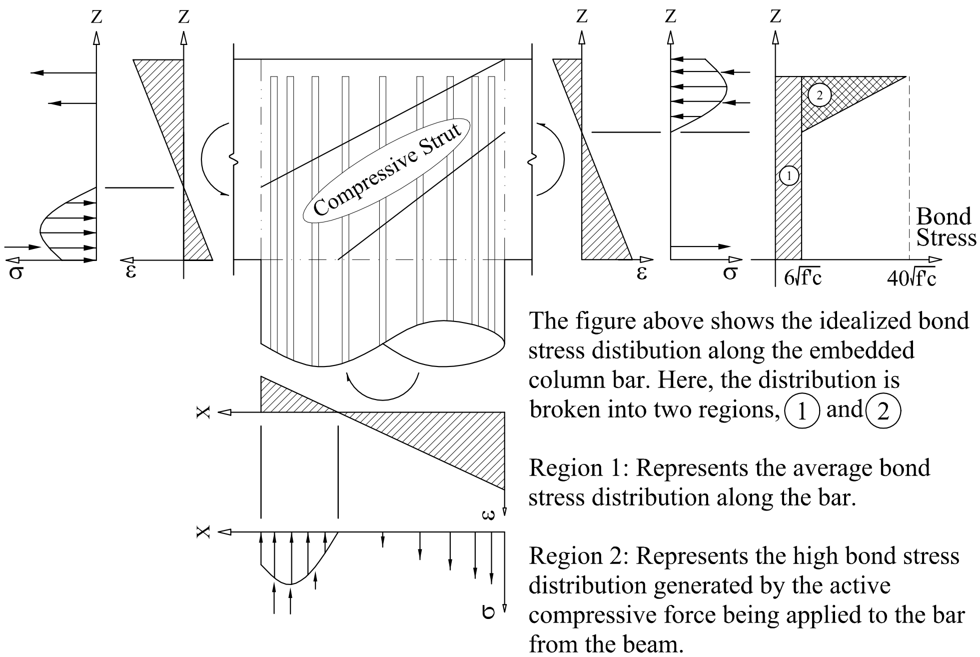

Figure 7-2: Bond stress input

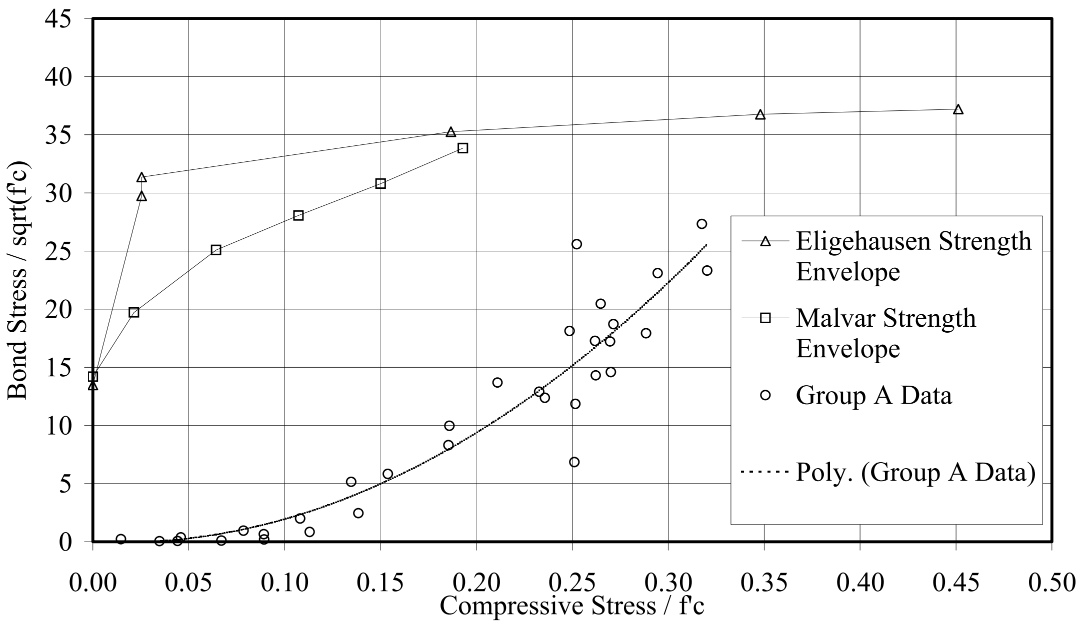

Figure 7-3: Bond stress-confining stress relationship

7.2.3 Specimen B1: Horizontal Transverse Reinforcement (X and Y)

To resist the bond demands placed on the joint from the column reinforcement, Specimen B1 uses horizontal transverse headed reinforcement oriented longitudinally and perpendicular to the axis of the cap beam. To determine the quantity of reinforcement, a conceptual model was developed to provide proper anchorage of the column reinforcement. The following section outlines the transfer mechanism from the column reinforcement anchorage to the confinement resistance required by the transverse bars.

The bond stress demand of $6\sqrt{f'c}$ is assumed to be distributed in a radial manner about the column bar (Figure 7-4). To anchor these stresses a compression cone is assumed to form at a 45-degree angle. Resolving the bond stress to the diagonal cone requires a confining stress of $6\sqrt{f'c}$. This in turn results in an equilibrating or *bursting* stress of $6\sqrt{f'c}$ normal to the bar cross section.

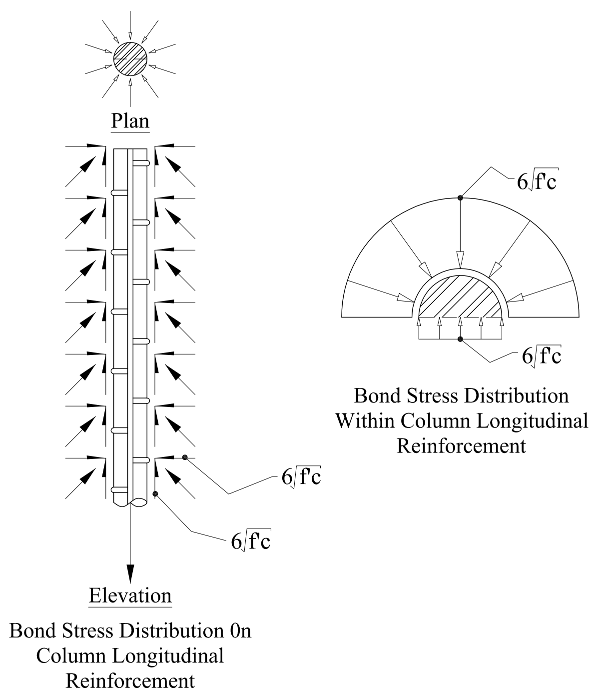

Figure 7-4: Bond transfer resolution

Thus if given a number of bars develop tensile forces, the amount of transverse reinforcement required can be determined by equating $F_{bursting}$ to $F_{resisting}$ (Figure 7-5). To safely account for damage in any orientation, two orthogonal distributions of transverse reinforcement are required. The formulation and suggested methodology are shown in the following design example.

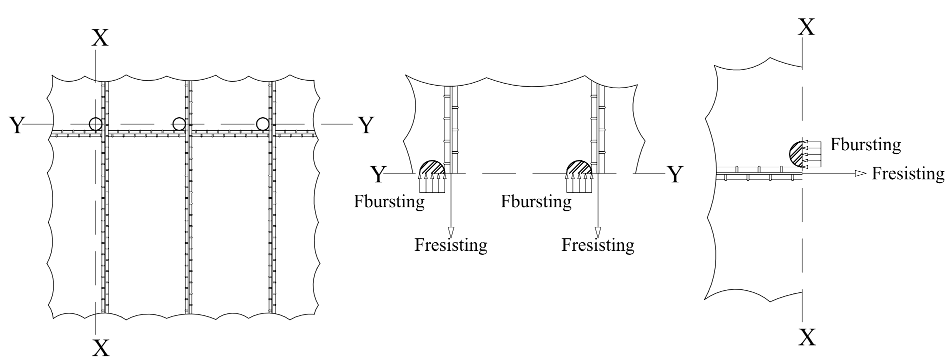

Figure 7-5: Internal forces on a horizontal section

The bursting force generated by one bundle (of two bars) of column longitudinal bars would thus be

$$F_{bursting_i} = 6.0\sqrt{f'_c} \cdot s_{vi} \cdot (2 \cdot d_b) \text{ [Per bundle]} \tag{7-1}$$

where f'_c is equal to the concrete compressive strength, s_{vi} is the vertical spacing between adjacent layers of transverse reinforcement, and d_b is the diameter of one column bar. The resisting force required is equal to

$$F_{resisting} = Av_{req.} \cdot fy \tag{7-2}$$

where Av_{req} is equal to the area of transverse joint reinforcement and fy is equal to the yield stress of the transverse reinforcement. Equating the bursting and resisting forces, the area of transverse reinforcement required can be computed

$$Av_{req_{ij}} = \frac{12\sqrt{f'c} \cdot s_{v_j} \cdot d_b}{fy} \text{ per layer } i\text{, oriention } j \text{ and bundle} \tag{7-3}$$

As shown in cut X-X of Figure 7-5, when the longitudinal bars are in-line, only one transverse bar is required to provide the $F_{resisting}$ force needed to support all the bars. To take advantage of this behavior when the bars are oriented in a circular configuration, the following multiplier should be applied to determine the necessary quantity of transverse bars across each section:

$$Avtotal_{ij} = Av_{req_{ij}} \cdot \frac{\left(\sum_k \ell_{kj}\right) + \ell_{sp}}{\ell_{sp}} \tag{7-4}$$

Where $Avtotal_{ij}$ equals the total quantity of transverse reinforcement required in orientation j at vertical level i, l_{sp} equals the circumferential center-to-center distance between adjacent bars (or bundles), and l_{kj} equals the center-to-center distance between an adjacent group of bars k projected to a plane normal to the orientation j under consideration. The design of joint horizontal transverse reinforcement for Specimen B1 is illustrated in Figure 7-6 and Table 7-3.

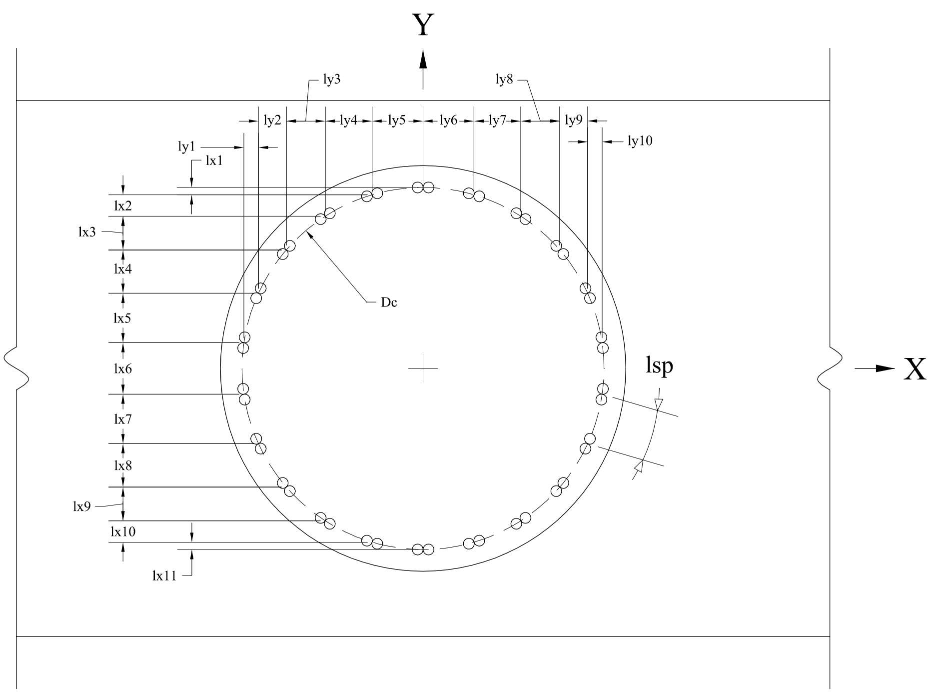

Figure 7-6: Design illustration

Table 7-3: Joint design example for Specimen B1

Required:

Determine the quantity of transverse bars required to anchor column reinforcement within the joint. Place the reinforcement in two orthogonal directions: along and perpendicular to the beam axis.

Given:

A. Diameter of column core, center-to-center of extreme reinforcement, dc = 25.0 in.

B. Column reinforcement, 22 #6 bundles of two bars, db = 0.75 in. (Figure 7-6)

C. Transverse reinforcement, #3 bars, Atr = 0.11 in.^{2}

D. Concrete compressive strength, $f'c$ = 4500psi.

E. Reinforcement yield strength, fy = 60 ksi.

F. $\ell sp = \dfrac{dc \cdot \pi}{\text{number of bundles}} = \dfrac{25.00 \cdot \pi}{22}$ $\qquad \sum_i \ell_{xi} = dc = 25.00 in.$ $\qquad \sum_i \ell_{yi} = 24.75 in.$

Solution:

1. Choose number of layers desired.

   Three layers of horizontal transverse reinforcement. A varied spacing is used so more reinforcement is placed near the interface where yield penetration is the highest (see Figure 7-7):

   $s_{v1} = 8\,in.,\ s_{v2} = 6.5\,in.,\ s_{v3} = 6.5\,in.$ $\qquad$ Note: $\sum s_v = \ell_d$.

2. Orientation 1, X:

$$Avtotal_{x1} = \frac{12\sqrt{f'c} \cdot s_{v1} \cdot d_b}{fy} \cdot \frac{\left(\sum_{k=1}^{k=11} \ell x_k\right) + \ell sp}{\ell sp} = \frac{12\sqrt{4500} \cdot 8 \cdot 0.75}{60000} \cdot \frac{25.00 + (25\pi/22)}{(25\pi/22)}$$

   $Avtotal_{x1}$ = 0.644 in.^{2}

   $Avtotal_{x2}$ = 0.523 in.^{2}

   $Avtotal_{x3}$ = 0.523 in.^{2}

3. Orientation 2, Y:

$$Avtotal_{y1} = \frac{12\sqrt{f'c} \cdot s_{v1} \cdot d_b}{fy} \cdot \frac{\left(\sum_{k=1}^{k=10} \ell y_k\right) + \ell sp}{\ell sp} = \frac{12\sqrt{4500} \cdot 8 \cdot 0.75}{60000} \cdot \frac{24.75 + (25\pi/22)}{(25\pi/22)}$$

   $Avtotal_{y1}$ = 0.639 in.^{2}

   $Avtotal_{y2}$ = 0.519 in.^{2}

   $Avtotal_{y3}$ = 0.519 in.^{2}

4. Thus use:

   Layer 1: X-orientation ⇨ 0.644 in.^{2} ~ 6 #3 bars, Y-orientation ⇨ 0.639 in.^{2} ~ 6 #3 bars

   Layer 2: X ⇨ 0.523 in.^{2} ~ 5 #3 bars, Y ⇨ 0.519 in.^{2} ~ 5 #3 bars

   Layer 3: X ⇨ 0.523 in.^{2} ~ 5 #3 bars, Y ⇨ 0.519 in.^{2} ~ 5 #3 bars

Sixteen #3 horizontal transverse reinforcing bars are required in both the X- and Y-orientations. To account for the beam longitudinal reinforcement oriented in the X direction, the joint reinforcement was reduced. The reduction in the number of bars was made relative to the beam flexural overstrength. Group B specimens provided a 3.8% overstrength in positive flexural capacity and 11.3% in negative flexural capacity. Given the location of the beam flexural reinforcement relative to the developed column bars, only the positive beam reinforcement and the second layer of negative reinforcement are assumed active in bond anchorage. This translates to a reduction of 0.22 in.^{2} and 0.40 in.^{2} in the Avx required for the bottom and top transverse reinforcement respectively. Due to the odd number of longitudinal bars, through which the Y-transverse reinforcement must pass, the quantity of bars in each layer was rounded up to an even number for symmetric arrangement. A total of 11 #3 bars were used in the X-direction and 18 #3 bars in the Y-direction (6 in each layer). The final details are shown in Figure 7-7.

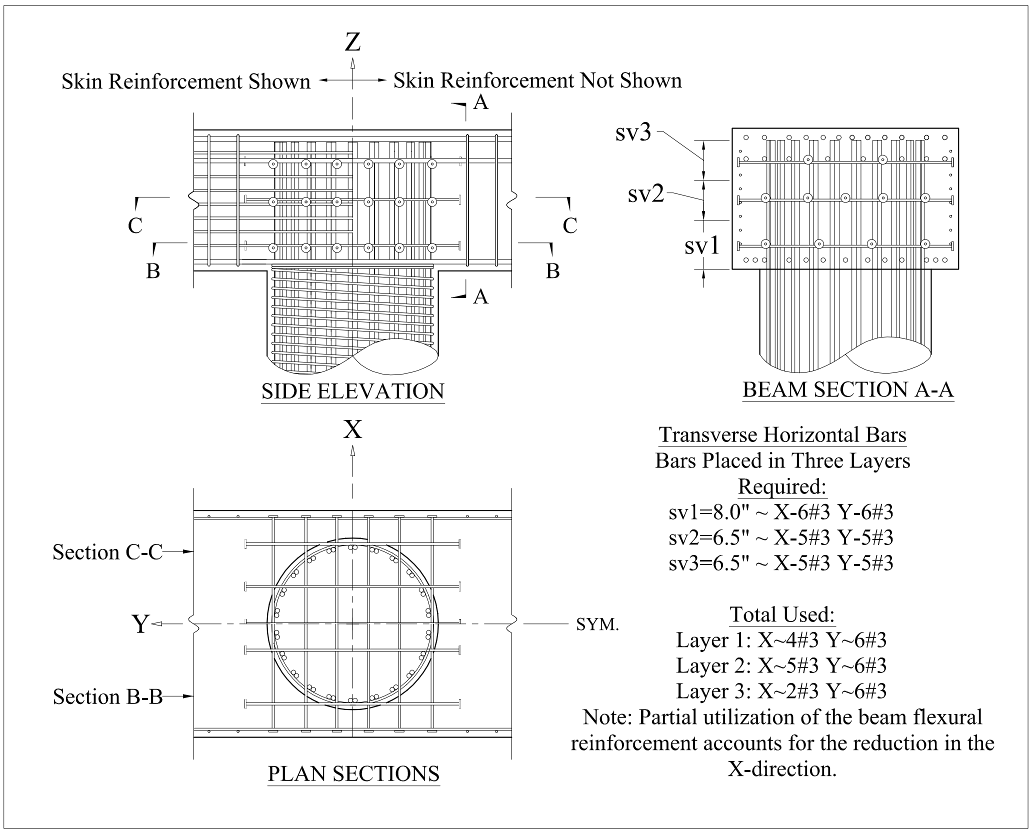

Figure 7-7: Joint details of Specimen B1

7.2.4 Specimen B2: Horizontal Transverse Reinforcement (Spiral)

Anchorage of column longitudinal reinforcement in Specimen B2 is achieved using joint spiral reinforcement. As with Specimen B1, a bond stress of $6\sqrt{f'c}$ is assumed to develop along the column tensile reinforcement and anchor in the surrounding joint through compression struts. The conceptual model used in Specimen B2 assumes that this results in the formation of at least two mechanisms of failure, referred to as crack mechanism 1 and 2 (Figure 7-8). In mechanism 1, a crack forms at the column longitudinal bars normal to the hoop. In mechanism 2, a crack forms at the bar tangent to the hoop. The amount of joint spiral reinforcement required is determined by conservatively *combining* the demand of each mechanism acting independently.

For crack mechanism 1, bond anchorage of the longitudinal reinforcement produces 45-degree compressive struts acting tangential to the circular orientation of the bars. The compressive struts, in turn, are resisted by the hoop reinforcement (Figure 7-9). This produces tensile hoop loads near the tensile column longitudinal reinforcement and reaches a maximum near the extreme tensile bars (Figure 7-9). In the case of crack 2 formation, the section is restrained through the confining action produced by the curvature of the spiral. The quantity of hoop reinforcement is determined by the amount needed to restrain the bursting force. The resisting force provided by the hoop is equal to the radial component. Using these rules, the total required area and spacing of hoop reinforcement can be determined as shown in subsequent paragraphs.

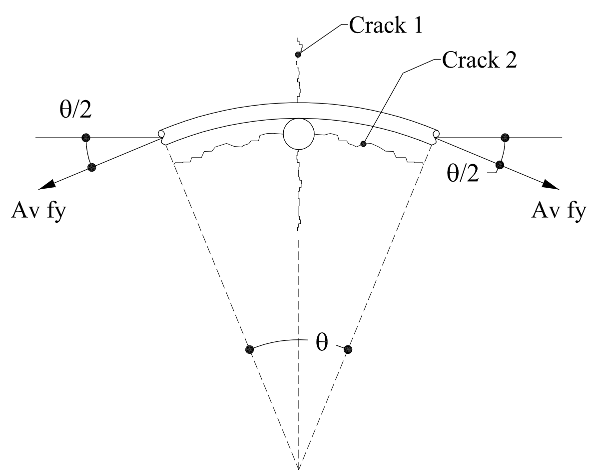

Figure 7-8: Joint hoop crack mechanism diagram

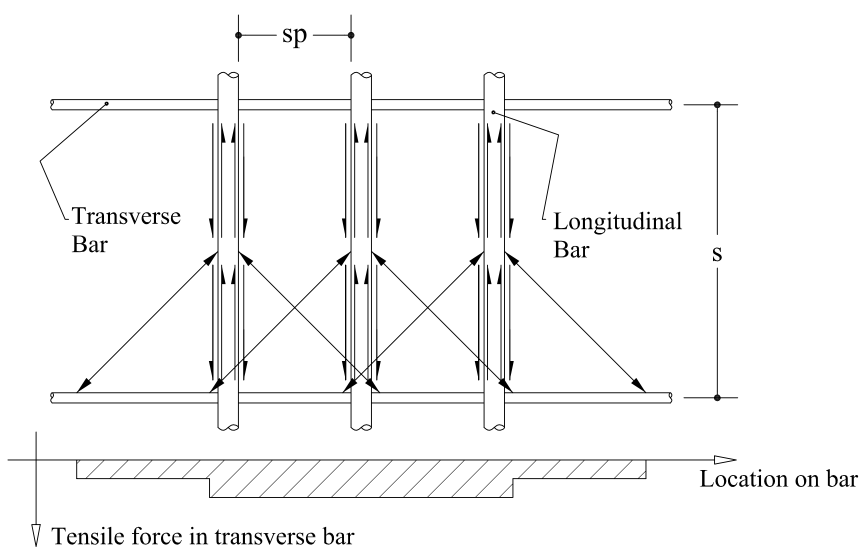

Figure 7-9: Hoop bond transfer — crack mechanism 1

Crack Mechanism 1 Resistance

Restraint of crack 1 is approached by providing enough reinforcement, Av_1, to resist the strut force. The bursting force resulting from the struts is equal to

$$Fh_1 = \frac{1}{2}\left[6\sqrt{f'c}\cdot\left(\pi \cdot d_{beffective}\right)\cdot s\right]\cdot \mathrm{C} \tag{7-5}$$

where *f'c* is equal to the concrete compressive strength, *s* is the vertical spacing between adjacent hoops, and $d_{beffective}$ is the effective diameter of the developed column bars. The effective diameter of the column longitudinal bars are computed as follows:

$$d_{beffective} = \left\{\begin{array}{c}\sqrt{4/\pi\left(\text{Total area of bars in bundle}\right)},\ \text{if column longitudinal bars are bundled} \\ \text{One bar diameter, if column longitudinal bars are NOT bundled}\end{array}\right\} \tag{7-6}$$

To account for the load increase in the transverse reinforcement when the column bars are closely spaced, a magnification factor C, equal to the ratio *s/sp,* is used, where *sp* is the clear spacing of adjacent column bars. The resisting force is equal to

$$Fh_{allowable} = Av_1 \cdot fy \tag{7-7}$$

where Av_1 is equal to the required area of transverse hoops and *fy* is equal to the yield stress of the transverse reinforcement. Equating the bursting and resisting forces, the area of the required transverse reinforcement for mechanism 1 can be computed

$$Av_1 = \frac{3\sqrt{f'c}\cdot\pi\cdot d_{beffective}\cdot s^2}{sp\cdot fy} \tag{7-8}$$

Crack Mechanism 2 Resistance

To resist crack formation tangent to the circumference of the spiral, the confining (radial) force from the orientation of the spiral is used. The bursting force is equal to

$$Fh_2 = \frac{1}{2}6\sqrt{f'c}\cdot\left(\pi\cdot d_{beffective}\right)\cdot s \tag{7-9}$$

where *f'c*, $d_{beffective}$, and *s* are the same quantities defined in equation 7-5. The resisting capcity of the spiral is equal to

$$Fh_{allowable} = Av_2 \cdot fy \cdot \left(2\sin(\theta/2)\right) \tag{7-10}$$

where Av_2 is equal to the required area of transverse hoops, θ is equal to the central angle between adjacent column bars, and *fy* is equal to the yield stress of the transverse reinforcement. Equating the bursting and resisting forces, the area of the required transverse reinforcement for mechanism 2 can be computed

$$Av_2 = \frac{1.5\sqrt{f'c} \cdot \pi \cdot d_{beffective} \cdot s}{fy \cdot \sin(\theta/2)} \tag{7-11}$$

The following example summarizes application of the conceptual design model given by equations 7-8 and 7-11. Note that the effective circumferential spacing, diameter of bundled bars, and central angle in this example were taken to be 1.06 in., 2.07 in., and 16.4 degrees, respectively.

Table 7-4: Joint spiral design example for Specimen B2

Procedure	Design Example
• Assume a spacing, s. • Compute $Av_{total} = Av_1 + Av_2$	• Say s = 2.0 in. • $Av_{total} = \frac{3\sqrt{4500} \cdot \pi \cdot 1.06 \cdot 2.0^2}{2.07 \cdot 60000} + \frac{1.5\sqrt{4500} \cdot \pi \cdot 1.06 \cdot 2.0}{60000 \cdot \sin(16.4/2)}$ $= 0.10$ in.^{2}
• Compute true bar spacing based on realistic Av, $s = (s_a \times Av) / Av_{total}$	• s = (2.0 x 0.11) / 0.10 = 2.19 in. ⇨ Use: #3 Spiral @2.0″o.c.

The joint reinforcement for Specimen B2 consisted of #3 hoops at 2 in. on center as shown in Figure 7-10.

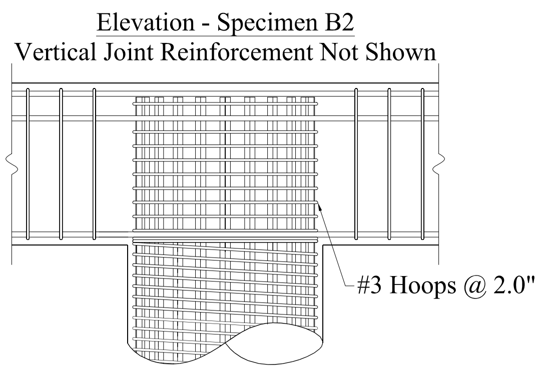

Figure 7-10: Specimen B2 joint confinement reinforcement

7.2.5 Group B: Vertical Transverse Reinforcement (Z-orientation)

The vertical joint transverse reinforcement is based on the quantity used in Specimen A2. The increased demand produced by the additional column reinforcement in Group B is accounted for by keeping the required ratio of vertical transverse reinforcement, *Av,* to column longitudinal reinforcement area, *As*, similar to that used for A2. Specimen A2 had 28 #4 vertical transverse bars and 32 #6 column bars, producing a ratio of 0.4 (note that Caltrans requirements recommend that 0.2*As* be used in addition to the continuation of beam shear reinforcement through the joint). To induce inelastic response in Group B joints, the relative quantity of vertical reinforcement was reduced. The amount of reduction was chosen to increase the demand so that the vertical bars approached yield. In Group A, the vertical reinforcement reached at most 74% of yield (Figure 7-11). To increase the demand on the vertical reinforcement, the ratio of *Av/As* was reduced by 26% to a value of 0.29*As* (28 #4 vertical bars). The same quantity was used in both specimens B1 and B2. The final details are as shown in Figure 7-12.

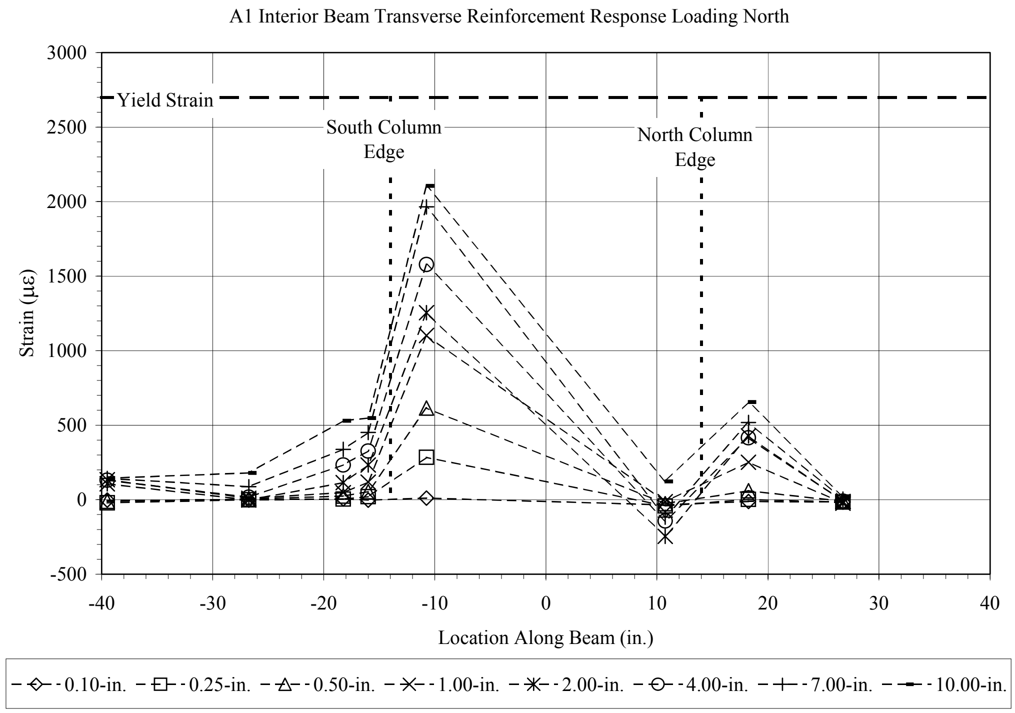

Figure 7-11: Strain in vertical transverse reinforcement along beam length (Specimen A1)

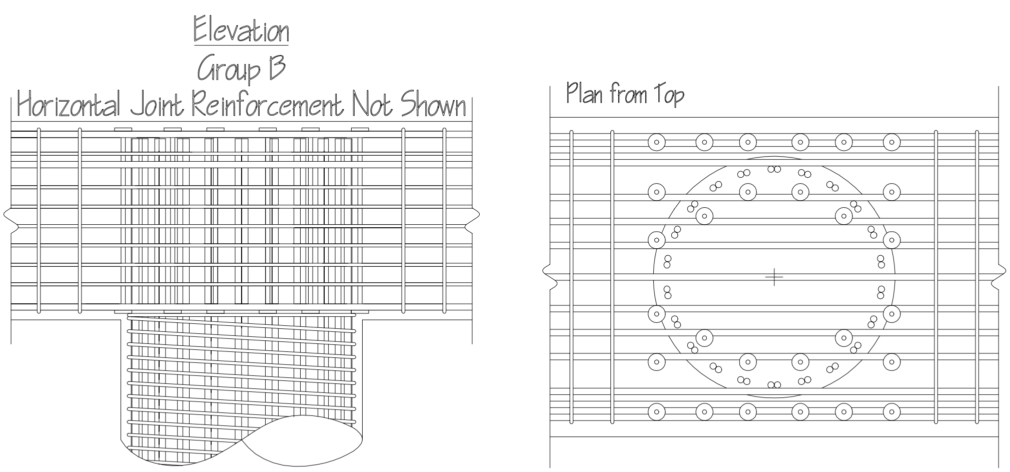

Figure 7-12: Group B vertical transverse joint reinforcement

7.3 Group B: Subassembly Details

This section summarizes the final details used in Group B subassemblies. Both the specimen details including the quantity of reinforcement, construction drawings, as-built photos, and material properties as well as the test subassembly details are presented.

7.3.1 Group B: Specimen Details

The reinforcement used in the cap beam and columns was the same in both subassemblies (Table 7-5). Beam reinforcement was placed in three layers: one layer of positive moment reinforcement and two layers of negative moment reinforcement. Column reinforcement was bundled in groups of two. Note that the column bars were developed straight into the joint without the use of hooks or heads. The final length of $28d_b$ was determined to be adequate using the assumed bond stress distribution. Skin reinforcement was placed on both vertical faces of the cap beam as required by Caltrans requirements.

Table 7-5: Group B specimen details

Column	*Beam*
44 #6 column bars (bundled in groups of two)	20 #6 total negative reinforcement
#3 Spiral at 1.5 in. within plastic hinge	13 #6 positive reinforcement
#3 Spiral at 3.0 in. outside plastic hinge	Skin steel 7 #3 each face
Plastic hinge length = column diameter = 28 in.	#3 stirrups at 4.75 in. (6 verticals and 3 horizontals)
Development length, l_d = 21 in. = $28d_b$	

The quantity of vertical and horizontal joint reinforcement is summarized in Table 7-6. The volume of vertical joint reinforcement used in both specimens is identical. The volume of horizontal reinforcement is higher in Specimen B1. The volumetric ratios were computed assuming a joint volume equal to the product of the cap beam width, cap beam height, and joint length (taken equal to the cap beam width).

Table 7-6: Group B joint reinforcement

Specimen	*B1*	*B2*
Effective joint volume Width x height x length (in.)	37 x 23 x 37	37 x 23 x 37
Horizontal transverse reinforcement	11#3 headed bars parallel to beam axis 18#3 headed bars perpendicular to beam axis	Joint hoops #3 at 2.0 in.
Vertical transverse reinforcement	28#4 headed bars	28#4 headed bars
Volumetric vertical transverse joint reinforcement ratio, ρ_{jv}	0.38 %	0.38 %
Volumetric horizontal transverse joint reinforcement ratio, ρ_{jh}	0.36 %	0.29 %

The final details used in subassemblies B1 and B2 are presented in Figure 7-13 and Figure 7-14, respectively. As-built photos of the reinforcement cages are presented in Figure 7-15.

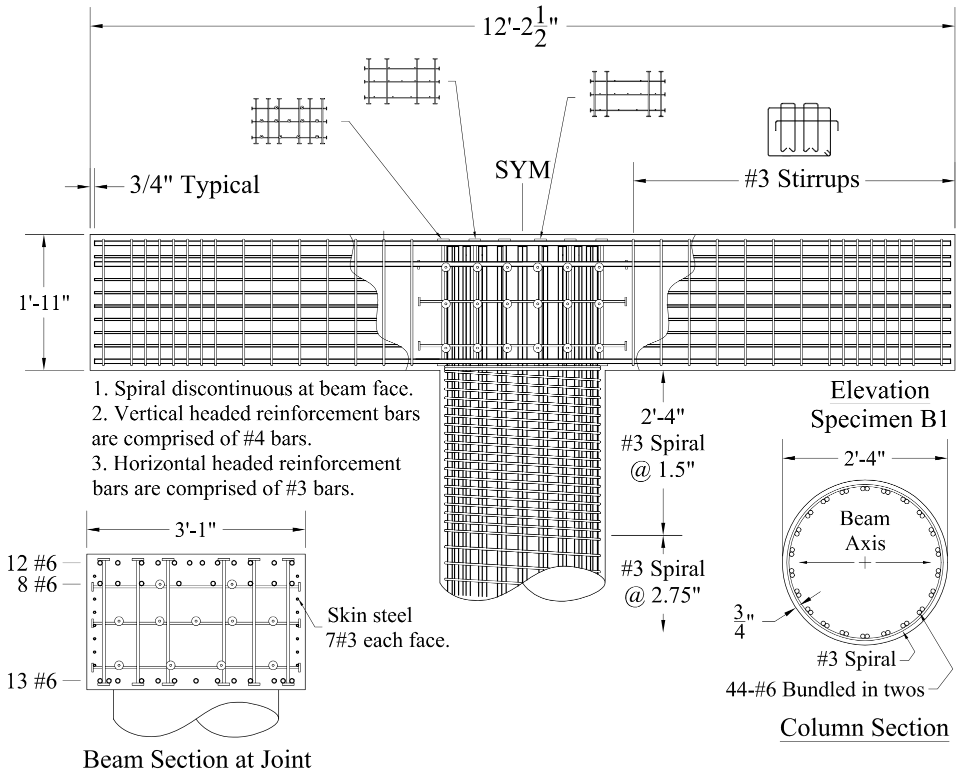

Figure 7-13: Specimen B1 details

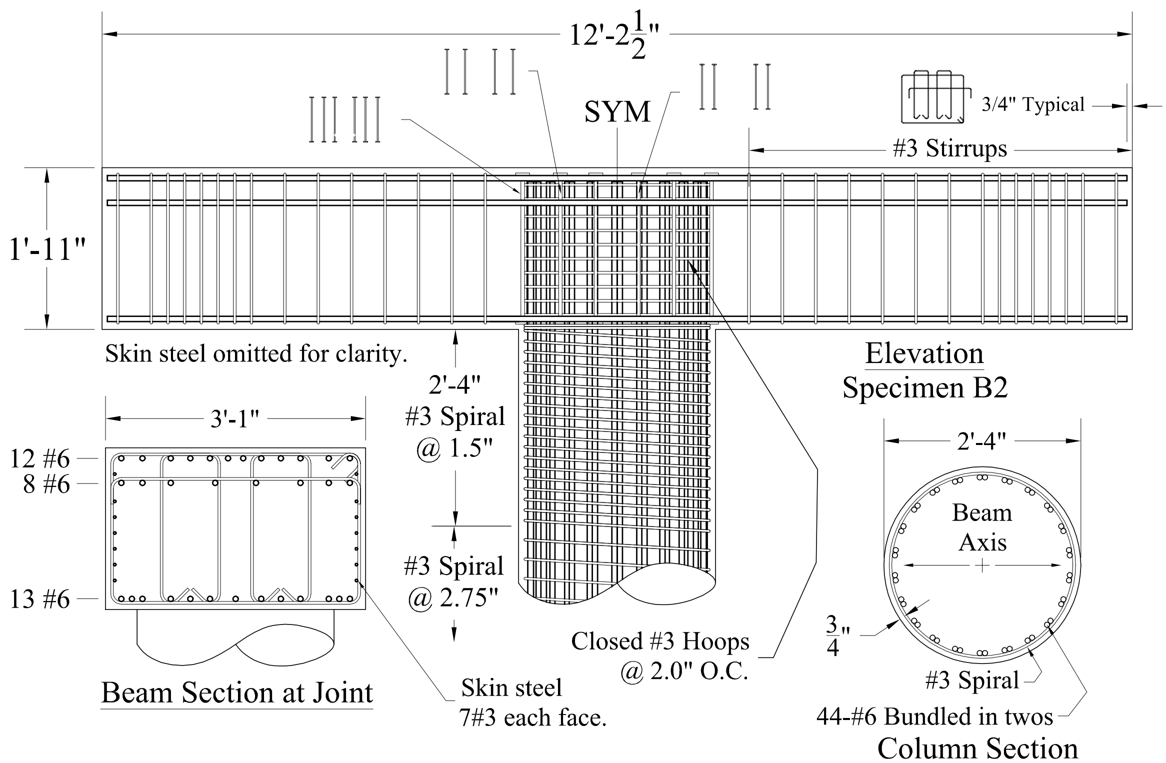

Figure 7-14: Specimen B2 details

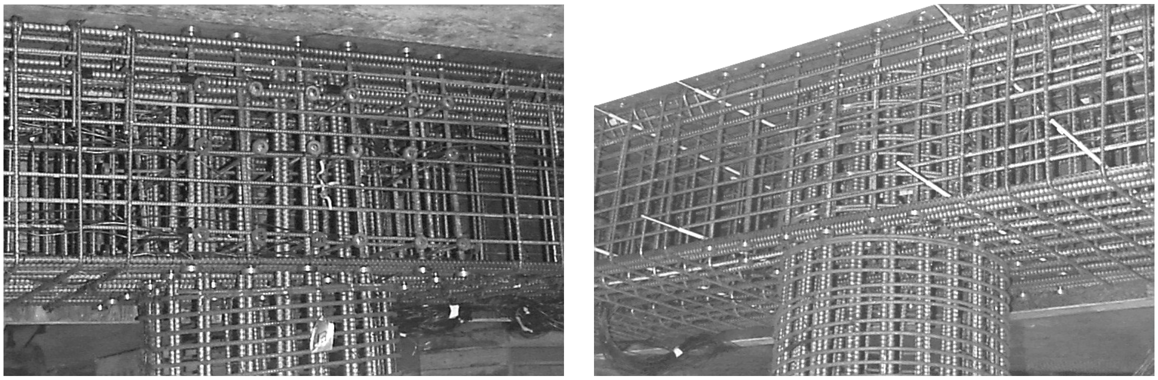

Figure 7-15: Construction photos of subassemblies B1 and B2

7.3.2 Group B Test Subassembly

Group B specimens were tested in an inverted position with the cap beam toward the floor and the column projecting upwards (Figure 7-16). Boundary conditions and load application were the same as the conditions used for Group A. Background and development are discussed in Chapter 3.

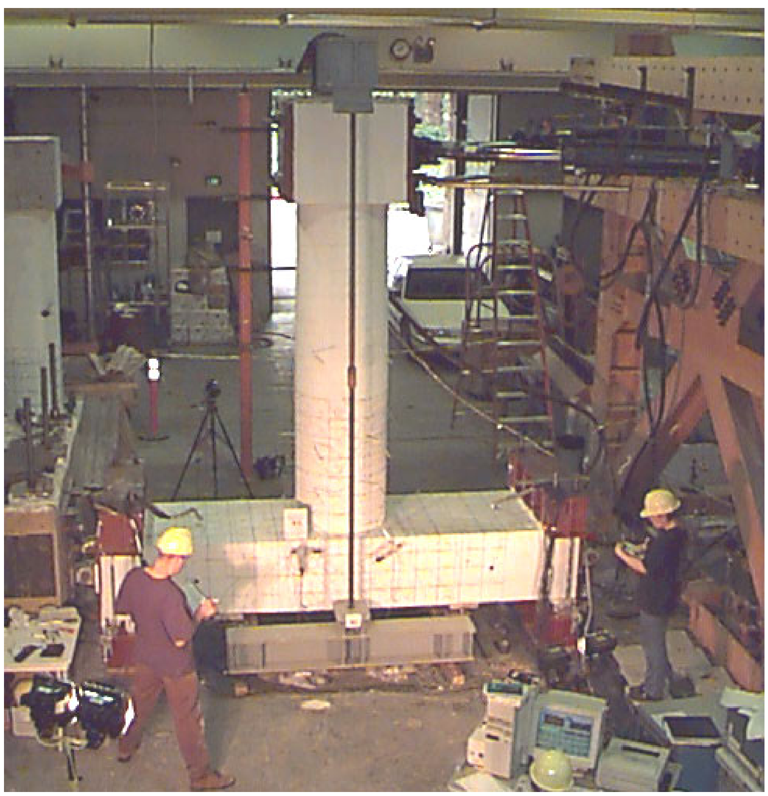

Figure 7-16: Setup used for Group B testing, (Specimen B2 shown).

7.3.3 Material Properties Group B

Material properties for specimens B1 and B2 were determined according to ASTM Standards and European testing methods [50-FMC] (Table 7-7 and Table 7-8). The testing methods are summarized in Appendix B.

Table 7-7: Group B reinforcement properties							
Bar Use		*Beam Skin and Joint Hoops*	*Beam Transverse*	*Column Spiral*	*Joint Horizontal Headed Transverse*	*Joint Vertical Headed Transverse*	*Beam and Column Longitudinal*
Bar size		#3	#3	#3	#3	#4	#6
ASTM specification		A615	A615	A615	A615	A706	A706
Elastic modulus	E_s	26600	26400	28000	26500	25100	27800
Yield stress	σ_y	67.2	84.6*	61.8*	67.2	74.5	69.1
Yield strain	ε_y	0.00253	0.00518*	0.00424*	0.00254	0.00296	0.00249
Plateau strain**	ε_{yp}	0.0121	None	None	0.0112	0.0142	0.0096
Ultimate stress	σ_u	105.9	112.2	108.9	107.4	103.1	103.6
Ultimate strain***	ε_u	0.129	0.0853	0.095	0.121	0.134	0.123
Fracture strain	ε_f	0.153	0.0954	N. A.	0.150	0.246	0.245

Note: All stresses are in ksi.
* Values computed using 0.2% offset.
** Strain at end of yield plateau.
*** Strain at ultimate stress.

Table 7-8: Group B concrete properties				
Test Subassembly			*B1*	*B2*
Column	Compressive strength	f'_c	4.22	4.38
Column	Corresponding strain	ε_c	0.00231	0.00238
Column	Splitting tensile strength	f'_t	0.364	0.441
Column	Modulus of rupture	f'_r	0.609	0.739
Column	Young's modulus	E_c	3260	3350
Column	Fracture energy [kip-in./in.^{2}]	G_f	0.00103	0.00070
Beam	Compressive strength	f'_c	5.23	5.44
Beam	Corresponding strain	ε_c	0.00244	0.00249
Beam	Splitting tensile strength	f'_t	0.471	0.481
Beam	Modulus of rupture	f'_r	0.711	0.708
Beam	Young's modulus	E_c	3500	3690
Beam	Fracture energy [kip-in./in.^{2}]	G_f	0.00053	0.00099

Note: All forces are in kips and lengths in inches.

7.4 Global Behavior of Joint Subassemblies Subjected to High Demands

The low beam depth combined with the high column and anchorage levels produce significant demand on the joint subassemblies. This section evaluates the experimental results observed and measured as the subassembly was subjected to increasing levels of drift. The observed progression of damage will be discussed relative to the drift levels and measured events such as yielding. It will be shown that the bond distribution model assumed in design was not achieved, leading to degradation of the joint followed by bar slip and consequently the loss of load capacity. The effectiveness of the spiral over that of the headed transverse bars is also discussed. It will be shown that the spiral is more effective in resisting slip, while the headed bars are more effective in reducing joint degradation.

7.4.1 Load and Displacement Response

The global behavior of the two specimens was similar. Column cracking, yielding, and ultimate capacity occurred at the same points in the displacement history (Table 7-9). Joint cracking occurred much earlier in Specimen B2. This could be indicative of a weaker joint configuration in the spirally reinforced specimen. Yielding also occurred earlier in B2; this may be attributable to construction variations. In both specimens failure consisted of joint shear failure and column reinforcement pullout.

The displacement history applied to each specimen is presented in Figure 7-17. The cycle numbers are indicated on the positive (northern) displacement peak. The number of cycles applied to each specimen was identical. The magnitude of the peak displacements, however, marginally varied as a result of differences in the subassembly geometry. The letters on each graph correspond to events that occurred during the test (Table 7-9).

Table 7-9: Group B test observations

Event Symbol	*Event Description*	*Column Tip Displacement (in.)*	
		B1	*B2*
A	Column Cracking	(0.25″ – N) Cycle 1	(0.25″ – N) Cycle 1
B	Joint Cracking and Beam Flexural Cracking	(1″ – N) Cycle 1	(0.50″ – N) Cycle 1
C	South Column Reinforcement Tensile Yield	1.56″ North (2″ – N) Cycle 1	1.46″ North (2″ – N) Cycle 1
D	North Column Reinforcement Tensile Yield	1.71″ South (2″ – S) Cycle 1	1.88″ South (2″ – S) Cycle 1
E	Peak North Lateral Load	4.40″ North (4″ – N) Cycle 1	4.40″ North (4″ – N) Cycle 1
F	Peak South Lateral Load	4.36″ South (4″ – S) Cycle 1	4.36″ South (4″ – S) Cycle 1
G	Column Spalling Initiates	(4″ – S) Cycle 1	(4″ – S) Cycle 1
H	Failure	Joint shear damage and column reinforcement pullout from joint.	

( ) denotes the displacement group and direction for which the listed event occurred.

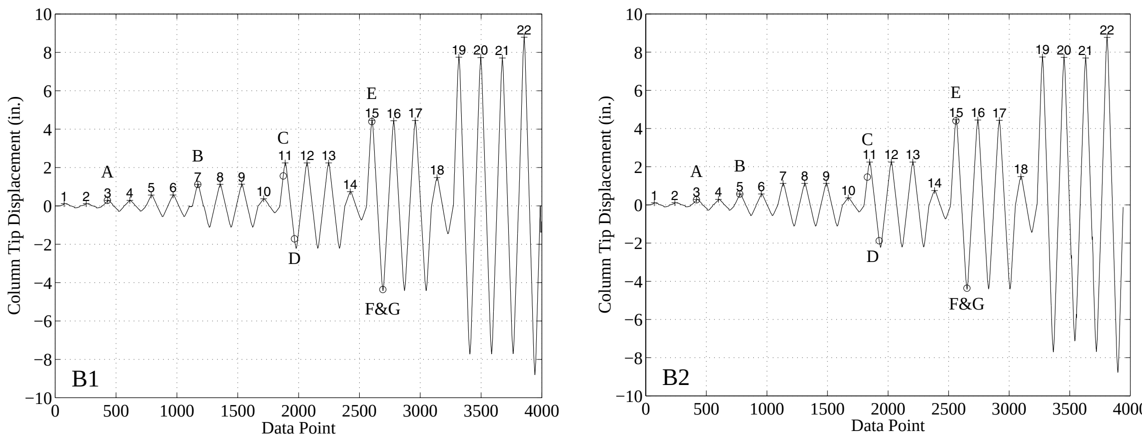

(a) Specimen B1 (b) Specimen B2

Figure 7-17: Group B displacement histories

The progression of damage occurred in the same pattern in B1 and B2 (Table 7-10). Column flexural cracking occurred first, followed at higher displacement demands by joint shear and beam flexural cracking. The amount of cracks on the joint, column, and beam continued to increase until the ultimate capacity was reached. At this level, spalling of the column occurred on the south face. Additional demand resulted in large joint-shear crack openings. Continued cycling at this displacement demand resulted in spalling of the joint face and beam top. Bond loss and pullout of the column reinforcement ultimately controlled capacity of the system.

Observations indicate that the joint with headed reinforcement (B1) was better confined and resisted shear deformation to a greater degree than the spirally confined joint (B2). In Specimen B2, joint cracking initiated during the 0.5-in. tip displacement (0.4% drift). Joint cracking of B1, however, was delayed until the 1.0-in. displacement. At the 2-in. and 4-in. displacement levels, a greater amount of cracking was observed in B2. This is indicative of greater joint shear damage in the spirally reinforced joint. At the end of the test, the joint in Specimen B1 had undergone spalling. Damage of the joint, however, was limited to a shear failure within the column diameter. No dilation was noticeable. Specimen B2, however, was subjected to noticeable dilation continuing into the beam. The shear deformation and associated damage present at earlier levels of demand were no longer observable, indicating a possible delamination of the beam face from the core.

Table 7-10: Progression of damage (B1 left, B2 right)

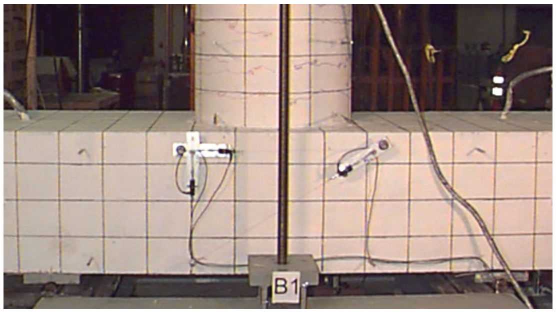 (a1) 0.5″ South – Cycle 1 Column flexural cracking	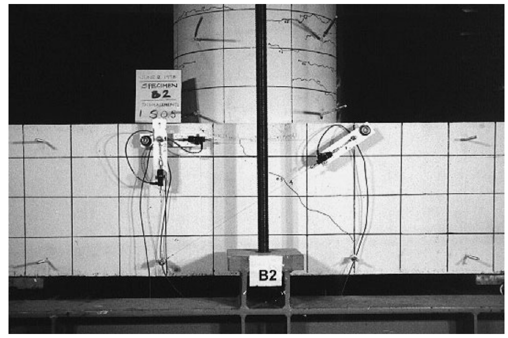 (a2) 0.5″ South – Cycle 1 Joint cracks form
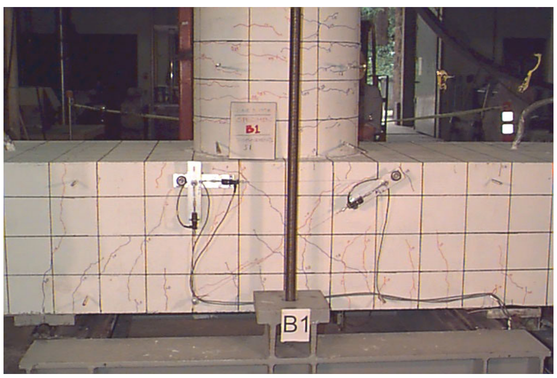 (b1) 1″ North – Cycle 1 Flexural beam and joint shear cracking	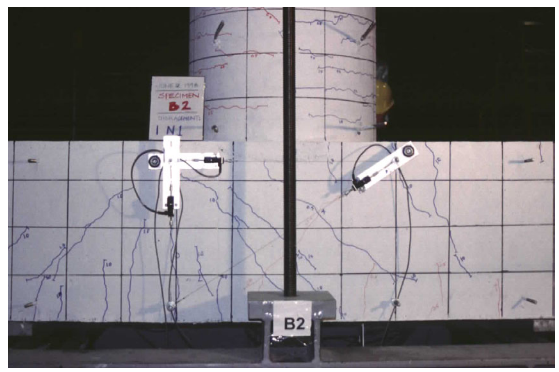 (b2) 1″ North-Cycle 1 Beam flexural cracking and greater joint cracking
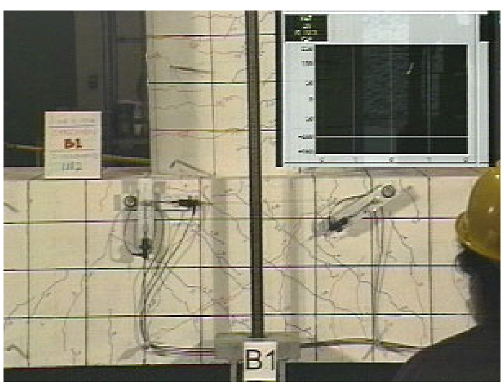 (c1) 2″ South – Cycle 1	 (c2) 2″ South – Cycle 1
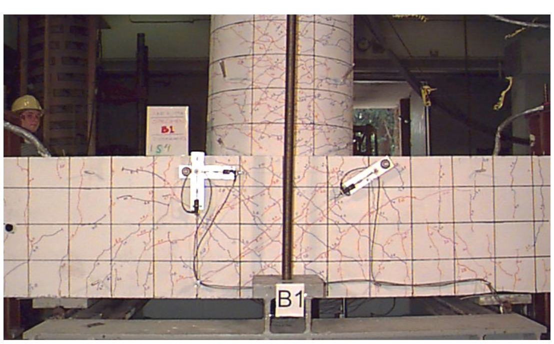 (d1) 4″ South – Cycle 1 – Ultimate capacity	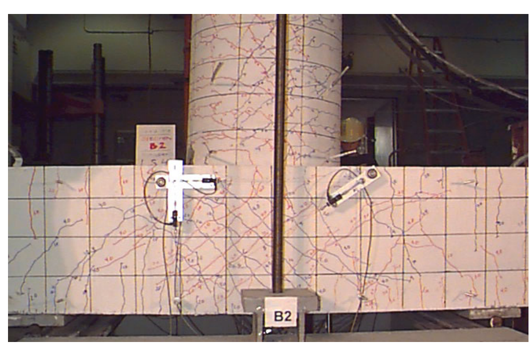 (d2) 4″ South – Cycle 1 – Ultimate capacity

Table 7-10: Progression of damage (B1 left, B2 right).

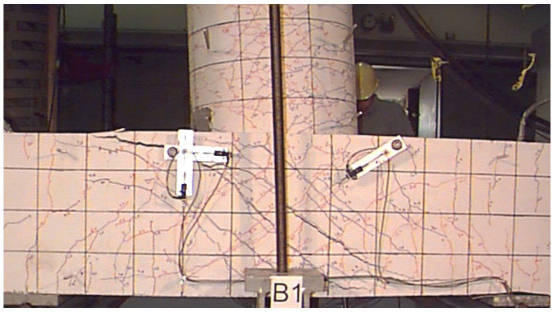

(e1) 7″ North – Cycle 1

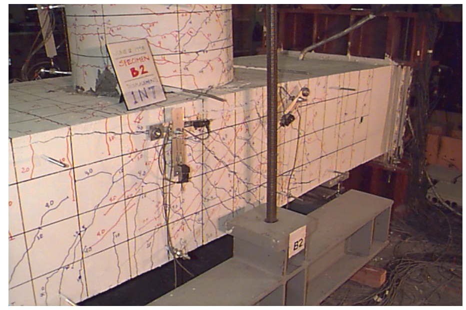
(e2) 7″ North – Cycle 1

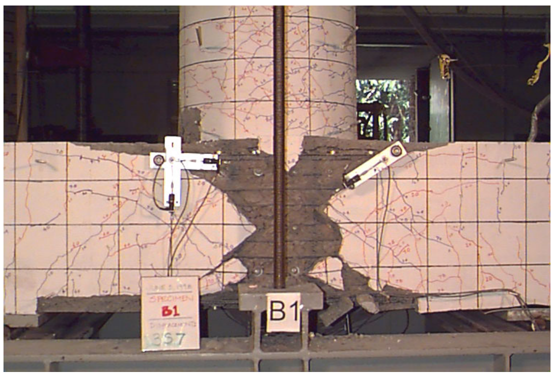

(f1) 7″ South – Cycle 3

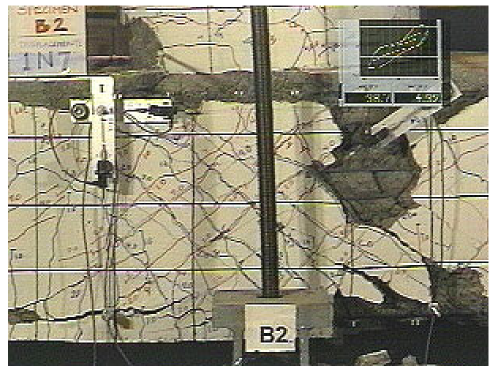

(f2) 7″ South – Cycle 3

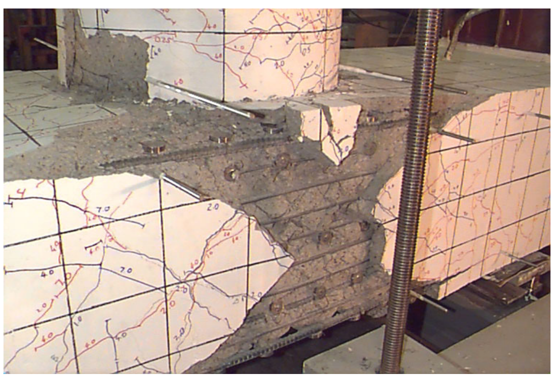
(g1) B1 End of test, close-up

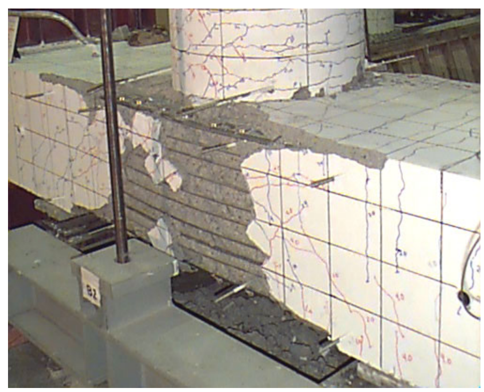
(g2) B2 End of test, close-up

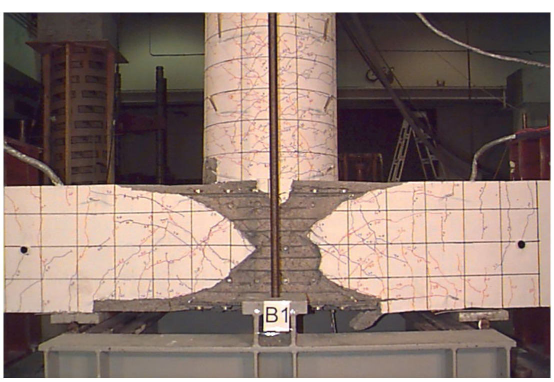

(h1) B1 End of test, overall

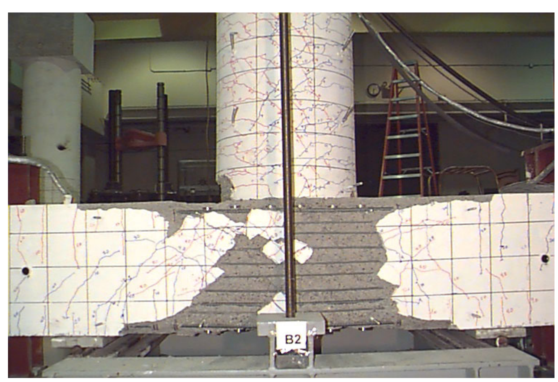

(h2) B2 End of test, overall

The hysteretic load-displacement behavior of the two specimens was similar (Figure 7-18 and Figure 7-19). The numbers listed on the graph correspond to the applied displacement cycles shown in Figure 7-17. The shape of the hysteresis and the ductility measured are comparable. Limited system yielding occurred up to the peak load capacity. This relatively low ductility is attributed to joint failure, which occurred prior to the formation of a column plastic hinge. Consequently, a yield plateau does not occur; instead, the load capacity rapidly decreases. At this level of demand, the column bars began to exhibit notable slip and joint shear damage. This led to slackness in the load-displacement hysteresis, producing pinching in the second and third cycles to 4-in. displacement.

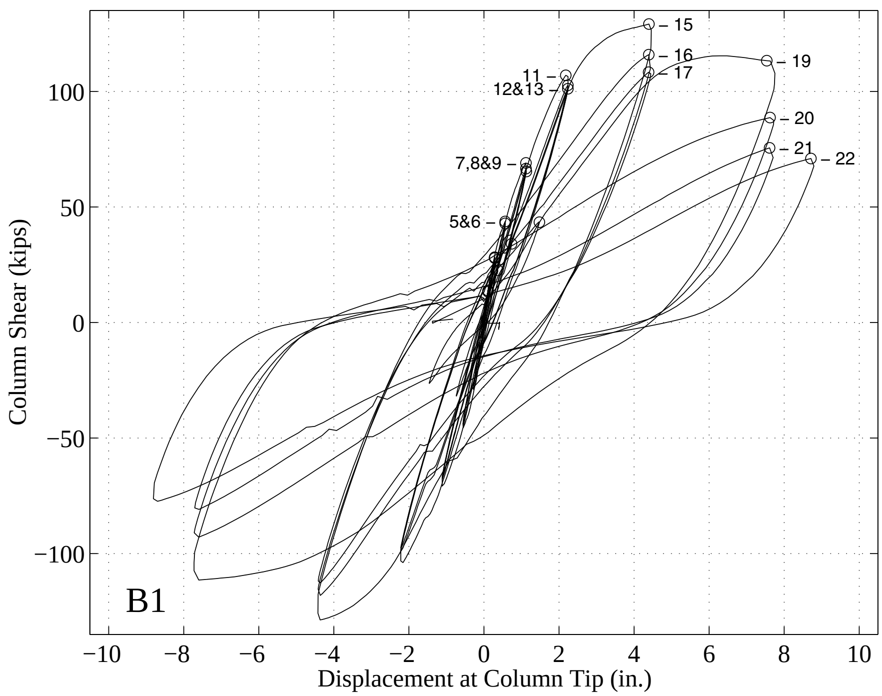

Figure 7-18: B1 load-displacement response

The global behavior is examined through the backbone or envelope of the load-displacement response. The backbone was computed by taking the intersection of the first cycle of displacement group (*i*) with the second cycle of displacement group (*i-1*) (Figure 7-20). This produces a lower bound representation of the response by accounting for any damage occurring between the first and second cycles. The upper-bound envelope was developed by connecting the maximum load measured in each displacement group.

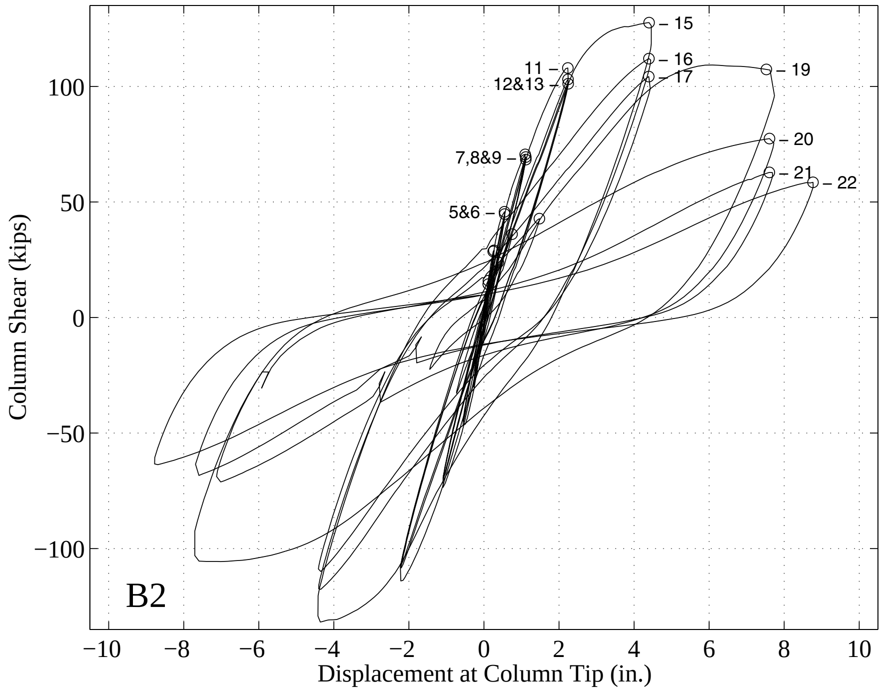

Figure 7-19: B2 load-displacement response

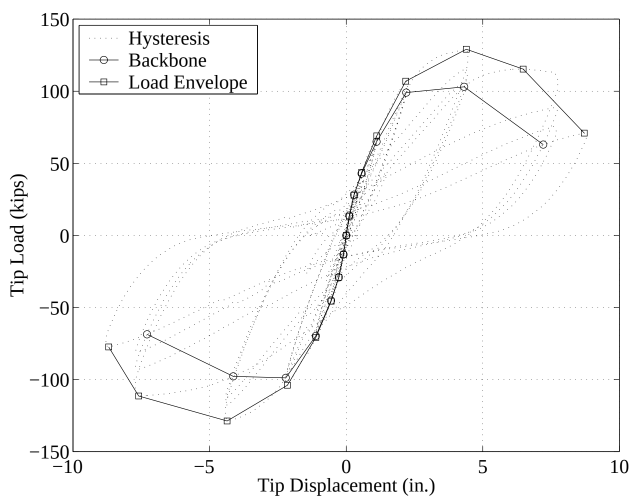

Figure 7-20: Definition of backbone and maximum load envelope

The backbone and load envelopes are marginally higher in Specimen B1 after the maximum load is achieved (Figure 7-21). However, differences between the envelopes (or backbones) for the two specimens are relatively minor.

Table 7-11 summarizes the global response measurements. Both specimens were tested with an axial load of 138 kips. The first yield and ultimate response occurred earlier in Specimen B2. This supports the earlier joint damage observed in B2. Maximum load capacity occurred at the same displacement for both configurations. Both subassembly columns were loaded into the plastic regime reaching at least 85% of their estimated ultimate capacity. The ultimate displacements presented were computed using the load envelopes. Ultimate displacement 1 corresponds to the intersection of the yield force with the descending branch of the envelope (assuming an idealization of elastic-perfectly plastic at the yield point). Ultimate displacement 2 corresponds to the point where the load decreases 20% from the peak load capacity. In comparison with Group A, Group B joints were heavily damaged. At drifts of 1.6% the joints crack openings were on the same order as the largest crack opening measured in Group A. After this level, cracks continued to increase reaching openings in excess of 0.125 in.

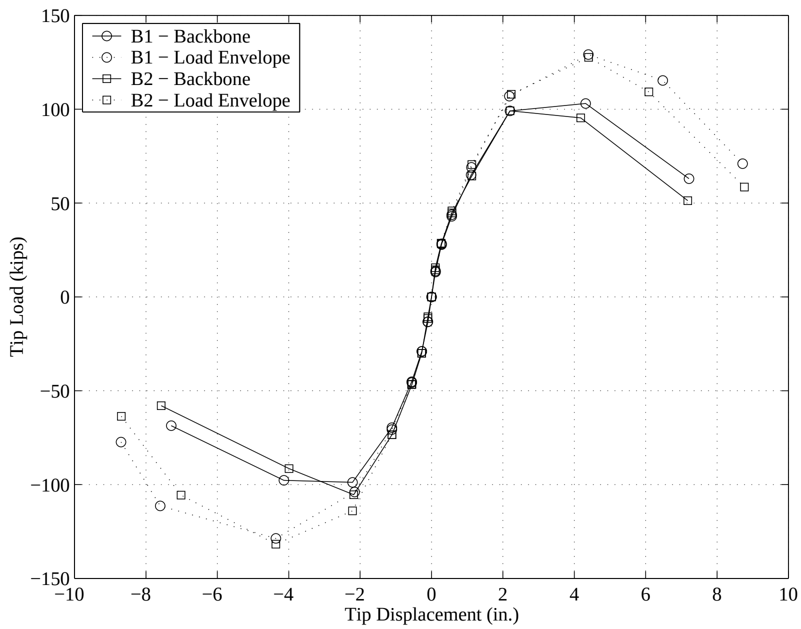

Figure 7-21: Group B load-displacement backbone and load envelope

The Group B specimens exhibited a similar amount of degradation in global stiffness (Figure 7-22). The global stiffness was computed as the tangent of the low-level load-displacement response taken from zero displacement. In both subassemblies, the stiffness decreases to 1/3 of its initial value by the onset of yielding. The degradation continues at roughly an exponential rate until the end of the test. The only noticeable deviation between the two responses occurs during the pre-yield cycles. Specimen B2 exhibits an earlier stiffness decrease. This correlates with the earlier formation of joint cracking in B2. Curiously, the stiffness degradation measured for Group B is very similar to that of Group A. This indicates that the global stiffness is not a good measure (i.e., not sensitive) to local damage if it took place in different components of the failing system.

Table 7-11: Group B experimental results			
Experimental Action		*Measured Values*	
		B1	*B2*
Column axial load		138	138
1st yield of column longitudinal reinforcement, column tip force	*Fy*	86.4	84.0
1st yield, column moment	*My*	9850	9576
1st yield, column tip displacement	*Dy*	1.56	1.46
Ultimate load, column tip force	*Fm*	129.1	127.6
Ultimate load, column moment	*Mm*	14706 89% of estimated Mm*	14546 85% of estimated Mm*
Ultimate load, tip displacement	*Dm*	4.40, $\mu_\Delta = 2.8$	4.40, $\mu_\Delta = 3.0$
Ultimate displacement 1	$Fu = F_y$	7.94, $\mu_\Delta = 5.1$	7.42, $\mu_\Delta = 5.1$
Ultimate displacement 2	*Fu = 80%Fm*	7.09, $\mu_\Delta = 4.5$	6.47, $\mu_\Delta = 4.4$
Maximum joint diagonal crack opening at 2 in.		0.02	0.013
Height of spalling on column		9.0	10.5

Note: All units are in kips and inches.
* Estimated Mm based on ARCS section analysis

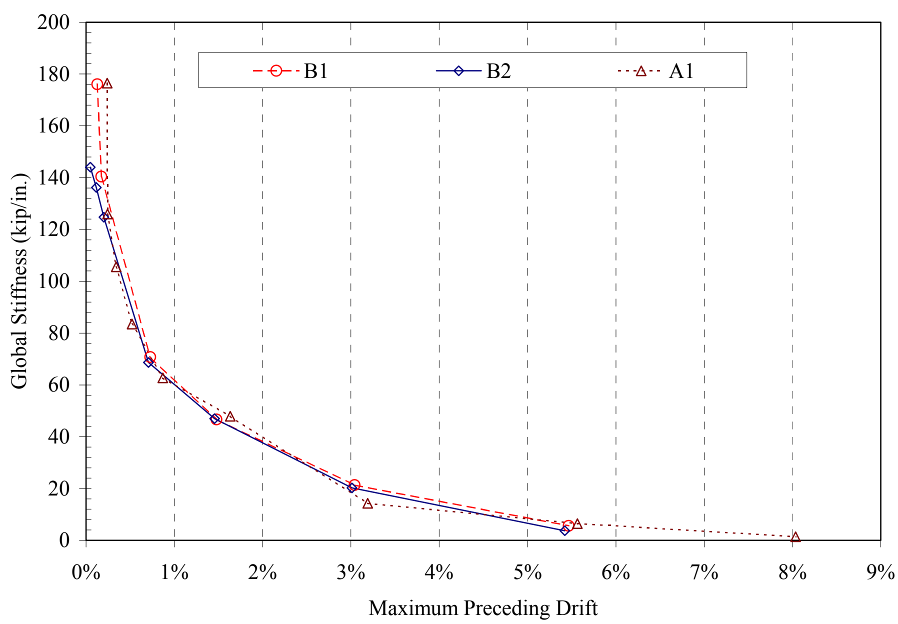

Figure 7-22: Stiffness degradation of Group B (and comparison with Specimen A1)

While the degradation of stiffness is comparable, the strength loss due to cycling in Specimen B2 is consistently higher than in B1 (Figure 7-23). Since beam and column designs are the same, the degradation can be directly attributed to the joint response. The measured response indicates that the details used for B1 are more effective in preventing degradation due to cyclic effects. Aside from this variation, the global response is comparable (refer to Figure 7-22). Strength degradation is minimal at lower levels of drift and does not increase considerably until significant damage and pullout of the column reinforcement is observed.

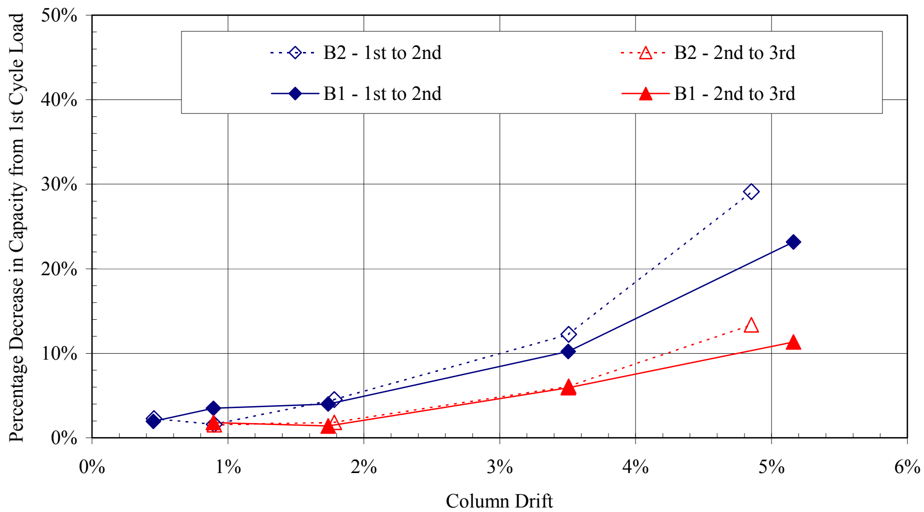

Figure 7-23: Loss in capacity due to multiple cycles to the same displacement

7.4.2 Different Contributions to Total Displacement of Group B

Deformation of the subassembly was assumed to consist of six distinct components: column flexure, column shear, beam flexure, beam shear, joint shear, and slip of column longitudinal reinforcement. Using an array of external instrumentation, the contribution of each component to the total displacement was estimated (see Chapter 3). These measurements were processed at the first northern displacement of each displacement cycle group. Due to the limited resolution of the instrumentation, low-level displacements are ignored. As with Group A, the largest contribution was from the column response (Figure 7-24). Unlike Group A, the column response was not controlled by plastic hinge formation but by slip of column longitudinal reinforcement.

The contribution of component displacements to the total drift varies between the specimens (Figure 7-24). At lower levels of drift, B1 is controlled by deformation of the column, while B2 is controlled by beam flexure. It should be noted that beam flexure consists of all deformation outside the column width. Observations indicated that joint damage in B2 extended into the beam area. This explains the lower joint shear and higher beam flexure contributions measured in Specimen B2. In both specimens, column and beam shear had similar contributions to the total displacement. Reinforcement slip and joint damage are notable as their contribution increases progressively. This behavior is considerably different than the response measured for Group A. In Group A, the full plastic hinge formed allowing further (stable) increase of column contribution with increase of drift. In Group B, column contribution decreases with increase in drift because of the instability due to the formation of a slip mechanism.

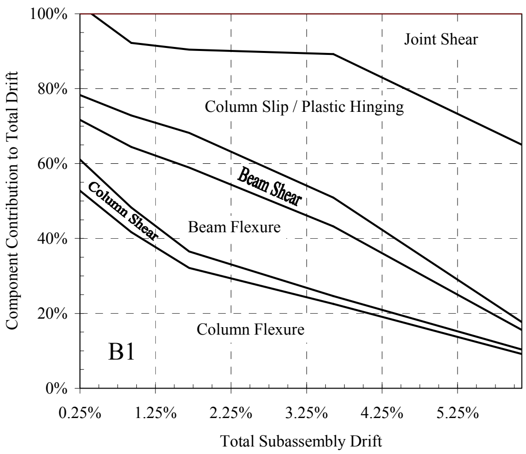

(a) Specimen B1

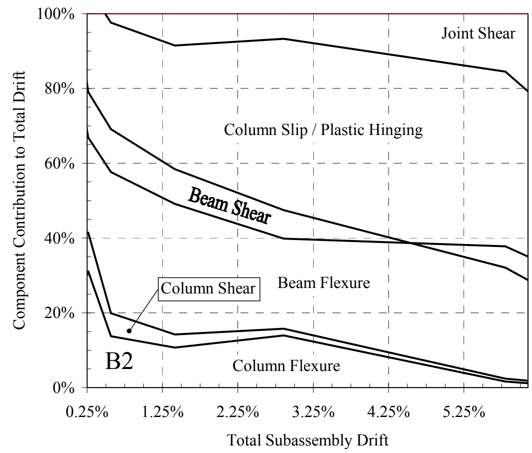

(b) Specimen B2

Figure 7-24: Contribution of components to total tip displacement

7.4.3 Slip of Column Longitudinal Reinforcement

The effectiveness of the two joint reinforcement strategies in restraining slip of the column reinforcement from the cap beam is evaluated through a comparison of the measured slip. To measure slip, a hole was prefabricated in the specimen from the cap beam top to the bar end (Figure 7-25). An external potentiometer mounted on the top of the cap beam and connected in bearing to the bar end was used to measure the relative displacement of the bar from the top surface. Any deformation measured was attributed to slip of the column bar from the cap beam. During the 7-in. displacement cycles, spalling of the cap beam top occurred causing the gage base to move. Therefore, the slip measurements are evaluated only up to the 4-in. cycles.

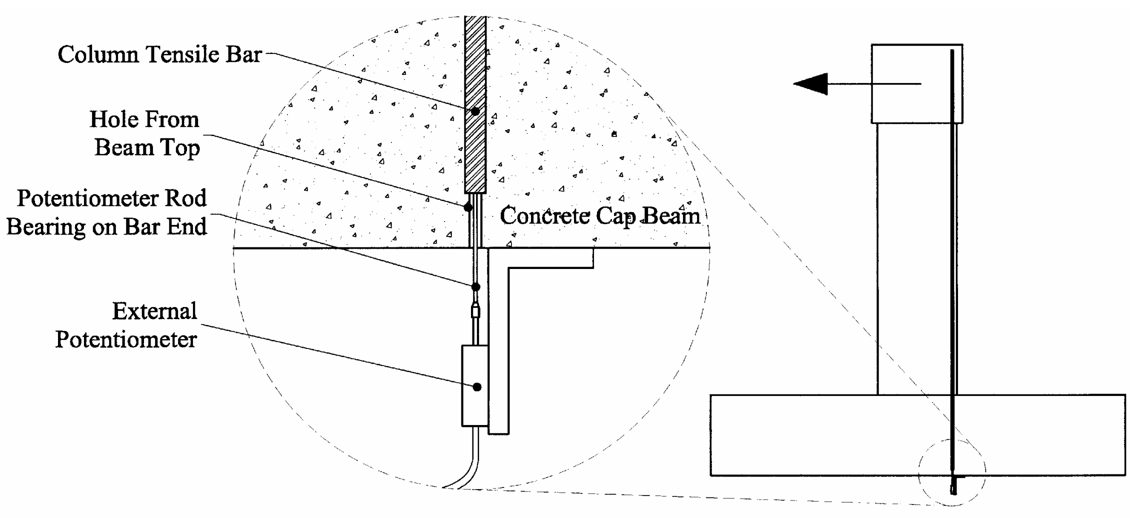

Figure 7-25: Setup of column reinforcement slip measurement

The measured slip in the spirally reinforced joint of Specimen B2 was consistently less than that measured in Specimen B1 (Figure 7-26). This indicates that continuation of the spiral into the joint provides a more effective restraint of the column bars. The headed bars are spaced uniformly around the joint and are not concentrated near the column bars. It seems plausible that the spiral provides superior pullout resistance over the headed bars because the spiral is in closer vicinity to the column reinforcement. In addition, the curvature of the spiral provides confining pressure on the longitudinal bar while headed straight bars only restrain cracks from widening.

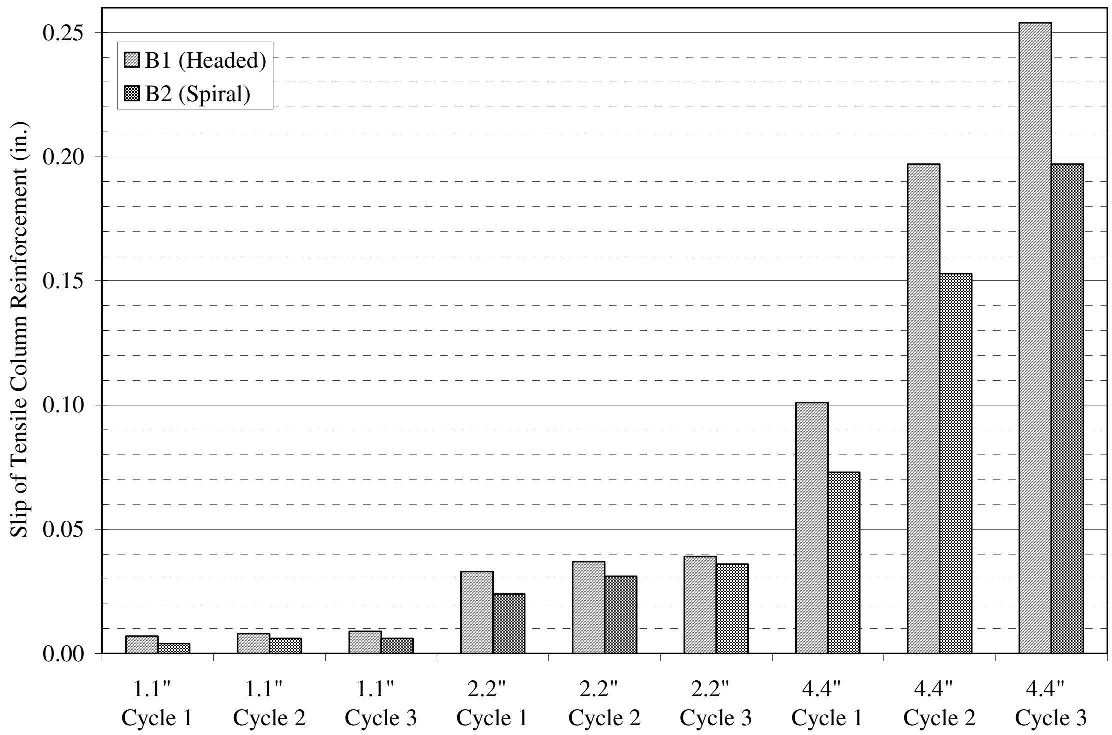

Figure 7-26: Slip of tensile column reinforcement from joint, throughout displacement history

Slip of the reinforcement from the joint follows a general pattern (Figure 7-26). Slip initiated prior to column reinforcement yielding. Under these lower force levels the column reinforcement slipped during tensile loading to a maximum of 0.01 in. and returned essentially to zero on unloading (Figure 7-27). During the entire history, no compressive slip was measured. Continued cycling at a given level of drift resulted in an increase in slip. During the ultimate load level cycles of 4.4 in., the slip does not recover on load reversal, but progressively increases. Consequently, the strength of the system decreases, producing a considerable loss in capacity during the second and third cycles to 4.4 in. In each case, the slip of the column reinforcement of specimens B1 and B2 are of the same order. Thus, neither joint configuration is entirely effective in eliminating slip under such high levels of demand.

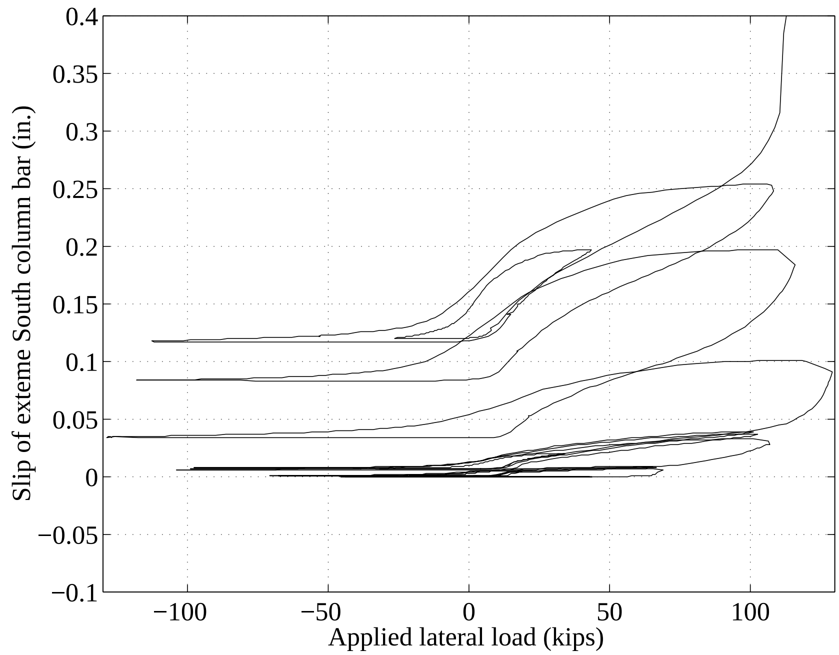

Figure 7-27: Slip history of column reinforcement from joint

7.4.4 Global Joint Shear Response

The joint shear response of the headed reinforced joint (B1) was more ductile than the spirally reinforced joint (B2). The joint shear stress-strain response was computed in a manner consistent with Group A (see Chapter 3). The shear stress-strain responses are presented in Figure 7-28 and Figure 7-29. By the end of the test, the joint potentiometers used in B2 reached their maximum stroke. Therefore, response curves are truncated over this range. The negative loading direction is used to develop backbone curves of the response as shown in Figure 7-30.

The joint shear behavior of B1 is superior to that of B2 (Figure 7-28). Specimen B1 sustains the peak shear force through shear strains as large as 0.023. Specimen B2, in contrast, loses a large degree of its capacity after the maximum load capacity of the system is exceeded. This is consistent with the test observations, which indicated that the headed reinforced joint remained confined, while the spirally reinforced joint did not. The difference in behavior is clearly visible in the backbone curves (Figure 7-30). Recall that backbone curves are developed by taking the intersection of the first cycle of displacement group (*i*) with the second cycle of displacement group (*i-1*). In comparison with Group A (Figure 6-23), the behavior of Group B specimens is highly inelastic. In Group A, maximum shear strains of 0.003 were recorded; in Group B the shear strains reached 0.03, which is an order of magnitude greater.

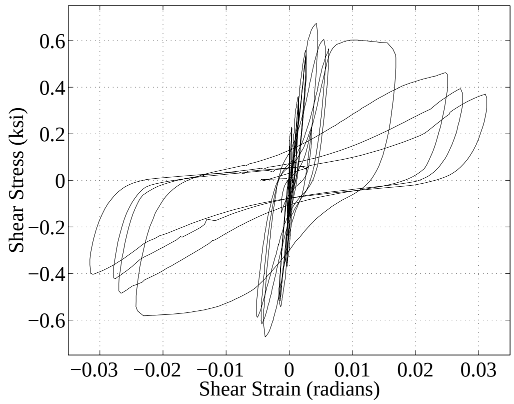

Figure 7-28: B1 joint shear response

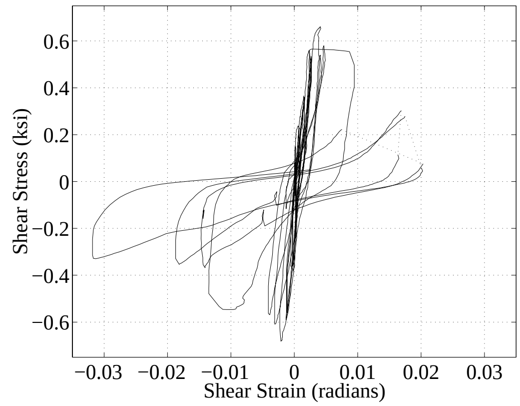

Figure 7-29: B2 joint shear response

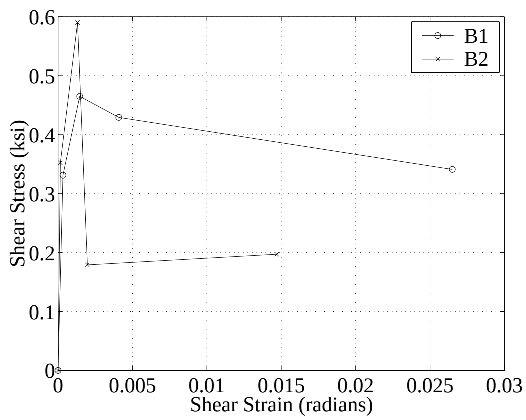

Figure 7-30: Joint shear response backbone curves

7.4.5 Summary of Global Behavior

In both cases, B1 and B2, joint failure controlled the ultimate response of the specimen. Column damage consisted of flexural and shear cracking and minor spalling on the extreme faces; buckling of the column reinforcement did not occur. Splitting failure of the beam edges occurred in the vicinity of the joint as well as spalling of the top of the cap beam. Overall system strengths were comparable, with Specimen B1 having a slightly higher yield and peak tip load than Specimen B2. Visual inspection indicated that the spirally reinforced joint (B2) underwent significant joint shear damage. The headed reinforced joint (B1) appeared better confined, exhibiting a more ductile shear-type failure. Maximum joint shear strains were approximately 0.03 radians for B1 and 0.015 radians for B2. The component contributions to the total drift indicated that the joint damage of Specimen B2 was not confined to the column width but extended into the beam. The spiral was more effective in limiting slip of the column reinforcement from the joint. Nevertheless, the measured slip in both specimens was on the same order of magnitude, and contributed significantly to the global drift. The localized strain distributions, bond, force transfer mechanisms, and the effectiveness of each reinforcement strategy are investigated in more detail in the next section.

7.5 Local Demand on Group B Subassemblies

Local demand is evaluated based on the strains on the reinforcement at increasing levels of drift. Strain was measured throughout the subassembly with the surface-mounted strain gages. These gages allowed for an evaluation of the bond anchorage capacities of the column and beam reinforcement, as well as the effectiveness of the two joint reinforcing strategies. Local measurements on the reinforcement support the global observations in the previous section.

7.5.1 Column

The strains measured on the column reinforcement of the two specimens were similar. The tensile and compressive strains were measured along the exterior reinforcement at increasing levels of drift (Figure 7-31 and Figure 7-32). The tensile and compressive responses for both subassemblies compare well under both elastic and inelastic demand levels. Initiation of tensile column yielding (within the joint region) is clearly noticeable during the 1.7% drift level. Compression yielding (outside the joint region) did not occur until the following cycle group to 3.4% drift. Note that tensile yielding was indicated to occur first in the cap beam and compressive yielding begins within the column. It is plausible that tensile yielding actually occurred first in the column but was not recorded; more gages were needed at the interface to capture the onset of yielding in the column because of the rapid change at the interface. In terms of effectiveness of the two joint details, both appear to provide comparable levels of anchorage capacity.

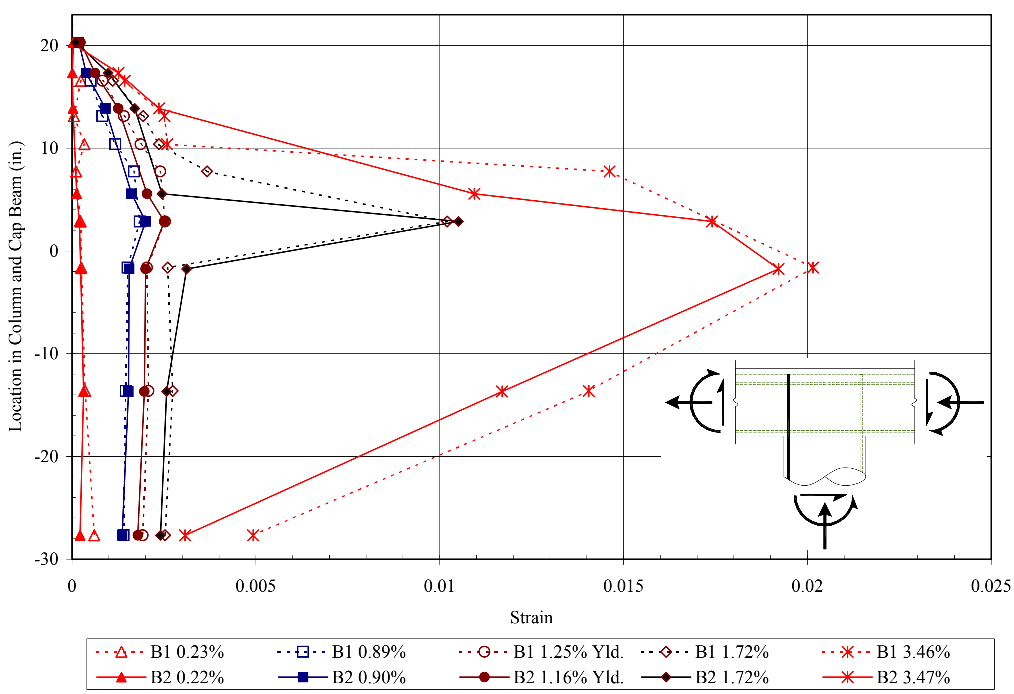

Figure 7-31: Tensile column reinforcement strain distribution at increasing levels of drift

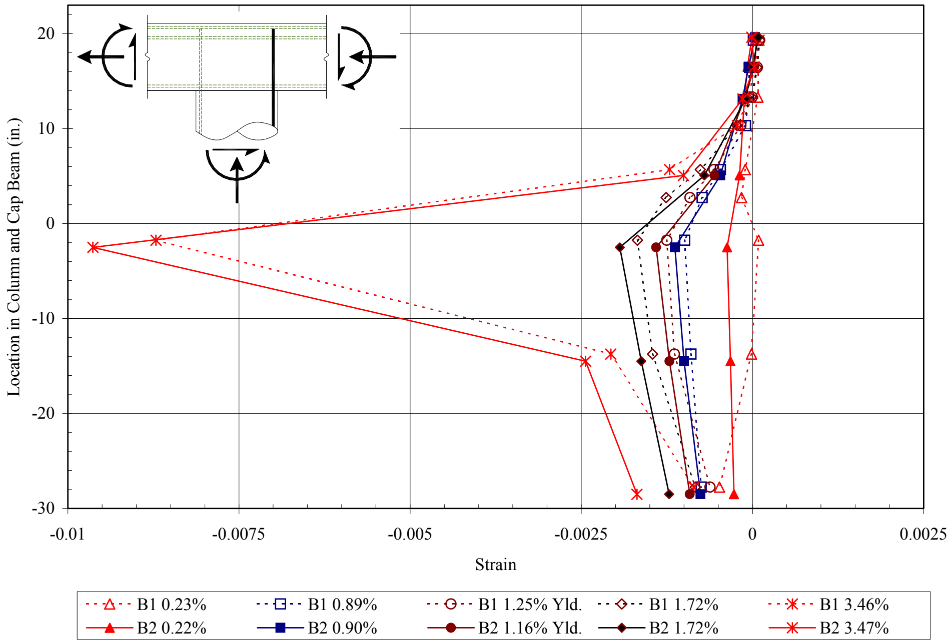

Figure 7-32: Compression column reinforcement strain distribution at increasing levels of drift

The inferred bond capacities were lower than expected in both subassemblies (Figure 7-33). Bond stresses between $20\sqrt{f'c}$ and $30\sqrt{f'c}$ were estimated (see Section 6.2.1 for description of procedure for estimating bond stresses). This is lower than the maximum bond stress of $40\sqrt{f'c}$ assumed in the conceptual model. Consequently, the column bars were unable to accommodate the anchorage demands, resulting in the measured slip. The distribution of bond forces along the tensile column reinforcement was consistent with the conceptual model and the bond stresses measured in Group A. The stresses are relatively low, between 5 and $10\sqrt{f'c}$ psi, at the beam-column interface and within the lower half of the joint, and increase rapidly toward the top of the cap beam. The maximum bond stresses are comparable to the maximum stresses measured in Group A. The assumed increase in the peak bond stress capacity as a result of the higher cap beam compressive stresses was not correct. The bond stress capacity in B1 was lower than that of B2. At the 3.5% drift level, Specimen B2 reached a bond stress capacity of $27\sqrt{f'c}$ psi while B1 reached a capacity of $21\sqrt{f'c}$ psi. This indicates that the joint hoops used in B2 provided superior anchorage to the headed bars in B1, supporting the lower slip measured in B2. In summary, if bridge geometry requires a short development of the column bars and congestion limits the use of hooks or headed reinforcement, the joint spiral should be used. In all other cases, headed transverse joint reinforcement will provide comparable levels of response, with less congestion.

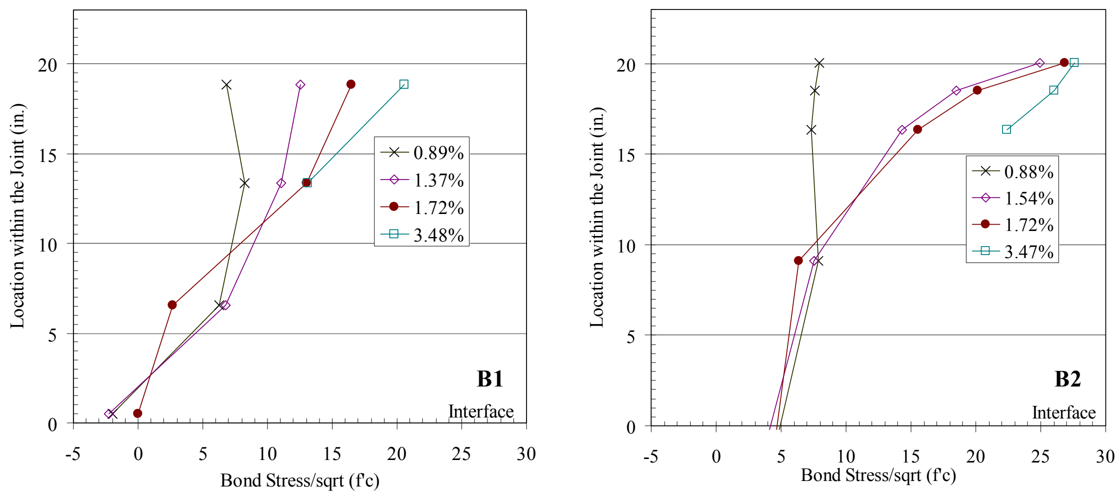

Figure 7-33: Tensile column reinforcement bond distribution at increasing levels of drift
(Note: f'_c in units of psi)

7.5.2 Beam Reinforcement Anchorage

Strain measurements were recorded along the primary beam longitudinal reinforcement. Figure 7-34 presents the values measured on the primary negative, secondary negative, and positive reinforcement at increasing levels of drift. The horizontal axis represents the location along the bar; the origin is at the center of the joint and +/- 14 in. is at each side of the column face.

The strain readings indicate that the beam longitudinal reinforcement is not adequately developed within the joint. This behavior is apparent on the secondary and primary (top) negative reinforcement. Tensile strains produced by flexural action on the right side of the joint are transferred to the left side without noticeable decrease. This pull-through may be attributed to inadequate vertical reinforcement. The limited amount of vertical reinforcement results in insufficient tie-down force acting to confine the beam longitudinal reinforcement, thus reducing the bond capacity. The positive (interface) reinforcement, in contrast, behaves according to conventional flexural assumptions: the right portion of the beam is in compression as a result of negative flexure and the left is in tension as a result of positive flexure. At the interface, the beam longitudinal reinforcement is able to develop its tensile forces within the joint width due to the large compression force produced by the column flexural response. This compression force provides an active confining stress allowing the interface bars to develop a high amount of bond stress within the joint.

Measurements revealed two regions of unexpected response on the longitudinal reinforcing steel within the joint. The first region occurs on the secondary negative reinforcement in the center of the joint. Specimen B1 exhibited a sharp increase in tensile strain in this region after the yield drift level. Similar behavior was measured on Specimen B2. After the occurrence of the 3.5% drift level, the measured tensile strain rapidly increased beyond the resolution of the gage. Thus while the 6% and 7% drift levels do not illustrate the increase, it did occur. This increase in tensile strain at the center of the joint could be attributed to shear failure of the joint. As shown in Figure 7-10(e) shear cracking crossed the secondary reinforcement in this region. Thus this tensile spike could be attributed to the joint shear failure of the specimens. The second region occurs on the interface reinforcement on the right column face. In this region, Specimen B2 undergoes a high tensile excursion when a compressive response is expected. This is attributed to permanent tensile strain hardening on the preceding positive moment application.

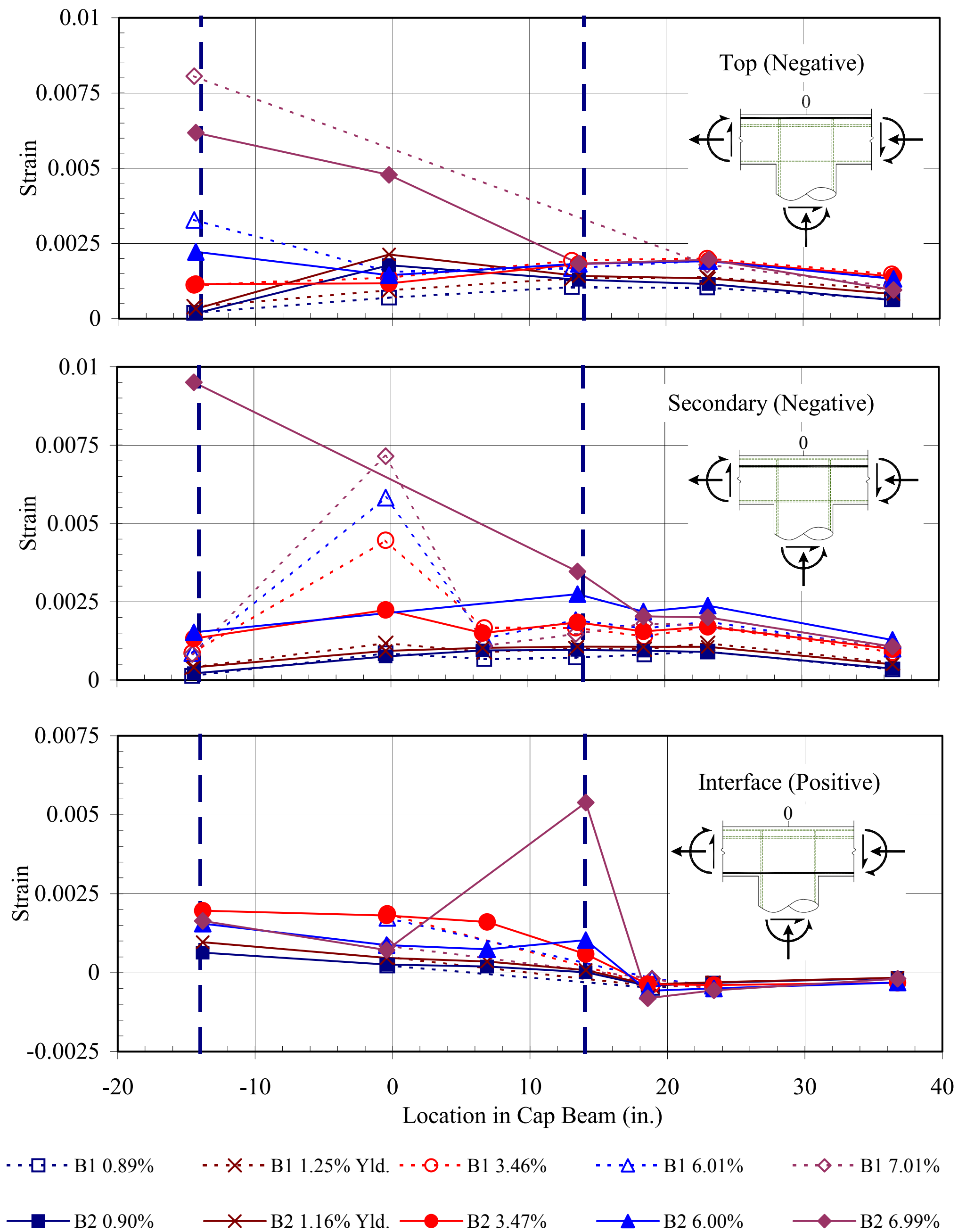

Figure 7-34: Beam longitudinal bar strain along cap beam/joint

7.5.3 Joint

The joint horizontal transverse reinforcement in Specimen B1 is highly activated (Figure 7-35). Yield is reached throughout the depth by a drift of 3.5%. Yielding of the interface lateral reinforcement begins on the south face of the joint near the tensile column reinforcement. This leads to permanent tensile strain on the following displacement to 7% drift. The high levels of strain measured on the lateral reinforcement at the top of the joint can be attributed to the anchorage of the beam longitudinal reinforcement. The demand on the lateral bars running parallel to the joint is less than the demand on the bars running perpendicular. Nevertheless, both types of horizontal transverse bars yield. The longitudinally oriented bars are strained the highest at mid-beam depth indicating their participation in resisting diagonal crack opening.

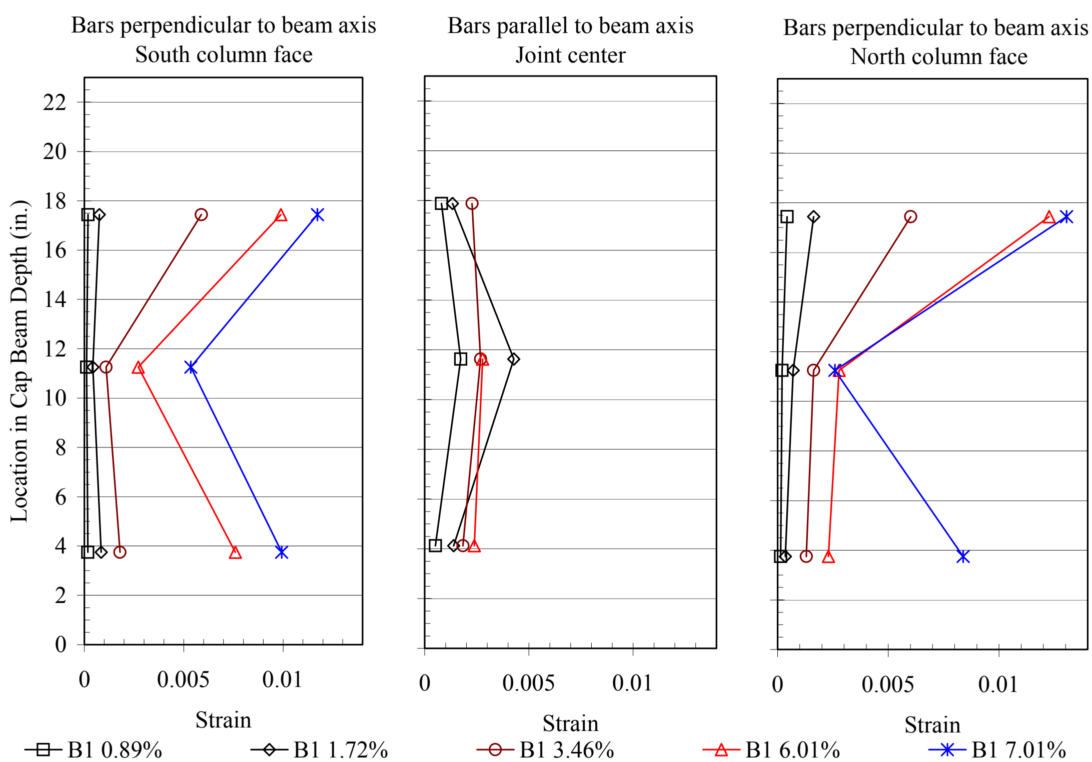

Figure 7-35: B1 horizontal joint transverse reinforcement response at increasing levels of northern drift

The joint hoops in Specimen B2 behave in a similar manner to the transverse reinforcement in B1 (Figure 7-36). Anchorage of the column tensile longitudinal reinforcement led to high strains on the joint hoops near the soffit on the tensile joint corner, i.e., the south joint face in Figure 7-36. This is consistent with the conceptual model used in design. Strains then decrease as the forces are developed in the joint. On the compression corner, the tensile hoop strain demand is considerably less. At the top of the joint, the reverse behavior is noted, with high tension on the north joint face and lower values on the south. This action is most likely attributed to the anchorage of the beam tensile reinforcement at the top north corner of the joint. The strain on the hoops at the face of the joint indicates that the spiral is active in resisting the joint shear.

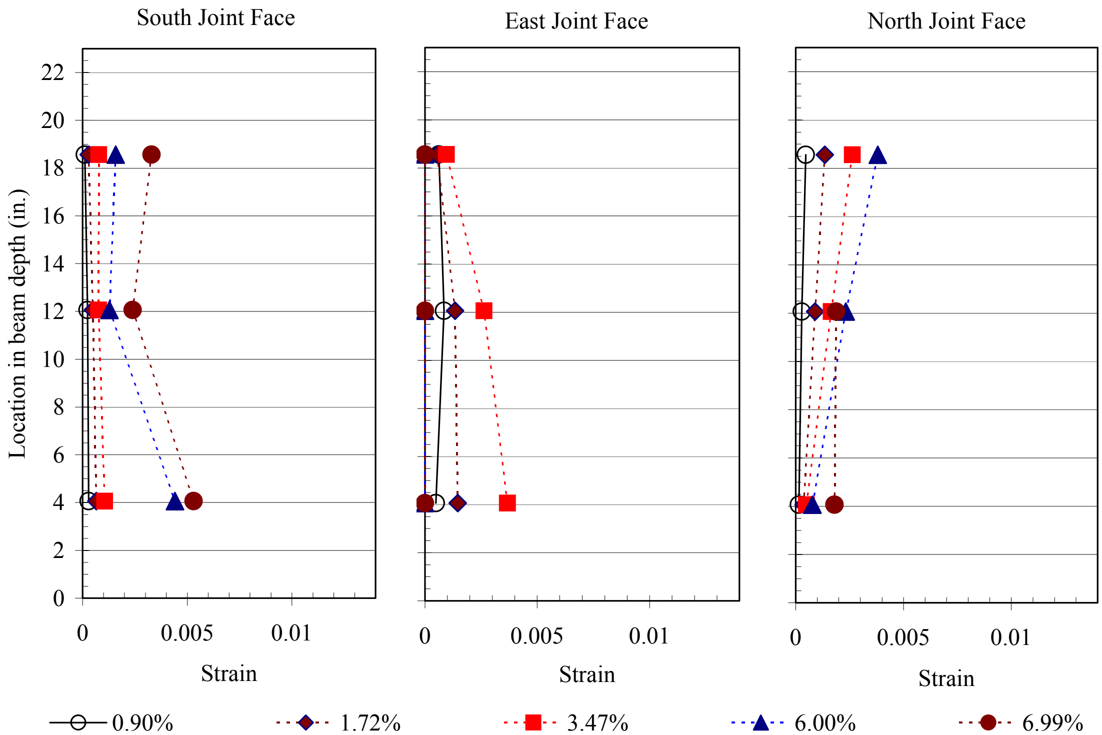

Figure 7-36: B2 horizontal joint hoop reinforcement response at increasing levels of northern drift

7.5.4 Summary of Local Behavior

The two joint designs provide similar resistance to shear demands and anchorage capacities. The bond demand provided by the spiral was superior to that of the headed reinforcement strategy, although the anchorage capacities were on the same order of magnitude. The peak bond stress of $40\sqrt{f'c}$ [$f'c$ in psi] assumed in design was not reached. Instead, the level of bond stress achieved in Group B was similar to that of Group A, i.e., in the range of 20–30 $\sqrt{f'c}$ [$f'c$ in psi].

7.6 Finite Element Modeling

To supplement the experimental results, finite element investigations were conducted. Three-dimensional nonlinear finite element models were developed using the as-built dimensions and measured material properties. The modeling techniques are discussed in detail in Chapter 4.

7.6.1 Correlation with Experimental Results

The load-displacement responses from the finite element analysis compare well with that of the tested subassemblies (Figure 7-37). However, the computational models produce a stiffer response than the experimental models. Since finite element modeling typically underestimates flexural deformation [Cook 1989] and the initial stiffness is controlled by the flexural column response, this underestimation is expected. The models do not directly account for slip of the reinforcement; consequently the load-displacement response does not decrease in capacity. Instead, the strength continues to increase as the column reinforcement strain-hardens. Consequently, comparison with the experimental measurements is only appropriate to a displacement of 4 in., i.e. up to the peak load.

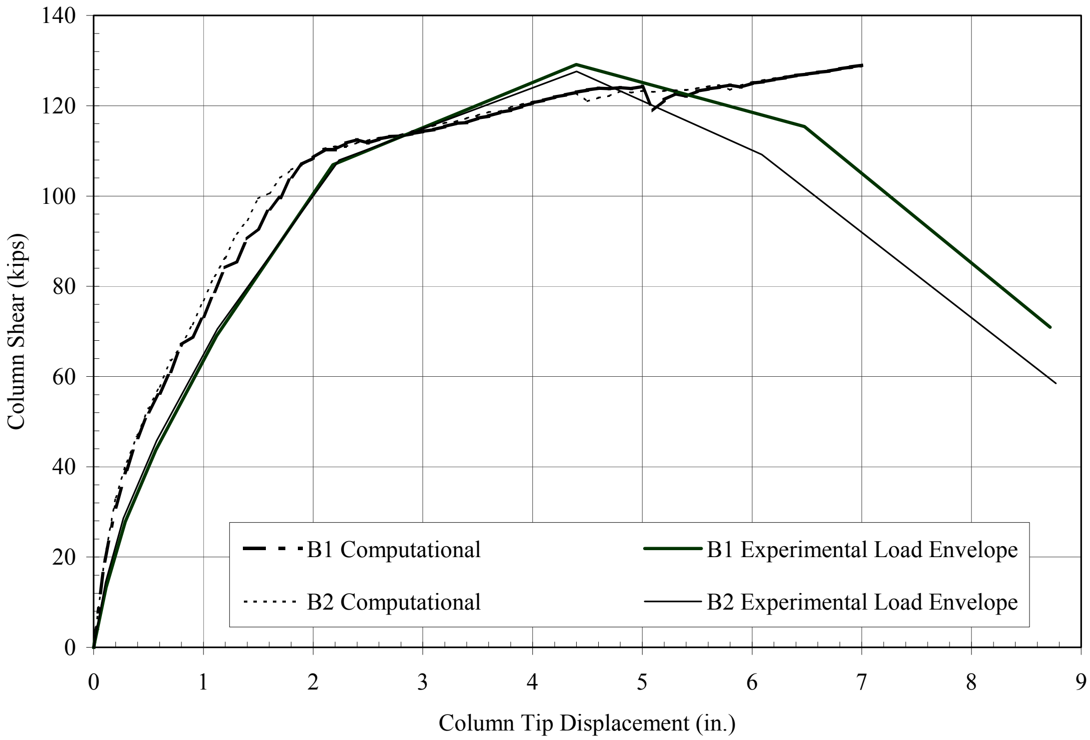

Figure 7-37: Group B load-displacement comparison

7.6.2 Evaluation of Displacement Contributions

Using the finite element results, the contribution of the various displacement components to the total tip displacement was evaluated. Both specimens B1 and B2 follow the same trend (Figure 7-38). At low demand, the column flexural behavior and the beam and column shear response control the tip displacement. As inelastic damage initiates, in the form of column flexural cracking, the contribution of the column and beam shear response becomes a smaller percentage. At this point, the column response controls the drift. Shortly afterwards, the cap beam forms flexural cracks thus increasing the beam contribution. This is followed by yielding of the column reinforcement, which controls the remainder of the response.

Figure 7-39 presents the experimental response previously discussed in Section 7.4.2. To provide comparison with the computational model, the slip component and the flexure are combined. Recall that the experimental displacement component calculations are determined from external instrumentation, which had reduced accuracy at low levels of displacement. Nevertheless, the resulting trends of the experimental models are similar to that predicted by the computational models. This lends support to the use of the computational modeling techniques.

Throughout the displacement history, calculated joint shear deformation does not contribute significantly to the global deformation. While this indicates that total joint failure has not occurred, it does not preclude significant joint damage. To evaluate the joint response, the load transfer mechanism and shear strain behavior are evaluated using the analytical models.

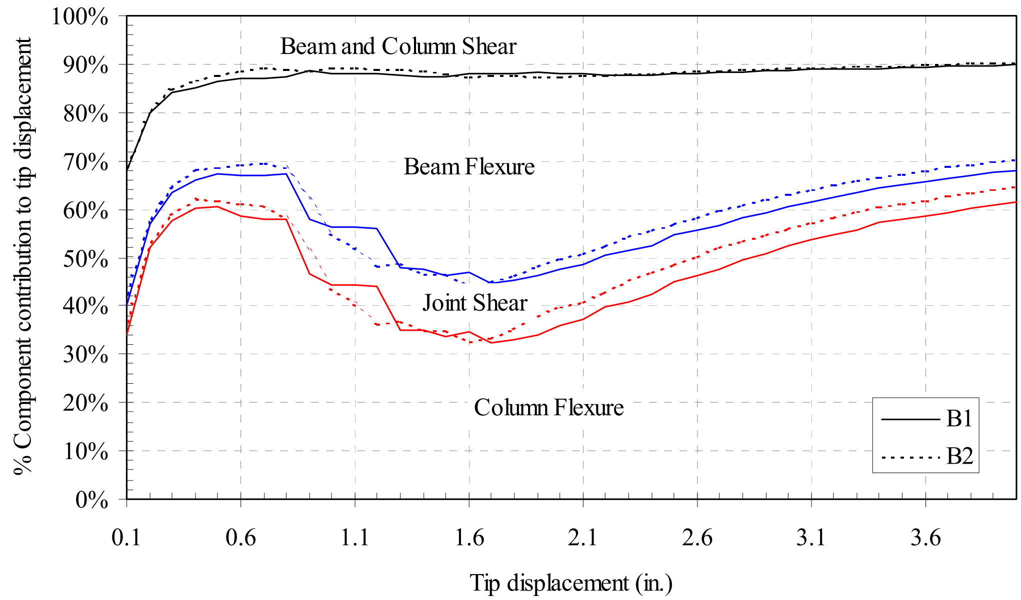

Figure 7-38: Component contribution in computational models

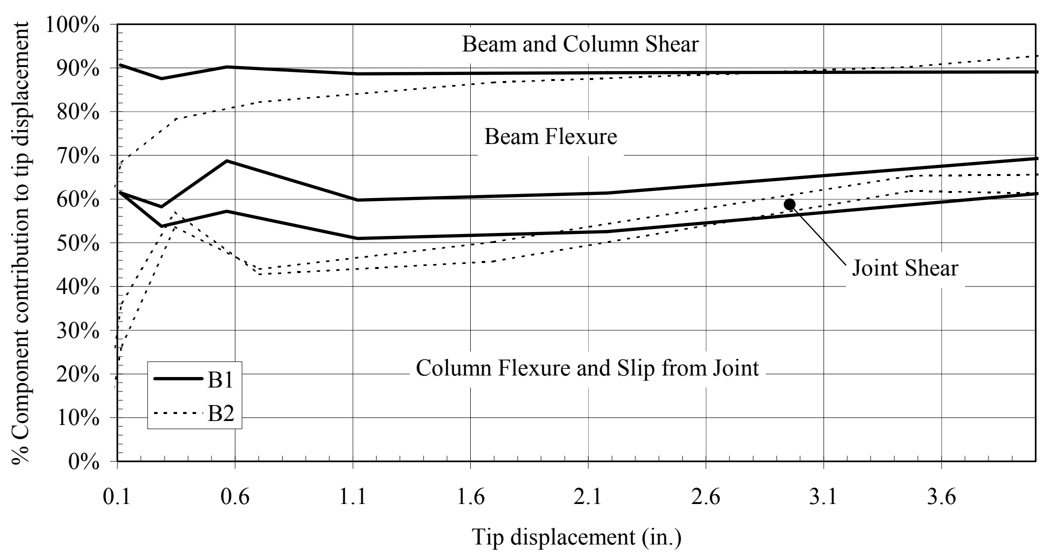

Figure 7-39: Component contribution in experimental subassemblies

7.6.3 Predicted Joint Response

The finite element analysis reveals that a principal compressive strut is a predominant contribution to load transfer in both joints. The principal compression strut is most highly activated within the column core

(Figure 7-41). The level of principal compressive stress measured in Specimen B1 indicates that the entire joint width is activated in transferring force across the joint (Figure 7-41(a) through Figure 7-41(c)). High levels of compressive stress are prevalent both in the interior and on the face of the joint. In Specimen B2, the compression forces are confined to the joint column core and are most highly activated around the spiral reinforcement and not at the joint center (Figure 7-41(d) through Figure 7-41(f)). This produces lower principal compressive stresses at the interior of joint B2. The headed transverse reinforcement activates a greater percentage of the joint width, while the use of joint hoops limits the compressive strut transfer to the circumference of the spiral (hoops).

The limited width of the compression strut in Specimen B2 is due to the high tensile strains present near the face of joint. Because of the lack of transverse hairpins, the core of the joint becomes dislocated from the cap beam. This is evident in the high principal tensile strains visible in B2 and not in B1 (Figure 7-42). This supports the experimental results, which indicated that the cap beam face delaminated from the core in Specimen B2 and remained confined in B1 (Figure 7-40). This dislocation manifests itself in the high tensile strain and low compressive stress measured outside the column core.

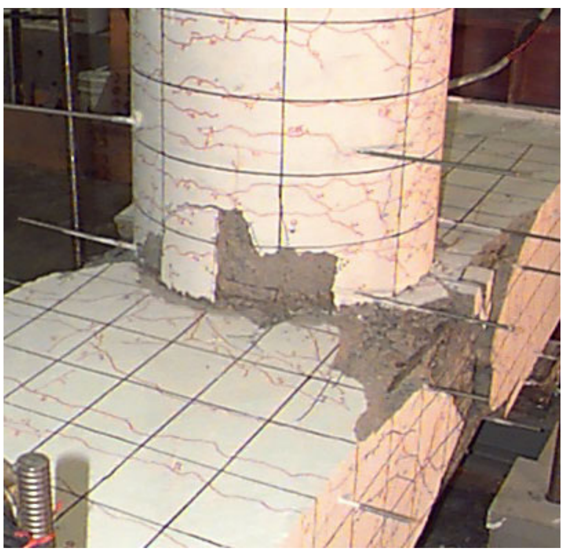

(a) Specimen B1 at end of test

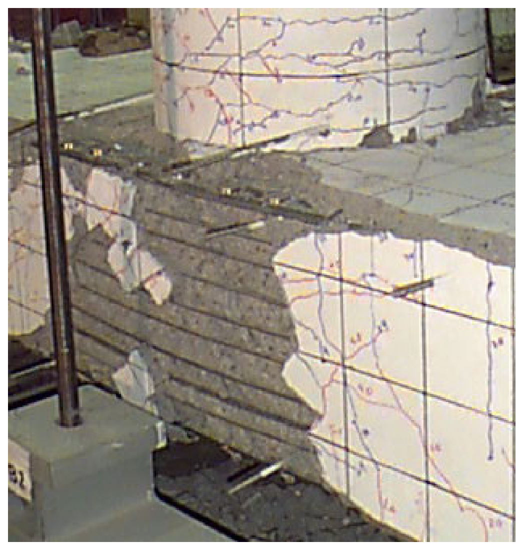

(b) Specimen B2 at end of test

Figure 7-40: Lateral joint dilation of Group B specimens

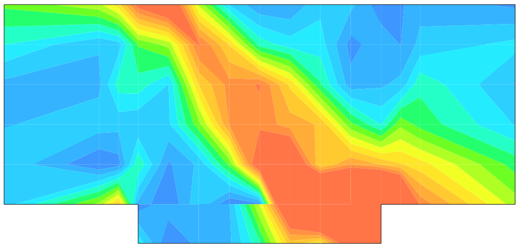

(a) Vertical cut through interior — B1

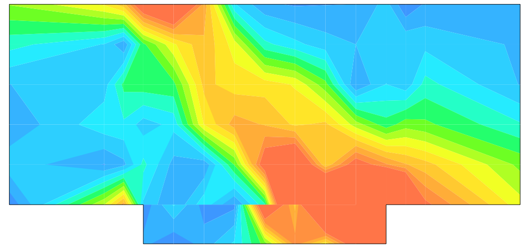

(e) Vertical cut through interior — B2

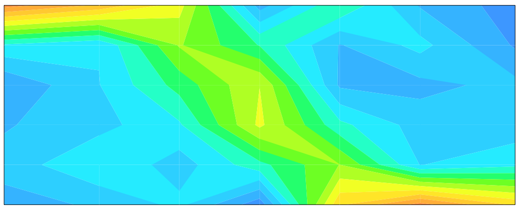

(b) Vertical section at face — B1

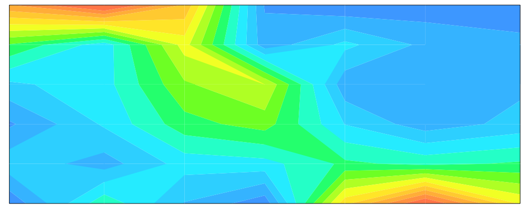

(f) Vertical section at face — B2

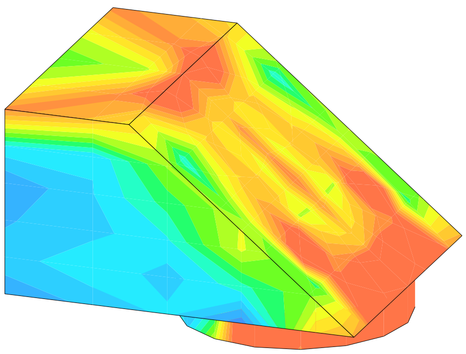

(c) Principal compressive stress — B1

(ksi)

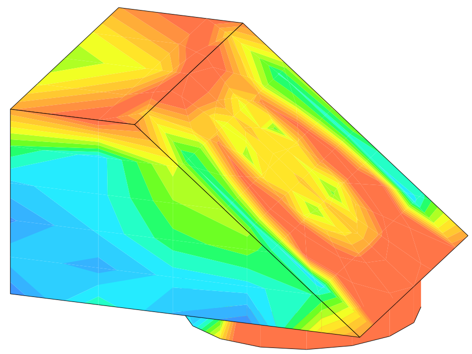

(f) Principal compressive stress — B2

Figure 7-41: Principal compressive stress at different sections through joint

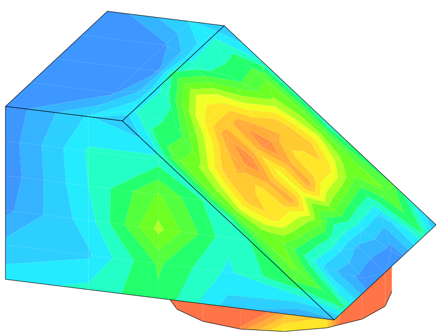

Principal tensile strain — B1

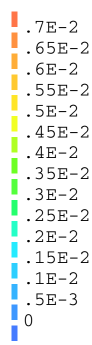

(strain)

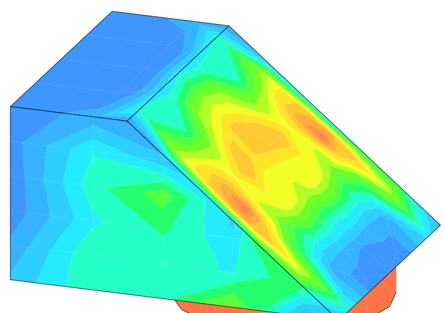

Principal tensile strain — B2

Figure 7-42: Principal tensile strain mapping along compression strut

To evaluate the effectiveness of the two joint details, joint shear strain response is compared. Joint shear strain was computed using the global deformations of the joint; the procedure is outlined in Chapter 3. For consistency, the same techniques were used for both the experimental and analytical models.

The estimated joint shear strain at increasing levels of lateral load correlate well with the measured experimental response (Figure 7-43). The finite element response is able to model the general trend of the experimentally determined shear response. Both the elastic response and decrease in stiffness due to the initiation of diagonal cracking are represented. In addition, the stiffness increase and eventual yielding due to the activation of the transverse reinforcement crossing the cracks are properly modeled. In the experimental subassemblies, shear strain was measured externally using linear potentiometers (see Chapter 3). The potentiometers were fastened to steel rods that passed laterally through the thickness of the joint. As a result, the shear strain measured in the experiment is a combination of the internal and external shear strain. Two computational shear strain responses are presented for each specimen: the shear strain measured on the face of the joint and the shear strain measured at the center of the joint. These two responses envelope the experimental response, lending support to the accuracy of the computational model. The finite element models, however, do not show the significant plastification measured in the experiment. This is most likely a result of the modeling techniques used, which did not account for slip. In both specimens B1 and B2, large slip of the column longitudinal reinforcement was recorded (see Section 7.4.3). At the 4-in. displacement level, slip on the order of 0.25 in. was measured. This slip most likely resulted in an allowance for further joint crack openings and shear strain. Since slip is not accounted for in the finite element model, the model in its current state cannot be used to estimate the behavior of the system under these conditions. Extrapolation of the finite element results to develop design rules using the current model can be conducted provided that the assumption is made that slip will be prevented in the design with proper development lengths, hooks, or headed longitudinal column reinforcement.

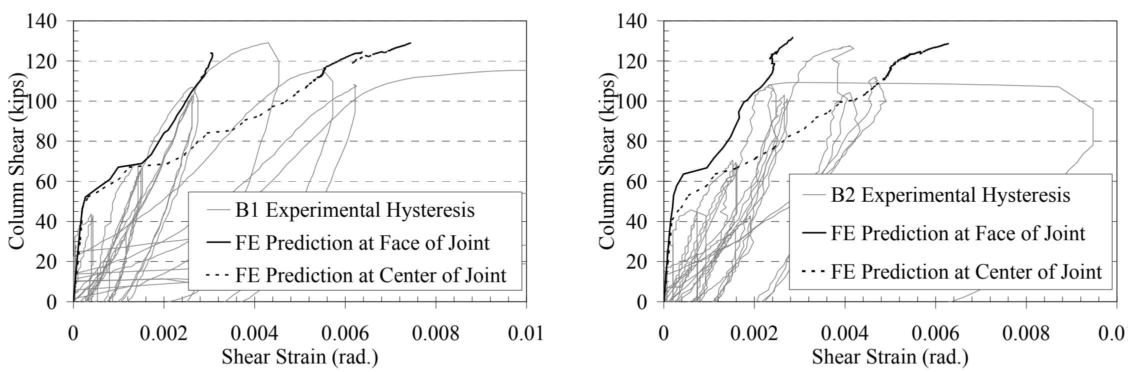

Figure 7-43: Lateral load versus joint shear response of Group B specimens

The analytical shear strain response calculated at the face and center of the joint indicates that the headed transverse reinforcement is more effective in activating the entire joint width (Figure 7-44). In both the spirally reinforced joint system (B2) and the headed reinforced joint system (B1), the shear strain response measured at the center and face of the joint was similar. A shift in the response of B1 occurred early in loading, mostly likely a result of earlier initiation of shear cracking. Nevertheless, the tangent stiffness of the two responses were similar. The difference in shear strain through the thickness of the joint indicates that the joint does not respond uniformly. The greater the deviation between the center and face, the less effective the joint is in being effectively utilized. Throughout the load history, the spirally reinforced joint exhibits a greater deviation between the percentage of shear strain measured at the face and that measured at the center. Thus, the spirally reinforced joint was less activated in shear than the joint confined with headed bars. This supports the experimental observations and previous analytical data presented which indicated that the spirally reinforced joint core becomes dislocated from the face of the cap beam.

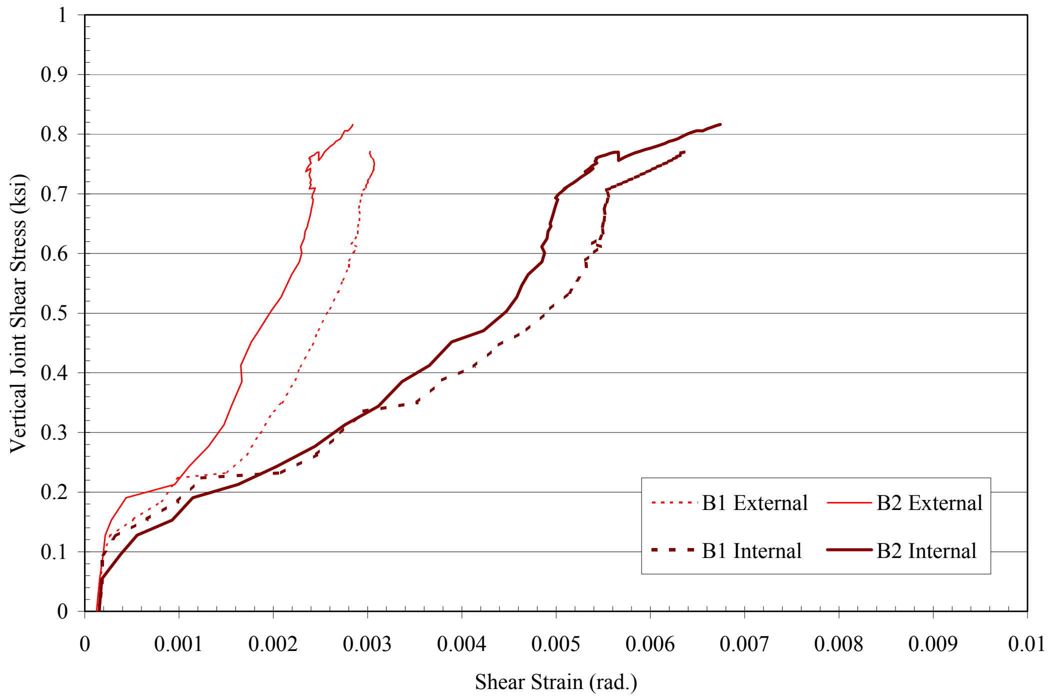

Figure 7-44: Analytical joint shear stress-strain response

7.6.4 Summary of Finite Element Analysis of Joints Subject to High Demands

The finite element modeling techniques used are reliable in predicting the global and local behavior of beam-column subassemblies up to the initiation of slip. Both the global load-displacement response and the joint shear strain responses were similar to the experimental behavior. The discussed finite element techniques provide a viable tool for evaluating joint design strategies and conducting parametric studies. The only detraction is that the described techniques do not account for slip. The assumption is made that slip of the column reinforcement will be prevented using adequate development lengths, hooks, or the use of headed reinforcement, and thus allowing the use of the presented finite element models for further studies to properly design beam-column joints as discussed in Chapter 8.

7.7 Conclusions of Group B

The conceptual design model was not entirely effective in estimating the load transfer mechanism. The primary discrepancy stems from the assumption of $40\sqrt{f'c}$ psi bond stress capacity for the tensile column bars. This was not achieved and instead the bars slipped excessively after reaching a maximum bond stress in the range of 20 to 30 $\sqrt{f'c}$ psi. The conceptual model was effective in estimating the demands on both the spiral and headed transverse reinforcement. The development of the beam reinforcement at the top of the joint led to variations in the transverse reinforcement strain distributions. This fact imposed difficulty in direct evaluation of the model.

The use of just spiral reinforcement in the joint region allowed for superior anchorage of the column reinforcement in comparison to the use of lateral joint transverse reinforcing bars only. Since the spiral is in contact with all the developed column reinforcement, it was more active in resisting slip by providing local anchorage. However, the sole use of the spiral resulted in poor activation of the cap beam width. In this case, the lack of horizontal transverse bars led to delamination of the column joint core from the cap beam face. Therefore, compressive strut transfer was confined to the interior of the column core and less shear strain occurred on the face of the joint.

The use of headed transverse reinforcement improved activation of the entire cap beam width. Experimental observations showed that the joint remained laterally confined at the ultimate level. This was supported by the analytical model that showed improved activation of the joint face in resisting applied shear stresses and improved the compressive strut mechanism.

7.7.1 Joint Design Concept

The preceding experimental and analytical investigations suggest that the joint reinforcement should consist of a quantity of vertical transverse reinforcement and horizontal hairpins. While the spiral led to improved bond of the column bars, the improvement was not dramatic, with the headed reinforcement also being effective in providing bond. Therefore, it would appear that no spiral reinforcement is necessary. However, tests on joints designed to avoid bond failure of the column bars and reinforced only with the headed bars are needed to verify this hypothesis. To activate the large cap beam widths used in current construction, horizontal lateral reinforcement (hairpins or headed bars) should be installed. In addition, vertical transverse reinforcement should be placed throughout the cap beam with higher concentration along the center of the joint to limit damage. This can be accomplished by developing a relationship between the quantity of vertical reinforcement and the maximum tensile strain in the joint at ultimate response. Chapter 8 conducts parametric investigations on a joint geometry typical of California construction and recommends quantities of joint reinforcement to be used.

8 Bridge Joint Reinforcement Requirements

Bridge joint designs should be constructable, efficient, and provide enough strength and stiffness such that only limited damage occurs under the ultimate demand. As a means of developing these ends, the analytical models are used to investigate the effect of other reinforcement details on joint performance. In addition, the experimental behavior coupled with the analytical results is used as a means of developing suggested damage limitation criteria for joint reinforcement requirements. It should be stressed that the computational models used in this study do not allow for slip of the reinforcement. While these models are only applicable to situations where slip is limited using adequate development length, hooked, or headed reinforcement, the models nevertheless form a solid basis for design guidelines and further refined computational studies.

8.1 Damage-Based Design Criteria

Results presented in Chapter 6 demonstrate that current joint designs are capable of resisting design forces. However, the methods may not always result in the most efficient designs. Current design procedures are based on force transfer models that do not directly address the associated level of deformation. Furthermore, inherent in the use of the most common force transfer model, the strut-and-tie model, is damage; cracks must form so that forces can be distributed to the tensile ties and compression struts. The problem with neglecting these issues is that the joint will either be over-reinforced or under-reinforced and subjected to an unknown amount of damage. First, the joint can be over reinforced (inefficiently reinforced) due to neglecting the presence of existing reinforcement such as cap beam skin and longitudinal reinforcement or simply from the use of large overstrengths. Consequently, the intended compression struts and tension ties do not form, producing an inefficient design. The second possibility is that the intended mechanism is reached. In this case, the joint becomes damaged; cracks form and joint tension ties become highly activated, i.e., yielding of reinforcing steel takes place. The joint is not only damaged, but also the damage level expected is difficult to determine. Thus, the use of current joint requirements could result in an ineffective design or an inefficient design.

To overcome these shortcomings, bridge beam-column joint requirements can be based on a criterion of limiting joint damage. This ensures that the intended yield mechanisms can form without loss of joint capacity, and with minimal and predictable damage to the joint region. To accomplish this goal, damage-based requirements can be adopted. As a means of developing such requirements, a finite element investigation was conducted. The prototype used in the study is based on a joint configuration typical in California. Construction details are discussed later in this section. Joint reinforcement is assumed to consist of two quantities of reinforcement: horizontal bars running transverse to the cap beam and vertical bars running through the depth of the joint. Joint spiral reinforcement is not used.

Joint performance of the model is based on two criteria: the entire joint width shall be active in resisting the shear deformation, and the growth of principal tensile strains will be limited after yield. Reinforcement requirements are determined by satisfying these criteria at a target displacement ductility for the bridge bent. At this level of displacement demand, the joint should have compatible shear deformation on the face and center of the joint. This ensures that the entire joint width is active in providing resistance to the applied demand. To accomplish this, the quantity and arrangement of lateral reinforcement (out-of-plane headed bars) required to produce the same joint shear strains on the interior and exterior were determined. Similarly, an acceptable damage level, in terms of calculated principal tensile strain at the center of the joint, was chosen as the target demand. The quantity and arrangement of vertical reinforcement was modified until the growth in the principal tensile strain after cracking was below an acceptable level.

8.1.1 Typical Bridge Joint Geometry

The studied bridge bent configuration is the same as that used for Group A (Table 3-1 and Figure 3-2). The geometry and longitudinal requirements represent typical values found in California construction based on the database presented in Appendix A. The study is conducted at 3/8 scale to conform to the models used in preceding chapters.

8.1.2 Finite Element Model Configuration

All parametric studies conducted in this chapter are based on 3D finite element analyses. The finite element techniques used are the same as those used for Group A (Chapter 4). The constitutive models and finite element parameters match those used for Specimen A2.

8.2 Target Displacement

The target displacement was determined from Caltrans recommendations and experimental results. The bridge system under consideration consists of a reinforced concrete box-girder deck with multi-column bents. Large diameter columns are used with high quantities of spiral reinforcement. Caltrans recommends a ductility risk reduction factor of 8 for this structure. As discussed in Chapter 6, a displacement ductility (μ_Δ) of only 7.7 was achieved, where yield displacement is defined as the displacement corresponding to initiation of yield in the column longitudinal reinforcement. While additional ductility may have been reached with less cyclic loading on earlier cycles, a displacement ductility of 8 can be considered a practical upper bound.

While direct usage of the Caltrans recommended ductility might be appropriate for column response, the ductility corresponding to the ultimate load would provide a better evaluation of the ultimate joint response. At this level, the joint is subjected to the highest demand. Specimens A1 and A2 reached their ultimate load at displacement ductility, μ_Δ, of 6.0 and 5.4, respectively. To be conservative, the target displacement value was assumed to be equal to a μ_Δ of 6.0. Since the bridge mechanism (plastic hinging) forms in the column adjacent to the cap beam, the displacement ductility of the column was used. The prototype model

(Specimen A2) reached this level of μ_Δ at a displacement of 7.8 in. This displacement is used as the target displacement for the study conducted in this chapter.

8.3 Horizontal Transverse Joint Reinforcement Requirements

To decrease the levels of joint shear stress present in bridge beam-column joints, codes recommend an increase in the width of the cap beam. Caltrans BDS [1994], for example, recommends that the cap beam be 2 feet wider than the column diameter. While this may increase the gross geometry of the joint, it does not ensure that the entire joint width will be active in resisting joint shear. To activate the face of the joint, horizontal hairpins can be used. This section evaluates the appropriate arrangement and quantity of horizontal ties (lateral reinforcement) required to effectively activate the entire joint width. Activation is determined by comparing the joint shear strain at the center and face of the joint. Convergence of the joint shear strains correlates to a greater degree of activation, with equal levels of joint shear strain (internally and externally) representing complete activation.

8.3.1 Current Lateral Reinforcement Requirements

Caltrans requirements result in a heavily reinforced joint (Figure 8-1). The lateral joint reinforcement consists of both hairpin/headed and spiral reinforcement. The arrangement used in the experimental investigation consisted of a dispersed array with concentrations at both the interface and top of the joint, near the extremities. This was done to assist in confining the joint at the interface (i.e., where the tensile column bars pull out). In addition to the lateral reinforcement, spiral reinforcement is continued into the joint from the column plastic hinge region, and vertical reinforcement is distributed in the joint. The combination of all these requirements produces a high level of congestion leading to constructability problems. To address this issue, this section studies the effectiveness of the spiral and lateral reinforcement on joint response.

Caltrans requirements produce incompatible shear strains between the exterior and interior of the joint. Figure 8-2 compares the joint shear strain, computed on the exterior and interior of the finite element model (Figure 8-3), with the subassembly drift. These results are obtained from the analysis of Specimen A2. The goal of the parametric study is to determine an acceptable level of deviation between the interior and exterior shear response of the beam-column joint.

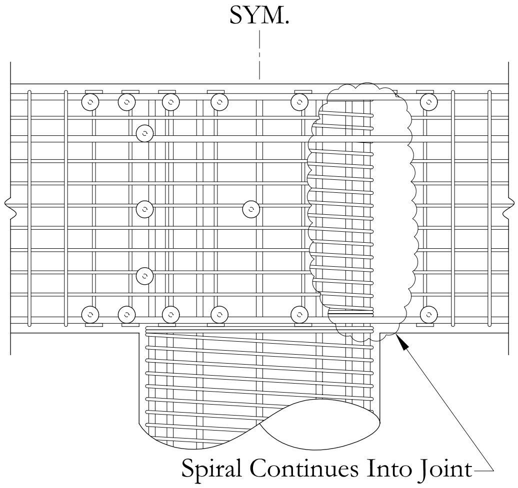

Figure 8-1: Experimental subassembly joint reinforcement configuration (Model A)

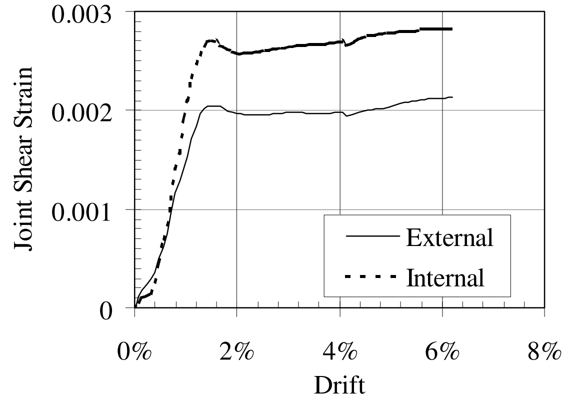

Figure 8-2: Joint shear strain response to a tip displacement of 7.8 in.

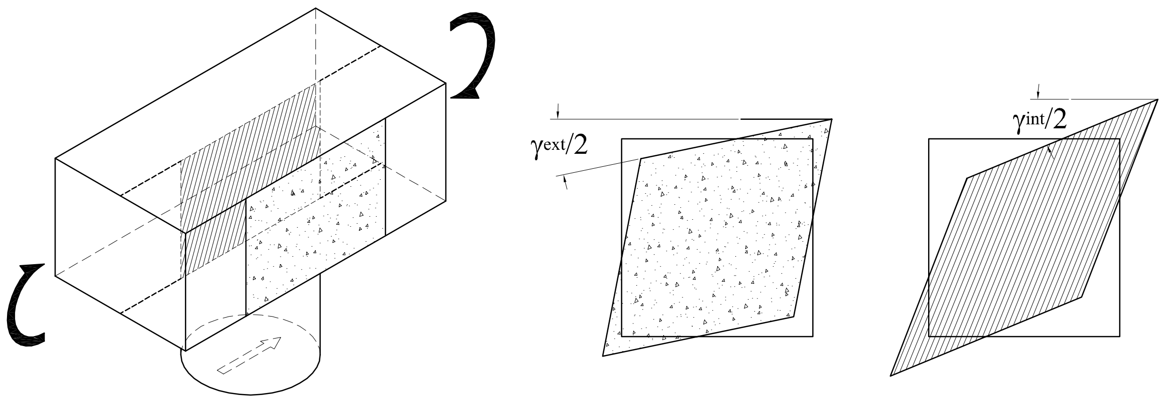

Figure 8-3: Shear strain deformations

8.3.2 Distribution of Lateral Reinforcement

The effectiveness of lateral reinforcement distribution on joint response was studied. The distribution was varied from that used for Subassembly A2. In addition to the Caltrans prototype (Model A representing Subassembly A2, Figure 5-5), four distributions of lateral reinforcement are studied (Table 8-1). As discussed in Chapter 6, headed lateral bars provided comparable, if not superior, behavior to that of conventional hooked (hairpin) bars. Furthermore, the primary resistive force of headed transverse reinforcement is along its axis. This provides a means of applying a localized discrete resistance to lateral deformation, allowing for a straightforward evaluation of transverse reinforcement strategies. Therefore, headed transverse reinforcement is used in the following studies. As discussed in Chapter 7, the joint spiral was ineffective in resisting joint shear and improving lateral compatibility. This is further justified in the following parametric studies on lateral and vertical joint reinforcement. In the distribution study, the volume of lateral joint reinforcement is kept constant between models. To account for the variation in the number of lateral reinforcement bars, the areas of the bars are altered.

Table 8-1: Lateral reinforcement details
(All distributions have the same volume of lateral reinforcement)

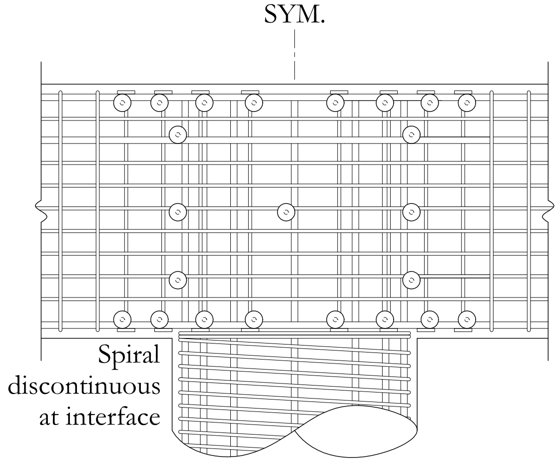

Model B —Subassembly A2 without spiral

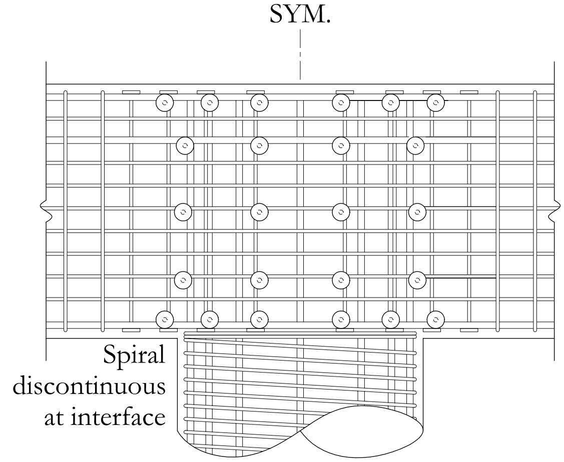

Model C

Table 8 -1 *(continued):* Lateral reinforcement details

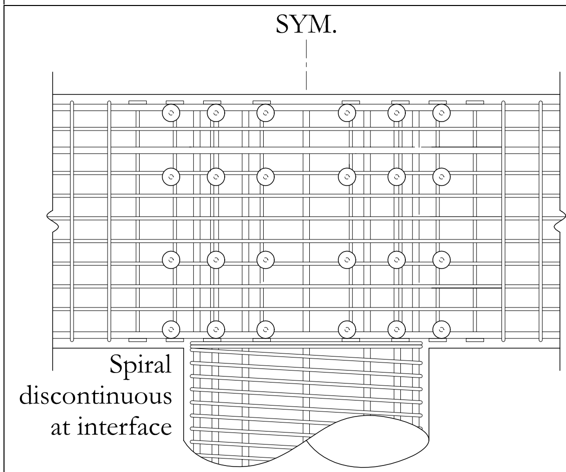

Model D

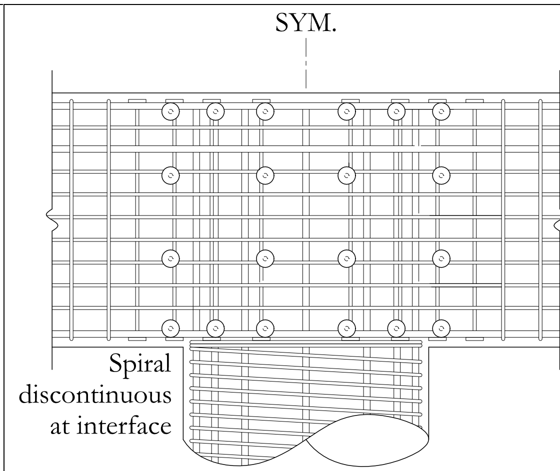

Model E

The joint shear strain at the target displacement is affected by the use of the joint spiral or lateral reinforcement arrangement; however, the effect is not significant (Figure 8-4). The presence of the joint spiral decreases the interior joint shear strain and increases the exterior shear strain. The difference relative to the internal joint shear strain is small, changing from 25% to 35%. While this may appear large, the corresponding quantity of reinforcement removed is significant. In this case, the benefits to constructability far outweigh the marginal increase in internal joint shear strain. Furthermore, a variation in the arrangement of the bars provides an effective substitute for the spiral. Model C, for example, while easier to construct than Model A, still provides a comparable variation in internal and external shear strains.

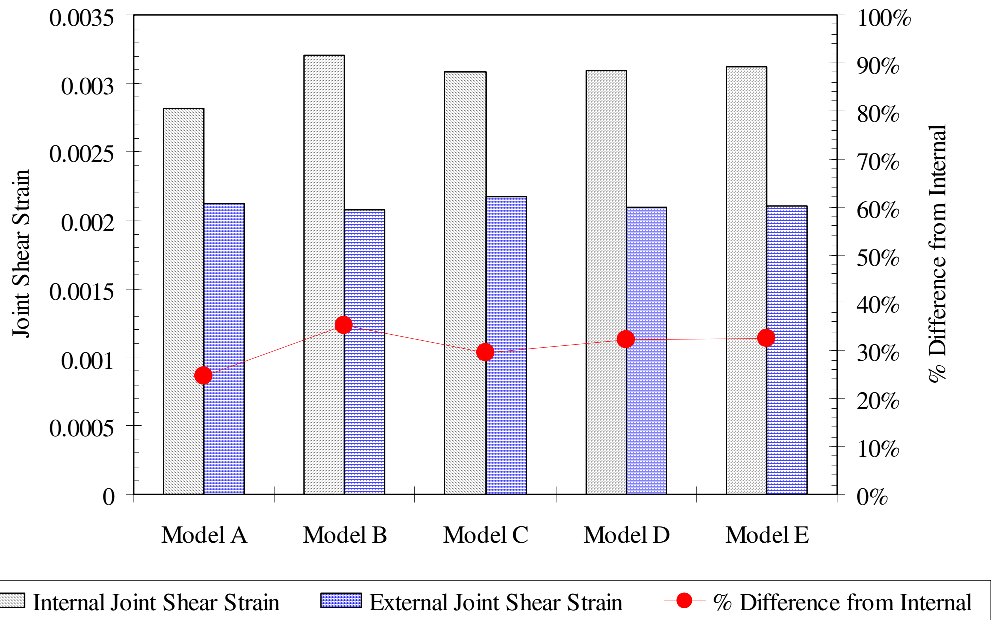

Figure 8-4: Effect of lateral reinforcement distribution on compatible joint response

Activation of the joint face is best achieved by placing lateral bars in the width of the column core. To actively resist column pullout, experimental results show that a higher concentration of bars should be placed at the beam-column interface. The small variation between models D and E shows that the number of bars within the joint does not significantly alter the activation of the joint. Consequently, distribution E was chosen as the ideal distribution, providing adequate activation with superior constructability.

8.3.3 Quantity of Lateral Reinforcement

The quantity of lateral joint reinforcement notably affects the behavior of the joint. To compare the effect of the quantity of reinforcement, the distribution presented by Model E was modified. Variations in the quantity of lateral reinforcement from 0 to 1.3As_{column} were studied (Table 8-2), where As_{column} equals the total area of column longitudinal reinforcement.

Table 8-2: Parameters used in the investigation of quantity of lateral reinforcement

Area of each lateral bar (in.^{2})	Total area of lateral reinforcement (in.^{2})	Total area of lateral reinforcement (% of As_{column})
No lateral bars	0.00	0 %
0.023	0.46	3 %
0.120	2.30	16 %
0.230	4.60	33 %
0.460	9.10	65 %
0.920	18.40	131 %

Activation of the joint is directly related to the amount of lateral reinforcement used. Figure 8-5 presents the internal and external joint shear strain response as a function of tip displacement for different levels of lateral reinforcement. The joint shear strain-displacement response follows a consistent trend. Up to the initiation of column yield, the internal and external joint response is comparable. After yield, the internal and external joint responses diverge. At this demand, the external portion becomes less effective.

Activation of the joint width is dependent on the amount of lateral reinforcement. As the quantity of lateral reinforcement is increased, the external joint shear strain increases and the internal joint shear strain decreases. Of the two, the external joint shear strain is more sensitive (Figure 8-6). As the level of lateral reinforcement is increased from zero, the external joint shear strain rapidly increases.

To directly evaluate the level of reinforcement required to activate the joint, an activation index, I_L, is defined at the target displacement as

$$I_L = 1 - [(\gamma_{int}\text{-}\gamma_{ext})_i \,/\, (\gamma_{int}\text{-}\gamma_{ext})_0] \tag{8-1}$$

Where $(\gamma_{int}\text{-}\gamma_{ext})_i$ is equal to the difference in external and internal joint shear strain for level of reinforcement i, and $(\gamma_{int}\text{-}\gamma_{ext})_0$ is equal to the difference in external and internal joint shear strain for the case of no lateral reinforcement. I_L has a value between 0 and 1. I_L equal to 0 corresponds to lowest level of joint activation (i.e., the case of no lateral reinforcement $(\gamma_{int}\text{-}\gamma_{ext})_i$=$(\gamma_{int}\text{-}\gamma_{ext})_0$), I_L equal to 1 corresponds to complete activation of the joint width (i.e., $(\gamma_{int}\text{-}\gamma_{ext})_i$=0).

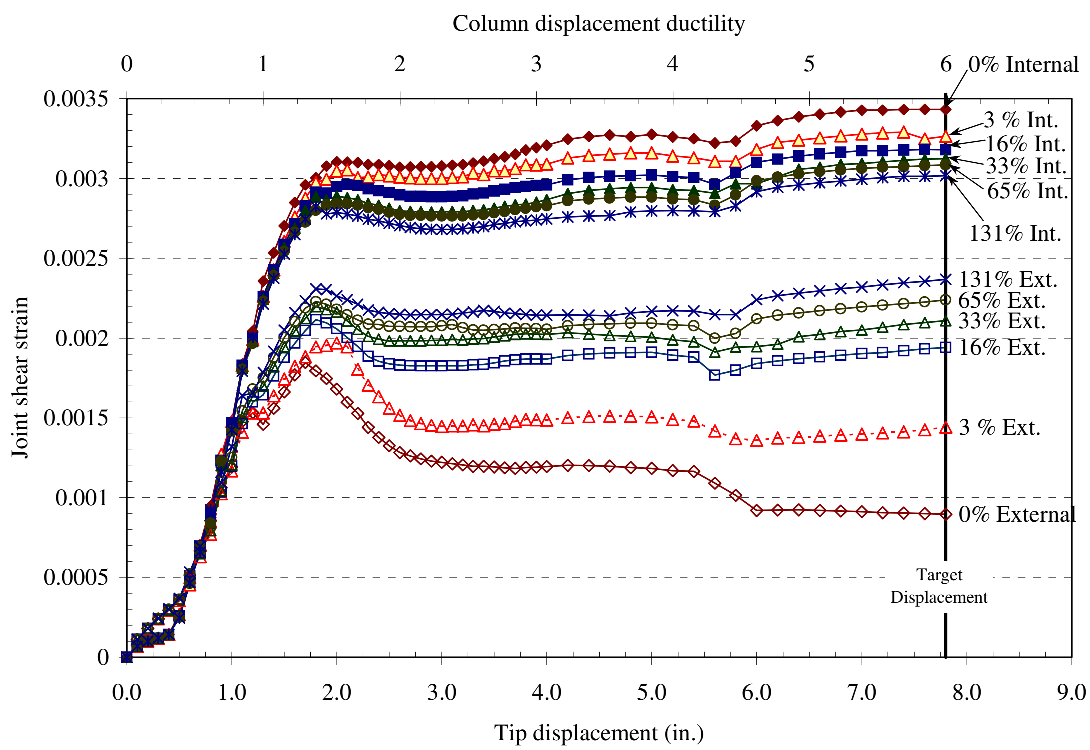

Figure 8-5: Effect of quantity of lateral reinforcement on compatible joint response

Activation is greatly improved by small levels of lateral reinforcement (Figure 8-7). Once the quantity of lateral reinforcement exceeds 25%As_{column}, the benefit of additional bars diminishes. Increasing the level of lateral reinforcement from 33%As_{column} to 65%As_{column} increases the activation index by only 0.07. To achieve significant activation of the joint, a high quantity of lateral reinforcement is required, possibly on the order of 4 or 5 times As_{column}. Since 100% activation (I_L=1.0) is not feasible and possibly not obtainable, an activation index of 0.6 is recommended. At this level only 33%As_{column} is required as lateral reinforcement, thus constructability is not adversely affected. Higher activation can be achieved, but at the expense of joint congestion.

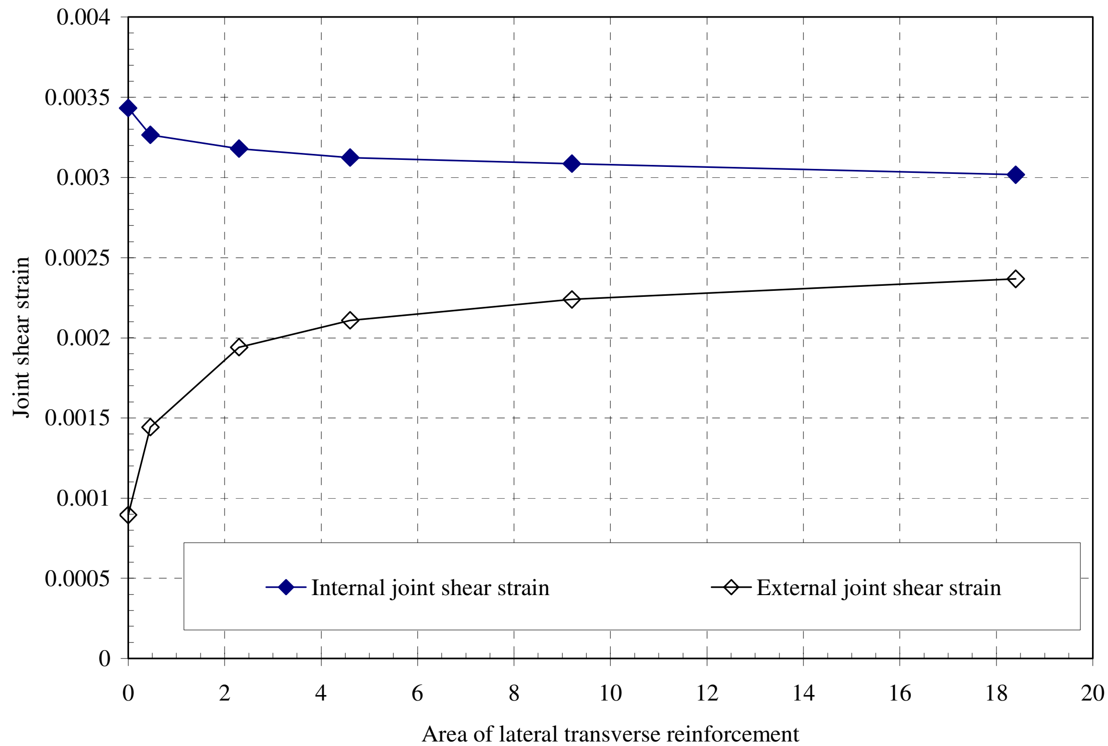

Figure 8-6: Joint shear relative to total area of lateral reinforcement [in.^{2}] at target displacement

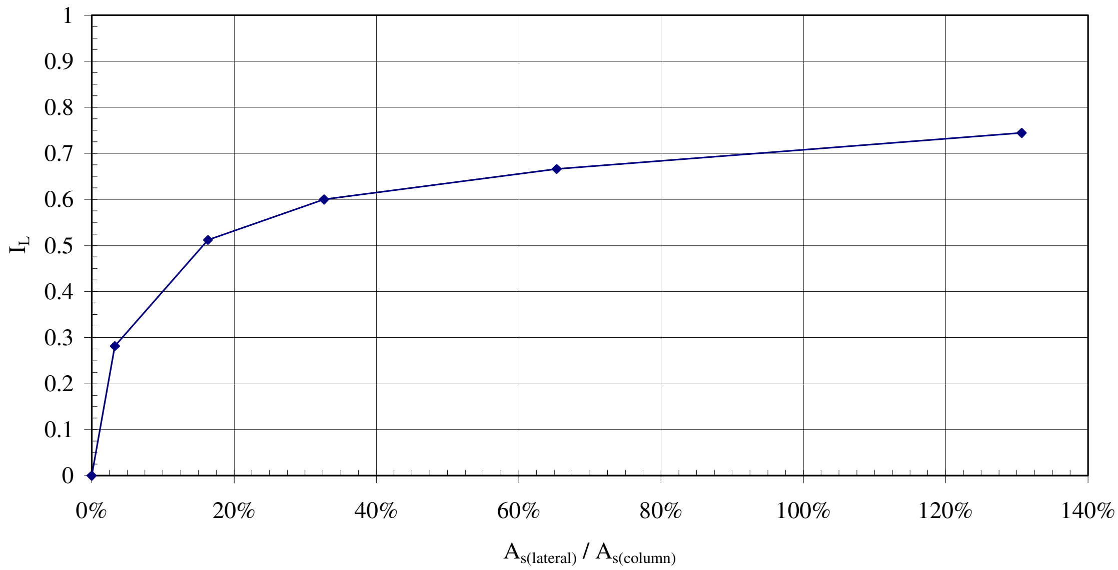

Figure 8-7: Joint activation index as function of quantity of lateral reinforcement

8.3.4 Summary of Horizontal Transverse Joint Reinforcement Requirements

The analytical study presented in Section 8.3.2 shows that joint activation is not significantly affected by the removal of joint spiral. This correlates with the experimental findings of Group B. Consequently, it is recommended to eliminate the joint spiral as a means of improving joint constructability.

Distribution of lateral reinforcement was most effective when bars were placed within the column core. Furthermore, in the experimental program it was shown that a concentration of lateral bars at the beam-column interface assisted in resisting yield penetration. Additional bars should be placed on the periphery of the joint adjacent to the extreme column reinforcement. This assists in both resisting pullout along the longitudinal column bar length and in improving confinement of the beam compression forces. An effective distribution is shown in Table 8-1, Model E.

Based on a target displacement ductility of 6.0, the effectiveness of the joint was evaluated for different levels of lateral reinforcement. Effectiveness was determined by evaluating the variation between the internal and external shear strains using a quantitative characterization through a defined activation index I_L. Based on this criterion, it is suggested that 33% As_{column} might be sufficient to use as lateral reinforcement.

8.4 Vertical Transverse Reinforcement Requirements

The effect of the vertical joint reinforcement on joint damage is studied in this section. Damage is evaluated using the magnitudes of the shear and principal tensile strain in the joint. Principal tensile strains directly correlate to the amount of cracking, and thus provide a good criterion for damage. Recommendations on the arrangement and quantity of vertical reinforcement are developed.

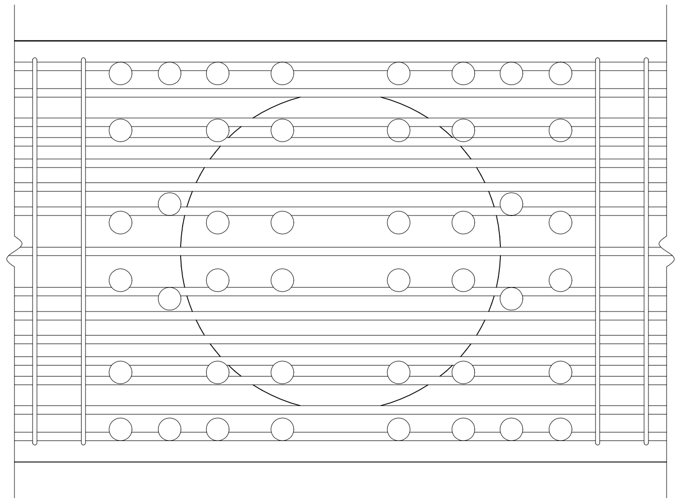

Figure 8-8: Plan view of vertical joint reinforcement layout Model 1

To determine the sequence of the parametric investigation on vertical reinforcement, two variations of the Caltrans prototype model are examined. The Caltrans prototype matches the design used for Subassembly A2 (Chapter 5). The joint reinforcement used in this model contains an area of vertical reinforcement, *Av* (Figure 8-8), horizontal reinforcement, *Ah* (Figure 8-1), and the continuation of the joint spiral from the column plastic-hinge region. In the first variation, the joint spiral is removed to directly assess the benefit of the spiral. The second variation looks at the response of the joint with no spiral, vertical, or horizontal transverse reinforcement. This model relies only on the joint concrete and the longitudinal column and beam reinforcement for lateral resistance. Consequently, the model bounds the ultimate level of damage that could be expected for the prototype joint geometry.

As discussed previously, joint response is not significantly affected by the presence of the joint spiral. Joint reinforcement reduces the average shear strain measured on the *interior* of the joint as expected, which lends confidence to the analytical modeling techniques (Figure 8-9). The removal of the spiral from the prototype reinforcement arrangement results in only 8% increase in the level of shear at the target displacement. Similar behavior is observed in a comparison of the principal tensile strains measured on the face of the joint (Figure 8-10). In this case, the removal of the joint spiral does not affect the level of *external* tensile strain. It should be noted that the complete removal of joint transverse reinforcement results in a progressive increase in the measured *external* principal tensile strain. This validates the necessity of transverse joint reinforcement in reducing external joint damage. The greatest variation in behavior occurs with the *internal* principal tensile strain (Figure 8-11). In this case, the tensile strain is notably affected by the presence of the spiral. This can be attributed to the confinement action provided by the spiral. While this action can be considered beneficial, the goal of this investigation is to find a means of reducing damage, and improving constructability. Since the removal of the spiral is not detrimental to the behavior (i.e., removal does not result in a progressive increase of strain), but results in only a marginal increase of *internal* principal tensile strain (0.00202 to 0.00272 at the target displacement), the spiral is recommended to be discontinued at the beam-column interface.

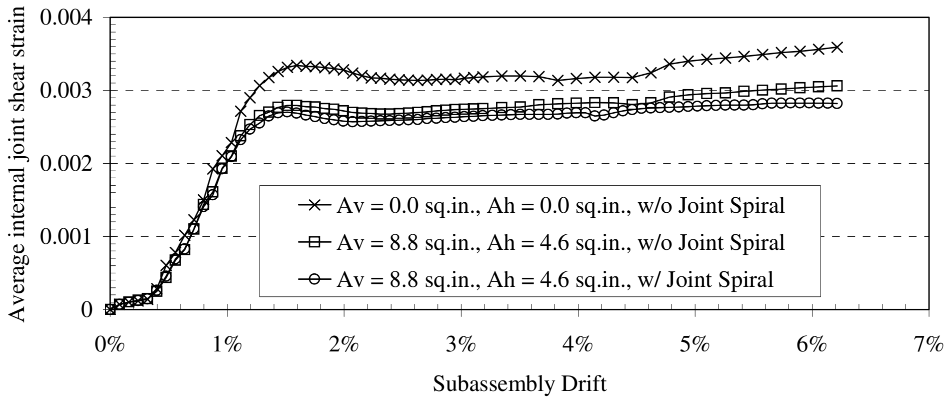

Figure 8-9: Effect of joint reinforcement on interior joint shear strain

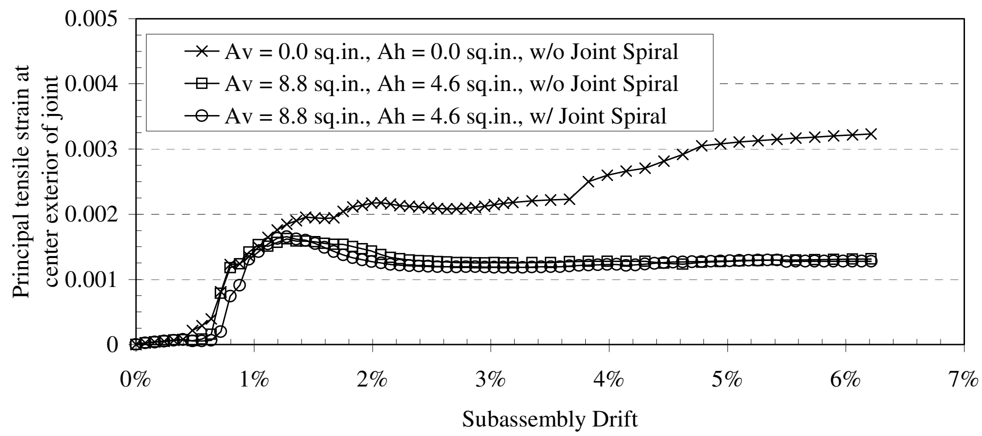

Figure 8-10: Effect of joint reinforcement on exterior joint principal tensile strain

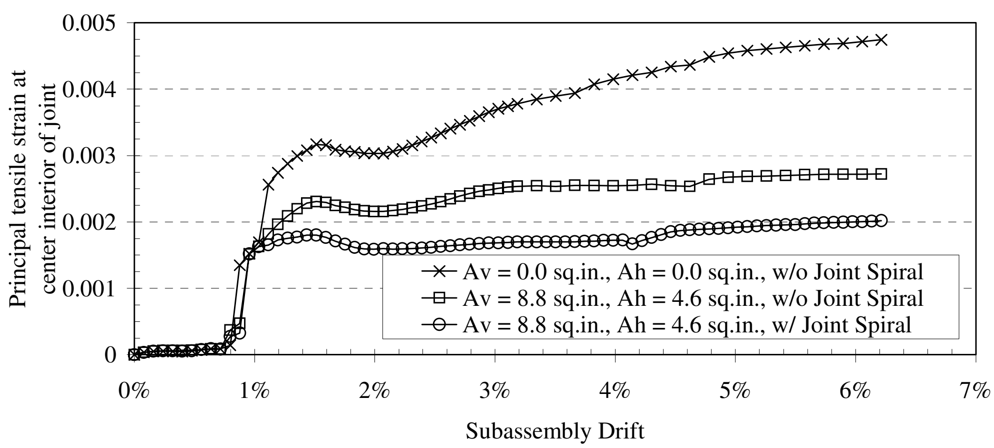

Figure 8-11: Effect of joint reinforcement on interior joint principal tensile strain

8.4.1 Distribution of Vertical Reinforcement

The prototype is compared to the response of two variants (Table 8-3), one with all vertical reinforcement placed on the exterior of the joint (Model 2), and the other with all reinforcement placed on the interior of the joint (Model 3). The effect of the distribution variation on activation of the entire joint width and limiting damage are evaluated. In both cases, a constant level of horizontal transverse reinforcement equal to the recommended level (Section 8.3) is used.

Table 8-3: Vertical joint reinforcement details (plan views)

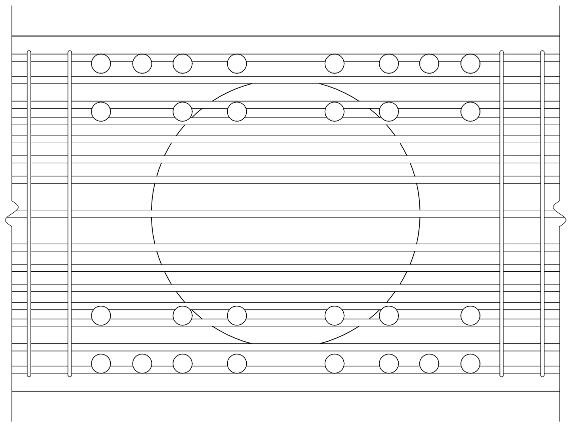 Vertical joint reinforcement, Model 2	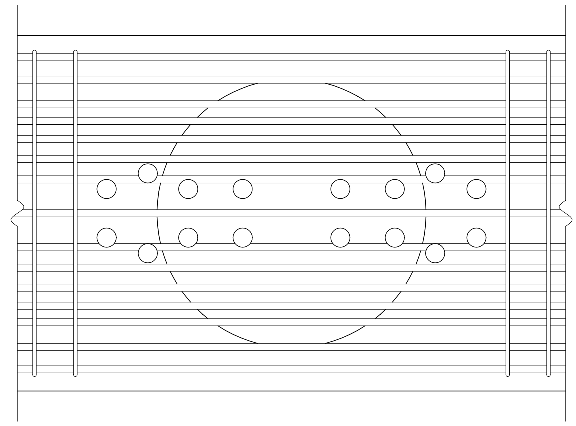 Vertical joint reinforcement, Model 3

Distribution of vertical reinforcement has minimal effect on joint deformation. The placement of reinforcement on the face (exterior) of the joint marginally increases the level of internal joint shear strain from that of the distributed response. Interior placement of vertical bars provides the lowest measured interior shear strain, however, the variation is not significant (Figure 8-12). At the target displacement of 7.8 in. (μ_Δ=6.0), the external joint shear strain is unaffected by vertical reinforcement distribution. Prior to column yield, however, the removal of vertical reinforcement from the face of the joint notably increases the magnitude of exterior joint shear strain. This can be attributed to the resulting decrease in the external joint stiffness. This effect, nevertheless, is short lived. Continued yielding of the column results in a rapid redistribution of the external shear strain. The principal tension strain in the joint is also marginally affected by the distribution. As expected, the removal of the external vertical reinforcement increases the external tensile strain, and removal of the interior vertical reinforcement increases the interior tensile strains. The change in strain in both cases is small, on the order of 0.0003 (Figure 8-13).

Distribution of vertical reinforcement does not significantly affect either the level of joint shear strain or the level of principal tensile strain measured at the center or exterior of the joint. Thus with the focus of limiting deformation and damage, any distribution can be used. Although it is not directly addressed in this study, a distributed arrangement (Model 1) is suggested. This will provide improved anchorage of the top beam reinforcement, allowing development within the column core (Chapter 6).

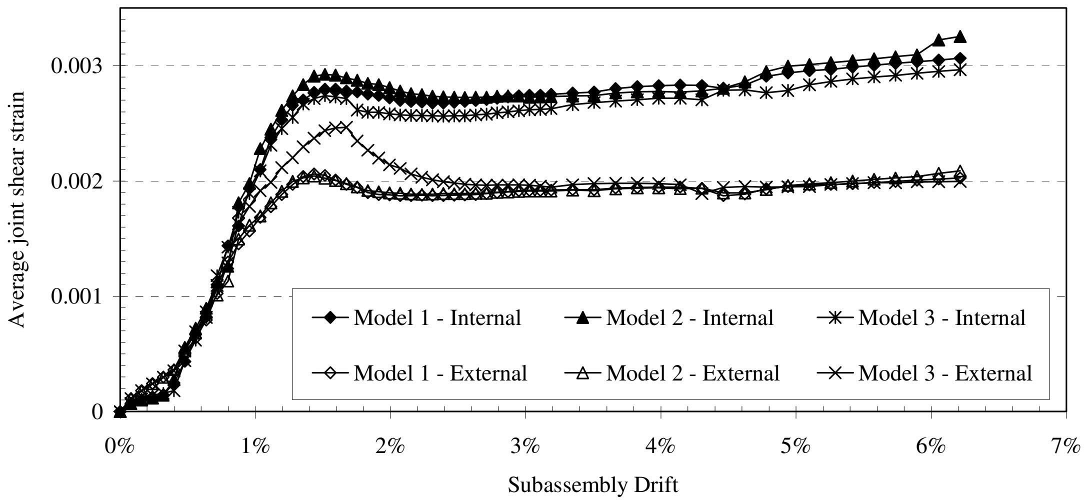

Figure 8-12: Effect of vertical joint reinforcement distribution on joint shear strain

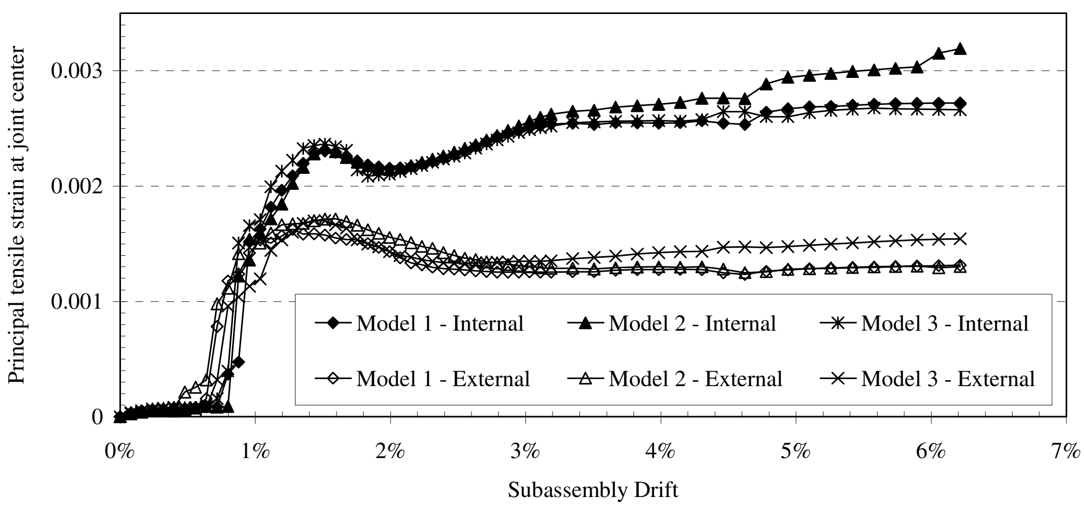

Figure 8-13: Effect of vertical joint reinforcement distribution on principal tensile strain

8.4.2 Quantity of Vertical Reinforcement

The quantity of vertical joint reinforcement affects the magnitude of damage on the interior of the joint. Comparison of principal tensile strains, $\varepsilon 1$, for the cases of no vertical reinforcement, prototype reinforcement distribution, and varying quantities of vertical reinforcement are presented (Figure 8-14). In all cases, the recommended level of horizontal reinforcement is used (Section 8.3). Under these conditions no significant variation in internal or external joint shear strain occurs.

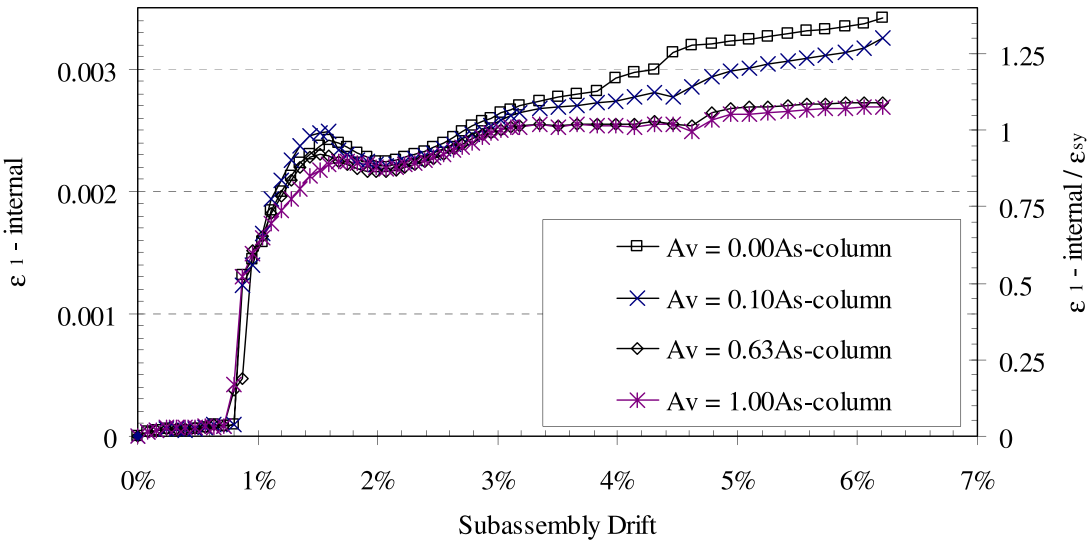

Figure 8-14: Effect of quantity of vertical joint reinforcement

To evaluate the resistance of each level of reinforcement to joint degradation, a factor I_s is developed. The level of degradation is defined relative to the increase in the measured principal tensile strain, $\varepsilon 1$, between subassembly yield and target displacements. The degradation factor is equal to

$$I_S = (\varepsilon 1_{target} - \varepsilon 1_{yield}) / \varepsilon 1_{yield} \quad (8\text{-}2)$$

where a degradation factor of zero is ideal. Comparison of the degradation factor relative to the level of vertical joint reinforcement (Av/As_{column}) is shown in Figure 8-15. Based on the trend of the relationship (i.e., quick convergence to a degradation factor of 0.6) only a low level of vertical reinforcement is necessary. From Figure 8-15 it is apparent that increase of A_v beyond 25% As_{column} has no effect in reducing degradation of the joint. To provide the most effective use of vertical bars, it is suggested that 25% As_{column} might be used.

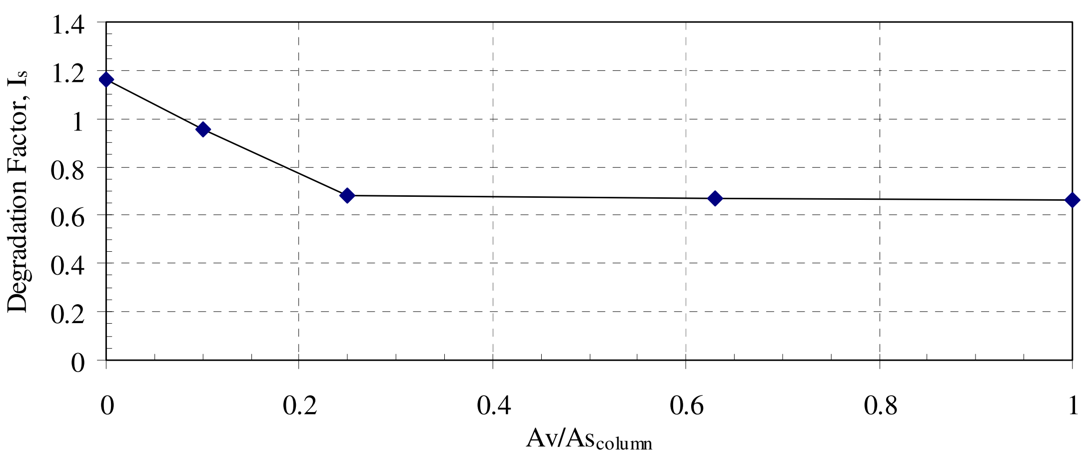

Figure 8-15: Influence of vertical reinforcement on joint degradation

8.4.3 Summary of Vertical Reinforcement Requirements

Joint response is not greatly affected by the distribution or quantity of vertical reinforcement. The parametric finite element study performed showed that a nominal level of vertical reinforcement equal to 25% As_{column} might be necessary to reduce degradation of the joint. Although distribution does not have significant effect on the joint response, it is recommended to distribute the bars evenly in the column depth and beam width. This will improve anchorage of the top beam longitudinal reinforcement.

8.5 Simplified Damage-Based Recommendations

The parametric study evaluated a typical joint configuration. For this prototype, the following observations and recommendations are made:

- The use of a joint spiral marginally improves the confinement of the core and decreases the principal tensile strain. This small improvement in joint behavior, however, does not justify the constructability expense. It is recommended to eliminate the joint spiral as a means of improving joint constructability.
- No evidence was found to support the placement of joint transverse reinforcement outside of the column depth.
- Lateral reinforcement is most effective when bars are placed within the column core (column depth). Furthermore, a concentration of lateral bars at the beam-column interface assisted in resisting yield penetration. Additional bars should be placed on the periphery of the joint adjacent to the extreme column reinforcement. This assists in both resisting pullout along the longitudinal column bar length and in improving confinement of the beam compression forces. An effective distribution is shown in Table 8-1, Model E.
- To effectively activate the entire joint width, (where effectiveness was determined by minimizing the variation between the internal and external shear strains), it is suggested that 33% As_{column} might be sufficient to use as lateral reinforcement
- Although distribution of vertical reinforcement does not have significant effect on the joint response, it is recommended to distribute the bars evenly in the joint zone (the area within the column depth and beam width). This will improve anchorage of the top beam longitudinal reinforcement.
- Joint response is not greatly affected by the quantity of vertical reinforcement. A nominal level of vertical reinforcement equal to 25% As_{column} might be sufficient to limit degradation of the joint.

9 Conclusions and Future Work

Investigations of the behavior of reinforced concrete bridge beam-column connections were carried out to identify their behavior and to advance models for assessment and design. Three areas are investigated: the evaluation of current bridge design requirements, investigation of methods for improving constructability, and the development of a recommendation for joints based on limiting damage. These objectives were achieved through both large-scale experimental investigations of bridge connections and three-dimensional finite element analysis. This chapter summarizes the work and results of each phase.

9.1 Review of Experimental Research

The experimental test program consisted of cyclic quasi-static testing of large-scale (3/8-scale) bridge beam-column connections. The geometry of the specimens coincided with geometry typical of California construction. A three-column reinforced concrete bridge bent with integral post-tensioned box-girder spans was chosen as the base structure. The test subassembly included the interior column (full height) and half the cap beam spans on each side; the box girder was not included. The test subassemblies were constructed and tested in an inverted position. For clarity, all future references in this conclusion will be presented with the assumption that the experimental subassemblies are in the true bridge orientation, i.e., the soffit is considered the bottom of the cap beam. The subassemblies were tested under increasing levels of displacement applied at the column base, parallel to the cap beam longitudinal axis (i.e., transverse to the bridge span). A constant gravity load of 5% of the column axial capacity was applied. The specimens were constructed using normal weight concrete and grade 60 reinforcement.

The experimental investigation was divided up into two phases: A and B. The first phase, Group A, consisted of four specimens: two with a circular column configuration, A1 and A2, and two with a square column configuration, A3 and A4. The cap beam and columns were designed according to Caltrans Bridge Design Specification. Column longitudinal reinforcement was developed straight without hooks to the rear of the joint and beam longitudinal reinforcement were continuous through the cap beam. The joints were also designed using Caltrans requirements; however, for specimens A2 and A4 all conventional joint reinforcement was replaced with headed reinforcement. Joint reinforcement consisted of vertical transverse bars in the form of beam stirrups, horizontal transverse reinforcement in the form of hairpins (U-shaped bars for the conventional design and straight bars with heads for the headed design) inserted on both vertical faces of the cap beam, and the continuation of the column spiral into the joint. In this phase, the state of current design, the use of headed reinforcement within the joint region, and force transfer mechanisms were evaluated. In the second phase, Group B, two specimens were developed to investigate the behavior of joints subjected to high demands and reduced joint reinforcement. To achieve a higher demand on the joint, the specimens, B1 and B2, had a reduced beam depth and significantly higher column strength from that of Group A. As was done in Group A, the column and cap beam were designed according to Caltrans recommendations with column longitudinal reinforcement developed straight to the rear of the joint. Specimen B1 joint reinforcement consisted of a nominal amount of vertical bars and an array of horizontal bars oriented transverse and parallel to the beam axis. Specimen B2 joint reinforcement consisted of a nominal amount of vertical bars and joint hoop reinforcement. These two designs investigated the effect of the joint spiral and further evaluated joint force transfer mechanisms.

9.2 Experimental Findings

Experimental findings show that Caltrans design requirements produce a well-behaved joint. The full capacity of the column was developed with little damage to the joint. The beam-column subassemblies developed a displacement ductility greater than 5.0 with column flexural plastic hinging controlling ultimate response. In these designs, joint damage was limited to a distributed array of small cracks. The strain readings indicated that the joint reinforcement remained elastic, and, furthermore, produced a force distribution that does not support the intended joint design mechanism. Consequently, reinforcement was not efficiently used.

Headed joint transverse reinforcement was equally as effective (as the conventionally reinforced joints) in transmitting joint forces and resisting shear deformation. Comparable levels of damage occurred in the joint reinforced with headed bars and the joint reinforced with conventional bars. Headed longitudinal column reinforcement reduced the measured slip of the column from the joint. This behavior was noticeable in a comparison of the two circular column subassemblies of Group A. In both specimens the column longitudinal bars were fully developed (development length >36 d_b). Nevertheless, the headed transverse reinforcement was activated leading to a greater degree of slip resistance than the conventional reinforcement. Based upon these experimental observations, the use of headed transverse joint reinforcement is recommended as a means of improving joint construction, and the use of longitudinal headed bars is suggested for systems where excessive slip may be an issue.

The strain distribution in the beam longitudinal reinforcement was not significantly affected by the details used in the joint. Nevertheless, the strain levels exceeded those predicted by conventional flexure theory within the joint region. In the regions adjacent to the joint the measured strains exceeded the predicted values on the top reinforcement (i.e., close to the bridge deck) and underestimated the strains on the interface reinforcement outside the joint region. The square or circular column configuration did not noticeably affect this distribution of the beam strain. In all cases, the development of the column tensile forces resulted in a localized increase in the beam strain on the interface longitudinal bars, often resulting in localized yielding.

The behavior of the vertical joint transverse reinforcement on the interior and exterior of the joint illustrates the three-dimensional response of the joint system. The strain distribution on the vertical transverse reinforcement was uniform on the face of the joint. On the interior of the joint, the strain distribution varied decreasing from a peak strain at the tensile face to a minimum at the compressive column face.

This behavior indicates that a shear panel mechanism may occur on the exterior of the joint, while at the same time, a principal compression strut forms on the interior of the joint.

The Caltrans design method was based on a mechanism dependent on both the spiral and out-of-plane transverse joint reinforcement. For the current details, dilation of the core occurred most significantly at the interface (soffit) and top of the joint. The dilation of the overall joint was greatest at the mid-depth. Note that the demands applied to the joints of Group A resulted in minimal joint damage. The elastic strain levels measured indicate that for these joints the levels of reinforcement used may be overly conservative.

The investigation of higher joint demand levels (Group B) has provided several conclusions with regard to reinforcement detailing. Horizontal joint hairpins, oriented perpendicular to the beam axis, are necessary to activate the large cap beam widths used in current recommendations. Without hairpins, the joint core can separate from the cap beam face, decreasing the effective joint width and increasing demand on the vertical transverse joint reinforcement. This, in turn, decreases the capacity of the joint. In addition, the vertical reinforcement is most highly activated within the core near the location of the extreme column tensile reinforcement. Consequently, vertical reinforcement should be concentrated in the center of the cap beam rather than on the face of the joint. Spiral joint reinforcement provides the best resistance to slip of the column reinforcement. Nevertheless, a well-distributed array of horizontal transverse reinforcement is expected to provide comparable levels of slip resistance. In addition, both horizontal transverse reinforcement and spiral reinforcement provide comparable levels of shear resistance. Therefore, the joint system may be constructed without the use of the joint spiral, thus allowing for a decrease in the quantity of joint reinforcement, and improved constructability.

9.3 Review of Analytical Models

Finite element modeling techniques were utilized for investigating the bridge beam-column joints. This study was intended to complement the experimental investigation. Trilinear concrete bricks and embedded reinforcement were used to model the specimens. This allowed for the investigation of three-dimensional effects. The use of embedded reinforcement, however, prescribed that the reinforcement has perfect bond and does not slip relative to the concrete. This is the only major shortcoming in the model. Constitutive properties were modeled using the measured response of the concrete and steel from material testing. Varieties of yield criteria were investigated. Steel behavior modeled using Von Mises yield criteria and concrete behavior modeled with the rotating-crack concept was found to produce good correlation with test results. The constitutive relationships were *not* altered to artificially produce a better match. With these rules, the behavior of both Group A and B specimens were investigated. The models were then used for parametric investigation of reinforcement strategies.

9.4 Analytical Findings

Analytical models were developed to expand understanding of the joint behavior measured in the experimental program. The models provided reliable estimation of the joint response. For Group A specimens, the models predicted a transfer mechanism consisting primarily of a compression strut in the interior of the joint. The strut is confined within the column core; however, additional tension ties occur outside the joint to anchor the localized pullout of the column tensile reinforcement. The width of the strut indicated that the placement of vertical reinforcement would be most effective within the joint core and not on the face of the joint. The demand levels for specimens A1 and A2 models, however, are below the compressive capacity, with maximum principal compressive stresses on the order of 2.0 ksi. Under these conditions, the joint is well behaved, and the joint reinforcement is elastic. To determine the behavior of the joint under significantly higher demand, Group B specimens were analyzed.

Analytical investigation of Group B indicated that the use of the spiral alone decreases the effectiveness of the joint. Large tensile strains occurred adjacent to the confined core indicating delamination of the cap beam. This was supported by a lower amount of principal compressive stress measured on the face of the joint. The use of lateral joint reinforcement increased the activation of the joint width, increased the compression forces on the face of the joint, and decreased the delamination of the cap beam. The inability of the modeling techniques to capture slip prevented complete evaluation of the shear failure mechanism.

The finite element modeling techniques used are reliable in predicting the global and local behavior of beam-column systems where slip of reinforcement is minimal. Both global load displacements, as well as joint shear strain response were comparable to the experimental findings. Accordingly, the used finite element techniques provide a viable tool for evaluating joint design strategies and conducting parametric studies.

9.5 Parametric Investigation Results

The parametric study evaluated a typical joint configuration. For this bridge beam-column prototype joint, the following observations are made:

- The use of a joint spiral marginally improves the confinement of the core and decreases the principal tensile strain. This small improvement in joint behavior, however, does not justify the constructability expense. Removal of the joint spiral may be used as a means of easing joint construction without significant impact to the joint behavior.
- No evidence was found to support the placement of vertical joint transverse reinforcement along the cap beam on each side of the column core.
- Horizontal joint transverse reinforcement is most effective when bars are placed within the column core (column depth). Furthermore, a concentration of lateral bars at the beam-column interface assisted in resisting yield penetration. Additional bars should be placed inside the core on the periphery of the joint adjacent to the extreme column reinforcement. This assists in both resisting pullout along the longitudinal column bar length and in improving confinement of the beam compression forces.

- To effectively activate the entire joint width (where effectiveness was determined by minimizing the variation between the internal and external shear strains), a quantity of lateral reinforcement equal to 33% As_{column} could be used (where As_{column} is equal to the total area of column longitudinal reinforcement).
- Joint response is not greatly affected by the quantity of vertical reinforcement. A nominal level of vertical reinforcement equal to 25% As_{column} could be used to limit degradation of the joint.
- Though distribution of vertical reinforcement does not have significant effect on the joint response, it is recommended to distribute the bars evenly in the joint zone (the area within the column depth and beam width). This will improve anchorage of the top beam longitudinal reinforcement.

With the preceding requirements, a well-behaved constructable joint is expected.

9.6 Future Work

While the presented research has provided good insights, additional work should be conducted to provide a comprehensive understanding of reinforced concrete bridge beam-column joints. This should consist of both analytical and experimental research. Further parametric studies focusing on different geometry and column demand levels should be conducted to complement the recommendations developed in Chapter 8. Extension of the analytical models to include longitudinal reinforcement slip should be carried out both to investigate the behavior of older joint systems where slip is a significant issue and to identify any shortcomings with the presented evaluations.

Testing of Group A subassemblies resulted in an elastic joint response and inefficient use of reinforcement, while testing of Group B resulted in inelastic joint response and high activation of reinforcement. Further study should be conducted to bridge these results. The test program should consist of beam-column subassemblies with Group A geometry and lower joint reinforcement quantities, as well as subassemblies with Group B geometry and increased quantities of joint reinforcement and headed column longitudinal reinforcement to eliminate the issue of slip.

Finally, experimental investigation of the joint system under bidirectional response should be evaluated. This should include the box-girder span to properly determine the force transfer mechanisms under longitudinal as well as combined longitudinal and transverse bridge response. This will provide improved understanding of the joint behavior by addressing the formation of joint mechanisms under bidirectional loading.

Appendix A California Bridge Parameter Investigation

To determine a geometry and reinforcement arrangement typical of California construction, detailed evaluations of 16 bridges were conducted (Table A-1). The investigation focused primarily on newer techniques used in bridge bent construction. The bridges studied include two-span overpasses and long-span viaducts. This appendix summarizes the details used in these bridges. All pertinent information was included: the bridge geometry, the column-to-footing connection, and the quantity of secondary positive beam longitudinal reinforcement. Unless noted, units are in kips and inches.

Table A-1: Bridges studied

Bridge Name	Original or replacement bridge	Caltrans Bridge ID #	Year Approved
East 20th St. Overcrossing	Original	12-109	1963
Crow Canyon Road Undercrossing	Original	33-233 R/L	1982
Crenshaw Boulevard Undercrossing	Original	53-2519	1985
52nd Place Overcrossing	Replacement	53-1094	1988
Imperial Highway Overcrossing	Replacement	53-941	1989
McFadden Street Overcrossing	Original	55-392	1990
Castro Valley Blvd. Undercrossing	Original	33-202 R	1991
Cottonwood Creek Bridge	Original	50-47	1991
Port of Oakland Connection Viaduct	Original	33-612 E	1993
Gavin Canyon UC	Replacement	53-2790 R/L	1994
Fairfax – Washington Undercrossing	Original	53-2792	1994
Bull Creek Canyon Channel Bridge	Replacement	53-2794R	1994
La Cienega – Venice Separation	Original	53-2791	1994
Mission – Gothic Undercrossing	Replacement	53-2793 R	1994
"CL" Line - 5th & 6th Street Viaduct	Original	33-0616L	1994
North Connector Overcrossing	Original	53-2796F	1994

The following pages tabulate the results of the investigation. A legend is included at the end.

Location	Column shape	Column geometry at mid-height	Column geometry at soffit	Gross area of column, Ag	Area of column core, Ac	Column to footing connection	Number of columns	Clear distance between columns	Core diameter
East 20th	Rectangle	30 x 42	Same	1260	?	P	2	234	
Crow Canyon	Octagon	66	132 x 66	3609	3019	P	3	255	62
Crenshaw Boulevard	Octagon	84	124 x 104	5040	4301	P	4	220	78
52nd Place	Wide Octagon	40 x 67	Same	2438	1990	P	3	217	36
Imperial Overcrossing	Octagon	72	Same	4295	3632	P	2	236	68
McFadden Street	Hexagon	66	142 x 66	3094	3019	M	1	N.A.	64
Castro Valley	Octagon	48	Same	1909	1521	P	4	288	44
Cottonwood Creek	Round	96	Same	7238	6648	M	1	N.A.	92
Port of Oakland	Rectangle	108 x 102	Same	11016	7543	M	2	216	
Gavin Canyon	Octagon	84	Same	5845	5027	M	3	336	80
Fairfax - Washington	Round	48	Same	1810	1521	P	5	90 to 156	44
Bull Creek Canyon	Round	66	Same	3421	?	P&M	4	336	
"CL" Line	Square	96	Same	9216	6648	M	2	312	N.A.
North Connector	Octagon	96	Same	7635	6648	M	1	N.A.	
La Cienega	Round	66	Same	3421	3019	P	3-4	213	62
Mission - Gothic	Round	84	Same	5542	5027	P	3	300	

Location	Clear height soffit to ground	Number of boxes along deck	Width of box	Wall thickness of box	Top slab thickness	Bottom slab thickness	Deck span (ft)	Cap beam width	Cap beam depth
East 20th	240	5	72	12	6	none	?	30	42
Crow Canyon	195	9	92	12	7.875	5.875	60&146	72	72
Crenshaw Boulevard	191	9	156	12	9.75	9.75	144.5	108	72
52nd Place	210	7	92	12	7.875	5.875	112&105	50	53
Imperial Overcrossing	352	5	89	12	7.75	5.625	148 &180	78	84
McFadden Street	215	4	72	12	7.25	5.5	125.5	72	60
Castro Valley	200	10	116	12	7.625	5.5	120 & 119	66	66
Cottonwood Creek	514	3	126	12	8.875	7.875	141 &108	102	69
Port of Oakland	?	Steel girder superstructure					?	108	108
Gavin Canyon	720	4	165	15	10	10	245, 290, 230	132	138
Fairfax - Washington	210	8	132	16	7.5	6	?	72	51
Bull Creek Canyon	180	10	?	?	8	7	?	96	96
"CL" Line	?	6	116	12	8.625	7.25	?	114	78
North Connector	?	2	138	12	8	7	?	132	78
La Cienega	228	9	106	14	8	?	?	99	72
Mission - Gothic	?	9	130	12	8.5	?	?	120	108

Location	Primary longitudinal reinforcement outer column	Primary longitudinal reinforcement inner column	Secondary longitudinal reinforcement	Total column longitudinal reinforcement, As	Column longitudinal reinforcement area ratio	Transverse column reinforcement at mid-height	Spacing of column reinforcement at mid-height	Transverse column reinforcement at soffit	Column transverse reinforcement volumetric ratio (relative to gross section)
East 20th	14#11	N.A.	-	22	0.0173	#4H w/ CT	12	?	?
Crow Canyon	56#14	39#14	22#8	126	0.0349	#5S	3.5	Same	0.00478
Crenshaw Boulevard	66#14	Same	14#6*	149	0.0295	#6S	3	Same	0.00713
52nd Place	30#9	Same	none	30	0.0123	2-3'Dia. #5S	3.5	Same	0.00411
Imperial Overcrossing	28#11	N.A.	none	44	0.0102	#5S	3.5	Same	0.00441
McFadden Street	34#14	N.A.	**	77	0.0247	#6S	3.25	Same	0.00880
Castro Valley	25#14	Same	none	56	0.0295	#5S	3.5	Same	0.00641
Cottonwood Creek	40#14	N.A.	none	90	0.0124	#6S	4	Same	0.00439
Port of Oakland	60#14	N.A.	32#5	145	0.0132	#8H Inner #7H Outer	4	#8H@3	?
Gavin Canyon	40#14	Same	20#14	135	0.0231	#8H	5	Same	0.00679
Fairfax - Washington	48#10	Same	none	61	0.0337	#6S	?	?	0.00560
Bull Creek Canyon	?	?	?	?	?	?	?	Same	?
"CL" Line	60#14	N.A.	none	135	0.0146	#8H	4	Same	0.01235
North Connector	42#14	N.A.	none	95	0.0124	#8H	5	Same	0.01193
La Cienega	36B#11s	same	none	112	0.0328	2-#6H	4.5	Same	?
Mission - Gothic	?	?	?	?	?	2-#6H	4.5	Same	?

Location	Column transverse reinforcement volumetric ratio (relative to core)	Straight development length	Development length in bar diameters	Horizontal joint transverse reinforcement in column width	Vertical joint transverse reinforcement in column width	Horizontal joint transverse reinforcement outside column width	Vertical joint transverse reinforcement outside column width	Quantity of top beam longitudinal reinforcement	Area of primary negative beam longitudinal reinforcement
East 20th	0.0026	30	21.3	1#5@?	2#5@?	1#5@4	2#5@4	?	?
Crow Canyon	0.0057	63	37.2	2#6@12	2#6@12	1#6@6	4#6@6	18#11	28
Crenshaw Boulevard	0.0075	60	35.4	2#6@12	6#6@12	1#6@4	6#6@4	32#11	50
52nd Place	0.0197	35	31.0	2#5@3	2#5@3	2#5@6	4#5@6	12#11	19
Imperial Overcrossing	0.0052	48	34.0	2#6@12	4#6@12	Same	Same	12#14	27
McFadden Street	0.0085	48	*	1#7@12	2#7@12	1#7,5@6",8 @9	4#7@6	23#11 & 6#6	39
Castro Valley	0.0081	54	31.9	2#7@12	4#7@12	1#7@7	4#7@7	16#14	36
Cottonwood Creek	0.0048	54	31.9	2#7@12	4#7@12	1#7@6	4#7@6	34#14	77
Port of Oakland	...	72	42.5	3#6@12	2#6@12	4#6@8	8#6@8	32#14	72
Gavin Canyon	0.0079	96	56.7	5#6@6	4#6@6	5#6@6	6#6@6	32#14	72
Fairfax - Washington	0.0067	46	36.2	10#6@12	3#6@12	Same	Same	20B#10s & 7#12	63
Bull Creek Canyon	?	?	?	8-2#7	8-2#7&2#8	3#7@8	6#7@8	24#14	54
"CL" Line	0.0171	63	37.2	6#6@9	6#8@9	4#6@4	6#6@4	28#18	112
North Connector	0.0137	63	37.2	5#6@12	4#6@12	4#6@9	8#6@9	26#14	59
La Cienega	0.0126	60	42.6	4#6@8	8#6@8	4#6@6	10#6@6	36#14	81
Mission - Gothic	?	?	?	3#6&1#8@ 6	6#8@6	3#6&1#8@ 16	6#8@16	48#14	108

Location	Quantity of secondary negative beam longitudinal reinforcement	Area of secondary negative beam longitudinal reinforcement	Location of secondary negative beam reinforcement, measured from top	Quantity of positive beam longitudinal reinforcement	Area of positive beam longitudinal reinforcement	Area ratio of negative beam reinforcement	Area ratio of secondary negative beam reinforcement	Area ratio of total negative beam reinforcement	Area ratio of positive beam reinforcement
East 20th	?	?	?	?	?	?	?	?	?
Crow Canyon	4#8	3.160	14.88	11#11	17.16	0.00542	0.00061	0.00603	0.00331
Crenshaw Boulevard	6#10	7.620	18.00	24#10	30.48	0.00642	0.00098	0.00740	0.00392
52nd Place	4#11	6.240	13.88	8#11	12.48	0.00706	0.00235	0.00942	0.00471
Imperial Overcrossing	4#11	6.240	23.75	10#11	15.6	0.00412	0.00095	0.00507	0.00238
McFadden Street	4#11	6.240	20.00	4#11	6.24	0.00892	0.00144	0.01036	0.00144
Castro Valley	4#9*	4.000	15.00	8#14	18	0.00826	0.00092	0.00918	0.00413
Cottonwood Creek	7#9	7.000	19.00	7#9	7	0.01087	0.00099	0.01186	0.00099
Port of Oakland	none	0.000	N.A.	23#11	35.88	0.00617	0.00000	0.00617	0.00308
Gavin Canyon	11#11	17.160	*	32#14	72	0.00395	0.00094	0.00489	0.00395
Fairfax - Washington	7#11	10.920	19.50	32#10	40.64	0.01725	0.00297	0.02022	0.01107
Bull Creek Canyon	7#14	15.750	15.00	20#14	45	0.00586	0.00171	0.00757	0.00488
"CL" Line	8#11	12.480	15.00	20#14	45	0.01260	0.00140	0.01400	0.00506
North Connector	6#11	9.360	15.00	8#11	11.28	0.00568	0.00091	0.00659	0.00110
La Cienega	10#9	10.000	17.00	24#14	54	0.01136	0.00140	0.01277	0.00758
Mission - Gothic	6#10	7.620	16.25	32#14	72	0.00833	0.00059	0.00892	0.00556

Location	Total quantity of skin reinforcement both faces	Total area of skin reinforcement	Skin reinforcement % of total column longitudinal reinforcement	Notes
East 20th	?	?	-	
Crow Canyon	10#5	3.10	6.40%	Middle column has less steel than exterior, 39#14
Crenshaw Boulevard	16#6	7.04	8.00%	Beam becomes slender between columns (b=90")
52nd Place	4#6	1.76	4.70%	Wide octagonal section has 27" center-center spirals
Imperial Overcrossing	8#5	2.48	5.08%	Bundled column bars
McFadden Street	6#5	1.86	3.65%	Longitudinal column bars bent 90 degrees outwards
Castro Valley	4#9	4.00	6.90%	
Cottonwood Creek	10#8	7.90	8.73%	Beam has a flange
Port of Oakland	14#8	11.06	10.25%	
Gavin Canyon	18#8	14.22	8.82%	
Fairfax - Washington	6#10	7.62	6.63%	
Bull Creek Canyon	10#9	10.00	8.71%	
"CL" Line	12#11	18.72	11.05%	
North Connector	10#8	7.90	9.98%	
La Cienega	10#11	15.60	10.76%	Ext. col. bars are developed straight, int. are hooked 90 & 135 deg alt.
Mission - Gothic	16#8	12.64	6.74%	

Legend: CT – Cross-tie; H – Hoops; S – Spiral; B – Bundled Bars; M – Moment connection; P – Pinned connection

Appendix B Material Testing Methods and Results

Extensive material testing was conducted as part of the experimental research program. This appendix summarizes the methods used and results compiled during the test program.

B.1 Concrete Testing

Concrete testing was conducted with the goal of establishing detailed constitutive relationships. Five separate tests were performed to get an overall view of the concrete response: compressive strength, compressive stress-strain under load control, compressive stress-strain under displacement control, modulus of rupture, splitting tension strength, and fracture energy. This section summarizes the testing methods used.

B.1.1 Compressive Concrete Response

Compressive response was measured using three testing protocols: compressive strength, hardening response, and softening response. Compressive strength tests were conducted to monitor the strength gain over time. These test were conducted on 6 in. by 12 in. cylinders taken during each pour. Note all concrete cylinders used for material testing were made according to ASTM C31 with full size cylinders measuring 6 in. in diameter and 12 in. in height. Cylinders were cured along the side of the specimen. Strength gain was measured in accordance with ASTM C39, (*Standard test method for compressive strength of cylinder cores).* Cylinders were capped using a sulfur compound and tested in compression with a calibrated universal testing machine at a rate of 35 psi/sec (Figure B-1).

Figure B-1: Compressive strength testing machine

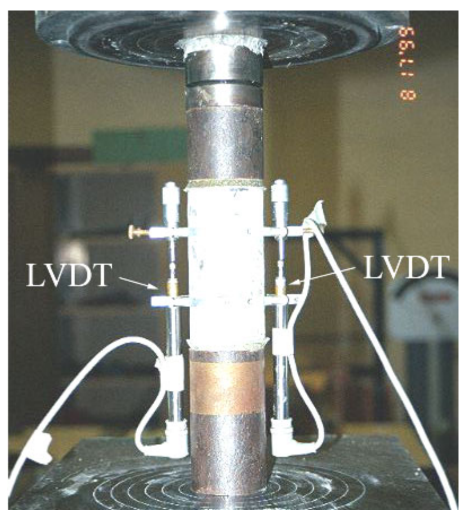

Figure B-2: Compression hardening test setup

To model compression hardening, the stress-strain response was evaluated by applying load (at a rate of 35 psi) and measuring the average external deformation. The external deformation was measured using two linear voltage displacement transducers (LVDT) placed on opposite sides of the cylinder. A gage length of 8 in. was used (Figure B-2). Strain was computed by averaging the measured displacements recorded on each LVDT and dividing by the gage length. The elastic modulus, Ec, was computed from the resulting stress-strain response. Ec was assumed to equal the secant stiffness of the concrete stress-strain response at a strain of 0.0005.

Compression softening was measured by displacement control testing of cylinders (Figure B-3). As was done in the preceding method, cylinders were capped with a sulfur compound and instrumented with two LVDTs (Figure B-4). Since the displacement of the machine piston could not be directly controlled, open loop feedback was used. The testing machine piston was moved such that the average displacement measured on the LVDT changed at a rate of 0.00022 in./sec.; the corresponding load was recorded.

Figure B-3: Compression softening response testing

Figure B-4: Compression softening test setup

B.1.2 Tensile Concrete Response

The concrete tensile regime was defined with three tests: modulus of rupture, splitting tensile strength and fracture energy. Modulus of rupture was used to evaluate the tensile response of the concrete when it is dominated by a flexural tension action such as that occurring in a cantilevered column subjected to lateral loading. Splitting tension was used to evaluate the response of the concrete when dominated by pure axial tension. This test provided a lower bound on the expected tensile concrete strength. Fracture energy tests were conducted to evaluate the amount of energy released as a result of cracking. The results were used in the finite element investigation (Chapter 4).

Modulus of rupture was determined using ASTM C293-94 S*tandard test method for flexural strength of concrete*. The test specimens consisted of 3 in. by 3 in. by 11 in. beams. The tests were conducted using simply supported conditions with center point loading (Figure B-5). A span length, L, of 9 in. was used. The load, P, was applied at a constant rate of 300 lbs./min. to the breaking point. Modulus of rupture, $f'r$, was computed with the relationship

$$f'r = 3PL / 2bd^2 \qquad \text{(B-1)}$$

Where b is the average width and d is the average depth of the beam at the location of fracture. Unless noted the presented results represent the average of three tests.

Splitting tension strength was determined using ASTM C496-96 *Standard test method for splitting tensile strength of cylindrical concrete specimens*. Testing consisted of subjecting concrete cylinders to diametrical compressive stress, applied along its length, until failure was achieved (Figure B-6). Load was applied at a rate of 150 psi/minute. The ultimate load, P, was recorded and converted to splitting tension strength, $f't$, according to

$$f't = 2P / \pi ld \tag{B-2}$$

Where l is equal to the specimen length and d is equal to the specimen diameter, measured prior to testing. The splitting strengths reported are the average of three tests.

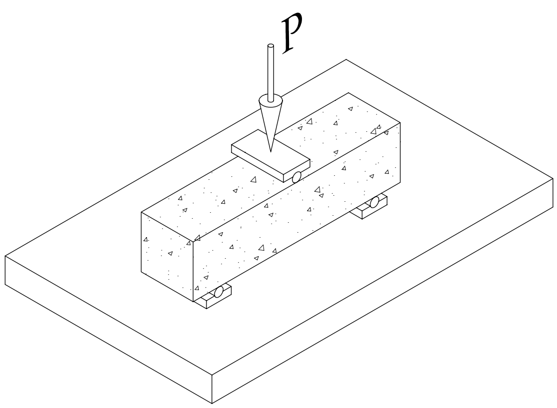

Figure B-5: Modulus of rupture test setup

Figure B-6: Splitting tensile test setup

Fracture energy tests were conducted according to the European recommendation 50-FMC *Determination of the fracture of mortar and concrete by means of three-point bend tests on notched beams*. The tests were carried out on notched beams with overall length, L, of 33 in., depth, d, of 4 in., and width, b, of 4 in. Notches were cast into the test specimens using wooden inserts. The area of the ligament above the notch, A_{lig}, was approximately half of the full cross section. The test was conducted under displacement control at a rate of approximately 0.001 in./minute. Load was applied at the center of the simply supported beam (Figure B-7). A span length, l, of approximately 31 in. was used in all tests. The load-displacement relationship was measured up to failure. Fracture energy, Gf, was computed with the following relationship:

$$Gf = (W_o + (m_1 + 2m_2)g\delta_o)/A_{lig} \tag{B-3}$$

Where W_o is equal to the area under the load-displacement curve, m_1 is equal to the weight of the specimen between supports, m_2 is equal to the weight of the loading arrangement not attached to the testing machine, and g is equal to the acceleration due to gravity.

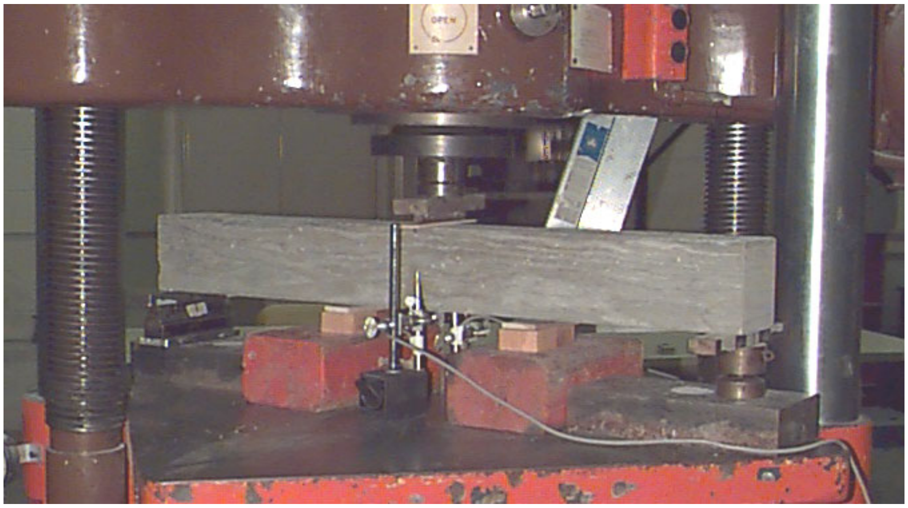

Figure B-7: Fracture energy specimen and test setup

B.2 Reinforcement Testing

All reinforcement used in construction was tested in tension in accordance with ASTM E8-98 *Standard testing method for tension testing of metallic materials*. The reinforcement coupons were fabricated to 24-in. lengths with a 3.5-in. section of deformations removed from the center of the bar. The bar was then marked with indentations at a 2-in. gage length for determination of fracture strain. A clip gage was installed and the coupon was pulled in tension until failure (Figure B-8 and Figure B-9).

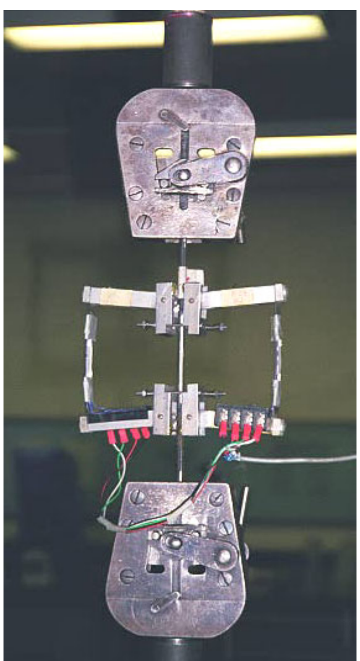

Figure B-8: Tension test setup for #2 reinforcement

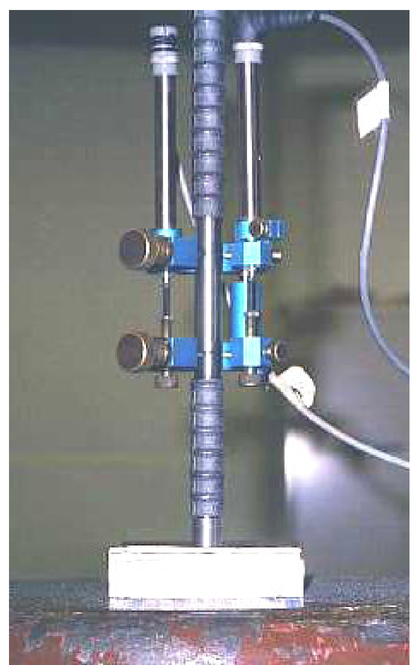

Figure B-9: Tension test setup for #3 reinforcement and greater, (#6 shown)

Reinforcement properties were derived from the measured stress-strain response of each bar. Elastic modulus was determined by taking the initial tangent stiffness of the stress-strain response. Yield and ultimate stresses and strains were determined in accordance with standard methods. If a well-defined yield plateau did not occur, yield was determined using a 0.2% offset of the initial stiffness.

B.3 Summary Material Properties

B.3.1 Concrete Properties

Normal weight concrete was used with a maximum aggregate size of 3/8 inch. The concrete constituents and typical batch weights are summarized in Table B-1. Concrete was supplied by a local ready-mix plant. Concrete was placed by pump using a 3-in. diameter hose. Following casting, all exposed concrete surfaces were covered with wet burlap and plastic. The concrete was kept moist for one week after casting.

Table B-1: Typical concrete batch weights for one cubic yard

Material	Absolute Volume [ft.^{3}]	Saturated Surface Dry Weights [lbs.]
3/8 in. X #8 (Specific gravity 2.68)	7.47	1250
Regular top sand (Specific gravity 2.67)	8.25	1374
Blend sand (Specific Gravity 2.60)	3.21	521
Cement-ASTM C150 Type 2	2.87	564
Water (36 gallons)	4.79	299
Water reducing admixture-ASTM C494 Type A		11.3 FL. OZ.
Retarder-ASTM C494 Type D	.41	10.9 FL. OZ.
Total:	27	4008

The same mix design was used in all specimens. Variations in measured properties can be attributed to changes in water content brought on by variability in weather or batching conditions. Nevertheless, the measured material properties were comparable throughout the test program (Table B-2, Table B-3, and Figure B-10).

Table B-2: Column concrete material properties

Test subassembly		A1	A2	A3	A4	B1	B2
Compressive strength	$f'c$	5.51	5.81	5.34	5.54	4.22	4.38
Corresponding strain	εcu	0.00294	0.00297	0.00280	0.00295	0.00231	0.00238
Tension strength	$f't$	0.540	0.425	0.503	0.465	0.364	0.441
Modulus of rupture	$f'r$	N.A.	N.A.	N.A.	N.A.	0.609	0.739
Young′s modulus steel	Ec	3360	3470	3280	3290	3260	3350
Fracture energy	Gf	0.00098	0.00077	0.00092	0.00085	0.00053	0.00070
Age at testing	days	77	105	116	129	30	37

Table B-3: Beam concrete material properties							
Test subassembly		A1	A2	A3	A4	B1	B2
Compressive strength	*f′c*	5.29	5.53	5.97	5.99	5.23	5.44
Corresponding strain	ε_{cu}	0.00296	0.00294	0.00279	0.00289	0.00244	0.00249
Tension strength	*f′t*	0.563	0.544	0.578	0.432	0.471	0.481
Modulus of rupture	*f′r*	N.A.	N.A.	N.A.	N.A.	711	708
Young′s modulus steel	*Ec*	3310	3480	3800	3680	3500	3690
Fracture energy	*Gf*	0.00103	0.00099	0.00105	0.00079	0.00103	0.00099
Age at testing	days	91	119	130	143	36	43

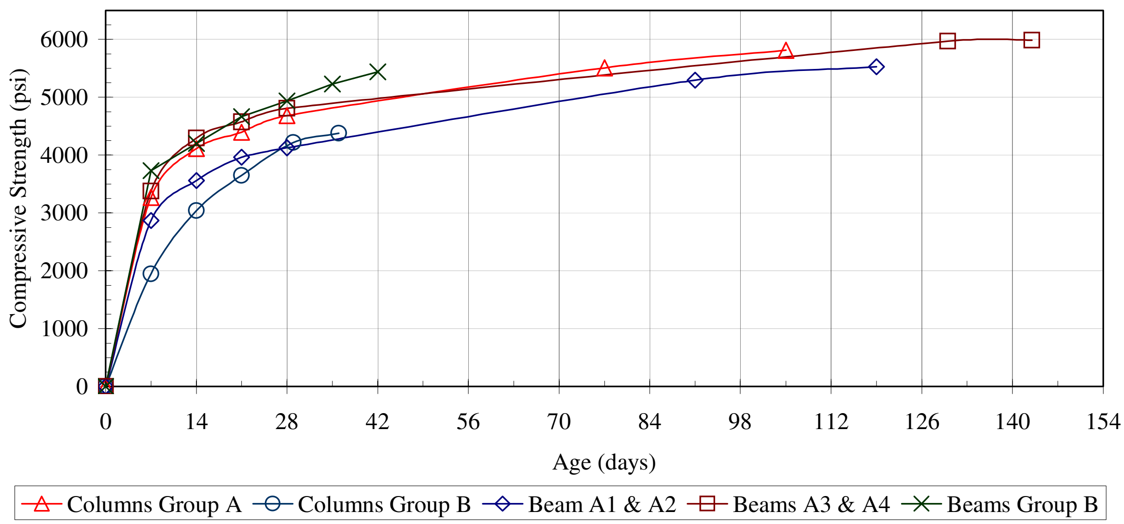

Figure B-10: Concrete strength gain

The concrete constitutive relationship for each specimen was derived by combining the average hardening response (Figure B-11) with the average softening response (Figure B-12). The final relationships are presented in Figure B-13 through Figure B-16.

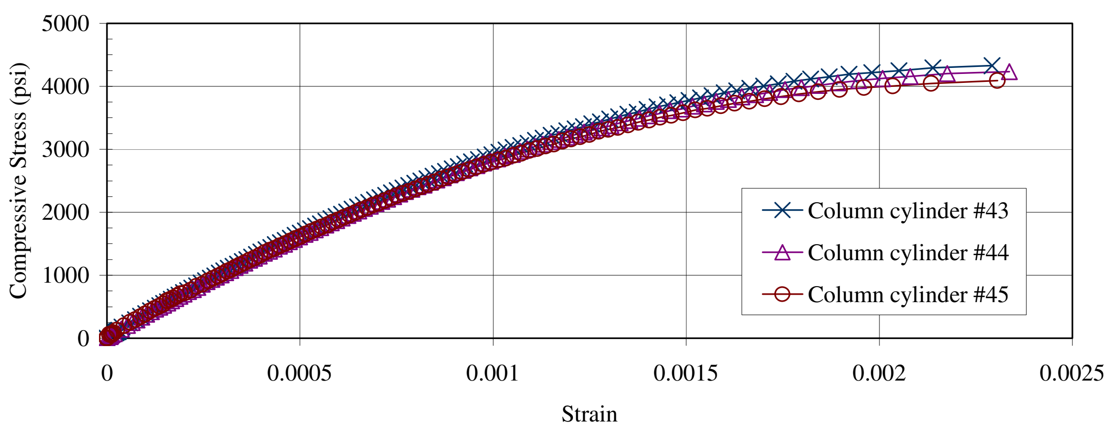

Figure B-11: Typical concrete compression hardening response (Subassembly B1 shown)

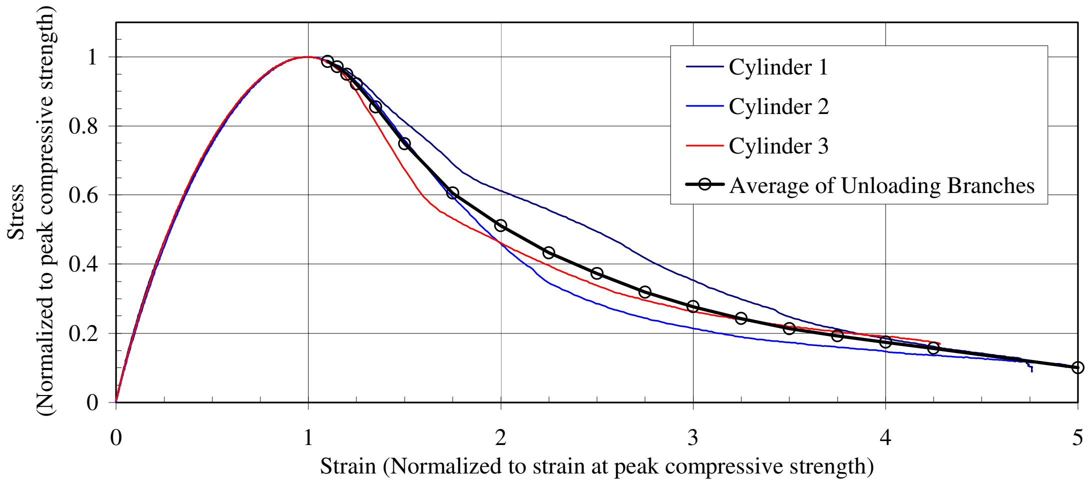

Figure B-12: Typical concrete compression softening response

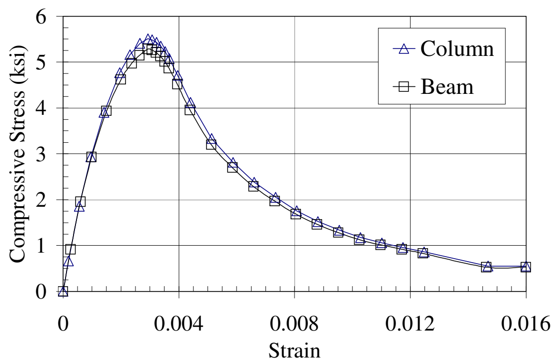

Figure B-13: Concrete compressive stress-strain relationship Subassembly A1

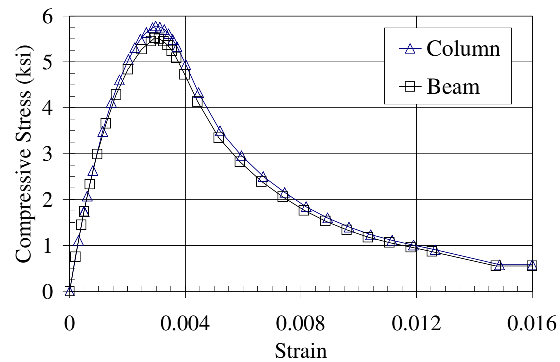

Figure B-14: Concrete compressive stress-strain relationship Subassembly A2

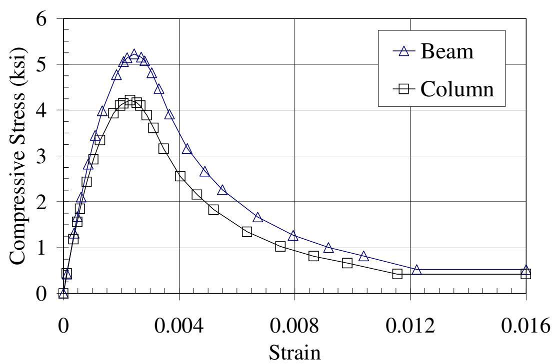

Figure B-15: Concrete compressive stress-strain relationship Subassembly B1

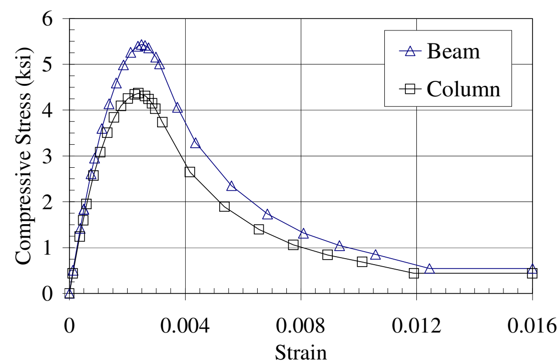

Figure B-16: Concrete compressive stress-strain relationship Subassembly B2

B.3.2 Reinforcement Properties

Three types of reinforcement were used. Primary longitudinal bars consisted of reinforcement meeting the requirements of ASTM A706. Due to the limited availability of A706 for bars of small diameter, transverse bars consisted of ASTM A615 material. To model the scaled column ties in specimens A3 and A4, #2 deformed reinforcement was used. This size of bar, at the time of writing, was no longer commercially produced. Consequently, the #2 reinforcement consists of ungraded material acquired from the University of California at Berkeley stockpile. The measured reinforcement material properties, including mill specifications where available, are summarized in Table B-4 and Table B-5.

Table B-4: Group A reinforcement material properties

Bar Use		Column Ties A3 and A4	Beam ties, skin, and spiral	Headed transverse	Anchor block transverse	Headed longitudinal	Conventional longitudinal
Bar size		#2	#3	#4	#4	#6	#6
Yield stress	σ_y	76.0	77.0	74.0	71.0	72.5	68.0
Yield strain	ε_y	0.00260	0.00270	0.00260	0.00245	0.00250	0.00250
Elastic modulus	Es	29231	28519	28462	28980	29000	27200
Plateau strain	ε_{yp}	0.032	N.A.	0.013	0.011	0.020	0.012
Ultimate stress	σ_u	104.0	122.5	109.0	113.0	98.5	102.0
Ultimate strain	ε_u	0.111	0.192	0.131	0.117	0.140	0.139
Fracture strain	ε_f	0.165	0.250	0.220	0.210	0.240	0.240
Heat Number		N.A.	310696	N.A.	Z4141	N.A.	70769
Manufacturer		N.A.	Cascade	N.A.	Tamco	N.A.	Tamco
ASTM Specification		Unknown	A615	A706	A706	A706	A706
Yield		N.A.	65	N.A.	67.000	N.A.	66.0
Tensile		N.A.	103	N.A.	93.000	N.A.	93.5
Elongation		N.A.	11	N.A.	15.500	N.A.	17
C		N.A.	0.38	N.A.	0.300	N.A.	0.28
Mn		N.A.	1.08	N.A.	0.760	N.A.	1.04
Cu		N.A.	N.A.	N.A.	N.A.	N.A.	0.42
Ni		N.A.	N.A.	N.A.	N.A.	N.A.	0.17
Cr		N.A.	N.A.	N.A.	N.A.	N.A.	0.18
Mo		N.A.	N.A.	N.A.	N.A.	N.A.	0.02
V		N.A.	0.002	N.A.	N.A.	N.A.	0.23
Carbon Equivalent		N.A.	0.58	N.A.	0.460	N.A.	0.49

The constitutive relationships used for the reinforcement used in Group A finite element models are presented in Figure B-17 through Figure B-20. Applications of these models are presented in chapters 4, 6, and 8.

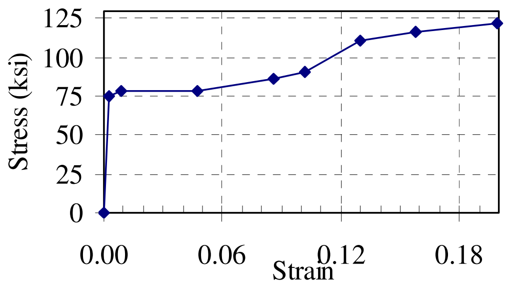

Figure B-17: Group A #3 beam ties, skin, and spiral

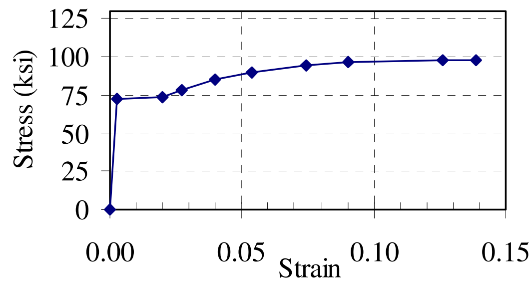

Figure B-18: Group A #4 headed transverse

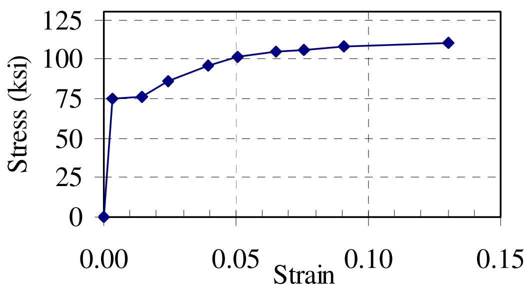

Figure B-19: Group A #6 headed longitudinal

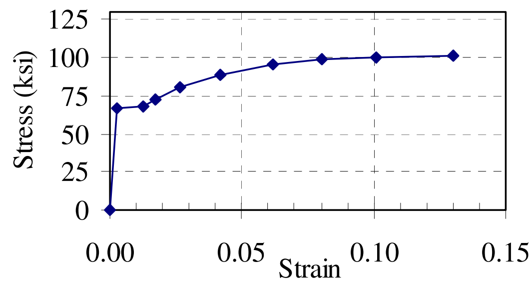

Figure B-20: Group A #6 conventional longitudinal

The constitutive relationships used for the reinforcement used in Group B finite element models are presented in Table B-5 and in Figure B-21 through Figure B-26. Applications of these models are presented in Chapter 7.

Table B-5: Group B reinforcement material properties

Bar Use		Skin and Joint hoops	Column spiral	Beam transverse	Horizontal joint transverse	Vertical joint transverse	Primary longitudinal
Bar Size		#3	#3	#3	#3	#4	#6
Yield stress	σ_y	67163	61790	84606	67178	74478	69076
Yield strain	ε_y	0.002526	0.00424	0.005176	0.002536	0.002962	0.002485
Elastic modulus	Es	26592	27965	26436	26490	25142	27797
Plateau stress	σ_{yp}	67409	No Plateau	No Plateau	67880	75337	69647
Plateau strain	ε_{yp}	0.01206	No Plateau	No Plateau	0.01123	0.01421	0.00963
Ultimate stress	σ_u	105862	108936	112237	107440	103067	103582
Ultimate strain	ε_u	0.1287	0.09460	0.0853	0.1212	0.1338	0.1229
Fracture stress	σ_f	97558	N.A.	105635	97363	70987	85299
Fracture strain	ε_f	0.1533	N.A.	0.0954	0.1502	0.2462	0.2453

Table B-5 *(continued):* Group B reinforcement material properties						
Bar Use	Skin and Joint hoops	Column spiral	Beam transverse	Horizontal joint transverse	Vertical joint transverse	Primary longitudinal
Heat number	96998	167249	6-6096	N.A.	N.A.	80992
Manufacturer	Cascade	Nucor	CF&I	N.A.	N.A.	Tamco
ASTM Specification	A615M	A615-94	A615	A615	A706	A706
Yield	64	65.636	62.2	N.A.	N.A.	67.5
Tensile	100	104.091	100.909	N.A.	N.A.	97.5
Elongation	14	14	13.6	N.A.	N.A.	15
C	0.37	0.36	0.44	N.A.	N.A.	0.26
Mn	1.08	1.19	0.81	N.A.	N.A.	1.06
Cu	N.A.	N.A.	0.2	N.A.	N.A.	0.35
Ni	N.A.	N.A.	0.09	N.A.	N.A.	0.18
Cr	N.A.	N.A.	0.07	N.A.	N.A.	0.24
Mo	N.A.	N.A.	0.021	N.A.	N.A.	0.03
V	N.A.	N.A.	0	N.A.	N.A.	0.022
Carbon Equivalent	0.55	0.56	0.58	N.A.	N.A.	0.48

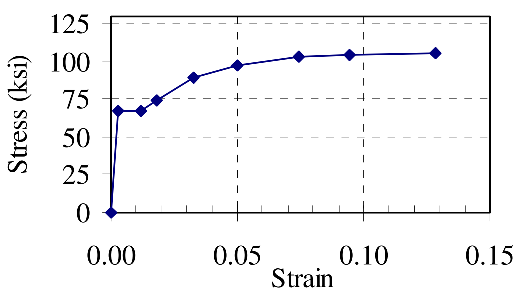

Figure B-21: Group B #3 skin and joint hoops

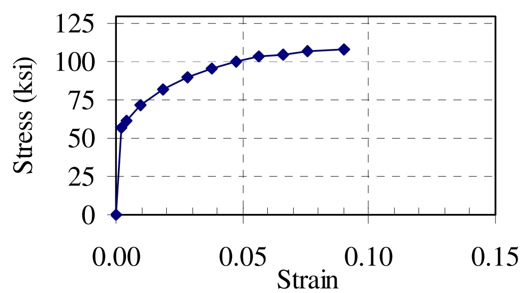

Figure B-22: Group B #3 column spiral

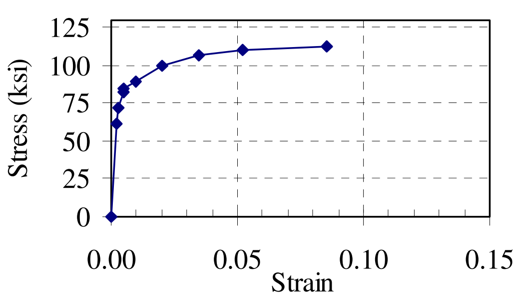

Figure B-23: Group B #3 beam transverse

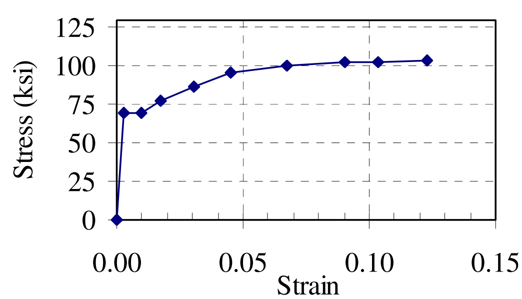

Figure B-24: Group B #6 primary longitudinal

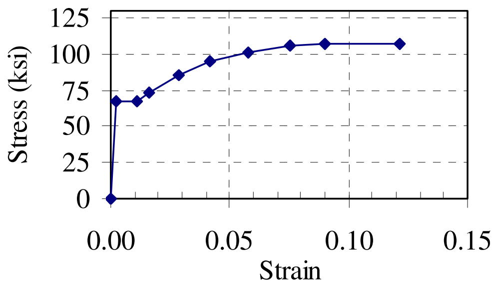

Figure B-25: Group B #3 horizontal joint transverse

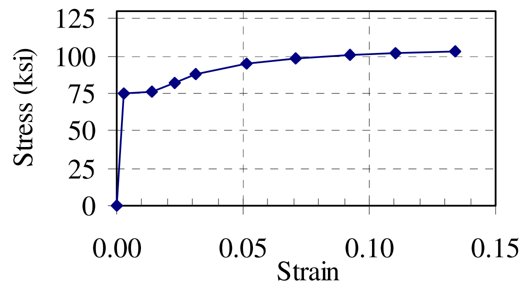

Figure B-26: Group B #4 vertical joint transverse

Appendix C Joint Design Study

To compare the effectiveness of code requirements an investigation was performed on the current recommendations used for beam-column joint design. A standard geometry and arrangement of longitudinal reinforcement was chosen (Figure C-1). The development requirements of each design varies; for illustration, the column bars are shown as hooked. Starting with a typical column longitudinal reinforcement ratio, ρ, of 2.2% and assuming that column plastic hinge formation controls the strength, the remaining components were designed. The resulting moment capacities are tabulated.

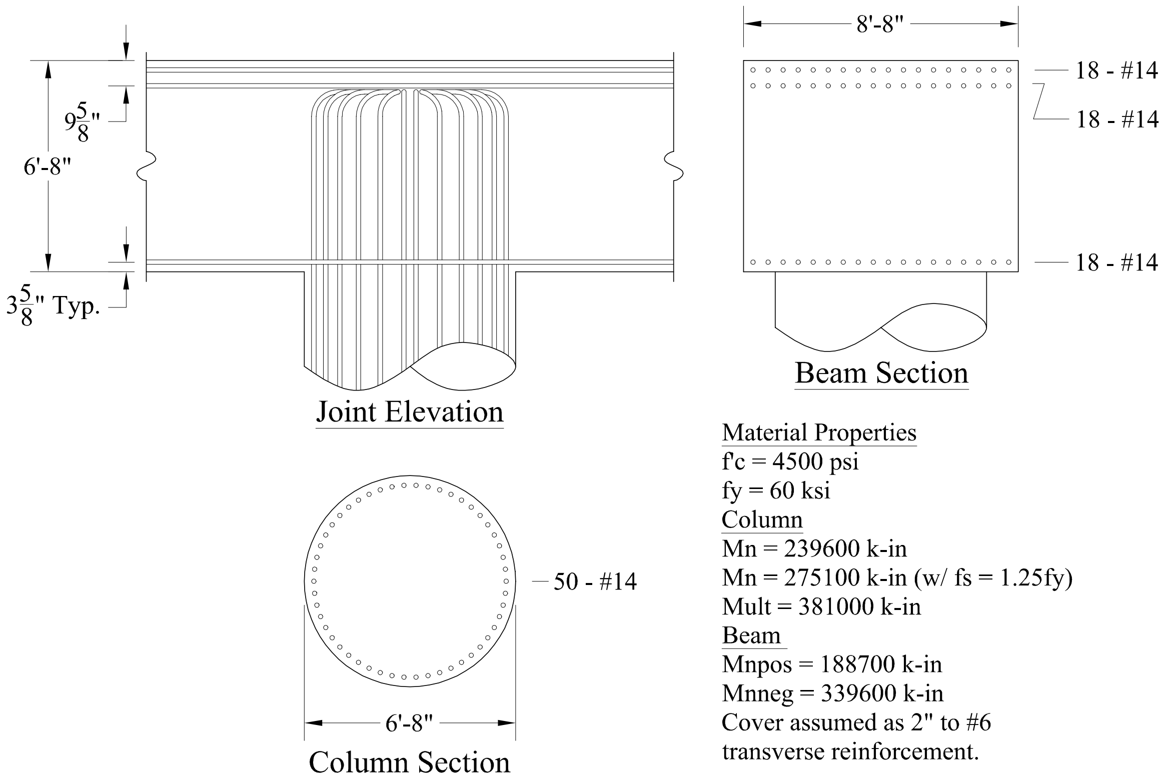

Figure C-1: Prototype joint geometry and longitudinal reinforcement

The joint recommendations listed in Table C-1 were evaluated.

Table C-1: Joint details

Design Method	*Joint Detail*
ACI 352 using column transverse reinforcement for confinement	A
ACI 352 using beam transverse reinforcement for confinement	B
Architectural Institute of Japan (AIJ)	C
California Transportation Bridge Design Specification	D
New Zealand-NZS 3101 — 1982	E
New Zealand-NZS 3101 — 1995	F
Applied Technology Council — ATC 32	G

The following details illustrate the amount of reinforcement required by each of the design specifications. This includes the amount of vertical and horizontal transverse reinforcement needed for joint shear or tension resistance, and the amount of horizontal spiral or hoops required for joint confinement. The level of transverse reinforcement needed to resist shear and/or to provide confinement in the beam and column outside the joint has not been investigated and is not included in the following details.

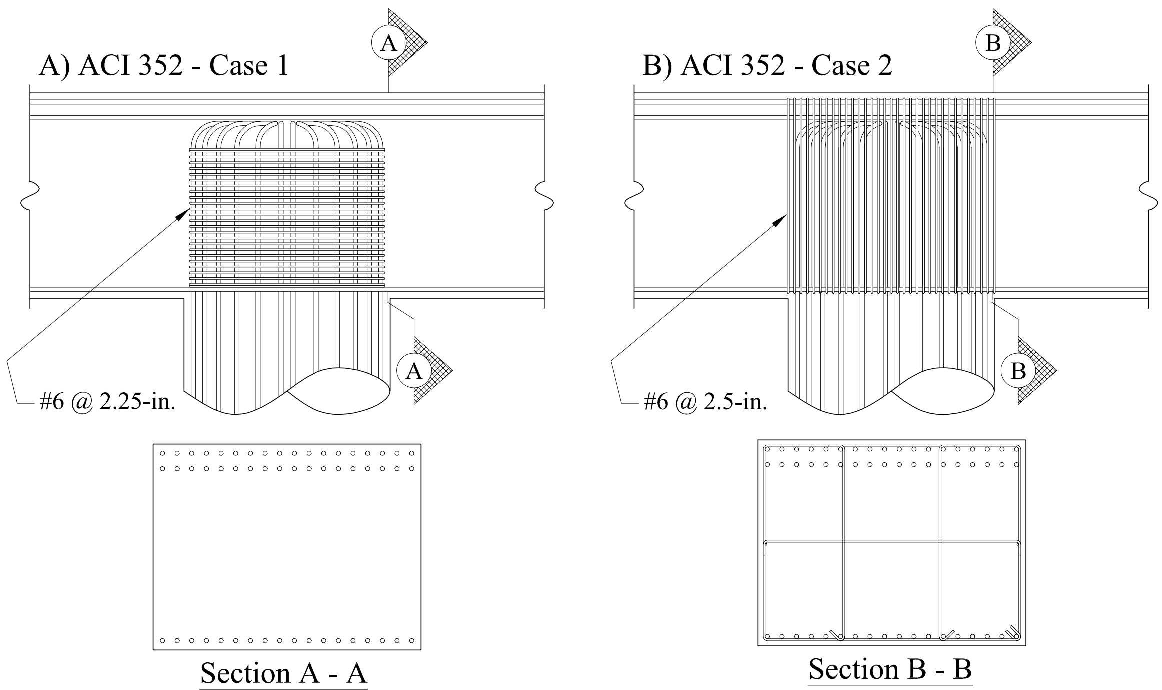

Figure C-2: Joint details (A) and (B)

Two arrangements of reinforcement were evaluated for ACI 352 (Figure C-2). The first assumes that horizontal transverse bars consisting of a spiral around the developed column reinforcement provide the joint reinforcement. The second case assumes that vertical transverse bars in the form of beam stirrups provide the joint reinforcement. In both cases the joint requirements do not consider the effects of axial load. Note that the column longitudinal reinforcement is extended to the far side of the joint and terminated with 90-degree hooks. As shown, both cases result in high quantities of joint reinforcement with detail A lending itself more to construction. To alleviate the congestion present in detail B, larger bars should be used for the joint stirrups. Due to the required bending involved it would be prudent to limit these bars to #8. For comparative reasons, however, these bars were kept as #6.

To provide shear resistance and to assist in confining the joint, AIJ requires that transverse joint reinforcement be placed perpendicular to the yielding member (Figure C-3 (C)). The bond limitations for the beam reinforcement requires that the #14 longitudinal bars be developed a minimum of 51 in. within the joint, the 80-in. joint depth was more than adequate. Note that since the bars terminate within the joint, they are to be extended to the far side of the joint and hooked to improve force transfer.

Caltrans BDS requires a considerable amount of joint reinforcement. Continuation of the column spiral into the joint is required to assist in confining the joint and improving anchorage of the longitudinal column reinforcement. To assist in the transfer of forces from the column to the cap beam, horizontal hairpins in combination with a concentration of beam transverse reinforcement are required outside the column core. In addition, skin reinforcement is required on both vertical faces of the cap beam to improve cracking resistance to large vertical accelerations.

New Zealand specifications require that the joint be reinforced to provide confinement of the core and resistance to shear forces. This is accomplished through the continuation of the column spiral into the joint region and the use of horizontal and vertical joint shear reinforcement in the form of beam stirrups (Figure C-4). As discussed in Chapter 2, an increase in the assumed capacity of the concrete compression strut leads to a considerable decrease in the required amount of horizontal joint reinforcement.

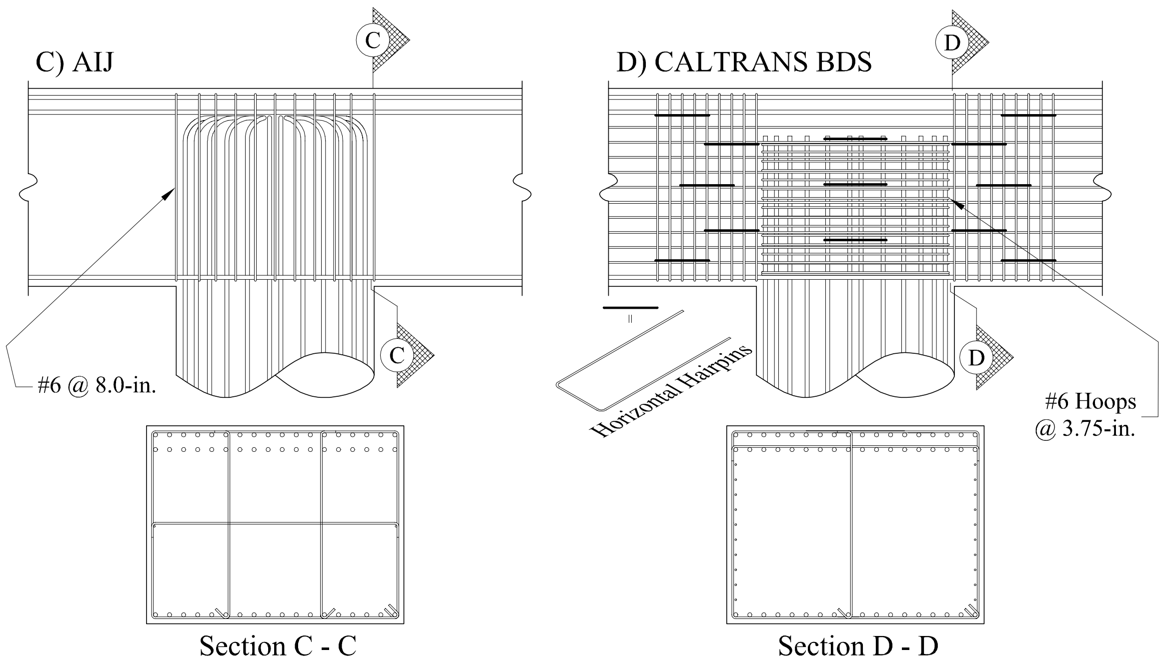

Figure C-3: Joint details (C) and (D)

ATC 32 requires that a spiral be provided in the joint to confine the column longitudinal reinforcement and to assist in carrying tension stresses in the joint. The code allows for a straight termination of the column bars with a development length of at least 43 in. To provide an added level of safety, the column bars are extended to the far side of the joint, directly below the top beam reinforcement (Figure C-5). Due to the high level of principal tension stress, $6.3\sqrt{f'c}$, additional transverse reinforcement is required for force transfer. It should be noted that the corresponding level of principal compressive stress, $0.14f'c$, meets the allowable value of $0.25f'c$. The additional reinforcement required by the ATC to effectively transfer forces is very excessive. The code requires forty-two vertical #6 bars on each face of the column core and four additional #14 beam longitudinal bars on the bottom of the cap beam to transfer tension generated by hinging of the column. Twenty-one vertical #6 bars are required within the column core to restrain the top beam longitudinal reinforcement from buckling. The code also requires a significant amount of spiral reinforcement in the joint to resist the thrust from the internal compression struts developed during hinging of the column. The code requires that a #6 spiral be used at 13/16 inch. This value is clearly unacceptable from a construction view since getting concrete to flow through a 1/16 in. clear spacing will not be possible. To alleviate this, the spiral was increased to a #8, resulting in 3/8 in. clear spacing. Increasing the spiral any larger may lead to other issues such as difficulties with handling and bending. Though the other requirements posed by this design will not produce any significant constructability issues, the required spiral spacing makes this design strategy unfavorable.

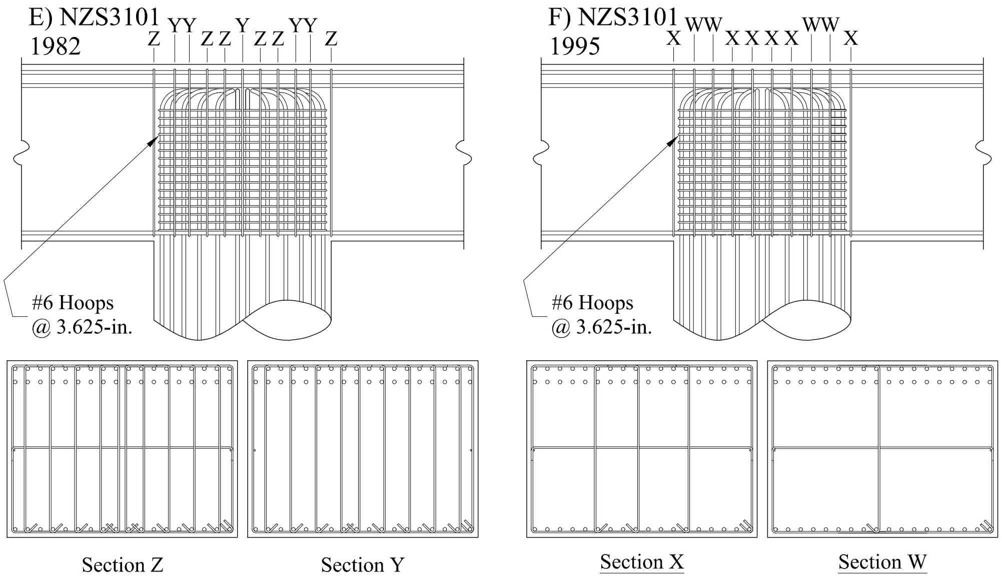

Figure C-4: Joint details (E) and (F)

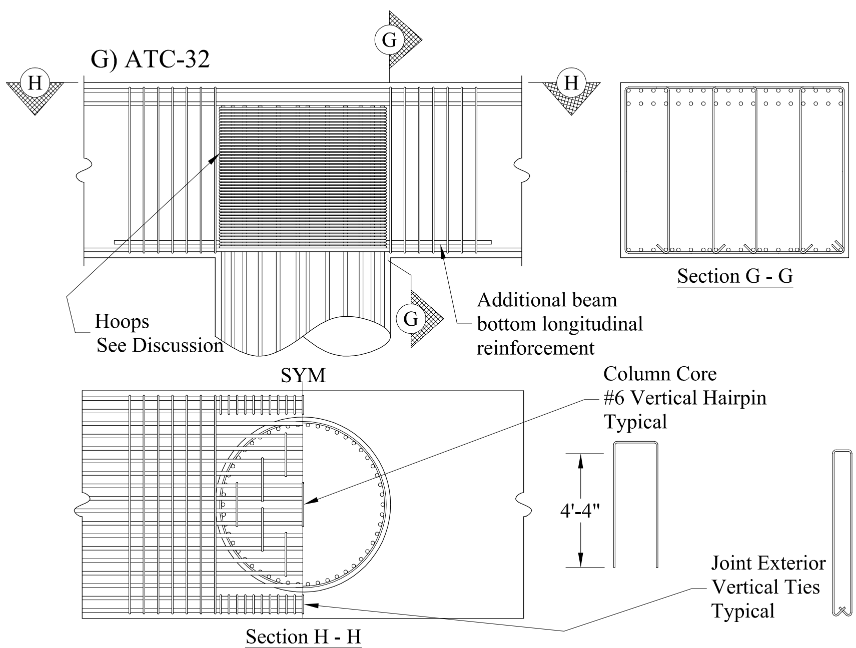

Figure C-5: Joint detail (G)

References

50-FMC Committee on the Fracture Mechanics of Concrete. 1985. Determination of the Fracture Energy of Mortar and Concrete by Means of Three-point Bend Tests on Notched Beams. *Rilem Draft Recommendation, Materials and Structures,* Vol. 18, No. 106, pp. 285–90.

ACI 318-95. 1995. *Building Code Requirements for Structural Concrete and Commentary.* American Concrete Institute.

ACI-ASCE Committee 352. 1983. *Recommendations for Design of Beam Column Joints in Monolithic Reinforced Concrete Structures*.

Agbabian, M. S., Higazy, E. M., Abdelghaffar, A. M., and Elnashai, A. S. (Reprint). August 1994. Experimental Observations on the Seismic Shear Performance of RC Beam-to-Column Connections Subjected to Varying Axial Column Force. *Earthquake Engineering & Structural Dynamics* 23(8)(August): 859–76.

Architectural Institute of Japan. 1994. *AIJ Structural Design Guidelines for Reinforced Concrete Buildings.*

Argyris, J., and Sharpf, D. 1969. Methods of Elasto-Plastic Analysis. *ISD, ISSC Symposium on Finite Element Technique, Stuttgart.*

ASTM. 1998. *Standard Test Methods for Tension Testing of Metallic Materials: Designation E8-98.* ASTM Standards. Philadelphia: American Society for Testing Materials.

ASTM. 1997. *Standard Specification for Welded Headed Bars for Concrete Reinforcement: Designation A970-97.* ASTM Standards. Philadelphia: American Society for Testing Materials.

ASTM. 1996. *Specification for Deformed and Plain and Billet Steel Bars for Concrete Reinforcement: Designation A615-96.* ASTM Standards. Philadelphia: American Society for Testing Materials.

ASTM. 1996. *Standard Test Method for Compressive Strength of Cylindrical Concrete Specimens: Designation C39-96.* ASTM Standards. American Society for Testing Materials.

ASTM. 1996. *Standard Test Method for Splitting Tensile Strength of Cylindrical Concrete Specimens: Designation C496-96.* ASTM Standards. Philadelphia: American Society for Testing Materials.

ASTM. 1994. *Standard Test Method for Flexural Strength of Concrete (Using Simple Beam with Center-Point Loading: Designation C293-94.* American Society for Testing Materials.

ASTM. 1993. *Standard Specification for Low-Alloy Steel Deformed Bars for Concrete Reinforcement: Designation A706-93.* ASTM Standards. Philadelphia: American Society for Testing Materials.

ATC-32. 1996. *Improved Seismic Design Criteria for California Bridges: Provisional Recommendations.* Applied Technology Council.

Bashandy, T. R. 1996. *Application of Headed Bars in Concrete Members.* Ph.D. Thesis. University of Texas at Austin.

Bazant, Z. P., and Oh, B. H. 1983. Crack Band Theory for Fracture of Concrete. *Materials and Structures* 16(93): 155–77.

British Standard 8101. *Structural Use of Concrete*. 1985.

BSSC. 1997. *NEHRP Guidelines for the Seismic Rehabilitation of Buildings.* Developed by the Building Seismic Safety Council and Applied Technology Council for the Federal Emergency Management Agency. (Report No. FEMA-273), Washington D.C.

California Department of Transportation. December 1995. *Caltrans Bridge Design Specifications.* Division of Structures.

Comité Euro-International du Bénton. 1990. *CEB-FIP Model Code.*

Comité Euro-International du Bénton. 1996. *RC Elements under Cyclic Loading State of the Art Report*.

Cook, R. D., Malkus, D. S., and Plesha, M. E. 1989. *Concepts and Applications of Finite Element Analysis*. 3rd Ed. New York: John Wiley & Sons.

DesRoches, R., and Fenves, G. L. 1997. *New Design and Analysis Procedures for Intermediate Hinges in Multiple-frame Bridges.* Report UCB/EERC 1997/12 Berkeley, Calif.: Earthquake Engineering Research Center, College of Engineering, University of California.

DeVries, R. A. 1996. *Anchorage of Headed Reinforcement in Concrete*. Ph.D. Dissertation. University of Texas at Austin. December.

Eligehausen, R., Popov, E. P., and Bertero, V. V. 1983. *Local Bond Stress-Slip Relations of Deformed Bars under General Excitations.* Report UCB/EERC-83/23. Berkeley, Calif.: Earthquake Engineering Center, University of California, Berkeley.

Favre, R., et. al. 1985. *CEB Design Manual on Cracking and Deformations.* Lausanne, Switzerland: Ecole Polytechnique Federale de Lausanne.

Feenstra, P. H. 1993. *Computational Aspects of Biaxial Stress in Plain and Reinforced Concrete*. Ph.D. Dissertation. Delft, The Netherlands: Delft University of Technology.

Frenary, J. W. 1990. Theory and Experiments on the Behavior of Cracks in Concrete Subjected to Sustained Shear Loading. *HERON* 35(1).

Hanson N. W., and Connor H. W. 1967. Seismic Resistance of Reinforced Concrete Beam-Column Joints. *J. of the Structural Division* 93 ST5 (October): 533–60.

Haroun, M. A., Pardoen, G. C., Shepherd, R., Haggag, H. A., and Kazanjy, R. P. December 1994. *Assessment of Cross-Tie Performance in Bridge Pier Walls*. Final Report to the California Department of Transportation.

Hordjik, D. A. 1992. Tensile and Tensile Fatigue Behavior of Concrete: Experiments Modeling and Analysis. *HERON* 37(1).

Ichinose, T. 1991. Interaction between Bond at Beam Bars and Shear Reinforcement in RC Interior Joints. *Design of Beam-Column Joints for Seismic Resistance*. SP 123-14, 1991. Ed. J. O. Jirsa. ACI.

Jirasek, M., and Zimmerman, T. 1997. *Rotating Crack Model with Transition to Scalar Damage. I: Local formulation. II: Nonlocal formulation and adaptivity.* LSC Internal Report 97/01. Lausanne, Switzerland: LSC — Laboratoire de Mechanique des Structures et Mileux Continus, Ecole Polytechnique Federale de Lausanne (EPFL).

Kaku, T., and Asakusa, H. 1991. Bond and Anchorage of Bars in Reinforced Concrete Beam-Column Joints. *Design of Beam-Column Joints for Seismic Resistance,* SP 123-15, 1991. Ed. J. O. Jirsa. ACI.

Kitayama, K., Otani, S., and Aoyama, H. 1991. Development for Design Criteria for RC Interior Beam-Column Joints. *Design of Beam-Column Joints for Seismic Resistance,* SP 123-4, 1991. Ed. J. O. Jirsa. ACI.

Kupfer H. B., and Gerstle K. H. 1973. Behavior of Concrete under Bi-axial Stresses. *J. Engineering Mechanics* 99(4): 853–66. ASCE.

Lehman, D. E., Elkin, S. J., Nacamuli, A. M., and Moehle, J. P. May 1998. Repair of Moderately and Severely Damaged Bridge Columns. *Proceedings of the Sixth U.S. National Conference on Earthquake Engineering.* Paper # 86.

Leon, R. T. Towards New Bond and Anchorage Provisions for Interior Joints. *Design of Beam-Column Joints for Seismic Resistance,* SP 123-16, 1991. Ed. J. O. Jirsa. ACI.

Lowes, L., and Moehle, J. P. September 1995. *Seismic Behavior and Retrofit of Older Reinforced Concrete Bridge Joints.* Report No. UCB/EERC-95/09. Berkeley, Calif.: Earthquake Engineering Center, University of California, Berkeley.

Lowes, L.. 1999. *Finite Element Modeling of Reinforced Concrete Bridge Beam-Column Connections*. Ph.D. Dissertation. University of California at Berkeley.

Malvar, L. J. 1992. Bond Reinforcement under Controlled Confinement. *Materials J.* 89(6): 593–601. ACI.

MacGregor, J. G. 1988. *Reinforced Concrete — Mechanics and Design.* Englewood Cliffs, N. J.: Prentice-Hall,

Mander, J. B., Priestley, M. J. N., and Park, R. 1988. Theoretical Stress-Strain Model for Confined Concrete. *J. Structural Engineering* 114(8)(August): 1804–49. ASCE.

McConnell, S. W., and Wallace, J. W. June 1994. *Use of T-Headed Reinforced Concrete Knee-Joints Subjected to Cyclic Lateral Loading*. Report CU/CEE-94/10. Clarkson University.

Mitchell, D. W., and Rooney, A. March 1994. T-Headed Bars in the Hibernia G.B.S. *Canadian Civil Engineer.*

Mosalam, K. M., White, R. N., and Gergely, P. December 1997. C*omputational Strategies for Frames with Infill Walls: Discrete and Smeared Crack Analyses and Seismic Fragility.* Technical Report NCFER-97-0021.

New Zealand Standard. 1982. *3101 — Code Practice for the Design of Concrete Structures*.

New Zealand Standard. 1995. *3101 — Code Practice for the Design of Concrete Structures*.

Paulay, T., and Loeber, P. J. 1974. Shear Transfer by Aggregate Interlock. *Shear in Reinforced Concrete.* ACI Special Publication 42, Volume 1, pp. 1–15. Detroit: ACI.

Paulay, T., Park, R., and Priestley, M.J.N. 1978. Reinforced Concrete Beam-Column Joints under Seismic Action. *ACI Journal Proceedings* 75(11)(November): 585–93.

Priestley, M. J. N. *Assessment and Design of Joints for Single-Level Bridges with Circular Columns.* February 1993. Report: SSRP-93/02. La Jolla, Calif.: Dept. of Applied Mechanics and Engineering Sciences, University of California, San Diego.

Rots, J. G. 1988. *Computational Modeling of Concrete Fracture*. Ph.D. Dissertation. Delft University of Technology. Delft, The Netherlands.

Schlaich, J. Schfer, K., and Jennewein, M. 1987. Toward a Consistent Design of Structural Concrete. *PCI J.* 32(3): 74–150.

Scott, R. H., Feltham, and Whittle. 1994. Reinforced Concrete Beam-Column Connections and BS8110. *Structural Engineer* 2(4)(February): 55–60

Scott, B. D., Park, R., and Priestley, M. J. N. 1982. Stress-Strain Behavior of Concrete Confined by Overlapping Hoops at Low and High Strain Rates. *American Concrete Inst. J.* 79(1): 13–27.

Sozen, M. A. 1974. Hysteresis in Structural Elements. Proceedings, *Applied Mechanics in Earthquake Engineering,* November 17–21, 1974, pp. 63–98 New York: The American Society of Mechanical Engineers.

Sritharan, S., Priestley, M. J. N., and Seible, F. 1997. Influence of Prestress on Column / Cap Beam Tee Joints. *4th Caltrans Seismic Research Workshop*.

Sritharan, S., Ingham, J. M., Priestley, M. J. N., and Seible F. 1997. Bond Slip of Bridge Column Reinforcement Anchored in Cap Beams. *ACI Spring Convention,* Seattle.

Thewalt, C. R., and Stojadinovic, B. 1993. *ARCS: Analysis of Reinforced Concrete Sections*. Berkeley, Calif.: University of California.

Vecchio, F. J., and Collins, M. P. 1986. The Modified Compression Field Theory Reinforced Concrete Elements Subjected to Shear. *J. American Concrete Institute* 83: 219–31.

Vecchio, F. J., and Collins, M. P. 1988. Predicting the Response of Reinforced Concrete Beams Subjected to Shear Using Modified Compression Field Theory. *ACI J.* 85(3)(May-June): 258–68.

Witte, F. C., et. al. 1998. *DIANA — Finite Element Analysis.* User's Manual: Release 7. Delft, The Netherlands: TNO Building Construction and Research.

Zelinski, R. January 1995. *Seismic Design Memo Various Topics Preliminary Guideline.* Internal memo, California Department of Transportation, Division of Structures.

Zhu, S., and Jirsa, J. O. 1983. *A Study of Bond Deterioration in Reinforced Concrete Beam-Column Joints.* PMFSEL Report 83-1. University of Texas.

Zienkiewicz, O. C., and Taylor, G. C. 1989. *The Finite Element Method*. Volume 1: Basic Formulation and Linear Problems. 4th ed. Berkshire, England: Mc-Graw Hill.

Zienkiewicz, O. C., and Taylor, G. C. 1991. *The Finite Element Method*. Volume 2: Solid and Fluid Mechanics, Dynamics and Non-Linearity. 4th ed. Berkshire, England: Mc-Graw Hill.